STRENGTHENING OF METALLIC STRUCTURES USING CARBON FIBRE COMPOSITE PLATES

By

Farzad Nikoukar Zanjani

For the degree of Doctor of Philosophy
University of Southampton

May 2004

Faculty of Engineering and Applied Science
Department of Civil and Environmental Engineering

Summary

The aim of this research was to identify the benefits of strengthening metallic structures with carbon fibre reinforced polymer (CFRP) plates whilst the structures are subjected to preload and imposed loading. When a carbon fibre plate is bonded to a metallic substrate there is a curing period during which the adhesive develops its full strength. When it is not economic to take a structure out of service, the adhesive will be subjected to imposed loading during curing and uncertainty remains with regard to the effectiveness of the bond, which needed to be investigated.

For the beams, it was found from laboratory testing that reinforcement using CFRP plates had increased the stiffness by approximately 35%. This increase was found to be greatly affected by exposure to imposed loading at an early stage of curing, where adhesive can sustain damage (debonding). Finite element analysis was carried out to investigate the effect of cyclic loading on the performance of the adhesive.

Another focus of this research dealt with strengthening of cast iron struts with existing preload and geometrical imperfection. Studies [Moy & Lillistone, 1999] have shown that the intensity of the preload affects the amount of benefit gained, as tensile strength of cast iron determines when failure occurs, thus preventing the CFRP composite from developing its full capability. Therefore, the effects of geometrical imperfections and different levels of preload prior to reinforcement on the stiffness and load bearing capacity of cast iron struts was investigated.

At present, the guidance for engineers/designers with regard to the use of CFRP plates in reinforcing metallic structure is not fully developed and only deals with fully cured adhesive. However, with the aid of FE analysis it is possible to obtain the material damage in the adhesive due to imposed loading and recalculating the structures stiffness.

Acknowledgements

I would like to thank NPL (National Physical Laboratory) for its support and contribution towards this research. I would also like to thank my supervisors, Dr Stuart Moy and Professor Marcus Lee for their supervision, support and guidance.

I would like to express special thanks to my partner Fiona Buckingham. Without her support and understanding I would not be where I am today.

Table of Contents

3. Steel beam reinforced with carbon fibre composites- an experimental investigation

4. FE modelling of reinforced steel beam

6. CONCLUSIONS AND RECOMMENDATIONS

CHAPTER 1

1. INTRODUCTION

1.1 BRIEF BACKGROUND

The UK transportation infrastructure is now facing demands on it for which it was not originally designed. With the increase in both volume and weight of traffic in recent years there is a need to replace, strengthen or rehabilitate many structures. The costs associated with these operations can be high, and so a need for lower cost solutions has arisen.

Fibre reinforced polymer (FRP) composites have been demonstrated [LINK, 2000] as one solution that enable the cost of replacement, strengthening or rehabilitation to be reduced and are being used increasingly in construction, especially for structural upgrade. The technology of reinforcing metallic structures using carbon fibre reinforced

polymer (CFRP) is still novel and relatively untested, however, it is therefore necessary to investigate the technical issues surrounding the use of this technique of increasing the structural capacity by using CFRP, to give asset owners the confidence in the efficiency and durability of the solution and to propose design guidance that would enable the technology to be utilised by non-specialist civil engineers.

Generally, carbon fibre reinforced polymers (CFRPs) are used because their strength and stiffness properties compare favourably with those of conventional material such as steel and concrete. CFRPs are light weight (density about 20% that of steel), expensive materials, although the development of cheaper fibres is leading to cost reductions. The use of CFRPs in construction can be justified when their lightweight and ease of application leads to simple low-cost falsework and overcomes difficult access problems. In addition their corrosion and fatigue resistance is considerably greater than that of conventional materials.

1.2 COMPOSITE MATERIALS

A structural composite is a material system consisting of two or more phases on a macroscopic scale, whose mechanical performance and properties are designed to be superior to those of the constituent materials acting independently [Daniel, 1994]. One of the phases is usually discontinuous, stiffer, and stronger and is called 'reinforcement', whereas the less stiff and weaker phase is continuous and is called 'matrix', see Figure 1.1. Sometimes, because of chemical interactions or other processing effects, an additional phase, called 'interphase', exists between the reinforcement and the matrix. The properties of a composite material depend on the properties of the constituents, geometry, and distribution of the phases. One of the most important parameters is the volume fraction of reinforcement, or fibre volume ratio. The distribution of the reinforcement determines the homogeneity or uniformity of the material system. The phases of the composite system have different roles that depend on the type and application of the composite material. In the case of low to medium performance composite material, the reinforcement, usually in the form of short fibre or particles,

provides some stiffening but only local strengthening of the material. The matrix, on the other hand, is the main load-bearing constituent governing the mechanical properties of the material. In the case of high performance structural composites, the usually continuous-fibre[1] reinforcement is the backbone of the material that determines stiffness and strength in the direction of the fibres. The matrix phase provides protection and support for the fibres and the local stress transfer from one fibre to another. The interphase, although small in size, can play an important role in controlling the failure mechanisms, the fracture toughness, and the overall stress-strain behaviour of the material.

1.3 Type and classification of composite materials

Metcalfe [1974] describes composites by their types, classifications and constituents. He concluded that composite materials are classified into three categories depending on the type, geometry, and orientation of the reinforcement phase. They are as follows:

Particulate composite – consist of particles of various sizes and shapes randomly dispersed within the matrix. Because of randomness of particle distribution, these composites can be regarded as quasi-homogeneous. Particulate composites may consist of non-metallic and metallic particles in a non-metallic matrix.

Discontinuous or short-fibre composites – contains short fibres or whiskers as the reinforcing phase. These fibres can be either oriented along one direction or randomly oriented. In the first instance the composite material tends to be markedly anisotropic[2] or, more specifically, orthotropic[3], whereas in the second it can be regarded as quasi-isotropic.

[1] Fibres with great or indefinite length that run parallel to each other
[2] Properties at a point vary with direction or depend on the orientation of reference axes
[3] Material having at least three mutually perpendicular planes of symmetry

Continuous fibre composites are reinforced by long continuous fibres and are the most efficient from the point of view of stiffness and strength. The continuous fibres can be all parallel (unidirectional), or can be oriented at right angles to each other (crossly or woven), or can be oriented along several directions (multidirectional).

Fibre-reinforced composites can be classified into broad categories according to the matrix used [Richardson, 1977]: polymer, metal, ceramic, and carbon matrix composites. These are described as follow:

1. Polymers are the most widely used matrix material for fibre composites. Their chief advantages are low cost, easy processibility, good chemical resistance, and low specific gravity. On the other hand, low strength, low modulus, and operating temperatures limit their use. They also degrade by prolonged exposure to ultraviolet light and some solvents.

According to their structure and behaviour, polymers can be classified as thermoplastics or thermosets. The polymers that soften or melt on heating, called thermoplastic polymer, consist of linear or branched-chain molecules having strong intramolecular bonds but weak intermolecular bonds. Thermosetting plastics have cross-linked or network structures with covalent bonds between all molecules.

Unlike metals and ceramics, polymers may be considerably influenced by external variables. In contrast, the mechanical properties of metals are only influenced near the melt temperature. Polyester and epoxy resins are the most common polymeric matrix materials used with high-performance reinforcing fibres. Both are thermosetting polymers. Easy processibility and good chemical resistance are their chief advantages.

2. Metals are, by far, the most versatile engineering materials. The properties that are particular important for their use as matrix material in composites include high strength, high modulus, high toughness (most metals) and impact resistance. Their greatest advantage over the polymer matrices is in applications that require exposures to

high temperature and other environmental conditions that could affect the polymer matrices but not metals.

The most commonly used metal matrices are based on aluminium and titanium. Both of these metals have low density and are available as alloys.

3. Ceramic matrix composites – consists of ceramic matrices (silicon carbide, aluminium oxide, glass-ceramic, silicon nitride) reinforced with ceramic fibres. They are best suited for very high temperature application.

4. Carbon/carbon composites – consists of carbon or graphite matrix reinforced with graphite yarn or fabric. They have unique properties of relatively high strength at high temperature coupled with low thermal expansion and low density.

In addition to the types discussed above, there are laminated composites. They consist of thin layers of different material bonded together, such as bimetals, clad metals, plywood, and formica.

Recent advances in composite technologies have increased the mechanical performance of laminated composites significantly. As a consequence, composite structures are used in sophisticated designs as primary load-carrying elements. Therefore, it becomes increasingly important that the behaviour of composite structures subjected to a variety of loading modes, particularly the failure mechanisms in the composites, is fully understood. One of the major interests in the current research is the in-plane failure of the laminate composite and the adhesive due to material damage.

Due to the complex nature of composite, failure modes in composites are strongly dependent on geometry, loading direction, and ply orientation [Lessard and Chang, 1989]. Considering only a unidirectional composite, there are basically five different in-plane failure mechanisms: matrix tensile cracking, matrix compression, fibre breakage, fibre-matrix shearing, and fibre buckling, as shown in Figure 1.2. All of the mechanisms,

with the exception of fibre breakage and matrix tensile cracking, can induce compression failure. In order to accurately analyse failure of composites, the analysis must not only be able to predict failure modes in the composites, but can also evaluate the reduction of the material properties within the damaged area. Failure in composite can be predicted by a set of proposed failure criteria for each mode of failure, and the material properties within the damaged area are evaluated according to the proposed property degradation models. Most traditional failure criteria are unable to distinguish failure modes in each layer. A set of failure criteria was proposed by Hashin [1980] for predicting failure of unidirectional composites based on each failure mode. With modification carried out by Chang [1986], the failure criteria take into account the nonlinear shear deformation in each layer.

1.4 CAST IRON

The overground railway system owned and maintained by Network Rail has 42,700 bridges, of which 39% are metallic. Many of these are in need of strengthening because of increased vehicle loading or under-investment in the maintenance regime. The Highways Agency and County Councils and Unitary Authorities are also responsible for large number of metallic structures.

Cast iron is essentially an iron-carbon alloy containing other important elements such as silicon, manganese, sulphur, and phosphorus, which modify the structure and properties of the resulting alloy markedly [Angus, 1960].

Cast iron is a granular material that behaves in a brittle manner. In tension gray cast iron is more brittle than most metals. This brittleness is attributed to the microstructure of the material, which consists of a distribution of graphite flake in an iron matrix.

The form and distribution in which graphite is deposited depends on numerous factors, such as melting temperature, nucleation, cooling speed etc., but the basic forms are flake graphite, aggregate or temper carbon, and nodular or spheroids [Angus, 1960].

- Flake graphite may form as kish, normal flake, and rosette or undercooled.
- The shape of the graphite precipitated on solidification can be markedly modified to the nodular or spheroidal form by additions, notably, of magnesium and/or cerium.
- Aggregate or temper carbon is formed using heat treatment of white iron.

It is important that the fundamental properties of cast iron should be understood. Although the structural constituents of steel can all be present in cast iron, there are two important constituents not normally present in steel that are responsible for the major characteristics of cast iron [Angus, 1960].

Angus [1960] said "the effect of graphite on the purely mechanical properties is substantially that of a void, i.e. a steel matrix carrying a substantial number of voids distributed, as graphite in cast iron would show similar stress-strain characteristics as cast iron. The effect of phosphorus is somewhat less fundamental, since there are many grades of castings produced in which the phosphorus content is purposely kept very low indeed".

It is often imagined that the presence of graphite in cast iron must mean that it will necessarily be porous even at appreciable thickness. This, however, is not the case, as the graphite flake in each eutectic cell is separated from those in the neighbouring cells, and a continuous network does not exist [Angus, 1960].

In tension, graphite acts as a discontinuity in the matrix. It would be expected, therefore, that the strength of a cast iron would be inversely proportional to the amount of free graphite that is present, although the character of the matrix itself also affects the strength [LINK, 2000]. In compression, on the other hand, the graphite flakes serve to transmit stresses, and the overall response is governed by the response of the iron matrix

alone. The above differences manifest themselves in the following macroscopic properties: (i) different yield strengths in tension and compression, with the yield stress in compression being a factor of three or more higher than that in tension; (ii) inelastic volume change in tension, but little or no inelastic volume change in compression; and (iii) different hardening behaviour in tension and compression [LINK, 2000].

Much of the infrastructure of the London underground (LUL) system relies on cast iron beams and struts for its structural integrity, and the cast iron is usually over one hundred years old. It is generally felt that drilling holes in, or welding to, old in-situ cast iron is very undesirable; which makes strengthening by direct attachment of steel almost impossible. In addition LUL has to run its trains for up to 20 hours each day, so that any maintenance or structural strengthening has to fit within a small window in the early hours when trains are not running. CFRP is an appropriate and financially attractive solution to strengthening cast iron in these circumstances.

1.5 AREAS TO BE INVESTIGATED

1.5.1 Effect of cyclic loading on performance of adhesive

The main attraction of carbon fibre strengthening is the simplicity of application and the fact that it minimises the impact on the normal use of the structure. However, when a carbon fibre composite plate is bonded to a metallic substrate there is a curing period, approximately 20 hours, during which the adhesive develops its full strength. Therefore, if a structure is subjected to continuous cyclic loading and it is not economic to close the services during the curing period, the adhesive will be subjected to cyclic loading while the curing process takes place. There is a possibility that the effectiveness of the bond between the metallic substrate and the CFRP will be affected. Therefore, tests need to be carried out to confirm that this does not impact on the integrity of the bond formed.

1.5.2 Strengthening of metallic structures using CFRP

In the case of the cast iron strut, it is the tensile strength of the cast iron or the compressive strength of the carbon fibre that governs structural failure. Previous tests by Moy & Lillistone [1999] have shown that reinforcing cast iron with CFRP plate is beneficial in increasing strength. With the typical cast iron beam section shown in Figure 1.3, which has enlarged tension flanges, the reinforcement moves the neutral axis closer to the tension flange. This reduces the tensile stress in the cast iron and also the volume of cast iron in tension. Hence there will be considerable stress redistribution after the reinforcement is applied and since the volume of cast iron in tension is reduced the probability of a casting defect occurring in the tension zone is reduced.

Also, from previous tests on typical struts by Moy & Lillistone [1999], shown in Figure 1.4, two main benefits derived from CFRP reinforcement have been highlighted. Firstly, the bending rigidity of the strut is increased, which reduces the lateral deflections and, hence, the bending moment under a given load. Thus it is likely that any tensile stress that may be present would be extremely small. Secondly it will provide higher tensile resistance in the strut. The result is that in a strengthened cast iron strut failure will occur in the compression zone when the compressive strength of the composite is reached, since the compressive strength of cast iron is greater than that of the composite plates.

The situation is more complicated when the carbon fibre reinforcement is use to strengthened structures that are already carrying load. Although the benefit can be significant, the amount will depend on the level of preload in the structure and on the tensile strength that can be developed by the cast iron structure.

Dier [1997] has showed that there are benefits to be obtained from strengthening cast iron struts with carbon fibres. The typical behaviour of struts means that the compressive strength of the carbon fibre will determine when the reinforced strut fails. The benefit of reinforcing preloaded struts are more difficult to quantify because of the

difficulty in assessing the level of preload and also because the initial curvature and eccentricity will vary from strut to strut.

The situation when reinforcing steel structures is different as the ductility of steel is considerably greater that of carbon fibre composite. Tests by Moy [2000] have shown that failure of strengthened steel beams is governed by the rupture of the carbon fibres, and generally the full benefit of the reinforcement will be gained whatever the preload on the bare steel before the reinforcement is applied.

There is a lack of design information concerning the use of CFRPs in construction. Although there is now a considerable body of research on the use of CFRP bonded to concrete structures, this is not so for use on metallic structures. As metallic structures are used extensively in the transport infrastructure, there are many of them that require strengthening and upgrading. Therefore the need for research in this area is urgent.

1.6 AIMS OF RESEARCH AND THESIS LAYOUT

The effectiveness of adhesive bond that is used for structural strengthening is investigated with regard to the strength development and debonding whilst subjected to imposed loading.

Another area of research is to identify the benefits of strengthening cast iron struts with CFRP while the cast iron is carrying a preload. Generally it is impossible to remove preload from an in-situ strut and theoretical studies by Moy & Lillistone [1999] have shown that the intensity of the preload affects the amount of benefit available. This is because the tensile strength of the cast iron determines when failure occurs, thus preventing the CFRP composite from developing its full structural capability. The focus of the current research is to:

- Carry out an extensive literature review into previous and existing methods, findings, and guidelines with regard to strengthening metallic structures, using CFRP.
- Investigate the benefit of reinforcing pre-loaded cast iron strut and steel beam with carbon fibre composite plates.
- Predict the extent of damage in adhesive during the curing period while subjected to cyclic loading.
- Develop a progressive damage model for predicting the type and extent of in-plane damage in both the adhesive and the composite plate as a function of applied load.
- Investigate the effect of initial imperfection on the stiffness of the struts.

The findings are presented in the following chapters:

- Chapter two details summarized reports dealing with carbon, adhesive and cast iron material, and their characteristics by reviewing the use of composites in all disciplines of engineering. It also examines the provisions of design standards and the recommendation of design guidance on the life extension and strengthening of metallic structures, together with the main findings of previous experimental and numerical research on carbon fibre composites and cast irons.
- Chapter three details the configuration, test set-up and observation of bonding process of CFRP to steel I-beams, while undergoing cyclic loading, which illustrated the effect of cyclic loading on bending stiffness, followed by ultimate load tests to determine the effect on the collapse load of the performance of the adhesive.
- Chapter four highlights the use of shell and solid finite elements to model the behaviour of composites, adhesives, and metallic substrates. By gaining an understanding of the adhesive behaviour and the progressive failure in composite material, more advanced models were developed and the accuracy is compared with experimental tests.
- Chapter five details the configuration, test set-up of reinforced cast iron struts, while carrying preload, which illustrated the effect of the reinforcement on the structural stiffness and strength. This has been backed up by complex finite element modelling

which furthered the research by looking at geometrical imperfections within the structure and the effect of preload on the overall performance of the structure.

- Chapter six details the conclusions and recommendations for further work.

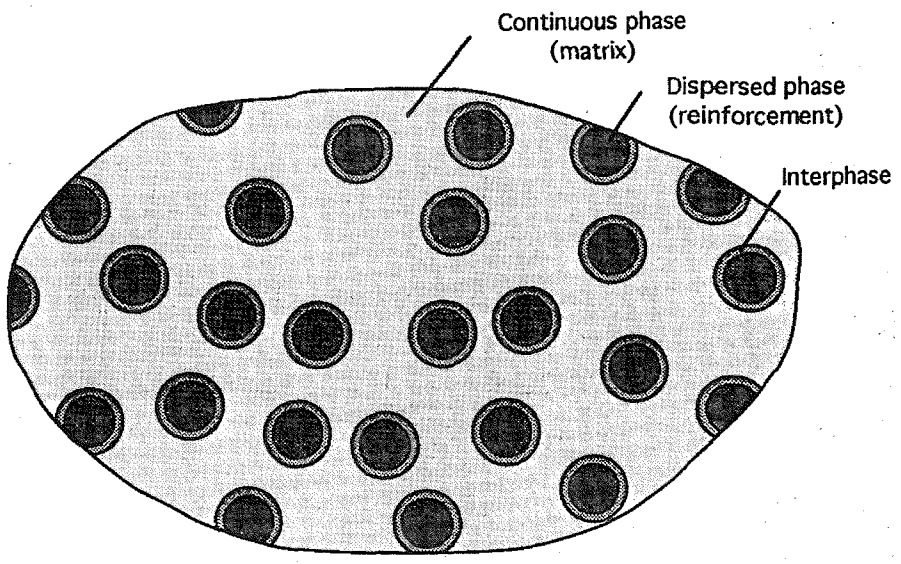

Figure 1.1 Phases of a composite material

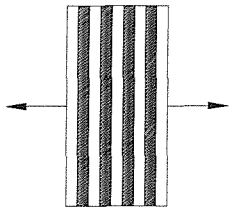

(a) Matrix tensile cracking

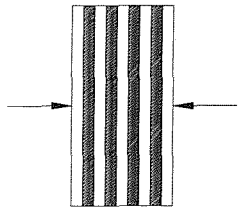

(b) Matrix compression

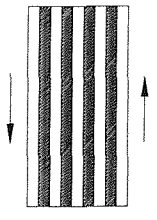

(c) Fibre-matrix shearing

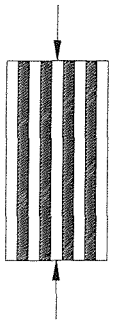

(d) Fibre buckling

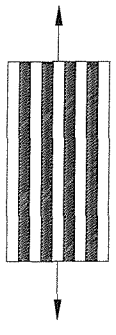

(e) Fibre breakage

Figure 1.2 Various failure modes in fibre composites under in-plane loading

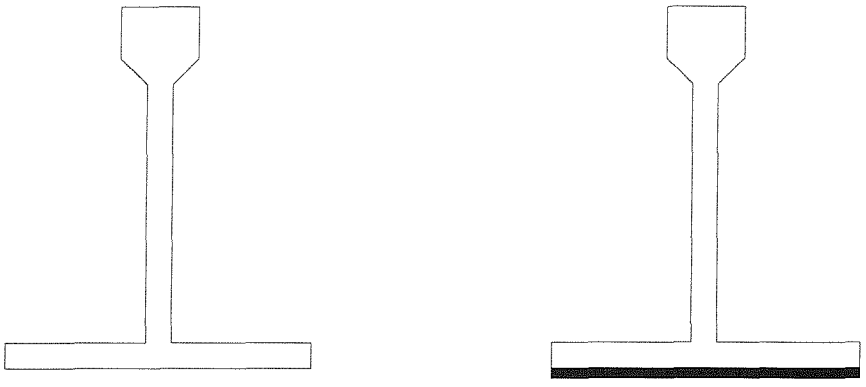

(a) Unreinforced (b) Reinforced

Figure 1.3 Typical cast iron beams

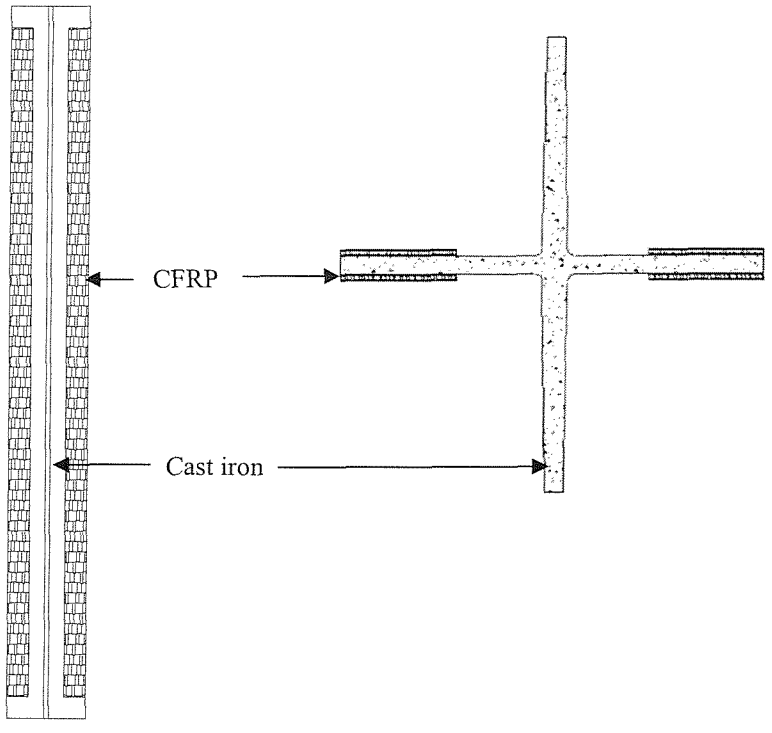

(a) Elevation (b) Section

Figure 1.4 A typical reinforced cast iron strut

CHAPTER 2

LITERATURE REVIEW

2.1 INTRODUCTION

Most metallic structures that were constructed during the second half of the nineteenth century are now in need of strengthening and life extension as a result of the significant increase in the live load they have to carry. Structures are strengthened generally when all avenues have been exhausted in assessing the strength of the structure and the loads on the structure, and the structure has still been found to be under strength [Kennedy, 2001]. At the start of the research a literature review was performed to study all aspects of strengthening metallic structures, especially metallic bridges. A review of previous and current methods of strengthening metallic structures in civil and other industries has been carried out, to see why the use of CFRP in strengthening will be an effective method.

An investigation was also carried out to highlight all aspects of adhesively bonded structures, which included: adhesives and adhesive selection, surface preparation and pretreatments, adhesive bonding and failures.

2.2 NEED FOR STRENGTHENING

A decision may be made not to strengthen a structure by reducing the load on the structure, by imposing a weight limitation, or by closing the bridge [Kennedy, 2001]. If these are not options, then the bridge will need to be strengthened. The following are possible reasons for strengthening:

- Faulty construction;
- More stringent code requirements since design;
- Deterioration due to corrosion or fatigue, including fatigue cracking;
- Impact damage;
- Increased loading since the original design

Gillett [1951] outlined the mechanical properties, fabrication, strength, and occurrence of failures within different metals, and highlighted fatigue in metallic structures as part of his review.

Under repeated stresses that may be well below the static yield strength, when no stress raiser is present, a stress raiser[1] can so concentrate the stress that a crack starts at the apex of the stress raiser and progresses further with each repetition until finally the solid section becomes so small that what remains tears apart. If overstressing (stress above the endurance limit) is applied many times, but the overstressing stopped before a fatigue crack has started and the piece is then run at a stress somewhat below the endurance limit, the piece might fail [Gillett, 1951].

[1] Such as scratches, toolmarks, sharp corner or shoulders, unrelieved press fits, corrosion pits, even a free surface.

Therefore, it is very important to reduce the stress level of the structure in order to enhance the life extension of the structure. This can be achieved through strengthening of the structure.

2.3 FACTORS TO BE CONSIDERED WHEN DESIGNING STRENGTHENING

Kennedy [2001] has written a report that engaged in assessing and strengthening steel and steel/concrete composite bridges. He has also identified strengthening solutions that may have application in civil engineering industry. The objective of his report was to disseminate the knowledge gained from relevant projects carried out to date and highlight areas that need consideration of a designer in reinforcing of metallic structures. Kennedy suggested the following factors that have to be considered when designing for strengthening:

(1) Minimum cost

Estimating the cost of strengthening is not straight forward as it can be dominated by overheads including traffic management and access. Burfsaas and Brustad [1993], has quoted that, '*Strengthening works are often highly labour intensive and the installation costs, particularly in confined spaces with their attendant health hazards, may be significantly greater than the material costs*'. Therefore great consideration needs to be taken to ensure easy manoeuvrability to reduce labour and installation.

(2) Traffic delay costs

Traffic delay costs often overwhelm the actual costs of strengthening and must therefore be considered in determining which strengthening option to choose [Pritchard, 1993]. They encompass traffic delay times due to queuing or diversions as a result of road closure, lane closure, speed or load restrictions, or restrictions on the road, railway or waterway passing below the structure. Therefore great consideration needs to be taken to ensure least disruption to the traffic.

(3) Minimum maintenance

Strengthening works can often complicate the maintenance process, providing awkward corners that cannot easily be inspected or painted [Das, 1996]. The ensuing maintenance costs and reliability must therefore be taken into account in choosing a strengthening option.

(4) Buildability

Some methods of strengthening are more straightforward than others to implement. If a method is prone to installation difficulties, then contractors will tender a high price if the risk lies with them, or submit expensive claims for delay if the risk remains with the client [Das, 1996]. Also safety has to be taken into account when considering different methods of strengthening.

Therefore, when designing for strengthening, special attention must be paid to all above factors, such as: safety, costs, traffic management, buildability and maintenance of the structure.

2.4 METHODS OF STRENGTHENING IN CIVIL ENGINEERING

Kennedy [2001] also summarises the most common strengthening methods for metallic bridges in order to improve their shear and bending capacities. They are as follows:

(1) Welding plates to flanges

Bending strength deficiencies in simply supported deck beams can be overcome by increasing the bottom flange cross-sectional area. This can be achieved by welding steel plates to these flanges [Kennedy, 2001]. These operations are costly and difficult as traffic access will be compromised and steel plates are extremely heavy, which makes the operation difficult, inconvenient and requiring special equipment for better manoeuvrability of the steel plates.

(2) Adding extra beams

When existing beams cannot be readily strengthened one option is to install a new steel beam between the existing ones [Kennedy, 2001]. This procedure is costly and time consuming.

(3) Prestressing

This can be an effective means of providing additional tensile capacity where the bending strength of a deck girder is inadequate [Evans, 1993]. This process is expensive, time consuming and mainly used for relatively large span bridges.

(4) Doubler plates

Where girder webs are weak in buckling or in shear, adding an additional ply of plate against the web can strengthen it [Kennedy, 2001]. This process is time consuming, restricts the traffic flow and might require special equipment.

(5) Adding cable stays

These can be a very effective means of enhancing bridge strength although somewhat elaborate and expensive [Albrecht and Haensel, 1996]. Care is required in designing and detailing the new or extended towers and the anchorages for the new cable stays.

(6) Strengthening of concrete structures using CFRP

The use of externally bonded composite materials for upgrading, strengthening and retrofitting of existing reinforced concrete (RC) structures has become widely accepted in recent years. This modern approach has many advantages over the traditional ones, mainly due to the lightweight, high strength, and improved durability of the composite material. Another advantage of this approach includes its ease of installation on site and the applicability of the method to a broad range of structural members such as beams, columns, slabs, or masonry walls.

The behaviour of 22 concrete specimens that were externally reinforced (wrapped) by carbon FRP sheets in low volumetric ratios was studied by Karabinis and Rousakis [2002]. The specimens were subjected to monotonic load conditions until failure. This experimental investigation [Karabinis & Rousakis, 2002] of the performance of carbon FRP sheet, as concrete confinement, indicated that FRP did effectively enhance the strength and ductility of concrete.

A recent approach carried out by [Rabinovitch, 2002] used circular patches made of composite materials which were bonded to the tensile face of the slab in the region of the extreme bending moments. It was shown that the strengthening patch method was suitable for strengthening and retrofitting of existing RC slabs of various layouts.

Tests carried out by Taljsten [2003] showed that concrete beams can also be strengthened for shear and those fabrics or laminates should be placed perpendicular to the shear crack if possible. Strain measurement in the investigation carried out by Taljsten [2003], showed that the thinner the fibre used the better the utilisation of the fabric.

From the reviews of using different methods in reinforcing metallic structures, it has been highlighted that buildability, manoeuvrability and public access management is some of the most important factors to be considered, when designing for reinforcement. It has also been shown that, reinforcing structures using CFRP has an advantage over the more traditional methods of reinforcing. This is due to its material properties such as low density, high strength, low maintenance and resistance to corrosive environment, which makes it an attractive candidate for strengthening.

(7) Strengthening of masonry structures using CFRP

Masonry structures are prone to extensive damage followed by failure and collapse when subjected to loads resulting from wind, earthquake and other natural or man-made events. Fibre reinforced materials in the form of externally bonded laminates and near surface mounted bars can be used for the strengthening of masonry structures

[Nanni A, 2003]. FRP composites are characterized by excellent tensile strength in the direction of fibres and negligible strength in the direction transverse to the fibres. Three most common type of FRP composites used in strengthening of masonry infrastructures are carbon, aramid and glass fibre. Due to its low cost and low elastic modulus, epoxy glass has been the fibre preference for the strengthening of masonry.

The dominant mode of failure in such structures is debonding of FRP laminate from the masonry substrate. Debonding is directly related to substrate characteristics such as roughness and porosity. For example, absorption of epoxy is limited in extruded bricks units as compared to that in moulded bricks leading to a reduction of the bond strength at the interface FRP laminate-masonry surface [Roko, 1999]. The experimental strengthening work carried out by Nanni [2003] showed a significant improvement in flexural and shear strengthening of masonry structures.

From reviewing the strengthening work carried out to date, one of the significant applications of FRP composites could be in historical structures where lack of corrosion problems, light weight, and versatility of installation are the features of primary interest and unique value.

(8) Bridge strengthening using CFRP plates

Recent development in FRP composite strengthening was led by ASSET [2002] project into developing the very first fully composite bridge in the UK. By producing a composite shape profile that satisfied the design requirements and by gaining the confidence of the highway and rail agencies that FRP composites can offered a viable alternative as to conventional methods of strengthening, numbers of bridges (cast iron mostly) have been strengthened using CFRP plates that were externally bonded to the beams supporting the bridges.

The strengthening work using CFRP plates have proven to be successful and an attractive alternative to conventional methods of strengthening. However, further research into material behaviour and issues surrounding the usability of FRP composites

under various loading environment is required to produce a complete design guidelines to gain the confidence and better understanding of FRP composites by engineers.

2.5 METHODS OF STRENGTHENING IN OTHER INDUSTRIES

Lawrence [1974] describes the use of composites in various industries, emphasising on the significance of replacing the conventional materials, followed by advantages gained in structural strength and performance. He detailed the history of composite involvement and more importantly the exploration for improvement in the structural strength, performance and installation in all industries which was carried out by reviewing the progression of each industry in form of case histories and justifications made for replacing conventional materials with composites.

2.5.1 Aerospace

Parmley [1974] outlined the use of composites in the military, highlighting their strength and mechanical properties. The potential for significant weight reduction in aerospace structures through the use of advanced composites was first realized on a broad scale by the military in the Air Force Project 'Forecast' conducted in 1963. This observation was based on the then recent development of the high-modulus, high-strength, low-density fibre and the superior mechanical properties that could be developed when these fibres were converted into composite laminates. Since that time, other filaments have been developed that offer equal or increased potential for reduced structural weight, increased stiffness, and lower cost. What this portends is a great variety of advanced composites from which the military aircraft designer can select to satisfy requirements for strength, stiffness, temperature, hostile environment etc.

Some of the most important repairs and strengthening in aerospace involve identifying a crack in the main frame and preventing growth of that crack by creating an alternative load path around the cracked region [Baker, 1988]. Most commonly used methods are welding steel plates or application of composite materials.

Repair based on adhesively bonded fibre-composite patches or reinforcements are more structurally efficient and much less damaging to the parent structure than standard repairs based on mechanically fastened metals. CFRP is widely used in aerospace as an efficient and effective means of repair or reinforcement. As a result of their excellent load transfer characteristics bonded reinforcements or patches provide a stiff alternative load path so they can be used very effectively to repair cracks [Baker, 1988]. In contrast, standard repairs, based on mechanically fastened metallic patches provide a relatively compliant alternative load path so they cannot effectively repair cracks and require prior removal of the crack region. Mechanical repairs also have several other disadvantages, compared to bonded repairs, as highlighted in Figure 2.1. The attributes of the composites include:

- High Young's modulus and strength, which minimises the required patch thickness.
- Highly resistant to damage by cyclic loads.
- Immunity to corrosion, forms excellent protective layer.
- High formability, which allows easy formation of complex shapes.

The main disadvantage of composites as patching materials results from their relatively low coefficient of thermal expansion compared to the parent material, which results in residual tensile mean stresses in the repaired component. Composite reinforcement can be used for a wide range of repairs/reinforcements to metallic aircraft components, as follows:

- Reduce stress intensity (crack patching)
- Stiffen under-designed regions
- Improve residual strength or stiffness

The use of composites in the Aerospace industry is well established and it can be seen that composites in repair and rehabilitation of most structures are more beneficial than conventional material. This is again due to material properties of composites, which makes it an ideal candidate for strengthening

2.5.2 Rail transportation & Ocean engineering

Noton [1974] outlined the use of composite materials in the transport industry. These materials were used to improve the performance and safety.

Rocca and Scott [1974] highlighted the history and the use of composite in the ocean engineering. The most striking example is the rapid replacement of wood with glass-reinforced plastic (GRP) in small boats. The high strength-to-weight ratios of GRP have proven beneficial in a number of applications to high-performance craft such as hovercraft.

Composite materials are becoming more and more recognised and used within most industries. This is again due to its favourably compared mechanical properties to most conventional materials.

2.6 FABRICATION OF COMPOSITES

Bhagwan [1990] describes the fabrication of composite materials with regards to types of matrix and fabrication methods. Fabrication or shaping of composites into finished products often combines the formation of the material itself during the fabrication process. The formation of the composite involves the combination of the matrix and the fibre such that the matrix impregnates, surrounds, and wets the fibres. With regard to polymeric matrix composites, there are two processing methods, thermosetting[2] and thermoplastic[3]. The choice of a fabrication process is strongly influenced by the chemical nature of the matrix and the temperature required to form, melt, or cure the matrix. The two main categories of resin matrix composite fabrications are as follow:

[2] Thermosetting matrix material typically involve material formation during final molding (e.g. hand lay-up, spray-up, vacuum-bag)

[3] It is more common in thermoplastic matrix composites to form the composite first and form or mold a shape in a second operation.

2.6.1 Fabrication of thermosetting resin matrix composites

Thermosetting resin systems become hard when cured by a chemical reaction and further heating does not soften them; the hardening is irreversible [Chawla, 1987]. During curing they undergo a chemical change or reaction called polymerisation, the linking of "monomers or prepolymers" [Chawla, 1987]. Fabrication processes for thermosetting resin matrix composites can be broadly classified as wet forming processes and processes using premixes or prepregs.

Different wet forming processes, and compounding of premixes and their subsequent used for final product fabrication are as follows:

- Hand lay-up technique- the hand lay-up technique is the oldest, simplest, and most commonly used method for the manufacture of both small and large reinforced products [Mallick, 1988]. Fibre reinforcements and resin are placed manually against the mold surface. The layers of materials placed against the mold control thickness. A chemical reaction initiated in the resin by a catalytic agent causes hardening to a finished part. Typical applications include boat and boat hulls, ducts, pools, tanks, furniture, and flat sheets. Operations involved in a typical hand lay-up process are: mold preparation, gel coating, hand lay-up, and spray-up.
- Bag molding processes- bag moulding is one of the oldest and most versatile of the processes used in manufacturing composite parts. The laminates are laid in a mold and resin is spread or coated, covered with a flexible diaphragm or bag, and cured with heat and pressure [Hull, 1981]. The general process of bag molding can be divided into three basic molding methods: pressure bag, vacuum bag, and autoclave.

  Vacuum-bag and autoclave methods are used to produce most bag-molded parts [Hull, 1981]. Their main advantages are that the tooling is relatively inexpensive

and the basic curing equipment can be used for an unlimited variety of shaped fibres.

- Filament winding- filament winding is a technique used for the manufacture of surfaces of revolution such as pipes, tubes, cylinders, and spheres [Rosato and Grove, 1964].
- Pultrusion- Pultrusion is an automated process for manufacturing composite material into continuous, constant-cross-section profile [Meyer, 1985].
- Preformed molding compounds- a large number of reinforced thermosetting resin products are made by matched die molding processes such as hot-press compression molding, injection molding, and transfer molding [Hull, 1981].

Wide range of processing methods is available for FRP composites, although generally the underlying principle is the same. Different methods are used usually to create different properties in composites for specific applications.

2.6.2 Fabrication of thermoplastic-resin matrix composites

The principal method used for the production of parts with short-fibre-reinforced thermoplastics is injection molding [Bhagwan, 1990], which has substantial use in domestic appliances.

As it can be seen there is a wide range of processing methods available for FRP composites. Although generally the underlying principle is the same, they can be made to suit most condition and have a variety of properties using different fabrication methods.

2.7 ADHESIVELY BONDED STRUCTURES

2.7.1 Introduction

Adhesion is the word used to describe the phenomenon of transferring stress across an interface [Mays, 1981]. Adhesives are bridges between substrate surfaces, whether they are the same or different materials. Generally speaking, secondary, or physical, forces are involved in holding the two surfaces together. These forces are collectively known as Van der Waals forces [Mays, 1981] and manifest themselves whenever two surfaces are brought into intimate contact, see Figure 2.2. These secondary forces may occasionally be supplemented by the presence of primary chemical bonds across the interface. However, for either secondary or primary forces to be developed, the two surfaces must be in extremely close contact and, because of the essentially rough nature of all solid surfaces on the molecular scale – however finely polished – it can be readily understood why two such surfaces cannot be stuck merely by pressing them together [Lee, 1984].

It is for this reason that all adhesives are liquids, or behave like liquids, when in the ready-to-use condition. It is only when materials are in the liquid state that they are mobile enough to flow and to make the intimate contact that is essential to the development of these strong adhesive forces. The word commonly used to describe the achievement of this close contact is "wetting" [Lee, 1984] but the word is used merely to describe the process whereby any liquid may spread freely and spontaneously over the surface of a solid, see Figure 2.3.

If such close contact is to be achieved, it is apparent that the wetting process must be complete before the liquid adhesive converts to a useful, load-bearing solid. Therefore it is important that the pot-life of the adhesive is sufficiently long. The problem is illustrated in Figure 2.4.

A further consideration is the problematic matter of the significance of surface topography, or roughness of the substrate. Intuitively it may be thought that the rougher

the surface the greater the adhesion [DML, 2000]. However, generally speaking one is interested in the strength of the adhesive joint and if the roughening of a surface increases its area then the gross interfacial strength could also be expected to be greater. In practice however, there can be problems with rough surfaces. From thermodynamic considerations, it can be shown that liquids may have difficulty in completely wetting rough surfaces [DML, 2000].

2.7.2 Surface preparation and pretreatment

Surface preparation is the most critical step in the adhesive bonding process. Unless a satisfactory surface preparation is accomplished, the bond will fail adhesively and unpredictably at the adherend-adhesive interface [DML, 2000]. With proper surface preparation, bond can be accomplished that will allow any failure to be cohesive in nature.

In dealing firstly with ferrous metals, a wide range of techniques may be employed. In most cases it is usual to start with a degreasing procedure involving the use of clean solvent, such as Genklene [Lee, 1984]. Generic processes include – chemical, abrasion, and blasting. For basic carbon steels, chemical-based processes are not indicated and can be discounted. Abrasion processes are readily available and often convenient. Lee [1984] outlined the following methods to be the most commonly surface pre-treatment methods used before external bonding. They include:

(1) Wire brushing

Simple but rather ineffective means for the removal of rust and millscale.

(2) Powered abrasive brush

Typically involving the use of silicon carbide particles in nylon bristles can be effective though the removal of corrosion products is accompanied by the deposition of traces of organic material from the bristles.

(3) Dry and wet grinding

The use of abrasive discs can be effective in removing weak inorganic layers but the technique has a tendency to introduce weaknesses of its own. The process can be likened to ploughing a very shallow furrow, with smears and flakes of metal being deposited over the surface and creating a weak boundary layer.

(4) Abrasive blasting techniques

They are widely regarded as those best suited to the surface preparation of most ferrous metals but whereas open blasting is often unacceptable for reasons of economy or because of arisings, Vacublasting or wet blasting may be feasible.

Pre-treatment can be helpful in a variety of ways. Primers are generally of lower viscosity and are often applied in order to achieve thorough wetting of the surface and to provide a sound base for adhesive proper [DML, 2000]. Certainly they can be useful in protecting a freshly prepared surface against corrosion, and if there is to be a delay in the application of the adhesive after surface preparation, it may well be wise to anticipate the problem of corrosion and to plan for the use of a brush coat of primer to be applied immediately.

Various methods of surface preparation are available and used to create a satisfactory surface condition prior to external bonding. The surface conditions, prior to bonding, are crucial part of allowing the bond to fail adhesively or cohesively [DML, 2000] and hence, imperative for a bond to fail cohesively and not adhesively.

2.7.3 Adhesive selection

An extensive review of adhesives was carried out by Lee [1984] where the mechanical properties, performance, and manufacturing of different type of adhesives were the main highlighted areas of this report.

There are some 12 major family groupings of adhesive likely to be of value to the engineer. No 'expert' could be expected to know everything about them – let alone their many sub-groups and individual formulations. Therefore, for the purposes of this research, the adhesives were divided into two main categories: structural and non-structural adhesives.

2.7.3.1 Structural adhesives

Adhesives that are commonly used for bonding laminations of woods or plate bonding where adherends are ranged from metallic to composites materials are as follows:

(1) Amino

Urea-formaldehyde adhesive comes as a water-based syrup or powdered solid for mixing with water [Lee, 1984]. These adhesives have few conventional engineering applications, being commonly used in the woodwork industry for bonding laminations of wood and wood-associated material.

(2) Epoxy

Epoxy adhesives are thermosetting resins that solidify by polymerisation and, once set, will soften but not melt on heating. Two-part resin/hardener systems solidify on mixing, while one-part materials require heat to initiate the reaction of a latent catalyst. Their properties vary with the type of curing agent – amine, amide, acid anhydride – and the resin type used [Lee, 1984]. Epoxies generally have high cohesive strength, are resistant to oils and solvents and exhibit little shrinkage during curing. Epoxies provide strong joints and their excellent low creep properties make them ideal for structural applications, but unmodified epoxies have only moderate peel and low impact strengths [Lee, 1984]. Although these properties can be improved by modifying the resin, to produce flexible materials with improved resistance to brittle fracture, real toughness is only obtained in the so called toughened adhesives in which resin and rubber combine to form a finely dispersed, two phase solid during curing.

Toughened adhesives contain a dispersed, physical separate, though chemically attached, resilient rubbery phase. The toughening of epoxy-based adhesive confers a substantial increase in the overall performance of both the two-part, mixed systems and the single-part, heat-cured variants [Lee, 1984]. Peel strength, impact resistance and durability are considerably enhanced without any corresponding fall in shear strength [Lee, 1984]. Whenever the absolute maximum performance is demanded from either a mechanical or structural assembly, the toughened epoxies must be considered because they currently offer the ultimate in adhesive performance.

Strength, durability, and great versatility give epoxies a wide diversity of application. They can be brittle, cure rate varies enormously with formulation and their viscosity can make use difficult on very small assemblies [Lee, 1984]. In general, their naturally very high strength may not modify readily. Their adherend compatibility is excellent, except with thermoplastic and rubber where performance is substantially reduced.

(3) Phenolic/resorcinoic

Adhesives of this type are usually medium- or high-viscosity liquids, but powdered and film forms are available [Lee, 1984]. The metal-compatible forms are usually heat cured. They are used for bonding and laminating wood, metal and a limited range or thermoplastics.

(4) Polyurethane

The family group is named after the polymer type formed on completion of reaction. The adhesives are usually two-component – one always isocyanate-based, the other formulated from one of several co-reactants, often amines or glycols [Lee, 1984]. They are used for bonding a wide range of components fabricated from metal, wood, and various plastics.

From the review of all structural adhesives, epoxy adhesive has the right characteristics to be considered the most suitable adhesive for the structural reinforcement. Their strength, durability, and great versatility give epoxies a wide diversity of application.

2.8 CAST IRON CHARACTERISTICS

Angus [1960] describes the physical and engineering properties of cast iron with regard to applications in industry. Cast iron is essentially an iron-carbon alloy containing other important elements such as silicon, manganese, sulphur, and phosphorus, which modify the structure and properties of the resulting alloy markedly.

2.8.1 Mechanical, physical and electrical properties of cast iron

In deciding to use cast iron for any given component, it is important that its fundamental properties should be understood. Although the structural constituents of steel can all be present in cast iron, there are two important constituents not normally present in steel, which are responsible for the major characteristics of cast iron.

The effect of graphite on the purely mechanical properties is substantially that of a void, i.e. a steel matrix carrying a substantial number of voids distributed, as graphite in cast iron would show similar stress-strain characteristics as cast iron [Angus, 1960]. The effect of phosphorus is somewhat less fundamental, since there are many grades of castings produced in which the phosphorus content is purposely kept very low indeed [Angus, 1960].

It is often imagined that the presence of graphite in cast iron must mean that it will necessarily be porous even at appreciable thickness [Angus, 1960]. This, however, is not the case, as the graphite flake in each eutectic cell is separated from those in the neighbouring cells, and a continuous network does not exist [Angus, 1960]. In tension, graphite acts as a discontinuity in the matrix. It would be expected, therefore, that the

strength of a cast iron would be inversely proportional to the amount of free graphite that is present, and this substantially correct, although the character of the matrix itself also affects the strength.

Since the strength depends considerably upon the total quantity of free graphite present, it would be expected that since graphite has a specific gravity of approximately 2.2, the stronger irons would be denser than the weaker irons.

2.8.2 Modulus of elasticity of cast iron

The presence of graphite as flakes or nodules, gives dispersed discontinuities which modify the stress/strain response [Angus, 1960]. The modulus of elasticity of graphite-free white iron is in fact about 207 GN/m^2, but the presence of dispersed discontinuities in grey, malleable or nodular cast iron lowers the apparent elastic modulus below that of the matrix, the effect being more pronounced with flake graphite grey irons [Angus, 1960].

2.8.3 Stress/strain properties of cast iron

The presence of graphite in the flake, nodular or aggregate form modifies the stress distribution within the casting so that no sudden yield occurs, but the curve of plastic deformation even in the ductile cast irons merges into the elastic portion [Lessells, 1954]. The use of the term 'yield point' is, therefore, inapplicable to cast irons.

2.8.4 Poisson's ratio

The ratio of elastic lateral strain across the bar to the elastic longitudinal strain is known as Poisson's ratio and in elastic materials the theoretical value is 0.25 and does not vary with stress [Angus, 1960]. For steel a value of 0.3 is usually employed. Since cast iron does not show elastic response to stress, Poisson's ratio may vary with stress and grade of iron.

2.8.5 Shear and torsional strength of cast iron

In general, it can be taken that the shear strength of grey cast iron is from 1.1 to 1.6 times the tensile strength [Angus, 1960]. The ratio is lower for high strength irons than for low strength irons.

2.8.6 Damping capacity

Damping capacity is that property which permits a material to absorb vibrational stresses. Cast iron has an exceptionally high damping capacity, particularly in its softer or weaker forms, the damping capacity is reduced as the tensile strength increases [Angus, 1976].

2.8.7 Corrosion of cast iron

Corrosion may be defined as a chemical or electro-chemical reaction of a metal to its environment [Angus, 1960]. When it occurs, the main points of interest are the distribution of the corrosion damage and the rate at which it occurs. The rate of corrosion of cast iron depends not only on the metal, but also on its environment. Surface finishes are usually applied for increased protection, such as: painting and plating.

Therefore, cast iron is a granular material that behaves in a brittle manner. As with many brittle materials there is considerable scatter in the results of material property tests. In tension the stress-strain relationship is non-linear, in compression it is practically linear. Hence, great consideration needs to be taken in dealing with cast iron material that takes into account for the variations.

2.9 LINK PROJECT

2.9.1 Introduction

The 'Link' Inland Surface Transport Project [Link, 2000] investigated the use of carbon fibre materials for the strengthening of metallic structures. In this project the specific cases of cast iron cruciform struts, cast iron beams and steel beams were investigated in detail. Design methods had been produced and validated at laboratory scale, large scale, and full scale. Installation issues were studied to enable procedures to be recommended that would lead to correct installation and performance of the strengthening system designed. Detailed experimental work had been completed to assess the long-term performance of the strengthening. The results indicated that the materials were indeed suitable.

The results from the work were drawn together in the form of a design guidance document [ICE, 2001]. The document aimed to support the non-specialist engineer in the design of a composite strengthening solution by detailing the issues that need to be considered and giving guidance on how to address them.

Due to the nature, the scale and the specialist expertise required, six organisations were involved to accomplish the objectives, which were to study typical carbon reinforced strengthening solutions likely to be used in the Civil Engineering Industry, to develop design methods and to validate them by full scale testing. The parties involved in this project were:

- Development Royal Dockyard Ltd, Composite Business Unit (DML), which carried out investigation on the degree of uncertainty over the surface preparation of substrates necessary prior to effective adhesive bonding. This led to producing guidance in relation to the preparation of steel, cast iron, wrought iron and concrete.

- Defence Evaluation and Research Agency (DERA), which investigated the use of composites in situations where unusual environments may be encountered. They

provided expertise in environmental exposure and durability of composites from their research of military and civilian structures.

- London Underground LTD (LUL) was the client, which provided specimens for full scale testing and access to the sites.

- MSL Engineering LTD (MSL) was involved in producing analysis and design of unreinforced and reinforced cast iron struts that were tested to failure. The reinforcement was provided by carbon fibre laminates bonded to the struts.

- Structural Static Ltd (StStL) was involved in monitoring the strengthened bridge and recordings of the relative data. This enabled comparison to be made as to the effectiveness of the strengthening.

- University of Southampton (UOS) examined the benefits of using CFRP as strengthening to various structural forms, in terms of enhancement of load bearing capacity, and was commissioned to carry out a series of tests on unreinforced and reinforced cast iron struts. This is discussed in detail in chapter five.

2.9.2 Plate bonding development trials

The Link programme had highlighted the need to investigate and develop the processes which can be used to install CFRP reinforcement plates. A series of plate bonding development trials were undertaken by DML [2000] in order to address this issue. The objective was to provide guidelines as to the most appropriate method of installation, which also covered adhesive selection, surface preparation, adhesive application, and the effects of temperature on cure times.

Several series of test were undertaken [DML, 2000] to study the material behaviour of four most commonly used adhesives. Approximately 25g of each of the following two part epoxy adhesives was mixed by hand:

- Sika-Sikadur 31 PBA
- SP system-Spabond 130
- Ciba-Araldite 136H
- SBD-Epoxy plus structural adhesive

The mixed adhesive was applied to a mild steel plate in a thick patch, and the plate stood vertically whilst the adhesive cured. The adhesives were quantitatively assessed for deformation during cure. The ease with which the two parts mixed was qualitatively assessed, as was the ease with which the mixed adhesive could be applied to the plate.

In order for an adhesive to be considered for plate bonding applications it must have sufficient viscosity not to run or sag when applied to vertical or overhead surfaces. A high degree of thixotropy (high viscosity displayed at low stress, decreased viscosity when an increased stress is applied) is also a desirable quality to aid mixing and adhesive application. Based on these criteria the Sikadur 31 PBA and the SBD-Epoxy plus structural adhesive were found to be the most suitable for plate bonding.

Lap shear tests conducted by DML [2000], had shown that the Sikadur provides a good combination of high mean strength and low variability. These findings emphasise the use of Sikadur in reinforcing applications, where metallic structures are reinforced using CFRP plates.

To adopt a suitable surface preparation procedure, a visual record was made of the surface finish achieved using different methods of preparation [DML, 2000]. It was found that, the use of shot blasting to prepare the surface was very rapid, completely remove all trace of rust and provided a uniformly rough surface. The use of hand tools was also rapid and provided a surface free from rust, although the surface roughness achieved was significantly less uniform than that obtained by shot blasting. This trial demonstrated that where the level of corrosion is such that it is practical to prepare the surface using hand tools, this does not result in a significant decrease in the bond strength achieved.

Therefore, as this method has provided a satisfactory result, the procedure could be adopted in reinforcing metallic structures, which will be used in this research.

An investigation was also carried out [DML, 2000] on how to achieve the best possible bond between plates. It was found that, the dome profile ensures that as load is added to the plate, the contact area between plate and adhesive moves from the centre of the plate toward the edges. This helps to ensure that no air is trapped within the adhesive layer. Overall, the method of applying the adhesive as a domed section was found to have worked well, ensuring that the contact area progresses from the centre of the plate toward the edges. This method reduced the likelihood of air voids becoming trapped in the bond line; both of the test plates produced contained zero air voids.

Individual lap shear specimens were prepared [DML, 2000] using Sikadur 31 PBA, in order to investigate cure development at low temperature. Testing was conducted at 5°C as this corresponds to the minimum temperature constraint imposed for site application of reinforcement plates. A number of specimens were used to confirm the gel time at 5°C of the adhesive, which the manufacturers quote as 6 hours. Following determination of the gel time, batches of five samples were tested after 16, 24, and 48 hours cure time at 5°C. The lap shear samples were prepared and tested in accordance with the CRAG standard 102 method of test for lap shear strength of fibre-reinforced plastics. It was found that after 16 hours cure at 5°C, the adhesive had not cured sufficiently for lap shear strength to be determined. After 24 hours cure at 5°C, the adhesive had started to gain strength. A "viscous" failure mode was exhibited, with the two parts sliding apart at failure. After 48 hours cure at 5°C, the state of cure was sufficient for a brittle failure mode. Overall, it was found that after 24 hours curing at 5°C, the adhesive has gained sufficient strength to resist live loading. After 48 hours of cure, the adhesive has gained 49% of the full strength achieved after a 7-day 25°C cure. This highlighted the problem that adhesives cannot gain sufficient strength at early stages of curing to withstand any live loadings, which should be taken into consideration.

Overall, the set of tests and findings by DML [2000] showed that the Sikadur provides a good solution to bonding CFRP plates to metallic structure. It also highlighted the importance of surface preparation, application method and the effect of temperature on duration of achieving the full strength. These findings have been taken into consideration in the current research. However, as this research is also dealing with applications where adhesive is subjected to cyclic loading, especially at the early stages of their curing hence adhesive mechanical properties need to be taken into account at early stages, where they have not gained enough strength and will sustain damage.

2.9.3 Durability of composite material

DERA [2000] investigated the durability of composite material with regard to environmental exposure. The effect of environmental exposure on composite materials is fundamentally more difficult to predict than with monolithic materials, as both the resin matrix and the reinforcing fibres determine the mechanical properties. Generally it is the matrix resin that is more susceptible to environmental degradation, but the interface between the fibre and the matrix can also be affected. This interface is crucial for load transfer from the resin to the fibre and therefore environmental degradation on this interface can alter many of the mechanical properties of the composite.

Any polymer composite material in proximity to moisture, whether in the form of humidity or complete immersion, will absorb a certain amount of water. Polymer composites exposed to moist environments will absorb moisture until equilibrium, or saturation point, is reached. The saturation point will not only be determined by the composite material, but also by the level of moisture in the environment. Higher temperatures will increase the rate at which saturation is reached. Accelerated environmental conditioning is carried out in high moisture environment at higher temperature in order to reach a high saturation level rapidly. Damage to the composite will occur in form of matrix plasticisation, matrix cracking caused by differential swelling rate and, in some situations, by osmosis causing blisters. Accelerated thermal ageing gives predicted strength losses caused by change in temperature during the service

life of a component. Composite was cycled between –20°C and +80°C, dwelled at the temperature extremes for 30 minutes and ramped between the two over 25 minutes, respectively, this represented a worst case service environment. This has highlighted the need for consistent monitoring of the surrounding environment of CRFP plates and if necessary create a more suitable condition, as to where the composite would not be susceptible to environmental degradation.

With moisture uptake and many other fluids once the composite has reached equilibrium there is no further reduction in the mechanical properties. Therefore it can be assumed that taking the specimen to equilibrium will give the ultimate performance drop-off. The concerns with acids and alkalis are that the materials will reach equilibrium for fluid uptake, the ionic components of the fluid will continue to attack the fibres and reduce the mechanical performance. A worst-case scenario would see that acid/alkali completely remove the interface between fibre and the matrix resin, as shown in Figure 2.5. The research is still in progress, however. When completed it will provide designers with a measure of the reduction in mechanical performance due to the effect of moisture.

The findings by DERA [2000] support the need to apply protection systems to all composite structures, which are expected to be exposed to moisture. Furthermore, there is a need for an appropriate design solution that takes into account of reduction in mechanical properties.

2.9.4 Design of strengthening schemes for cast iron strut using CFRP

The effect of the carbon fibre reinforcement in enhancing the load capacities of in service cast iron struts needs to be determined. Therefore, MSL were commissioned to carry out an investigation as to describe the analysis and design of the unreinforced and reinforced cast iron struts [MSL, 1999].

The carbon fibre composite was to be designed to increase the strength of the unreinforced strut by 50%. The carbon fibre composite needed to be applied to the strut

whilst the strut was sustaining an axial load. The loads would then be applied at a constant eccentricity, which is 10% of the distance over the cruciform short arms, from the centre line of the longer arms and the struts will be free to rotate at the ends.

An analytical technique for the design of strengthening schemes for column was developed. This technique formed the basis of the procedure for the preliminary sizing of the laminate, when used in conjunction with the Claxton Fidler formula.

FE models were created and analyses carried out to determine the load capacities of both unreinforced and strengthened strut under eccentric loads. When comparison was made by University of Southampton with experimental data [Moy, 1999], however, it was discovered that the finite element analyses underestimated the failure loads. It was found that difference in material properties had accounted for much of the discrepancy.

The need for further research is therefore identified, as there is little understanding on behaviour of cast-iron undergoing axial loading. This research will carry out extensive FE analyses on behaviour of cast-iron strut under axial loading, validated by experimental data [Moy, 1999], which has monitored strain reading through cross sections of cast-iron struts.

2.9.5 Design and practice guides, FRP composites, ICE [2001]

There is considerable interest in the use of fibre reinforcement polymer (FRP) composites in construction and one of the major aims of the Institution of Civil Engineers is to provide its members with opportunities for continuing professional development. One method by which the institution is achieving this is the production of design and practice guides on topics relevant to the professional activities of its members. The purpose of the guide is to provide an introduction to the main principles and important aspects of the particular subject, and to offer guidance as to the appropriate source of more detailed information. This report has focused on the repair of cast iron and steel structures using FRP composite.

The recommendations contained in the guide [ICE, 2001] mainly covered the structural strengthening or repair of metallic components of onshore structures, using CFRP. The recommendations were concerned with strengthening and repair schemes in which either the CFRP was bonded to an existing structure, such that the existing structure and CFRP act together, or the new composite structure provided an alternative load path to the existing structure. The recommendations were of limited application when applied to substrates other than metallic substrates, as each may require unique bonding materials and surface preparation techniques.

Selection of the type of laminate was considered in this guide [ICE, 2001]. As there should be a concurrent activity with the structural design and the laminate. Careful considerations were given to exactly what function the components were to perform. Key consideration was strain compatibility between the laminate and the substrate material, and ultimate strength of the laminate.

The method of design was the other main finding of the report [ICE, 2001] where designing a structure would depend on the material from which the structural component is made and on the geometry of the cross section. The behaviour of cast iron is very difficult to predict accurately [ICE, 2001], as there is a large variation in material properties from casting to casting. The stress-strain behaviour will vary according to the quality and coarseness of the graphite flakes present. The low elastic limit in tension coincides with the first localised yield at the ends of the graphite flakes, which act as stress raiser. In compression the graphite flakes can transfer stress, which results in the higher compressive strength. For the purposes of design, cast iron is usually assumed to be a linear elastic material and is assessed using simple elastic bending theory and suitable failure criterion. However, a new method was introduced to account for the non-linearity of the cast iron. As for steel, it has been used for structural purposes since 1890, largely replacing wrought iron by 1900. Design methodology appropriate to steel construction is well understood and is covered by current British Standards. Design guidelines for steel take two different approaches, depending on the cross-section of the

beam. Where rolled or fabricated sections meet the geometric requirements set out in BS5400, the full plastic moment can be developed before, and maintained after, the onset of local buckling. Sections of this type are referred to as being 'compact'. Where the sections are to be reinforced using CFRP, the onset of fully plastic bending results in strain in the extremes of the section exceeding the permissible strain in the CFRP.

Designing from the first principles can only be done for strengthening schemes where the strength of the component can be estimated reasonably accurately from a fundamental understanding of the failure behaviour. Thus, it can be used for 'simple' elements such as beams and columns. The analysis of structures made out of cast iron should take into account the non-linear stress-strain behaviour in tension and compression. When designing a strengthening or repair scheme using first principles, the resistance of a reinforced member shall not be obtained by simply adding the maximum theoretical resistance of each material acting alone.

An elastic analysis approach assumes that plane sections remain plane during bending and that the material exhibits a linear elastic stress-strain response [ICE, 2001]. It is also assumed that the CFRP reinforcement is perfectly bonded to the tensile (or compressive) flange of the beam, i.e. that no slip occurs at the interface. The design philosophy is to transform the reinforced section to an equivalent section of a reference material, normally that of the metal. The resulting transformed section behaves in the same manner as a member composed of only the reference material. The thickness of composite reinforcement to be added is designed, using an elastic analysis, such that stresses within the original section are limited to a permissible value. The reinforced section is transformed by increasing the width of the carbon fibre laminate, by multiplying the actual width by the modular ratio (elastic modulus of the composite divided by elastic modulus of the metal). The plane sections remaining plane assumption may then be employed in order to calculate stresses in the section. Using this approach the bending characteristics of a cross-section made from a number of materials with different elastic modulus may be calculated.

An elastic-plastic approach assumes that plane sections remain plane during bending and that the metal exhibits a linear elastic or perfectly plastic stress-strain response [ICE, 2001]. It is also assumed that the CFRP reinforcement is perfectly bonded to the tensile (or compressive) flange of the beam, i.e., that no slip occurs at the interface. An elastic-plastic analysis is required, rather than a fully plastic analysis, as a result of the fundamental differences in the behaviour of the metal and the reinforcing CFRP. The metal will deform in a linear elastic manner up to the limit of proportionality, after which it will deform plastically to failure at a large ultimate strain, whereas CFRP will deform elastically to failure. The long-term design allowable strain of CFRP is between 0.1% and 0.3%; at this strain limit it is unlikely that a full plastic hinge will have developed.

The reinforced section is analysed by assuming a plane sections remaining plane distribution with an assumed location for the NA. The location of the NA is then iterated until the resultant force blocks (tension or compression) balance; this is illustrated in Figure 2.6. Due to the fact that the metal is permitted to yield, the full benefit of the reinforcement will be realized irrespective of the pre-load prior to reinforcement. Stress is transferred into the CFRP reinforcement via shear stress across the adhesive interface with the beam. This shear stress must be assessed against a design allowable value for the adhesive using standard engineering formulae.

Overall, the design procedures have been created to allow engineers determine basic structural characteristic in form of hand calculations. However, these procedures are based on assumptions, which are not always met, i.e. knowing the amount of preload sustained by structures, and more importantly assuming full bond between CFRP and metallic substrate. The former assumption, fully bonded reinforcement, discards the fact that adhesive requires a minimum of 18 hours to reach it full strength and may sustain damage if subjected to live loading and this is the case in some metallic structures which undergo strengthening, i.e. bridges. Therefore, it is imperative to take into account the effects of loadings on the performance of cured adhesive, which in turn determines the overall strength of the structure.

2.11 CONCLUSIONS

Carbon fibre composite was highlighted for application of strengthening of metallic structures. Therefore, series of investigations that formed the LINK project (2000) were carried out. However, due to lack of knowledge on material behaviour, the design guides were limited to simple scenario where it is assumed that CFRP is fully bonded to its metallic substrates. However, it is not uncommon that the structure will continue to be exposed to live loading while the adhesive is curing, which in turn will affect the load carrying capacity of the structure. Hence, further research is necessary, which can investigate the effect of live load on performance of adhesives, whilst curing.

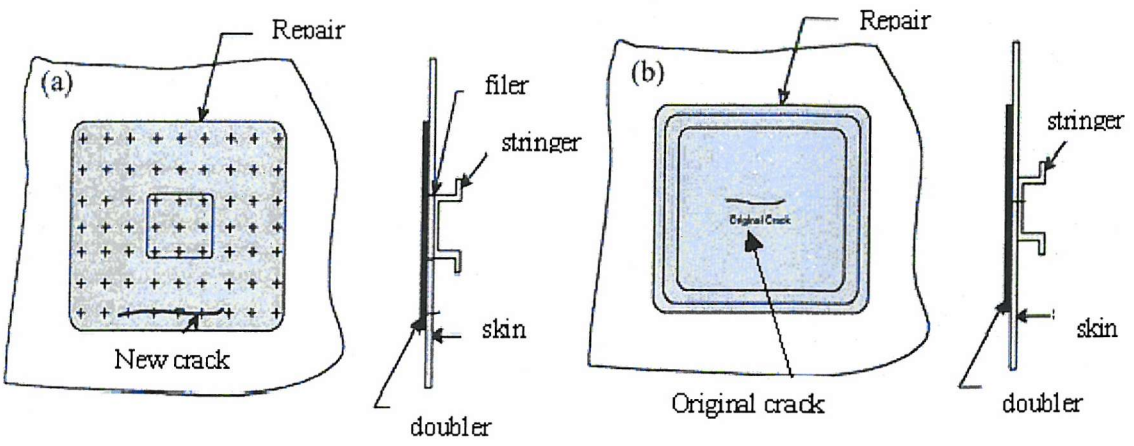

- No damage to structure or hidden components.
- Minimizes stress concentrations
- Slow crack growth even on exit from patch
- High patch efficiency, can repair crack
- Can detect crack growth under patch
- No corrosion problems, sealed interface

- Stress concentrations at fastener holes
- Difficult to detect cracks under patch
- Low patching efficiency, cannot patch cracks
- Rapid crack growth on exit from patch
- Danger of corrosion under patch

(a) Bonded repair

(b) Mechanical repair

Figure 2.1 Advantages of using bonded repair instead of mechanically repair method.

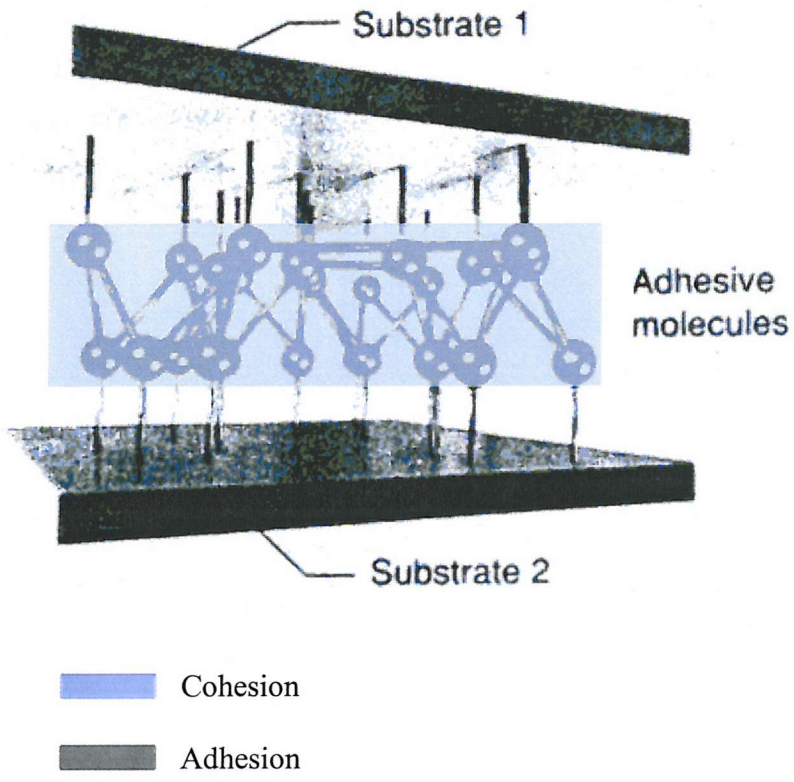

Figure 2.2 Adhesively bonded joint

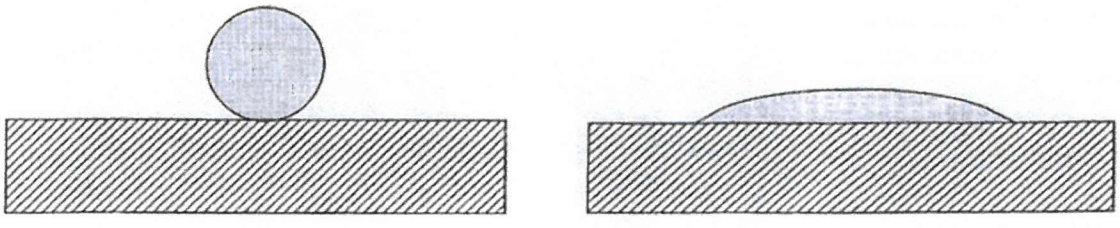

Figure 2.3 Showing a non-wet liquid on the left and a liquid wetting and spreading spontaneously over an idealised solid surface on the right

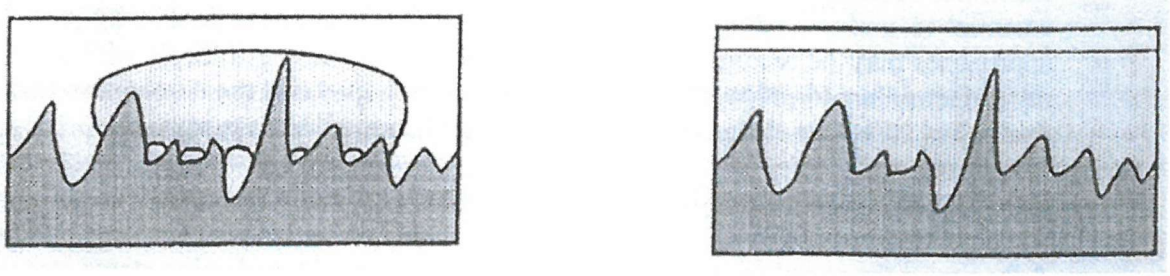

Figure 2.4 Schematic illustration showing incomplete wetting on the left and the creation of an idealised adhesive/substrate on the right

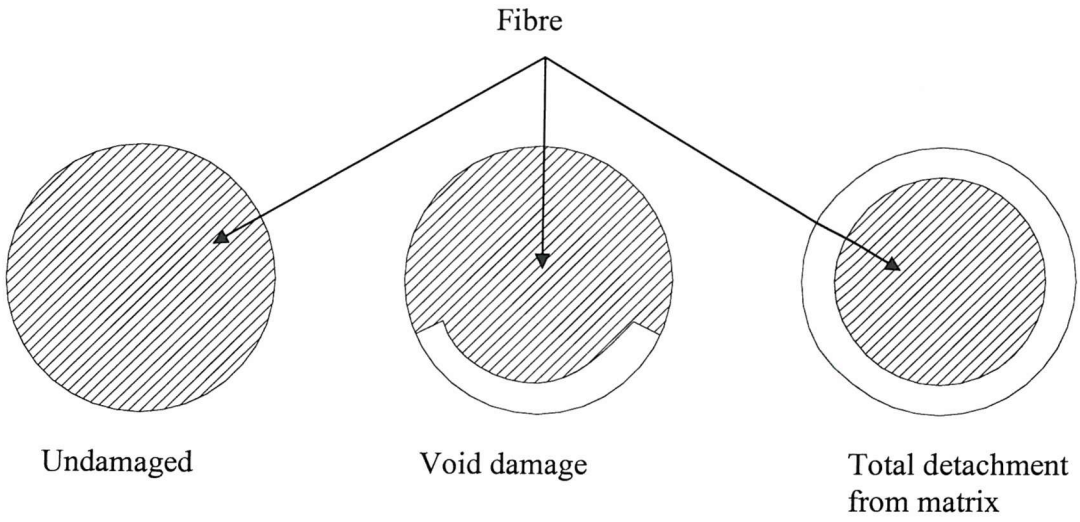

Figure 2.5 Fibre damage caused by fibre dissolution (DERA, 2000)

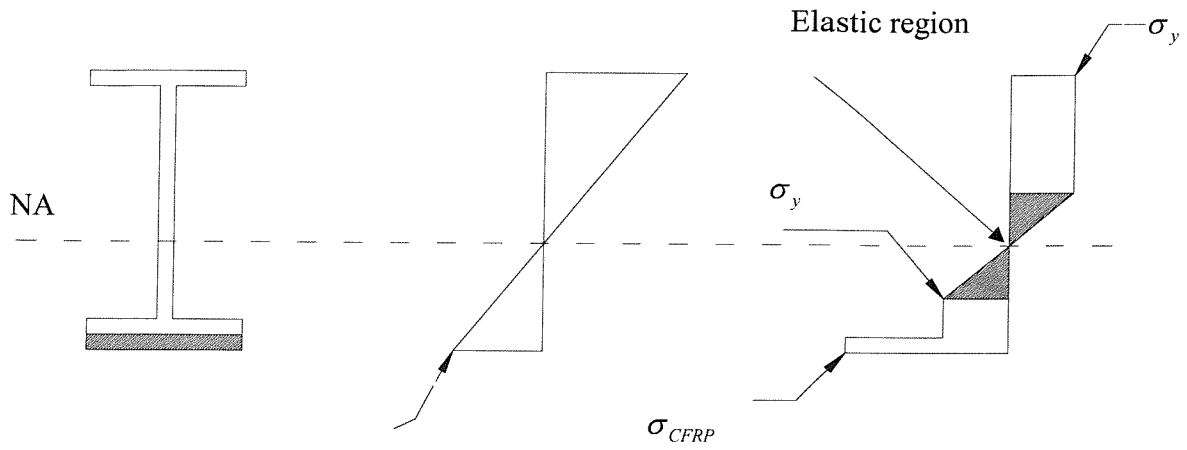

(a) Cross section (b) Strain distribution (c) Stress distribution

Figure 2.6 Elasto-plastic analysis

CHAPTER 3

STEEL BEAM REINFORCED WITH CARBON FIBRE COMPOSITES-AN EXPERIMENTAL INVESTIGATION

3.1 INTRODUCTION

This chapter details an experimental investigation of steel beams reinforced with CFRPs. A preliminary study had been conducted prior to the current research [LINK, 2000], and the ensuing report was utilised to create test specimens with the appropriate materials. The experiment was carried out in two phases: first to investigate the effect of the cyclic loading on the performance of the adhesive, which was followed by static strength testing to determine the load carrying capacity of each specimen.

When a carbon fibre composite plate is bonded to a metallic substrate there is a curing period during which the adhesive develops its full strength. When a railway bridge is strengthened in this way it is not usually economic to close the bridge during the curing period. Thus the adhesive will be subjected to cyclic loading each time a train passes over the bridge. Uncertainty remains with regard to the effectiveness of the bond between the metallic substrate and the CFRP, which is the subject of the current investigation.

To extend the life of the structure, it will be critical that the working stress in the structure be reduced sufficiently that repeated cyclic loading could not cause fatigue and degradation.

3.2 EARLY AGE CURING UNDER CYCLIC LOADING

3.2.1 Test specimens

A total of six specimens were tested (with the help of Miss Penny Penollopi, a Southampton University undergraduate). Each specimen consisted of a 1.2m long 127 x 76UB13 steel beam reinforced in one flange with a 0.98m long carbon fiber composite plate. The composite plate was made of K13710 ultra high modulus (Young's modulus of 1.5 times greater than steel) unidirectional carbon fiber in an epoxy matrix; each plate is 7.6mm thick and 76mm wide. The specimens were numbered for identification, as shown in Table 3.1. The number indicates the magnitude, in kN, of the cyclic load applied during the adhesive curing period. The minimum and maximum cyclic load magnitudes were selected in such way as the stress created in the specimens as a result of the cyclic load will be small and near to yield stress of steel used in the specimens, respectively.

Each specimen was prepared in an identical manner. One flange of the steel was grit blasted to the SA21/2 standard. Within one hour the carbon fiber plate was attached to the flange using a two-part epoxy adhesive (Sikadur BPA31). As described in the literature review (Chapter 2), epoxies were found to be very suitable for structural bonding and their properties can be altered to suit all applications, varied from flexibility to high strength. Sikadur was chosen due to its high strength capability over its flexibility.

After mixing, using weighed proportions of constituents, a layer of adhesive was applied to the steel and the carbon fiber plate. The adhesive was shaped as shown in Figure 3.1. When the carbon fibre plate was placed on the steel and pressed into position the shaped adhesive allowed air to be expelled, resulting in an even layer of adhesive over the whole contact area. G-clamps were used to hold the carbon in place, although they were only done up finger-tight. The mechanical properties of carbon fibre and adhesive are given on Table 3.4.

3.2.2 Test set-up

The tests were carried out in a servo-hydraulic Instron 8032 test machine, using the three-point bending arrangement shown in Figure 3.2. The Instron machine was calibrated to ensure accurate readings. A heavy steel beam was placed on the lower platen to support the test specimen via two rollers placed at 1.1m apart. A sinusoidally varying load was applied to the specimen at a frequency of 0.25Hz, and this loading was continued for up to 48 hours. At certain intervals the cyclic load was removed and a static test was carried out to measure the load-deflection response of the specimen. The test was also carried out on the control specimen by which no cyclic loading was applied during the curing period of the adhesive. Hence comparisons can be made between specimens with regard to the effectiveness of the adhesive bond and the level of the cyclic loading that cause debonding in the specimen.

In the cyclic loading stage the minimum load was set at 1kN but the maximum load was varied with each specimen, Table 3.2. The range of the loading was selected in such way that the biggest of the range represent a cyclic loading that would produce stress values near to yield stress of steel in the structure and the rest were selected to represent a practical range of applied load that we would be expecting. During the static tests mid-span deflections of the reinforced beams were measured in three ways. The Instron machine gave platen displacement and two transducers were also used. The platen displacements included the elastic displacement of the test rig and the spreader beam and were not used further. The transducers were mounted so that they gave specimen

displacement relative to the roller supports and the displacements were recorded using a data-logger (see Appendix A for further detail).

3.2.3 Results

Figures 3.3 to 3.7 show load-deflection graphs for the five specimens subjected to cyclic loading. Each graph contains the results of all the static tests carried out on that particular specimen; the time elapsed for each test after bonding the carbon plate is also shown. Each curve has the same form, there was an initial non-linear region (At low load this is a characteristic of the servo-hydraulics of the test machine, as the machine is 'bedding in'. This was removed from the graph to give a clearer view of the stiffness change with respect to time). This was followed by almost a linear region, where a line of best fitted has been plotted. The slope of the best-fitted line has been taken as a measure of the bending stiffness of the reinforced beam. Figures 3.8 to 3.12 show the build up of stiffness with time for each beam.

3.2.4 Discussion

The results contained in Figures 3.8 to 3.12 shows the bending stiffness of the specimens with time. The final time varies with each specimen, as time interval of each test was different. However, the final recorded time represent the stage where no significant change in stiffness was monitored. However, there is small variation in test results, as can be seen in Figure 3.6, where the recorded stiffness value of the beam SB50 has significantly decreased from times 20:05 to 40:07. There is no explanation for this, as the adhesive will be fully cured after approximately 20 hours. This variation could be due to lack of accuracy in obtaining the data as the transducers, which were used to record the deflections, might have shifted as a result of the high level of cyclic loading.

The stiffness values were calculated by making a best straight line fit to a portion of the original results (Figures 3.3 to 3.7, for calculating the bending stiffness). Despite this variation it is still possible to draw important conclusions from the test results.

The results confirm that in general the bending stiffness of the reinforced beam increases with time as the adhesive cures. However, this was not the case with specimens SB50 and SB62, as shown in Figures 3.11 and 3.12. For these beams the bending stiffness at the later stages of curing did not increase with time. Inspection of the specimens after the test showed that for Beam SB50, there was a crack running along the glue line in one half of the beam showing that the reinforcing plate had not been bonded to the steel and as for specimen 62, the CFRP was close to full debonding from the beam, which was caused by the cyclic loading in both case. Therefore, continuous excessive loading will cause progressive damage with time, which will have an effect on the structure's stiffness. In Beams SB25 and SB34 the final bending stiffness achieved was close to that of the control beam. However in Beam SB42, the final stiffness was less than that of the control beam, which was expected due to the cyclic loading. It was believed that some problems were experienced with the equipment (transducers), as stiffness of the beam at later stage of curing was significantly lower than early stages and not consistent with other specimens, Figures 3.11 and 3.12.

Upon applying the load to the reinforced steel beam, the tension flange will increase in length. During the early stage of the curing process, although the carbon plate is in contact with the steel, no shear is transferred across the adhesive, and consequently, there is slip between the steel and the plate. This slip is equal to the extension of the steel beam, depending on the magnitude of the load, since the change in length of the carbon plate will be negligible. Hence, the slip at end of each carbon plate is as follow,

$$\int_{L_1}^{L/2} \varepsilon.dx = \int_{L_1}^{L/2} \frac{Mh}{EI}.dx \qquad 3.1$$

where h is the half of the depth of section and L_1 is the distance between end of the carbon plate and steel flange. M, h, E and I are the moment, half the depth of the beam, Young's modulus and second moment of area, respectively (see Appendix C for full derivation). The importance of calculating slips will be explained in detail in Chapter 4.

The shear force is constant over each half span and is equal to the reaction force. Hence the shear stress τ is also constant. Using Engineering Bending Theory, we can derive an expression for the shear stress by taking horizontal equilibrium over half of the span, as shown in Figure 3.13. After full bending has been achieved the theoretical shear stress in the carbon is,

$$T = Bt.\ \frac{M}{I}\left(\frac{\bar{y} + [\bar{y} - t]}{2}\right) \qquad 3.2$$

$$\therefore \qquad \tau = \frac{Q}{I}\frac{L}{L_c}\left(\bar{y} - \frac{t}{2}\right)t \qquad 3.3$$

where B is the width of carbon plate, t the thickness of carbon plate, L the span of beam, L_c the length of the carbon plate, T the horizontal force (see Figure 3.13), Q the shear force, t the thickness of the carbon plate and $\bar{y}$ the distance from the centre of plate to the neutral axis.

Table 3.1 gives the bending stiffness values of approximately 40kN/mm for fully bonded beam and 30kN/mm for unreinforced beam that were calculated from Figure 3.16. These values are about 96% and 91% of the predicted values of 29kN/mm and 44kn/mm, respectively (for detailed calculations see Appendix C, 1m-Bending stiffness calculations). The reasons being are: the difference in the experimental span and the calculated span, great care was taken to ensure the correct length is placed between supports. However, small errors in the span have a significant effect on the bending stiffness since it is inversely proportional to span cubed. Also, the predicted calculations assume fully bonded specimens, but there was always the possibility that full bonding was not achieved due to air entrapment.

The predicted ratio, $\frac{reinforced - stiffness}{unreinforced - stiffness}$, of the fully reinforced beam to the steel beam is 1.46 ($\frac{44}{30}$, Appendix C, 1m-Bending stiffness calculations) and the average experimental value is 1.33 (40kN/mm for reinforced and 30kN/mm for unreinforced

beam, see Figure 3.16). This indicates that the performance of the adhesive layer may have affected the bending stiffness of the CFRP reinforced beam.

3.3 ULTIMATE TESTS

3.3.1 Test specimens

Subsequent to the cyclic load test, each specimen was tested to failure.

3.3.2 Test set-up

Again, the specimens were subjected to three-point bending. Platens of a column-testing machine were used as to provide rigid boundary supports, followed by applying load through a hand-operated jack. Figure 3.14 shows the schematic of the test set-up. This was chosen because it matched the loading used in the cyclic load tests. Two of the specimens were extensively strain gauged on both the steel and the composite (see Appendix B for full details). Mid-span vertical deflections were also measured during the test.

The test procedure was identical for each specimen. A small load was applied and removed to allow the specimen to bed-in. Initial readings were taken on all gauges and the load was then increased in increments of approximately 1.5 to 2 tonnes until failure occurred, at each increment of load all the gauges were scanned. As failure was approached the magnitude of the increments was reduced.

3.3.3 Results

Strain and displacement were recorded using data-logger, tabulated, and presented in a series of graphs. Specimen SB25 was tested first and failed prematurely due to local buckling in the compression flange. To rectify this all the other specimens were welded with stiffeners at critical locations - under the central loading point and the support at each side, as shown in Figure 3.15. Calculations were carried out to ensure against local

buckling and the remaining five specimens were tested following the former procedure. Figure 3.16 shows the load-deflection curves obtained from the tests. Due to large quantities, strain measurements graphs are presented separately in Appendix B. Each curve followed the same pattern: there is an initial linear region followed by a non-linear region. This non-linearity is due to yielding formation, initially under the point load and progress rapidly through out the surrounding areas, primarily in the compression flange and then to the web, which was observed during the experimental tests. The load levels experienced slight variation, which was due to instability on keeping the load level consistent during the non-linear phase of the test, as drop in load level was imminent when the section was gradually yielding.

3.3.4 Discussion

The unreinforced steel beam is classified as plastic according to BS5950, and was also satisfactory against web crushing but no check was made against crushing of the web of the reinforced beam. Specimens SB25 experienced web crush during the test and as a result web stiffeners were welded into the remaining specimens at mid-span and the support positions, as shown in Figure 3.15. There were no further problems with web crushing. Failures were due to either steel yielding accompanied by very large deflections when effectively a plastic hinge had formed at mid-span or debonding of the CFRP plate from the steel. The rotation capacity of the plastic hinge would have been limited by the strain capacity of the CFRP but the tests were stopped before failure of the CFRP.

It can be seen from Table 3.1 that there was a reduction in the failure load when the beam has been subjected to a higher level of cyclic loading. It is thought that failure in specimen, SB34, with no sustainable damage (debonding) resulted from yielding in the compression extreme fibers spreading into the section, producing eventually a plastic hinge. In the other specimen, SB62, failure was due to debonding of the CFRP plate.

Figure 3.17 shows the strain distribution across the depth of the section of the control beam at various load level. It can be seen that the readings lie on or very close to

the best-fit straight line as would be expected if there were perfect bond between steel and CFRP. Also the position of the neutral axis in the figure is very close to the predicted centroid of the reinforced section (see Table 3.3). Figure 3.18 confirms that the behaviour of the reinforced control beam was linear up to approximately the failure load. This behaviour confirms that the method of transformed section is good enough for predicting the reinforced section behaviour although it will need to be modified eventually to take account of the adhesive debonding.

3.4 CONCLUSIONS

This chapter has investigated the effect of cyclic loading on the performance of adhesive during curing and structural load carrying capacity. It is important to consider that, in strengthening structures where CFRP plate are attached using adhesives, which will reach their full strength on average over 18 hours (depending on temperature), the adhesive will be susceptible to damage from cyclic loading at the early stage of curing. In this chapter, we have studied the extent of damage with regard to structural stiffness sustained by adhesive at various levels of cyclic loadings.

From the ultimate load test, it was shown that, the overall stiffness of the structure (Figure 3.16) as a result of reinforcing using CFRP was increased by as much as 33%. However, this effect will be greatly reduced, if the adhesive is subjected to cyclic live loading, where it can sustain damage in the form of debonding.

It was shown that the behaviour of the reinforced beam was linear up to approximately the failure load, which confirmed that the method of transformed section is good enough for predicting the reinforced section behaviour. However, this is only valid where adhesive is not introduced to any live load while curing, which in most cases cannot be avoided. Hence, design guidelines have to be modified, so they can account for adhesive performance.

Specimen	Bending stiffness (kN/mm)	Failure load (kN)	Failure mode
Control beam	39.0	162	Formation of plastic hinge in steel beam
SB25	37.7	103*	Premature failure due to web crushing
SB34	35.9	162	Formation of plastic hinge in steel beam
SB42	32.9	127	Partial (10-15%) debonding of CFRP plate followed by formation of plastic hinge
SB50+	28.2	127	Partial (50%-60%) debonding of CFRP plate followed by formation of plastic hinge
SB62	31.0	122	extensive (90%) debonding of CFRP plate followed by formation of plastic hinge

+ Problems with experimental equipment, leading to inaccurate readings
* first specimen test with no added stiffeners

Table 3.1 Summary of test results (Figure 3.16)

Specimen	Maximum load (KN)	Slip in half span- hand calculation (mm)	Shear stress – hand calculation (N/mm^2)
SB25	25.0	0.13	0.67
SB34	34.0	0.17	0.86
SB42	42.0	0.22	1.00
SB50	50.0	0.26	1.26
SB62	62.0	0.32	1.60

Table 3.2 Slip and shear results

Section	Distance of centroid from top (mm)	Second moment of area, I (cm^4)	Section elastic modulus (cm^3)	
			top	bottom
Unreinforced	63.5	473	74.5	74.5
Reinforced	86.8	732	84.3	231.5

Table 3.3 Beam section properties

Properties	Carbon (an-isotropic material)	Adhesive (isotropic material)	Steel (isotropic material)
E1	310 kN/mm^2	2 kN/mm^2	194 kN/mm^2
E2	2 kN/mm^2	2 kN/mm^2	194 kN/mm^2
G12	5.35 kN/mm^2	0.75 kN/mm^2	
υ_{12}	0.29	0.34	0.3
υ_{13}	0.01	0.34	0.3
σ_{1T}	1031 N/mm^2	29.7 N/mm^2	*
σ_{1C}	310 N/mm^2	29.7 N/mm^2	*
σ_{2C}	40 N/mm^2	29.7 N/mm^2	*
σ_{2T}	29.7 N/mm^2	29.7 N/mm^2	*
τ_{12}	57 N/mm^2	15 N/mm^2	*

* Properties of steel are obtained from the stress/strain graph presented on Figure 4.3

Table 3.4 Material properties of the structural components

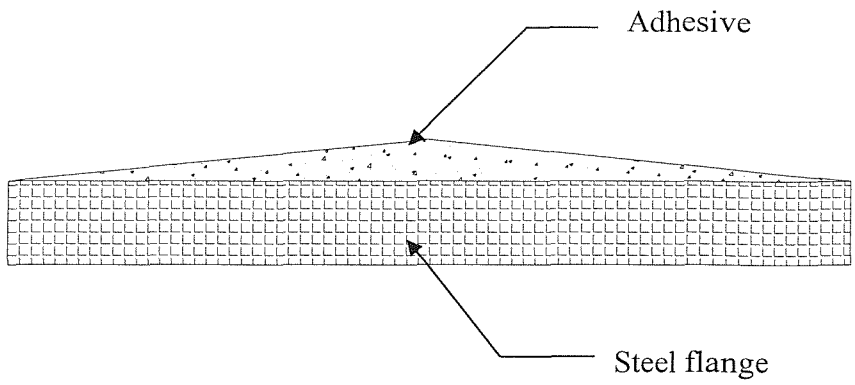

Figure 3.1 Shaped adhesive on substrate.

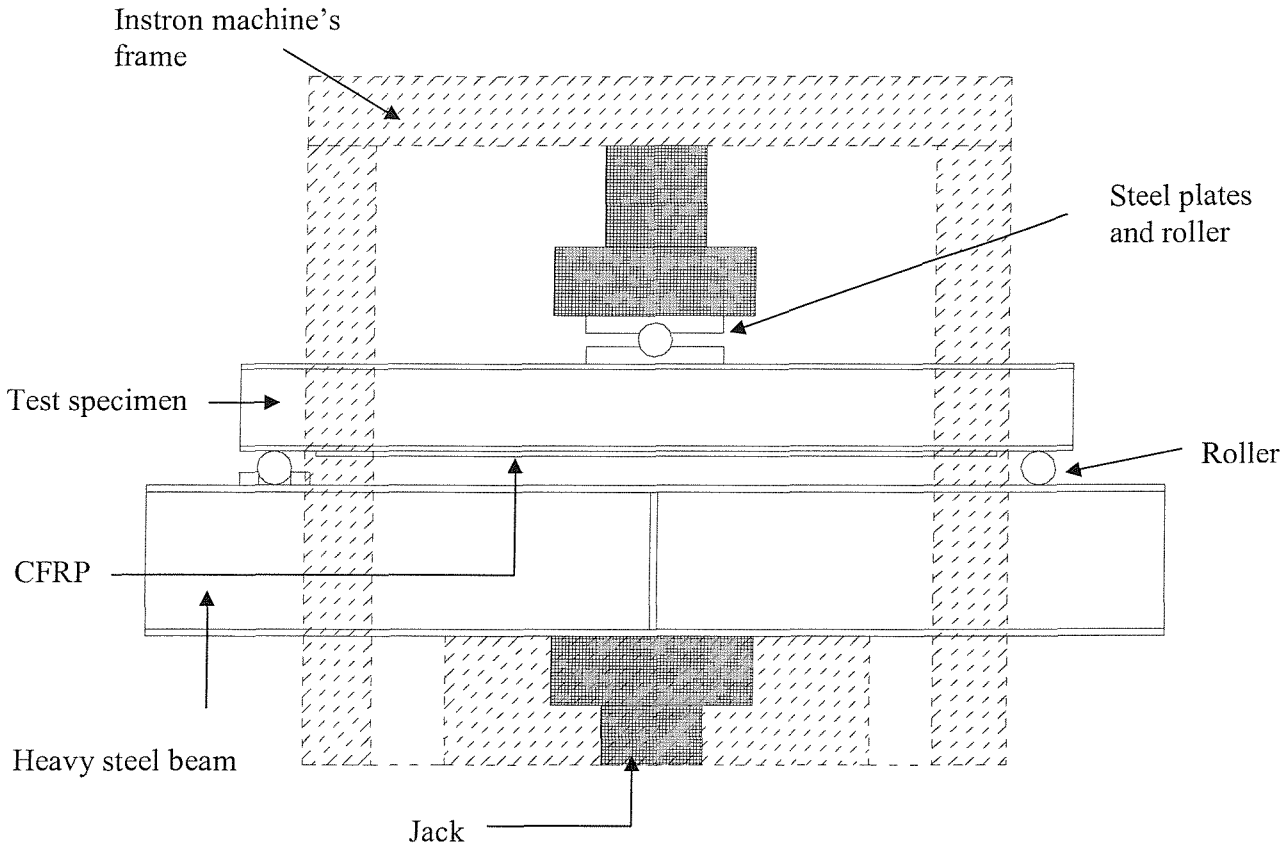

Figure 3.2 Schematic arrangement of the test set-up.

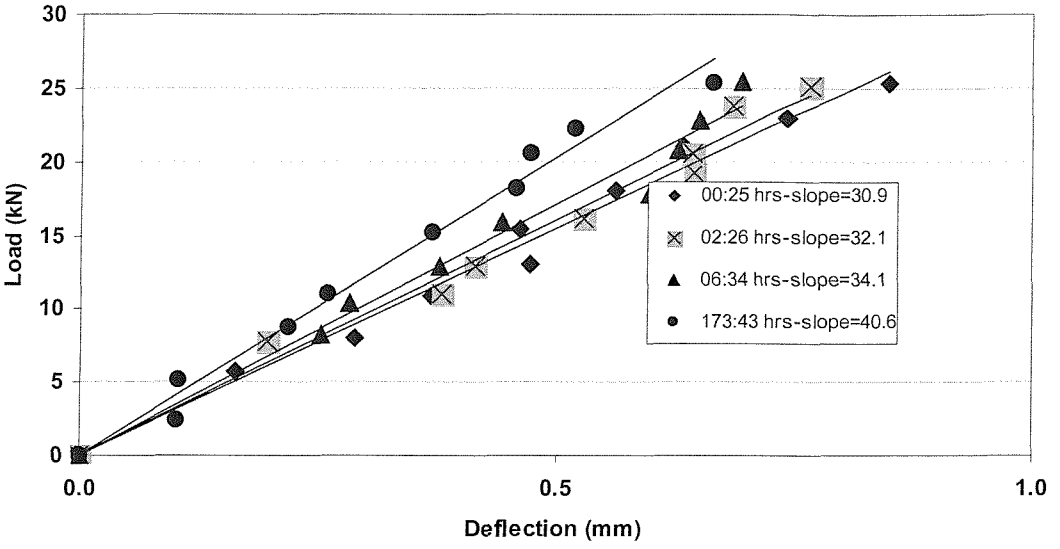

Figure 3.3: Beam SB25, load-deflection curves, average transducer data

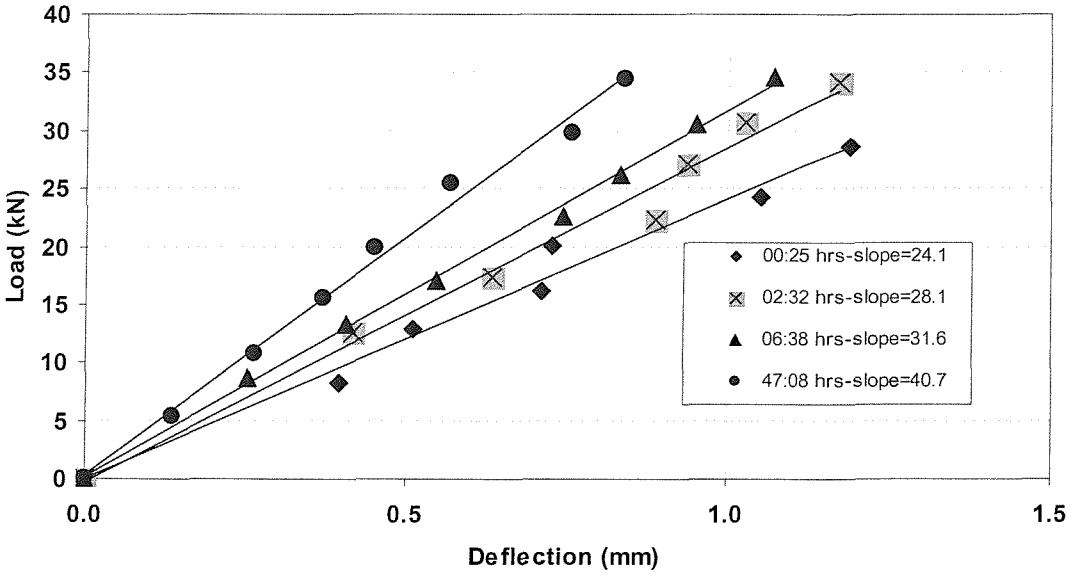

Figure 3.4 Beam SB34, load-deflection curves, average potentiometer data

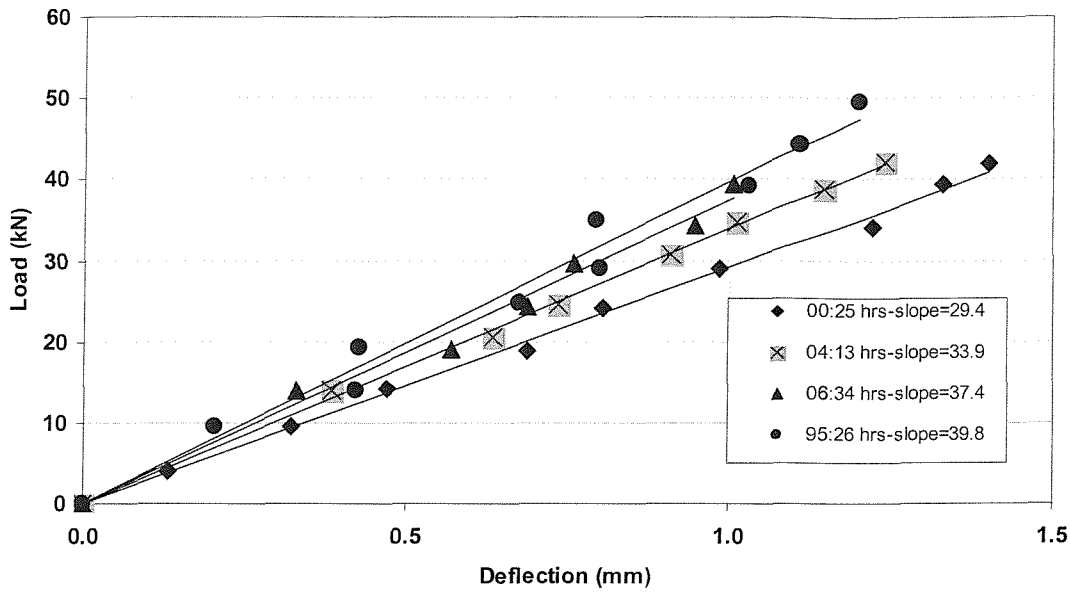

Figure 3.5 Beam SB42, load-deflection curves, average potentiometer data

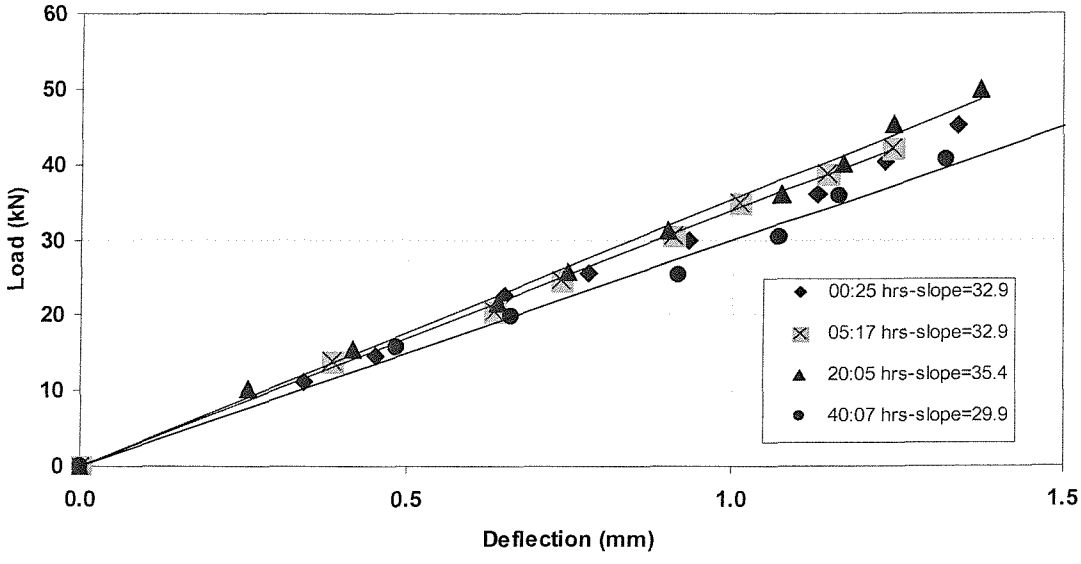

Figure 3.6 Beam SB50, load-deflection curves, average potentiometer data

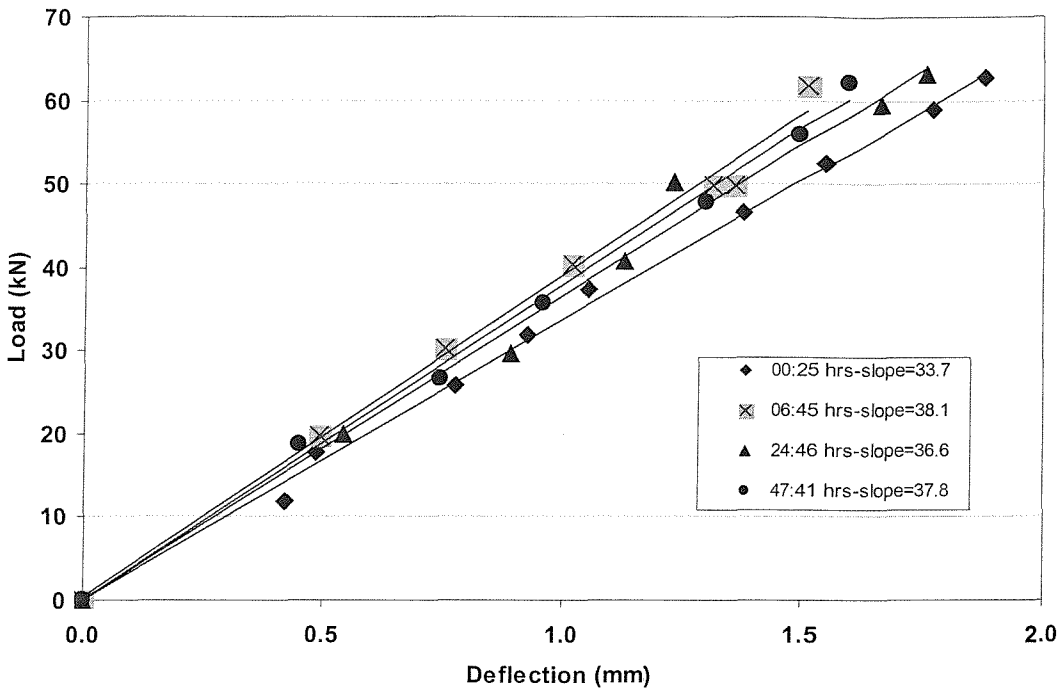

Figure 3.7 Beam SB62, load-deflection curves, average potentiometer data.

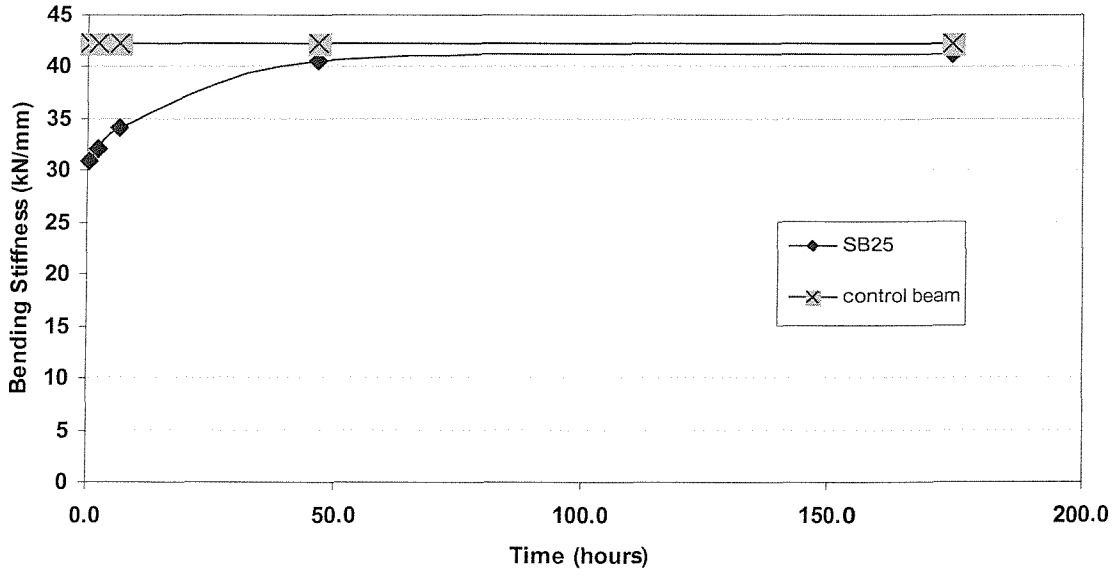

Figure 3.8 Bending stiffness versus time, Beam SB25

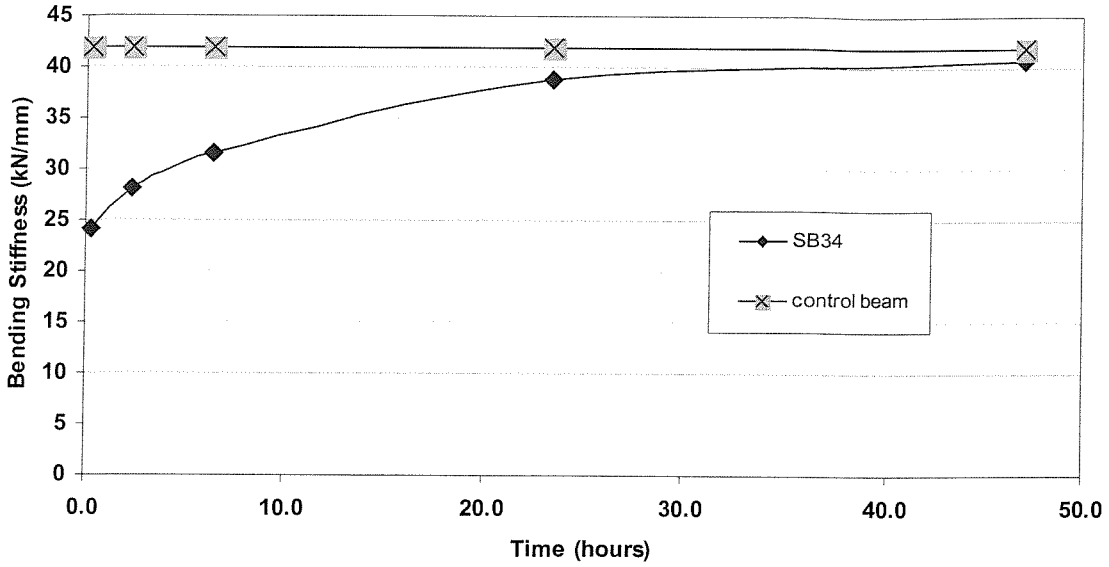

Figure 3.9 Bending stiffness versus time, Beam SB34

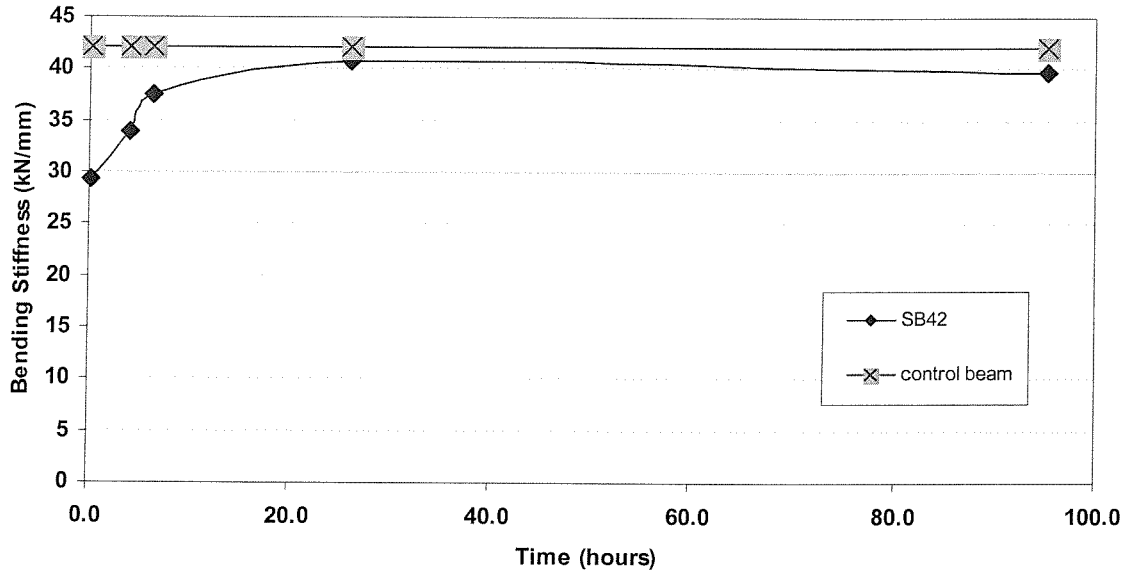

Figure 3.10 Bending stiffness versus time, Beam SB42

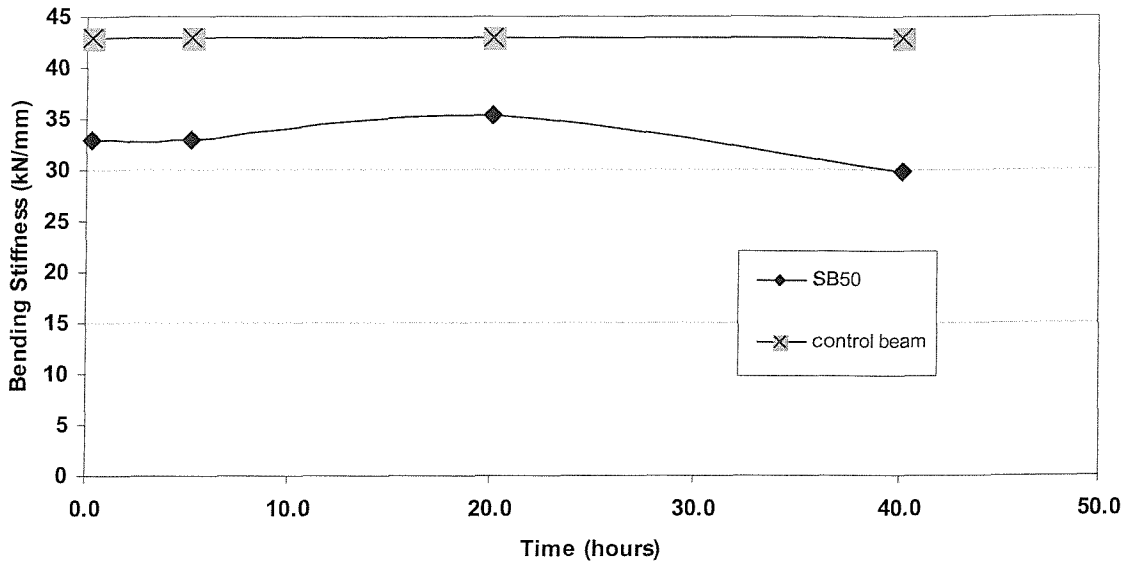

Figure 3.11 Bending stiffness versus time, Beam SB50

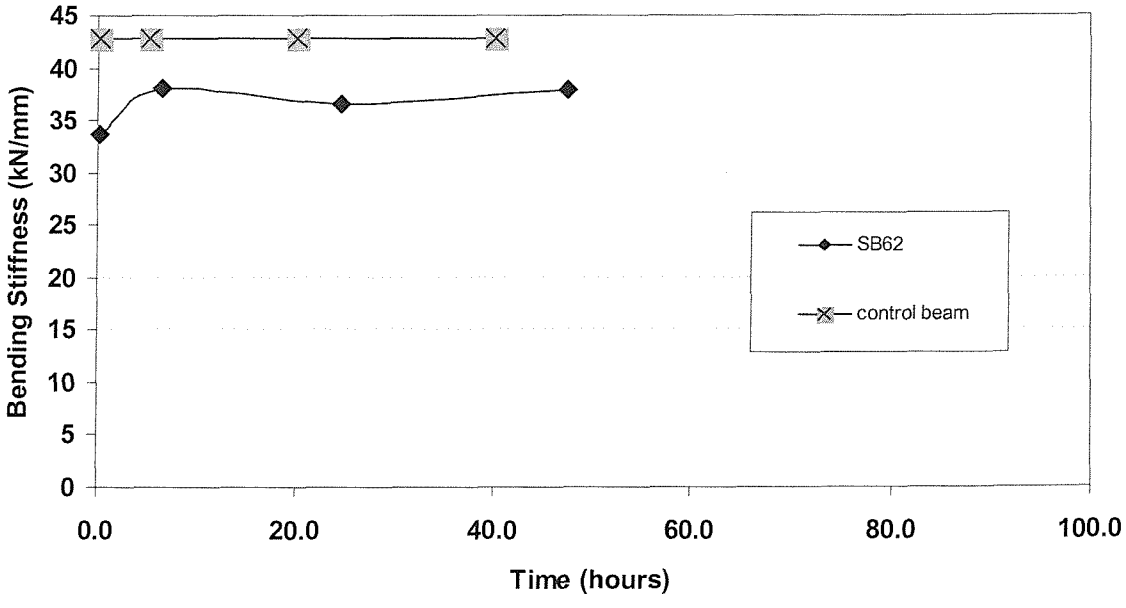

Figure 3.12 Bending stiffness versus time, Beam SB62

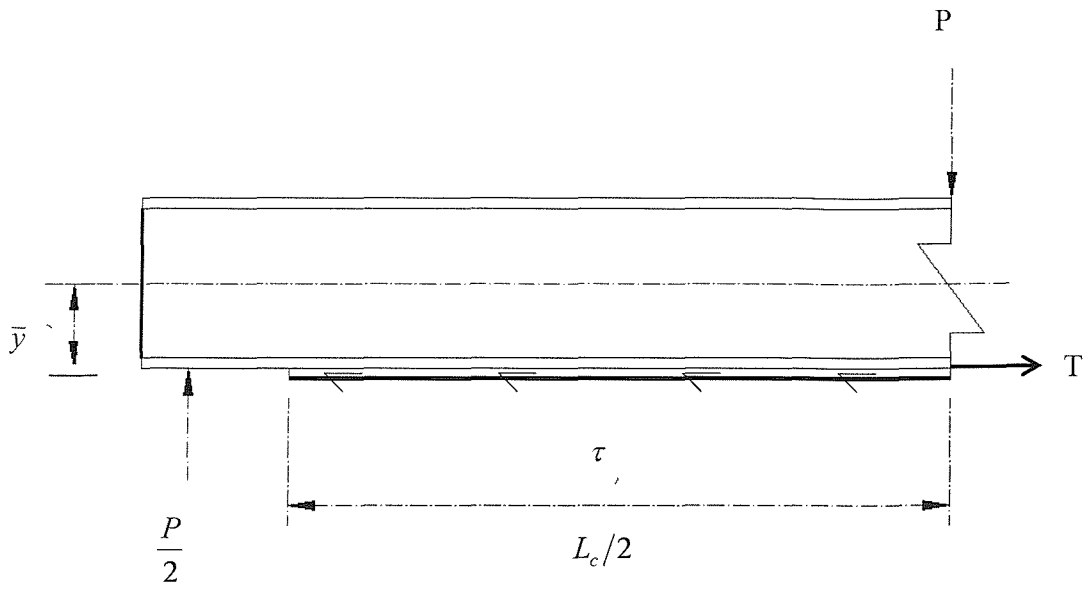

Figure 3.13 Forces across the reinforced beam

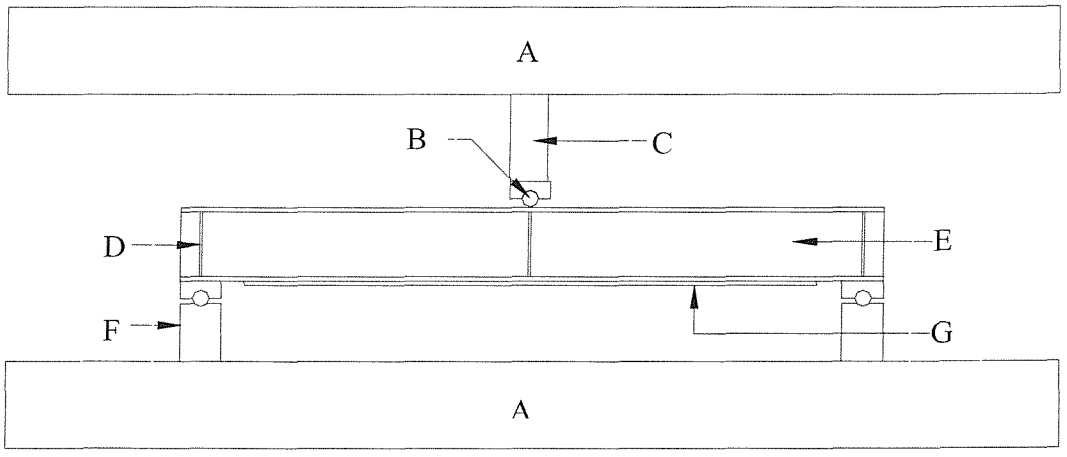

A: Platens of the column-testing machine
B: Roller
C: Hydraulic jack
D: Stiffeners
E: Steel beam
F: CFRP

Figure 3.14 Schematic of the test set-up

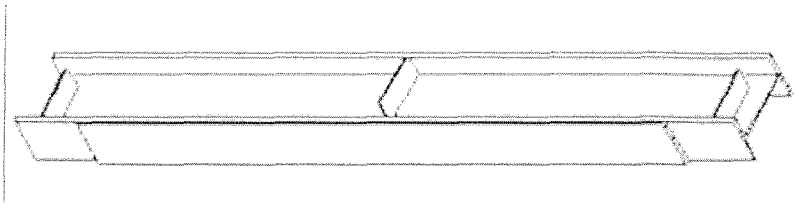

Figure 3.15 Schematic showing a typical specimen with added stiffeners.

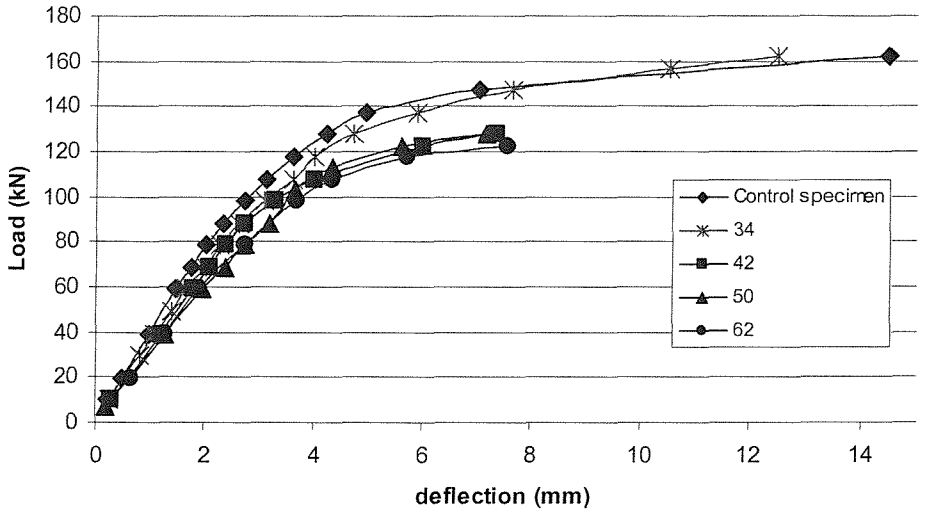

Figure 3.16 Load-deflection curve, for all specimens

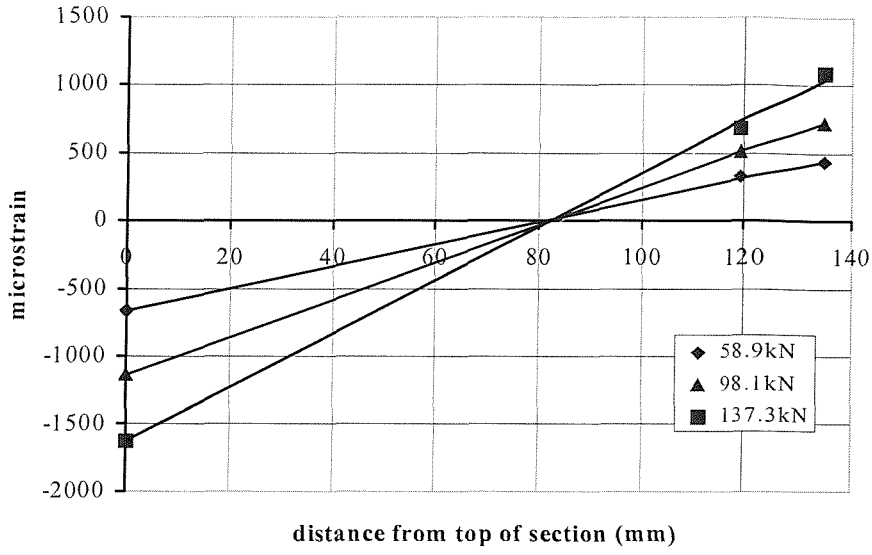

Figure 3.17 Strain distributions across the depth of the section of control specimen at various loads

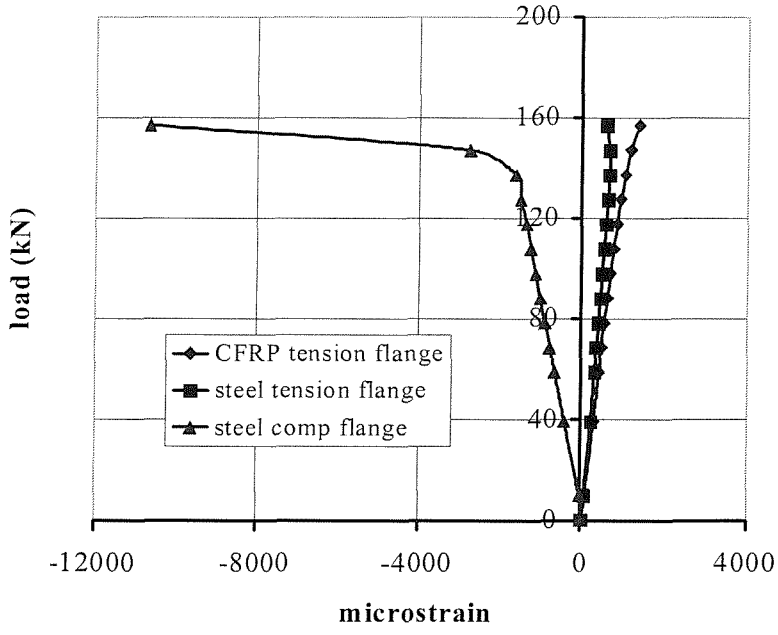

Figure 3.18 Strain gauge readings at key locations, control specimen

CHAPTER 4

FE MODELLING OF REINFORCED STEEL BEAM

4.1 INTRODUCTION

The use of the non-linear Finite Element (FE) Method for composite material is now well established. Studies by Lessard and Chang [1989] have shown that carefully calibrated numerical models can adequately model the required behavioural characteristics of composites. The commonly used mesh generation and FE analysis practices are described here with reference to the ANSYS and ABAQUS software used in the present study.

FE analyses were carried out to investigate the effects of cyclic loading on the performance of the adhesive, which is difficult to establish using experimental methods.

The FE analysis provided information on shear forces and stresses in the adhesive and the adherents. This led to the completion of a calibrated model that was used for a parametric study, where models of the beams of practical dimension (3m and 5m length) were analysed and the effects of the cyclic loading were determined throughout the adhesive.

Brief investigation was also carried out looking at shear stress distribution across the adhesive layer by using FE analysis, ultimate test, of lab shear specimen. This investigation was carried out only to raise awareness of the problem within reinforced structures using plates.

4.2 GENERAL DETAILS

4.2.1 Software

The FE procedure adopted was the same as that detailed in Chang and Lessard, 1989. The general-purpose software package ANSYS [1999] was used for the mesh generation and the ABAQUS [1997] package was used for the analysis and post-processing.

4.2.2 Introduction to the plasticity model

In this investigation a non-linear model was adopted to simulate the behaviour of a CFRP reinforced steel beam and a simple introduction is given below to highlight the fundamental principles behind the plasticity model used.

Plasticity models are written as rate-independent or as rate-dependent models. A rate-independent model is one in which the constitutive response does not depend on the rate of deformation – the response of many metals at low temperatures relative to their melting temperature and at low strain rate is effectively rate independent. In a rate-dependent model the response depends on the rate at which the material is strained.

A basic assumption of elastic-plastic models is that the deformation can be divided into an elastic part and an inelastic (plastic) part. In its most general form this statement is written as

$$F = F^{el} . F^{pl}$$

where F is the total deformation gradient, F^{el} is the fully recoverable part of the deformation at the point under consideration, and F^{pl} is the inelastic part. The rigid body rotation at the point can be included in the definition of either F^{el} or F^{pl} or can be considered separately before or after either part of the decomposition. This decomposition can be used directly to formulate the plasticity model. Historically, additive strain rate decomposition,

$$\dot{\varepsilon} = \dot{\varepsilon}^{el} + \dot{\varepsilon}^{pl}, \tag{4.1}$$

has been used in its place. Here $\dot{\varepsilon}$ is the total strain rate, $\dot{\varepsilon}^{el}$ is the elastic strain rate, and $\dot{\varepsilon}^{pl}$ is the plastic strain rate.

4.2.3 Geometry and element selection

The dimensions of the models were the same as the experimental specimens. The steel beam was modelled with 4-node doubly curved general-purpose shell elements[1], which had reduced integration[2] with hourglass control[3] and finite membrane strains. The adhesive and the carbon were modelled with 8-node linear brick elements[4], which had

[1] Shell elements allow the modelling of curved, intersecting shells that can exhibit nonlinear material response and undergo large overall motions. They can also model the bending of composites. There are three categories of shell elements consisting of general-purpose, thin, and thick.

[2] Reduced integration uses a lower-order integration to form the element stiffness. The mass matrix and distributed loading use full integration. Reduced integration reduces running time, especially in three dimensions.

[3] Hourglassing [ABAQUS, 1997] can be a problem with first-order, reduced-integration elements in stress/displacement analyses. Since the elements have only one integration point, it is possible for them to distort in such a way that the strains calculated at the integration point are all zero, which in turn, leads to uncontrolled distortion of the mesh. Second-order reduced-integration elements, with few exceptions, do not have the same difficulty.

[4] The solid element includes isoparametric elements: quadrilateral in two dimensions and "bricks" in three dimensions. These isoparametric elements are generally preferred for most cases because they are usually the more cost-effective of the elements. They are offered with first- and second-order interpolation.

reduced integration with hourglass control to prevent shear locking[5]. Figure 4.1 shows the finite element mesh used. Advantage was taken of any symmetry condition in loading and geometry to reduce computational effort. Discretisation of the geometric model into a finite element mesh is an important but subjective aspect of any FE study, relying on the experience of the researcher to obtain a compromise between creating a sufficiently fine mesh to yield accurate solutions and minimising CPU analysis time. This is particularly important if the mesh is to be used for a large number of analyses within a parametric study. Therefore, efforts were taken to create a mesh that yielded accurate solutions but at the same time minimising the analysis time as much as possible.

An extensive study was carried out into adopting an appropriate[6] mesh for the finite element model. This consisted of refining a default[7] mesh by up to 200%. This procedure was carried out in four stages whereby each stage was 50%, 100%, 150% and 200% finer than the default mesh. An investigation was carried out into monitoring the convergence[8] level, and the overall data of geometrical deflections[9] and element stresses in each refinement. Appropriate mesh was selected where no significant benefits were gained by further refining the mesh.

[5] Volumetric locking [ABAQUS, 1997] occurs in fully integrated elements when the material behaviour is incompressible. Spurious pressure stresses develop at the integration points, causing an element to behave too stiffly for deformations that should cause no volume change, [ABAQUS, 1997].

[6] Sufficiently fine mesh to yield accurate solutions and minimising CPU analysis time.

[7] The default mesh controls that the FE software program uses may produce a mesh that is adequate for the model. Therefore, a generated mesh that meets acceptable energy error estimate criteria [ANSYS 6.2].

[8] A convergence monitor is calculated for each degree of freedom at each global iteration. It is loosely normalized rate of change of the solution from one global iteration to the next and is calculated for each DOF [ANSYS 6.2]. The iterative solvers included in ANSYS, is a robust solver. The solver can solve indefinite matrix equations, when the solver encounters an ill-conditioned matrix, the solver will iterate to the specified number of iterations and stop if it fails to converge. When this happens, it triggers bisection (Automatic Time Stepping). After completing the bisection, the solver continues the solution if the resulting matrix is well-conditioned. Eventually, the entire nonlinear load step can be solved.

[9] Bending stiffness

4.2.4 Boundary conditions

Only one half of the beam was considered because of symmetry. All nodes at mid-span were restrained to produce the required symmetry, and nodes at the end of the beam were restrained to represent simply supported conditions. This is illustrated in Figure 4.2.

4.2.5 Material properties

The material properties of the adhesive and the carbon fibre composite plates were obtained from the DML database tests [LINK, 2000], which had been built up from earlier. As for the steel, tensile tests were carried out on steel coupons from different steel beams and average properties were obtained. These are shown in Figure 4.3 and the input stress-strain curve is the average curve.

4.2.6 Loading

Point load was applied at mid-span, using the "STATIC" function, whereby the step was analysed as a static load step and increments were selected using an automatic procedure. Thus ABAQUS automatically selects the increment size during the analysis, which is usually more efficient because ABAQUS can react to nonlinear response that the inexperienced user cannot predict. This method is particularly valuable in cases where the response to load varies widely through the step. Due to anticipated deformation, the geometric non-linearity function was turned on during analysis.

4.2.7 Failure criteria

Due to the complex nature of polymer composites, failure modes for these composites are strongly dependent upon geometry, loading direction, and ply orientation [Lessard and Chang, 1989]. Since the composite is loaded in-plane, only in-plane failure

modes need to be considered. For the CFRP plates subjected to tensile loading two failure modes were considered: tensile and shearing failure.

It is known that in-plane failure is the dominant mechanism in tensile failure of fibre-dominated composites [Chang, 1986]. Tensile failure can result from a combination of the tensile stress σ_x and the shear stress σ_{xy}. A failure index e_t can be defined in terms of these stresses and the strength parameters X_t, Y_t and S_c (to be defined later). When the failure index exceeds 1.0, material failure is assumed to occur. The failure index is defined as follows:

$$e_t = \left(\frac{\sigma_x}{X_t}\right)^2 + \frac{\int_0^{\gamma_{xy}} \sigma_{xy} d\gamma_{xy}}{\int_0^{\gamma_{xy}^u} \sigma_{xy} d\gamma_{xy}} \tag{4.2}$$

where e_t is the tensile failure , σ_x and σ_{xy} are the tensile stress and shear stress, respectively, in each layer of plies in a laminate. X_t is the longitudinal tensile strength and γ_{xy}^u the ultimate shear strain. The shear stress-shear strain relationship is written as

$$\gamma_{xy} = \left(\frac{1}{G_{xy}}\right)\sigma_{xy} + \alpha\sigma_{xy}^3 \tag{4.3}$$

where G_{xy} is the (initial) ply shear modulus and α [10] a nonlinearity factor. Introducing the ply shear stress-shear strain relationship of equation (4.3) into equation (4.2) gives

$$e_t = \left(\frac{\sigma_x}{X_t}\right)^2 + \frac{\frac{\sigma_{xy}^2}{2G_{xy}} + \frac{3}{4}\alpha\sigma_{xy}^4}{\frac{S_c^2}{2G_{xy}} + \frac{3}{4}\alpha S_c^4} \tag{4.4}$$

where S_c is the in-situ ply shear strength and for laminates with linear elastic behaviour ($\alpha = 0$), Equation 4.4 can be reduced to

$$e_t^2 = \left(\frac{\sigma_x}{X_t}\right)^2 + \left(\frac{\sigma_{xy}}{S_c}\right)^2 \tag{4.5}$$

Therefore, the tensile failure criterion states that when the stresses σ_x and σ_{xy} in any one

[10] α is a constant that was determined experimentally by Chang. Kuo and Chang. Yen, 1986

of the plies in a laminate satisfy Equation (4.4) (with $e_t^2 \geq 1$), tensile failure occurs in that layer. When tensile failure occurs in a layer, the longitudinal modulus E_x and Poisson's ratio ν_x of that layer are reduced to zero, i.e. the matrix can no longer carry any load in tension. However, the transverse modulus E_y, and the shear stress-strain relations remain unchanged, i.e. in the failed layer the in-plane properties are reduced as follows:

For $\sigma_x > 0$ and $e_t^2 \geq 1$

$$\begin{bmatrix} \dfrac{E_x}{1-\nu_x\nu_y} & \dfrac{E_y\nu_x}{1-\nu_x\nu_y} \\ \dfrac{E_x\nu_y}{1-\nu_x\nu_y} & \dfrac{E_y}{1-\nu_x\nu_y} \end{bmatrix} \longrightarrow \begin{bmatrix} 0 & 0 \\ 0 & E_y \end{bmatrix}$$

$$\overline{G}_{xy} = \frac{\partial f(\gamma_{xy})}{\partial \gamma_{xy}} \longrightarrow \frac{\partial f(\gamma_{xy})}{\partial \gamma_{xy}} \text{ (i.e. unchanged)}$$

For predicting fiber-matrix shearing failure, the criterion can be expressed as:

$$e_{fs} = \left(\frac{\sigma_y}{Y_t}\right)^2 + \frac{\int_0^{\gamma_{xy}} \sigma_{xy} d\gamma_{xy}}{\int_0^{\gamma_{xy}^u} \sigma_{xy} d\gamma_{xy}}$$

or

$$e_{fs} = \left(\frac{\sigma_y}{Y_t}\right)^2 + \frac{\dfrac{\sigma_{xy}^2}{2G_{xy}} + \dfrac{3}{4}\alpha\sigma_{xy}^4}{\dfrac{S_c^2}{2G_{xy}} + \dfrac{3}{4}\alpha S_c^4} \tag{4.6}$$

where e_{fs} is the shearing failure, σ_y and Y_t are the transverse tensile stress and strength, respectively, in each ply. For linear elastic laminates, Equation (4.6) can be reduced, as before to

$$e_{fs}^2 = \left(\frac{\sigma_y}{Y_t}\right)^2 + \left(\frac{\sigma_{xy}}{S_c}\right)^2 \tag{4.7}$$

The fibre failure criterion states that when, in any one of the plies in a laminate, the stresses σ_y and σ_{xy} in combination satisfy the criterion $e_{fs}^2 > 1$, that layer fails by

fibre-matrix shearing. In fibre matrix shearing failure mode, the material can still carry direct load in the fibre direction, but shear loads can no longer be carried. This is modelled by reducing the shear modulus and the Poisson's ratios, ν_y, and ν_x, to zero.

For $\sigma_x < 0$ and $e_{fs}^2 > 1$

$$\begin{bmatrix} \frac{E_x}{1-\nu_x\nu_y} & \frac{E_y\nu_x}{1-\nu_x\nu_y} \\ \frac{E_x\nu_y}{1-\nu_x\nu_y} & \frac{E_y}{1-\nu_x\nu_y} \end{bmatrix} \longrightarrow \begin{bmatrix} E_x & 0 \\ 0 & E_y \end{bmatrix}$$

$$\overline{G}_{xy} = \frac{\partial f(\gamma_{xy})}{\partial \gamma_{xy}} \longrightarrow 0$$

Similar failure criteria were used to determine the material failure in the adhesive. The parameters were changed to account for the adhesive stiffness and strength properties.

4.3 MODEL CALIBRATION

FE models are mathematical representations of the physical behaviour of structures and therefore need to be calibrated against experimental tests, to demonstrate their accuracy and compatibility. The models can then be modified to predict the behaviour of the structure under different geometry and material parameters. The FE analysis procedure in this investigation consisted of two stages: cyclic bending and ultimate strength analysis. The cyclic analyses were used to investigate the effect of cyclic loading on the curing of the adhesive. These effects were then added to the ultimate strength analyses. In this way it was possible to investigate the overall effect of cyclic loading on adhesive cure and the efficiency of the composite strengthening in terms of on the load carrying capacity of the reinforced steel beam.

4.3.1 Cyclic loading stage

The most important part of this stage was to take account of the change in the material properties of the adhesive with time while the adhesive is curing. The FE model was created to deal with material property changes, taking account of the increase in adhesive strength and stiffness during the curing period. It was assumed that the adhesive stiffness has a linear form over approximately 18 hours until reaching its peak value. Similar assumption was made with regard to strength properties.

The sinusoidal loading imposed in the test, detailed in chapter 3, was replaced by linear changes in the cyclic loading as shown in Figure 4.4. This was done to minimise the computing time and to reduce the model complexity. Two loads defined each load cycle - one was the peak, which was the maximum value of the cyclic load and the other the trough, which was set at 1kN. This was done to give similar loading conditions to those in the experiments.

The cyclic model was calibrated against experimental bending stiffness data obtained in Chapter 3 (Figure 3.10). Therefore, for a given value of adhesive's stiffness and strength with respect to time, the stiffness of the FE model reinforced beam was calibrated against the experimental stiffness. Figure 4.5 shows a comparison between the calibrated FE and the experimental specimen. Same procedure was carried out for all the specimens.

A special macro was used in the cyclic loading model to identify the occurrences of failure indexes (tensile and shear failure) in elements and reduce the mechanical properties of those elements accordingly. Figure 4.6 shows the progression of material failure in the adhesive, as a function of the maximum cyclic loading.

4.3.2 Ultimate strength analysis stage

The second phase of the analysis accounted for the progressive failure in the adhesive from cyclic loading phase (debonding) and also included web stiffeners added at the load and support points to prevent premature failure of the compression flange (as discussed in Chapter 3). Concentrated load was applied at mid-span and analyses were carried out to failure, which was reached when large increases in deflection were caused by a very small load increment. Initial yielding appeared around the mid-span loading point and progressed throughout the web and the compression flange with increase in load. The behaviour was similar to the formation of a plastic hinge within the structure.

4.3.3 Results

Figures 4.7 to 4.11 compare the load-deflection curves predicted by the FE models with the corresponding experimental curves. The results of the FE analyses can be seen to be in good agreement with the experimental results. It also can be seen from Figure 4.12 that the stiffness and load carrying capacity of the structure decreases with higher magnitude of cyclic loading

As expected, the FE models confirmed that all the specimens failed due to steel yielding in the compression flange and the web near the applied concentrated load. Table 4.1 gives a comparison between the FE and the experimental bending stiffness values and shows that the FE predictions overestimated the stiffness by up to 9%. The variation in material properties (see Figure 4.3) could account for the difference, but the differences between the FE and the experimental results are small enough to be considered acceptable.

No further material failure was found in the adhesive during the ultimate strength analysis, as the fully cured adhesive was capable of transferring the shear stress across the steel composite interface and was able to also withstand quite large strain. Also no failure occurred in the CFRP plate, due to CFRP plate strength being much greater than

that of the steel so that while the steel beam experienced extension yielding, the stresses in the CFRP plate only reached around half of the failure stress level.

Tables 4.2 and 4.3 show the results of FE and hand calculations for the shear and the slip in the adhesive, respectively. There is a good agreement between the calculated slip values in the adhesive and the finite element values. It also shows that the predicted shear stress values in the model were much lower than the maximum shear stress allowed in the design. The design shear stress distribution is assumed to be constant over the length of the adhesive for simplicity purposes; however, this is not the case as the shear stress distribution tends to have a lower value in middle and peaks toward the plate's ends. This will be described later in this chapter. Hence the design shear stress values tend to be higher than the FE values.

Overall, the model has shown good correlation and agreement with the experimental and theoretical values. Hence, it was felt that the model did represent the physical structure and was adequate for further parametric studies.

4.4 PARAMETRIC STUDY

The calibrated model was used in further analyses to investigate the effect of cyclic loading on the performance of the adhesive used in I-beams of more practical dimensions. Therefore, the result of the model was extrapolated to 3m and 5m beams. Table 4.4 shows the range of specimens used in the FE analysis. The beam identifications are similar to those used for the model beams, i.e. SB17/3 is 3m steel beam subjected to a cyclic loading of 17kN. Control and unreinforced beams were also analysed and the load-deflection graphs are shown in Figures 4.13 and 4.16.

It was discussed in Chapter Three that during the early stages of curing of the adhesive, although the carbon plate is in contact, no shear would be transferred across the adhesive. Consequently there will be relative slip between the steel and the carbon fibre plate, which beyond a certain limit would lead to debonding.

The range of the loadings for the 3m and the 5m beams was selected in such a way that, the biggest of the range represent a cyclic loading that would produce stress values near to yield stress of steel in the structure and the rest were selected to represent a practical range of applied load that we would be expecting.

The FE cyclic models were calibrated by varying the adhesive stiffness value so that the initial slip in the FE analyses was in close agreement with the hand-calculated slip values in which the slip was determined only by the extension of the tension flange, as in the slip calculations explained in Appendix C.

Shear stress calculations for the 3m and the 5m specimens for different load magnitudes are shown in Tables 4.5 to 4.8. The results follow similar patterns to the model specimens and showed extremely good correlation between the finite element and hand-calculated results.

4.5 MATERIAL FAILURE IN ADHESIVE UNDER THREE POINT BENDING CONDITIONS

Figures 4.13 to 4.16 show the load-deflection graphs for the 3m and the 5m span reinforced I-beams and it can be seen that the bending stiffness decreases with higher magnitude of initial cyclic loading. This was expected, as higher magnitude of cyclic load will increase the material failure within the adhesive (debonding) and hence decreases the overall stiffness.

It is believed that the adhesive in the early stages of curing can only withstand a small amount of lateral movement (slip), and if the slip is greater than a certain limit it will cause material failure (debonding) in the adhesive. Since the initial material failure in the adhesive is achieved when lateral movement in the adhesive exceeds a certain value, it is reasonable to assume that this would be valid in all beams irrespective of their size. An investigation was carried out to verify that this was the case.

Using the model beam adhesive property, stiffness and strength with respect to time under curing process, it was found that initial failure occurred in all specimens at a lateral movement of approximately 0.17mm and continued up to a value of 0.32mm at which there was a loss of approximately 90% of the adhesive contact. Table 4.9 summarises the results of the investigation and Figure 4.17 shows the percentage loss of adhesive contact (Table 4.9) with respect to lateral movement in the tension flange and it can be seen that all specimens (1m, 3m and 5m spans) have followed the same pattern. Figure 4.18 shows the best-fit curve that represents the loss of adhesive contact on all specimens.

Therefore, for any reinforced steel beam, it is possible to determine the amount of material debonding in the adhesive, when it was subjected to continuous cyclic loading while curing. It is then possible to calculate the bending stiffness of the reinforced steel beam using the area transformation method [LINK, 2000].

The steps to calculate the stiffness of the reinforced metallic structure, after it has been subjected to continuous cyclic loading while the adhesive was curing, are as follows:

1. Calculate the slip for any given load using the procedure explained in Chapter 3 (section 3.2.4).

2. Plot the curve which shows the amount of debonding with respect to slip in the adhesive for reinforced beams subjected to three point bending, using the equation curve shown in Figure 4.18:

$$y = 90\left(1 - e^{-24(x-0.14)}\right) \tag{4.8}$$

where y is the percentage adhesive strength loss, and x the slip in the adhesive layer.

3. Recalculate the effective area of the CFRP plates to account for the amount that is no longer in contact with the beam due to loss of adhesive.

4. Calculate the new composite stiffness, using the transformed section method, given in Appendix C.

This procedure was carried out for all three length of specimens. Tables 4.10 to 4.12 show the comparison between the FE and the hand calculated bending stiffness values. The results show very good agreement between the two methods, with hand-calculated method slightly overestimating the bending stiffness by up to 5%.

4.6 PARAMETRIC STUDY ON SHEAR STRESS DISTRIBUTION ON ADHESIVELY REINFORCED STRUCTURES

Debonding of the plate from the structure is an important failure mode as it prevents the full ultimate flexural capacity of the retrofitted structure from being achieved. Debonding failure depends largely on the interfacial shear and normal stresses between the structure and the bonded plate. This problem is described in term of adherends 1 and 2, where adherend 1 is the beam and adherend 2 is the soffit plate. Under normal stresses in the thickness direction, the adhesive layer will deform, so the vertical displacements at the bottom of adherend 1 and the top of adherend 2 differ. As a result, the curvature of the beam differs from that of the soffit plate. It is usually allowed in theoretical analysis of the interfacial shear stress that the curvature of both adherends is the same and also assumed that the shear stress in the adhesive layer do not vary through the thickness [Shiuh-Chuan, 1999].

At the ends of the plate, however, there is a sudden change in the cross-section from the basic unplated member to the plate-reinforced member. Consequently, the axial plate force is discontinuous at the end of the plate and leads to stress concentration at the plate ends. In some circumstances [Ascione, 2000], the investigation has shown that the

shear stress at the ends of the plate exhibited values much higher than the mean value predicted by classical theory.

In this study the variation in the shear stress across the adhesive layer will be investigated by conducting ultimate strength FE analysis of lap shear specimens with dimensions given in Figure 4.19. Based on the findings, recommendations will be made as to taking appropriate precaution in designing reinforced structures.

4.6.1 FE analysis

The dimensions of the model were the same as the experimental specimen, shows in Figure 4.19. All materials were modelled with 8-noded linear brick elements, which had reduced integration with hourglass control to prevent shear locking. Figure 4.19 shows the finite element mesh produced for this investigation. A convergence study was carried out similar to that of the model beam to optimise CPU time and geometrical mesh that yield accurate solutions. The whole specimen was modelled due to lack of symmetry. One side of the specimen was restrained to represent fully fixed conditions, as shown in Figure 4.20 and tensile loading was applied to the other side of the specimen.

The inputted material properties for the adherends in the FE analysis were the same as those used in modelling the reinforced beam, which was shown to be in good agreement with the experimental results. Therefore, by inputting the same FE data into the lap shear model, it would be a reasonable assumption that the model will represent the material behaviour of the specimen with good accuracy.

Adhesive was taken to be fully cured and CFRP plate to be fully bonded to the steel plate. After imposing a tensile force on the specimen, the shear force was monitored over the lap-joint area. Similar macro to that of the model beam was used in the model to identify the occurrence of failure and to reduce the material properties accordingly. However, for the purpose of this investigation, the distribution of shear force was monitored until failure had occurred in the specimen. This was done so that comparison

can be made between the FE results and the classical theory of calculating the shear force in lap joint structures.

4.6.2 Theoretical calculations

Shiyh-Chuan (1999) presented a one-dimensional solution for calculating the shear stress in the adhesive layer in a single-lap shear joint, as shown in Figure 4.21. The eccentric load path, due to dissimilar adherends, may result in bending deflections and joint edge moment at the free ends of the overlap region. To simplify the model, the thickness of the adherends was assumed to be small enough so that the bending effect would be neglected. The following assumption were also made:

- The shear stress in the adhesive layer did not vary through the thickness.
- The longitudinal stresses in the adherends did not vary through the thickness.
- The adherends and adhesive layer were linear elastic, and joint edge moment was neglected.

The dimension notation of the joint is shown in Figure 4.21. The free-body-diagram of an infinitesimal element in the overlap region is shown in Figure 4.22. As a result of tensile force, the longitudinal tensions T_0 and T_i in the upper and the lower adherend, respectively, and the shear stress τ in the adhesive layer can be expressed in the following forms (Appendix D):

$$T_o = P\left[-\frac{1}{2}\frac{\sinh(\lambda x)}{\sinh(\lambda l)} + \frac{E_i t_i - E_o t_o}{2(E_i t_i + E_o t_o)}\frac{\cosh(\lambda x)}{\cosh(\lambda l)} + \frac{E_o t_o}{(E_i t_i + E_o t_o)}\right] \tag{4.9}$$

$$T_i = P\left[1 + \frac{1}{2}\frac{\sinh(\lambda x)}{\sinh(\lambda l)} - \frac{E_i t_i - E_o t_o}{2(E_i t_i + E_o t_o)}\frac{\cosh(\lambda x)}{\cosh(\lambda l)} - \frac{E_o t_o}{(E_i t_i + E_o t_o)}\right] \tag{4.10}$$

$$\tau = \frac{P\lambda}{2}\left[\frac{\cosh(\lambda x)}{\sinh(\lambda l)} - \frac{E_i t_i - E_o t_o}{(E_i t_i + E_o t_o)}\frac{\sinh(\lambda x)}{\cosh(\lambda l)}\right] \tag{4.11}$$

$$\lambda^2 = \frac{G_a}{\eta}\left(\frac{1}{E_i t_i} + \frac{1}{E_0 t_0}\right)$$

where l is the half-length of the bonded region (Figure 4.21), E_o and t_o the Young's modulus and the thickness of the upper adherend, respectively, E_i and t_i the respective properties of the lower adherend. G_a is the shear modulus of the adhesive, and γ and η are the shear strain and thickness of the adhesive layer, respectively.

EUROCOMP [Clarke, 1996] used an alternative, more complex analysis by taking into account the severe shear stress change with discontinuity of cross section. This was achieved by calibrating several theories [Adams and Wake-1984, Hart Smith-1973, the ESDU-1978] and creating a design based on peak shear values. The design was based on the maximum shear stress, which occurs at the end of the joint. However, the shear stress decreases rapidly within a short distance from the joint end. It should also be noted that this peak stress occurs immediately after a load is applied, but owing to the viscoelastic nature of polymer adhesive, this peak flattens in the course of time. However, there is uncertainty with regard to the distribution of peak shear stress as a function of time.

The solutions for the adhesive shear stress, τ_x, was:

$$\tau_x = \frac{\sigma t}{8c}\left[\frac{\beta c}{t}(1+3k)\frac{\cosh\frac{\beta x}{t}}{\sinh\frac{\beta c}{t}} + 3(1-k)\right] \tag{4.12}$$

where

$$c = \frac{L}{2}$$

$$\sigma = \frac{P}{t}$$

$$\beta = \sqrt{8\frac{G_a}{E}\frac{t}{t_a}}$$

$$\lambda = \frac{c}{t}\left(\frac{6E_a t}{Et_a}\right)^{\frac{1}{4}}$$

$$R_1 = \cosh\lambda \sin\lambda + \sinh\lambda \cos\lambda$$

$$R_2 = \sinh\lambda \cos\lambda - \cosh\lambda \sin\lambda$$

$$k = \frac{cish(u_2 c)\sinh(u_1 L)}{\sinh(u_1 L)\cosh(u_2 c) + 2\sqrt{2}\cosh(u_1 L)\sinh(u_2 c)}$$

$$k' = k\frac{c}{t}\left(3(1-\nu^2)\frac{\sigma}{E}\right)^{\frac{1}{2}}$$

$$u_1 = 2\sqrt{2}u_2$$

$$u_2 = \frac{1}{\sqrt{2}t}\sqrt{3(1-\nu^2)\frac{\sigma}{E}}$$

and

P	is load per unit width
$2L$	is length of the overlap
t	is adherend thickness = $t_1 = t_2$
E	is adherend tensile modulus = $E_1 = E_2$
G_a	is adhesive shear modulus
t_a	is adhesive layer thickness
E_a	is adhesive tensile modulus
ν	is adherend Poisson's ratio

4.6.3 Results and discussions – elastic stress distribution

A series of FE analyses were carried out, with the first set of analyses using identical adherends and the second using different adherends. Analyses were carried out over a range of adherends thicknesses that were selected in such way that the biggest of the range represent a practical thickness that is commonly used in reinforcing of steel structures and the rest were selected to represent a practical range of thicknesses that we would be expecting. The specimens were referenced and numbered for identification, as shown in Table 4.13 and 4.14. The letters indicates the type of adherends used (i.e., SS is steel and steel and SC represent steel and carbon plate) and the number indicates the thickness of the adherends. The results are presented in Tables 4.13 and 4.14.

Figures 4.23 to 4.28 represent the shear distributions over the joint-lap region. It can be seen that the Figures 4.26 to 4.28, corresponding to different adherends do not show symmetrical behaviour, which is expected due to the difference in the mechanical properties of the adherends. Generally, for simple design tasks, theoretical calculations are adequate in predicting the overall level of shear stress in the adhesive layer. However, due to sudden change in cross-sectional area, one of the specimens experienced significant increase in shear at the end of the plate. In 2mm adherends cases (thin plates) the increases was significantly higher than the predicted value.

Tables 4.13 to 4.15 compare the peak shear stresses from the FE analyses and the hand-calculations values. In some cases, the peak FE shear stress values were up to 2.2 times greater than the predicted theoretical values. Although, the total value of shear stress * length (area covered under the curves) did exceed the FE requirement in all cases, as shown in Tables 4.16 and 4.17, there was still a level of uncertainty with regard to peak shear values at end corners and their effect on plate debonding. However, it should be mentioned that the EUROCOMP calculations produced lower shear stress values compared to the other theories, as can be seen from Table 4.15. All cases were satisfactory except for 2mm thick adherends, which are very thin flexible plates. Therefore, it would be advisable to introduce safety factors into the theoretical calculations involving thin adherends.

The required safety factor will differ, depending on the thickness and material properties of each adherend, Tables 4.13 to 4.14. For the current problem (reinforced I-beam), involving two dissimilar adherends (carbon and steel), a safety factor of 20% was identified from the FE analysis. Therefore, by applying the relative safety factor to the theoretical method of calculating the shear stress within the adhesive layer, the required shear distribution can be achieved to account for the peak values.

4.8 CONCLUSIONS

The FE analyses have successfully simulated the effect of cyclic loading on the performance of the adhesive in the reinforced steel beams and also shown that there is a good agreement between the FE analyses and experimental data.

The FE analyses have shown that excessive slip movement causes debonding of the adhesive layer and the behaviour is consistent throughout specimens, with different length and sizes. Therefore, it was concluded that, for reinforced beams, it is possible[11] to determine the amount of material debonding in the adhesive, when it is subjected to continuous cyclic loading during adhesive curing by using equation (4.8). It is then possible to calculate the bending stiffness of the reinforced steel beam using the area transformation method.

The FE analyses have also shown that in adhesively bonded joints with relatively thin adherends, the shear stress at the ends of reinforced plates could exhibit peak values 2 to 3 times greater than the mean values predicted by classical theory. To account for this problem, safety factors should be introduced into classical theories .

It has to be noted that further research is required with respect to shear and normal stress distribution in adhesively jointed structures. However, for the propose of this research, this problem was highlighted in small scale and tackled with aid of FE analysis to identify the exact stress distributions. Hence the use of FE analysis is recommended with regard to analysis of adhesive connections since it can provide a better understanding and more accurate results until further developments of the theory are achieved.

[11] Given similar material properties as was used in this investigation.

Specimen Ref.	Bending stiffness Experimental (kN/mm)	Bending stiffness FE (kN/mm)	Experimental /FE
Control beam	39.0	42.6	0.91
SB34	35.9	37.8	0.95
SB42	32.9	32.1	1.02
SB50	28.2	31.1	0.91
SB62	31.0	30.3	1.02

Table 4.1 Bending stiffnesses for the model beam specimens, FE and experimental results

Specimen Ref.	Maximum load (KN)	Shear stress – Hand calculation (N/mm^2)	Average Shear stress FE (N/mm^2)	Hand-calculation/FE
SB25	25.0	0.67	0.5	1.34
SB34	34.0	0.85	0.6	1.41
SB42	42.0	1.05	0.7	1.5
SB50	50.0	1.26	0.9	1.4
SB62	62.0	1.60	1.1	1.45

Table 4.2 Shear stress in the adhesive for the model beam specimen, FE and hand calculations

Specimen Ref.	Maximum load (KN)	Slip in half span-hand calculation (mm)	Slip in half span-FE (mm)	Hand-calculation/FE
SB25	25.0	0.129	0.124	1.04
SB34	34.0	0.176	0.168	1.05
SB42	42.0	0.217	0.208	1.04
SB50	50.0	0.258	0.247	1.04
SB62	62.0	0.320	0.304	1.05

Table 4.3 Slip calculations at each end of the carbon, for the model beam specimen - FE and hand calculations

Specimen Ref. 3m beam	Maximum load (KN)	Specimen Ref. 5m beam	Maximum load (KN)
SB17/3	17.0	SB13/5	13.0
SB21/3	21.0	SB16/5	16.0
SB25/3	25.0	SB19/5	19.0
SB31/3	31.0	SB23/5	23.0

Table 4.4 3m and 5m beams analysed in the parametric study (the last digit signifies the span of beam in metres)

Specimen Ref.	Maximum cyclic load Supplied (KN)	Shear stress – hand calculation (N/mm^2)	Average Shear stress FE (N/mm^2)	Hand calculation/FE
SB17	17.0	0.141	0.12	1.17
SB21	21.0	0.174	0.15	1.16
SB25	25.0	0.207	0.17	1.21
SB31	31.0	0.257	0.21	1.22

Table 4.5 Shear stress in adhesive for 3m span beam specimen, FE and hand calculations

Specimen Ref.	Maximum cyclic load supplied (KN)	Slip in half span-hand calculation (mm)	Slip in half span- FE (mm)	Hand calculation/FE
SB17	17.0	0.159	0.157	1.01
SB21	21.0	0.197	0.194	1.01
SB25	25.0	0.234	0.231	1.01
SB31	31.0	0.291	0.286	1.02

Table 4.6 Slip calculations at each end of the carbon, for 3m span beam specimen -FE and hand calculations

Specimen Ref.	Maximum cyclic load Supplied (KN)	Shear stress – hand calculation (N/mm^2)	Average Shear stress FE (N/mm^2)	Hand calculation/FE
SB13	13.0	0.060	0.05	1.2
SB16	16.0	0.074	0.07	1.1
SB19	19.0	0.088	0.08	1.1
SB23	23.0	0.106	0.09	1.2

Table 4.7 Shear stress in adhesive for 5m span beam specimen, FE and hand calculations

Specimen Ref	Maximum load (KN)	Slip in half span-hand calculation (mm)	Slip in half span-FE (mm)	Hand calculation/ FE
SB13	13.0	0.159	0.155	1.02
SB16	16.0	0.196	0.191	1.02
SB19	19.0	0.233	0.226	1.03
SB23	23.0	0.283	0.273	1.03

Table 4.8 Slip comparisons at each end of the carbon, 5m span beam specimen

Slip in half span(mm)	Adhesive debonding % Beam-1m	Adhesive debonding % Beam-3m	Adhesive debonding % Beam-5m
0.14	0	0	0
0.17	42	39	38
0.22	72	68	69
0.26	79	75	77
0.32	86	82	84

Table 4.9 Adhesive debonding relative to slip

Specimen	Bending stiffness Hand calculation KN/mm	Bending stiffness FE KN/mm	Hand calculation/FE
Control	44.65	42.65	1.04
SB34	39.29	37.87	1.04
SB42	34.49	32.16	1.07
SB50	33.17	31.14	1.06
SB62	31.77	30.28	1.05

Table 4.10 Bending stiffness comparisons, model beam specimen

Specimen	Bending stiffness Hand calculation KN/mm	Bending stiffness FE KN/mm	Hand calculation/FE
Control	18.07	17.38	1.04
SB17/3	16.23	15.68	1.03
SB21/3	14.50	13.76	1.05
SB25/3	14.03	13.18	1.06
SB31/3	13.53	12.85	1.05

Table 4.11 Bending stiffness comparisons, 3m span beam specimen

Specimen	Bending stiffness Hand calculation KN/mm	Bending stiffness FE KN/mm	Hand calculation/FE
Control	11.1	10.67	1.04
SB13/5	10.03	9.68	1.04
SB16/5	8.95	8.44	1.06
SB19/5	8.6	8.19	1.05
SB23/5	8.29	7.97	1.04

Table 4.12 Bending stiffness comparison, 5m span beam specimen

Specimen Ref.	Shear stress Hand calculation (N/mm^2)	Maximum Shear stress – FE (N/mm^2)	FE/hand calculation
SC2	14.8	17.6	1.19
SC4	19.2	22.9	1.19
SC6	23.5	28.1	1.19

Table 4.13 Maximum shear stress with respect to plate thickness-SC: steel to carbon fibre plate

Specimen Ref.	Shear stress Hand calculation (N/mm^2)	Maximum Shear stress – FE (N/mm^2)	Ratio FE/HC
SS2	14.9	32.5	2.17
SS4	17.7	18.1	1.02
SS6	20.7	20.2	0.97<1

Table 4.14 Maximum shear stress with respect to plate thickness-SS: steel to steel

Specimen Ref.	Shear stress Eurocomp (N/mm^2)	Maximum Shear stress – FE (N/mm^2)	Ratio FE/HC
SS2	17.8	32.5	1.82
SS4	19.9	18.1	0.91<1
SS6	22.8	20.2	0.97<1

Table 4.15 Maximum shear stress with respect to plate thickness-SS: steel to steel (EUROCOMP)

Specimen Ref.	Total area FE kNmm	Total area Theory kNmm	Satisfactory
SS2	245	268	Yes
SS4	268	334	Yes
SS6	334	401	Yes

Table 4.16 Total area covered under the shear stress curve-SS: steel to steel

Specimen Ref.	Total area FE kNmm	Total area Theory kNmm	Satisfactory
SC2	190	269	Yes
SC4	302	332	Yes
SC6	402	434	Yes

Table 4.17 Total area covered under the shear stress curve-SC: steel to carbon fibre plate

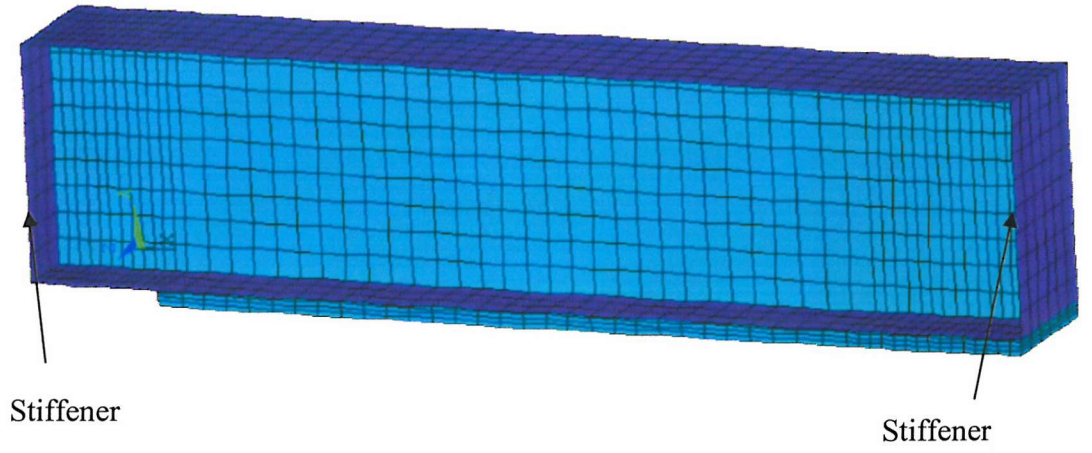

Figure 4.1 FE mesh

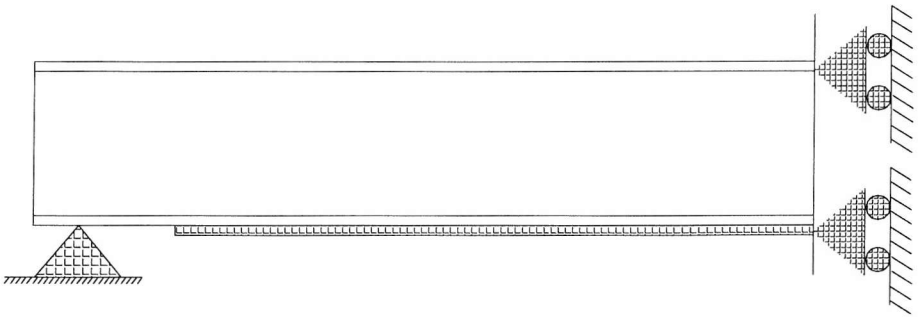

Figure 4.2 Boundary conditions for a half model

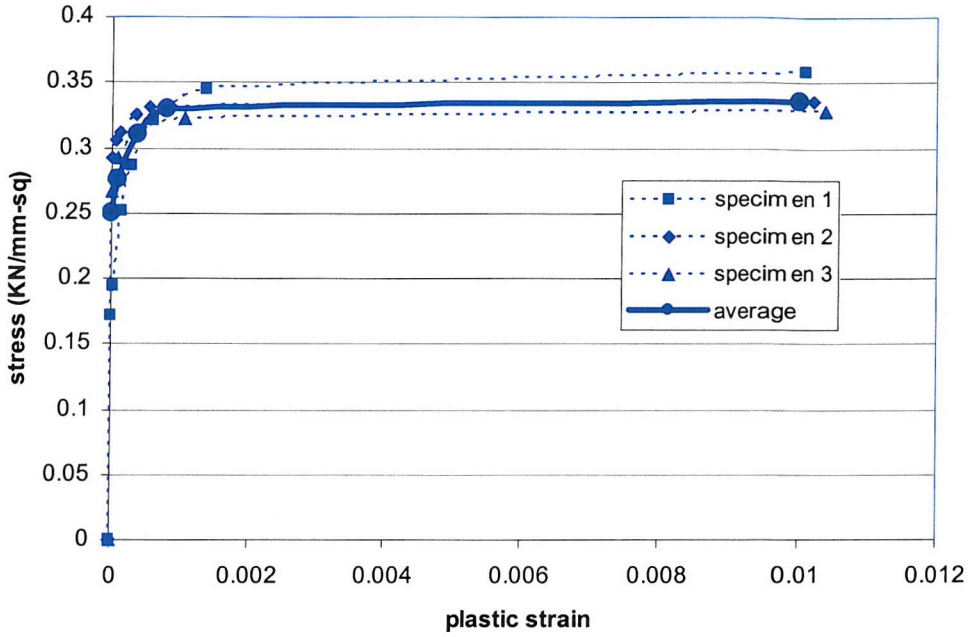

Figure 4.3 Stress-strain curve for steel

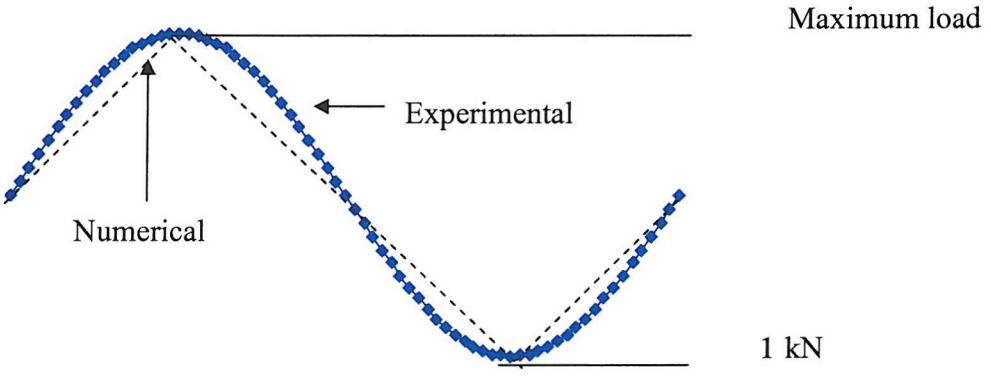

Figure 4.4 Alternative load curve

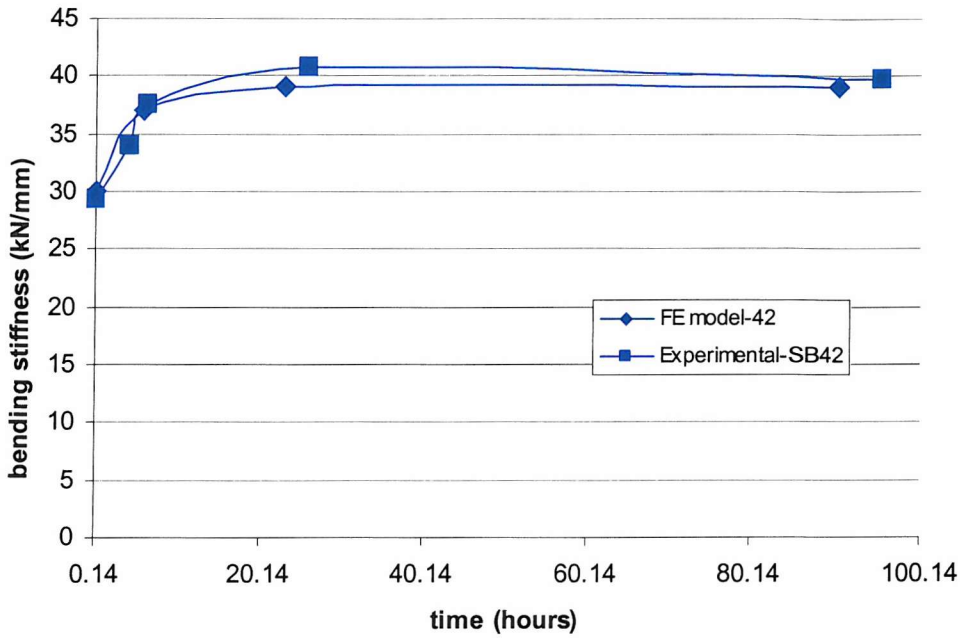

Figure 4.5 Model validation for beam SB42

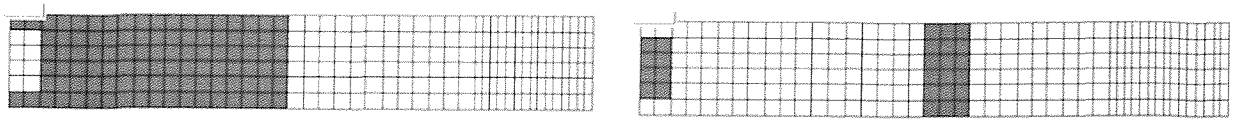

Tensile failure Shear failure

(a) SB34

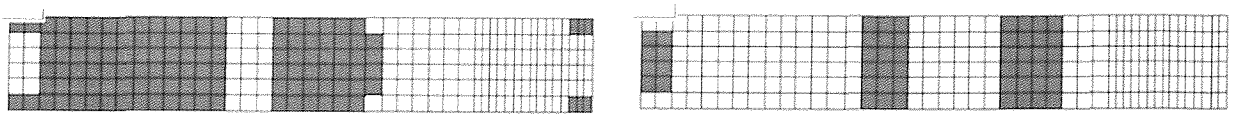

Tensile failure Shear failure

(b) SB42

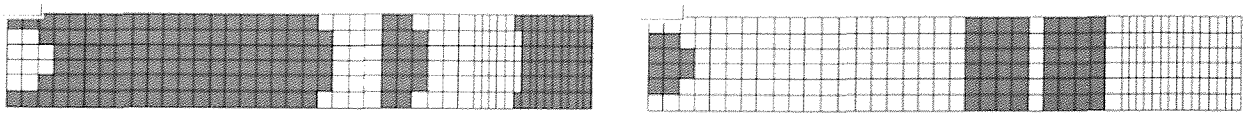

Tensile failure Shear failure

(c) SB50

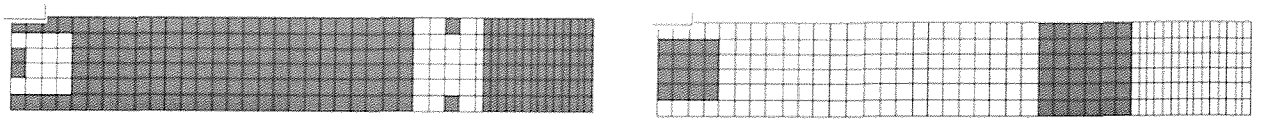

Tensile failure Shear failure

(d) SB62

Figure 4.6 Material failure (shown as shaded areas) in the adhesive due to cyclic loading

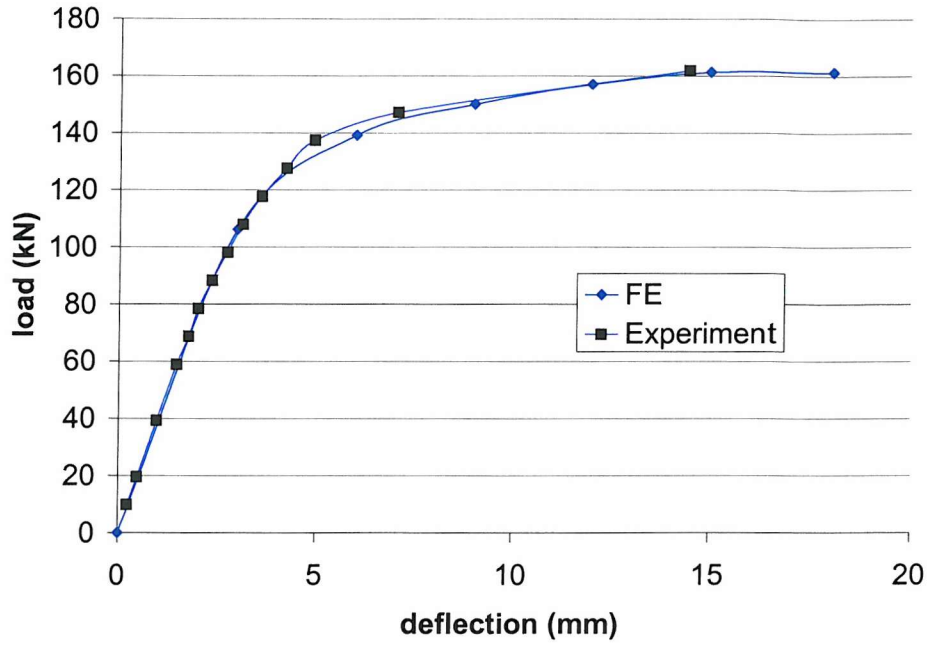

Figure 4.7 Load-deflection graph for control specimen

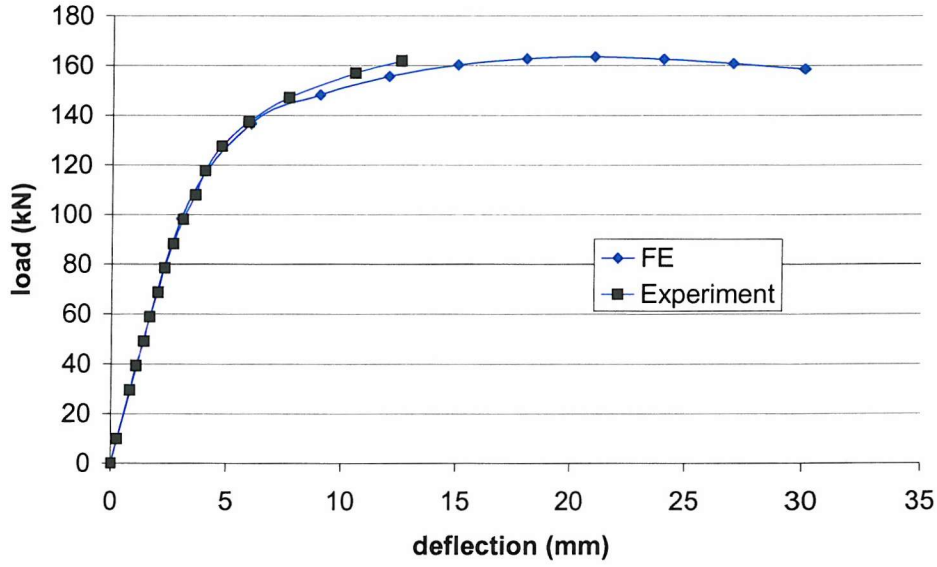

Figure 4.8 Load-deflection graph for SB34

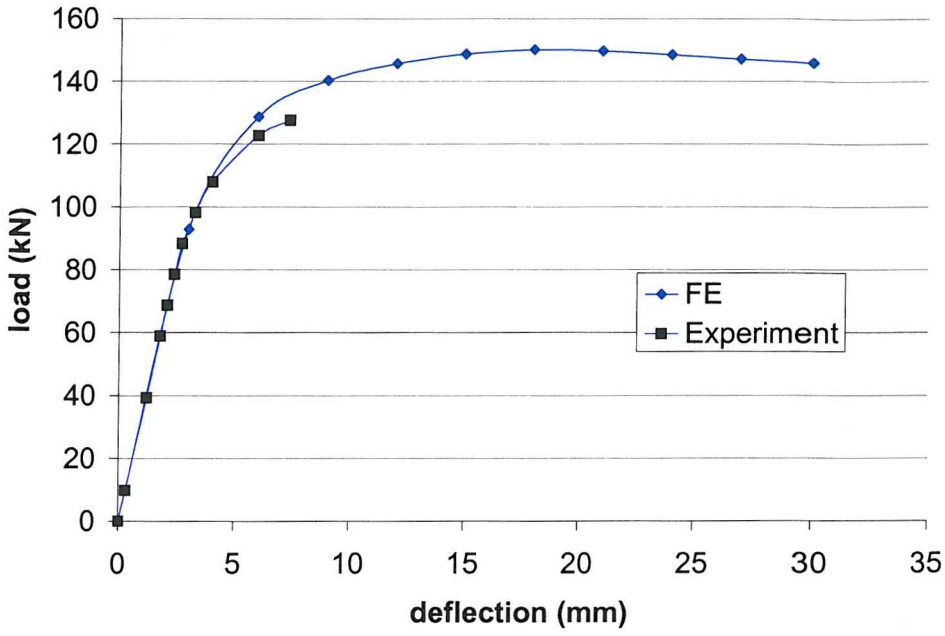

Figure 4.9 Load-deflection graph for SB42

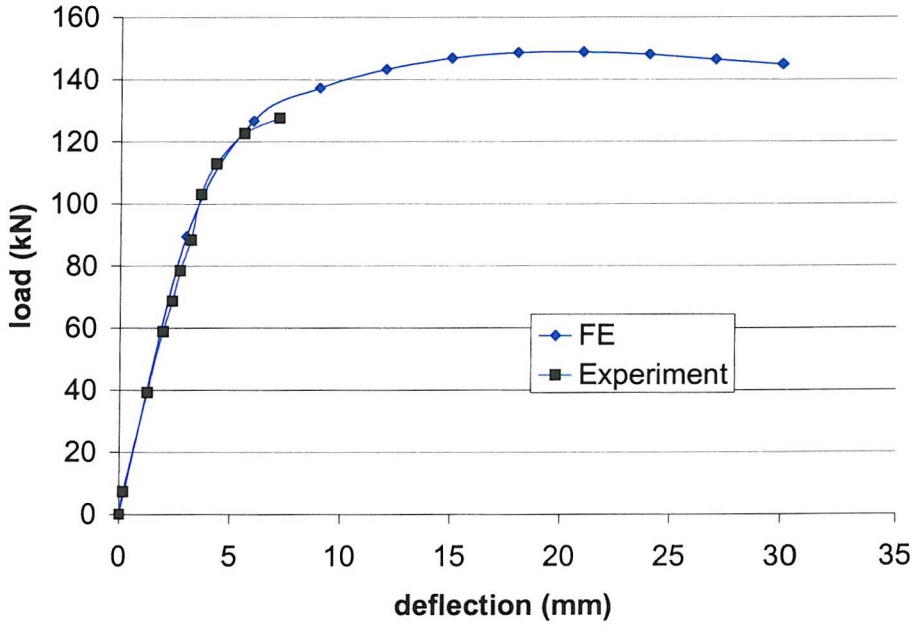

Figure 4.10 Load-deflection graph for SB50

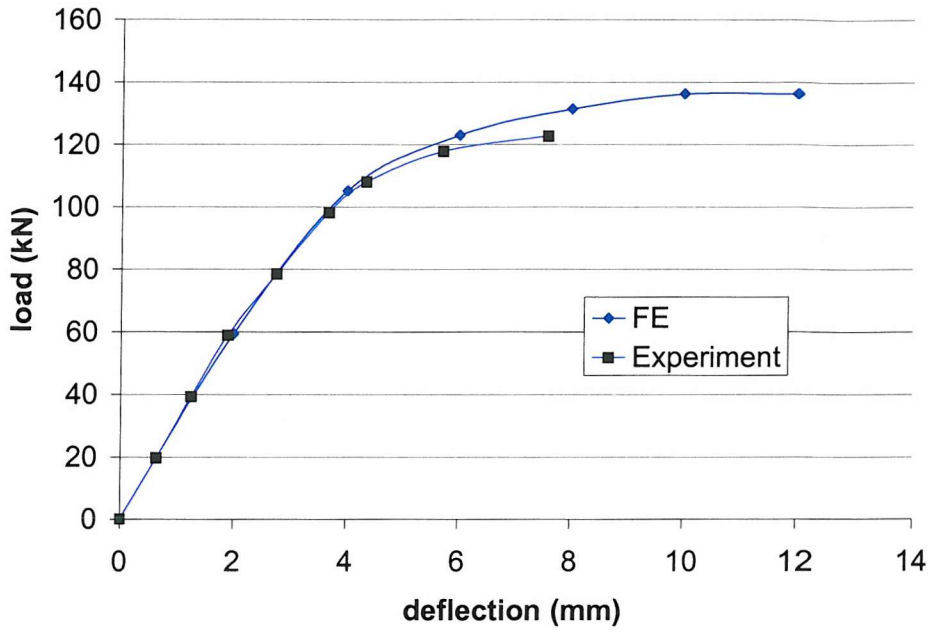

Figure 4.11 Load-deflection graph for SB62

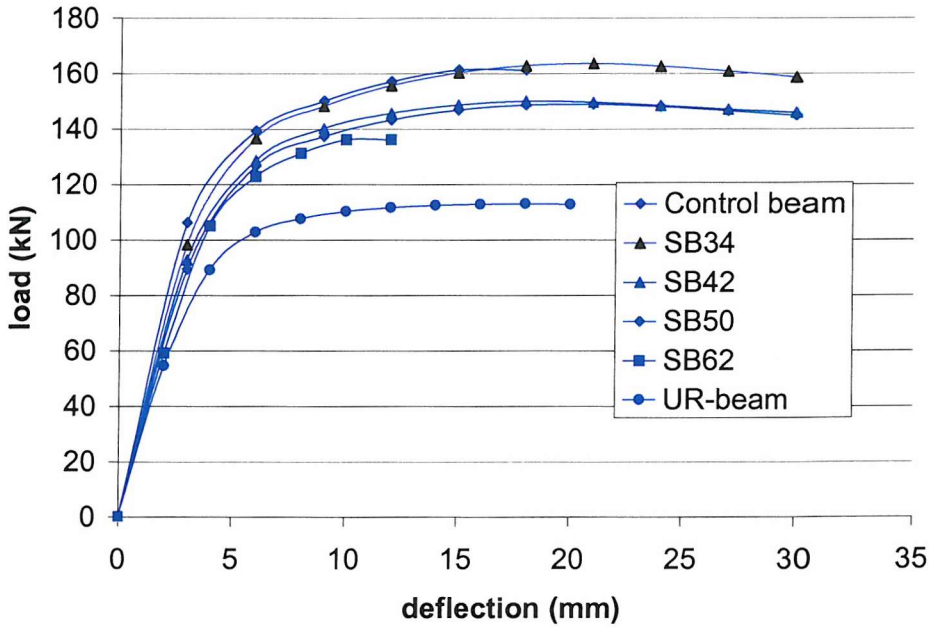

Figure 4.12 Load-deflection graph

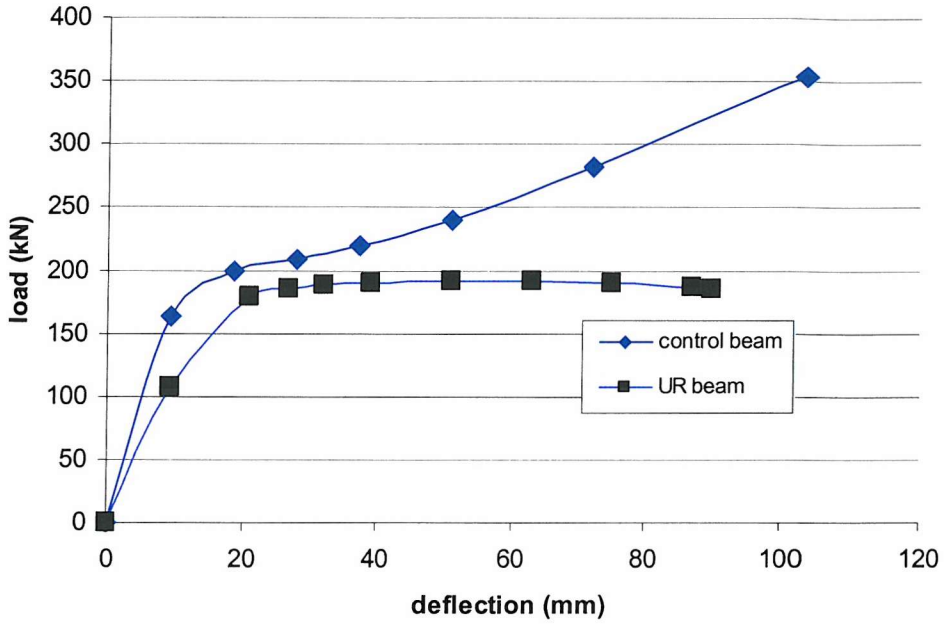

Figure 4.13 Load-deflection graph for 3m span reinforced and unreinforced specimen

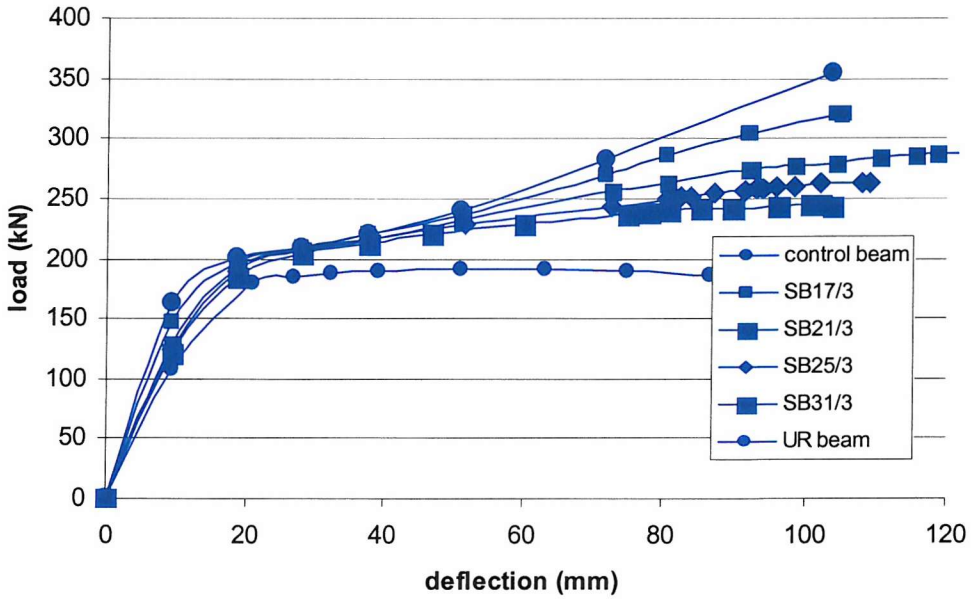

Figure 4.14 Load-deflection graph for 3m span specimen

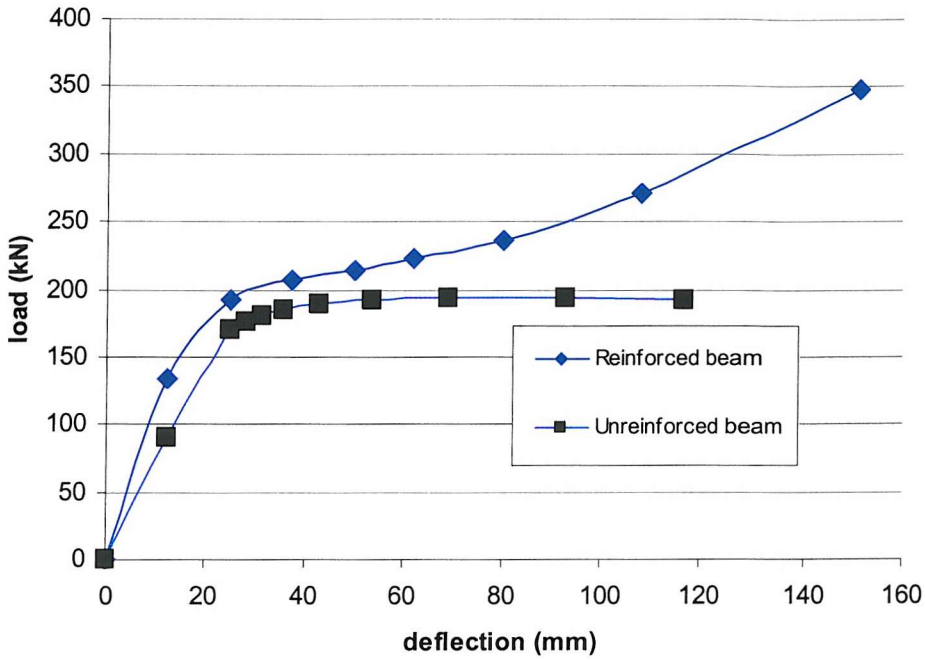

Figure 4.15 Load-deflection graph for 5m span reinforced and unreinforced specimen

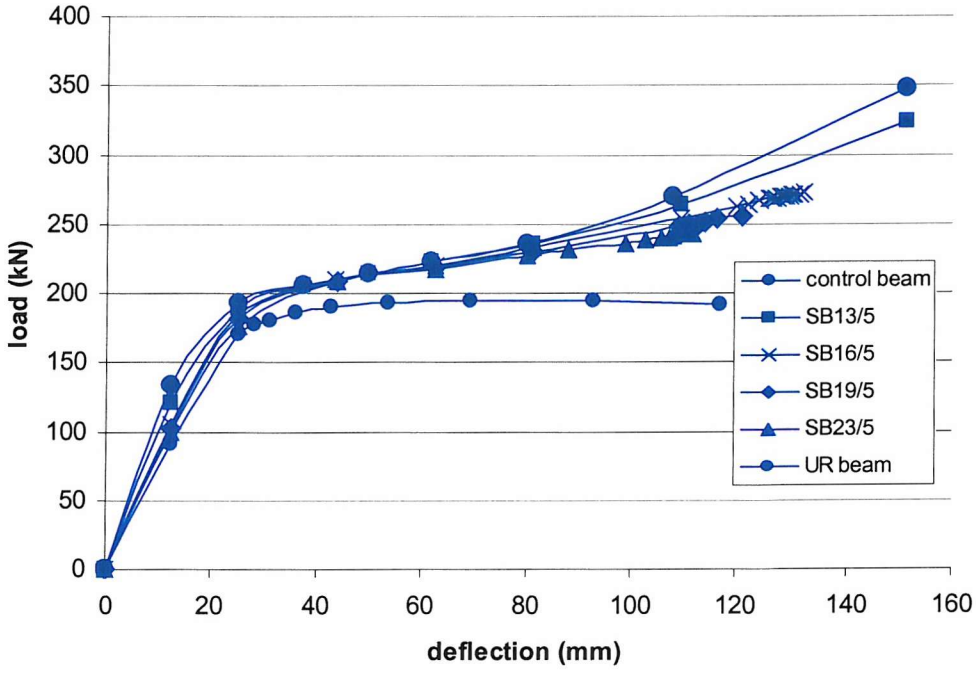

Figure 4.16 Load-deflection graph for 5m span specimen

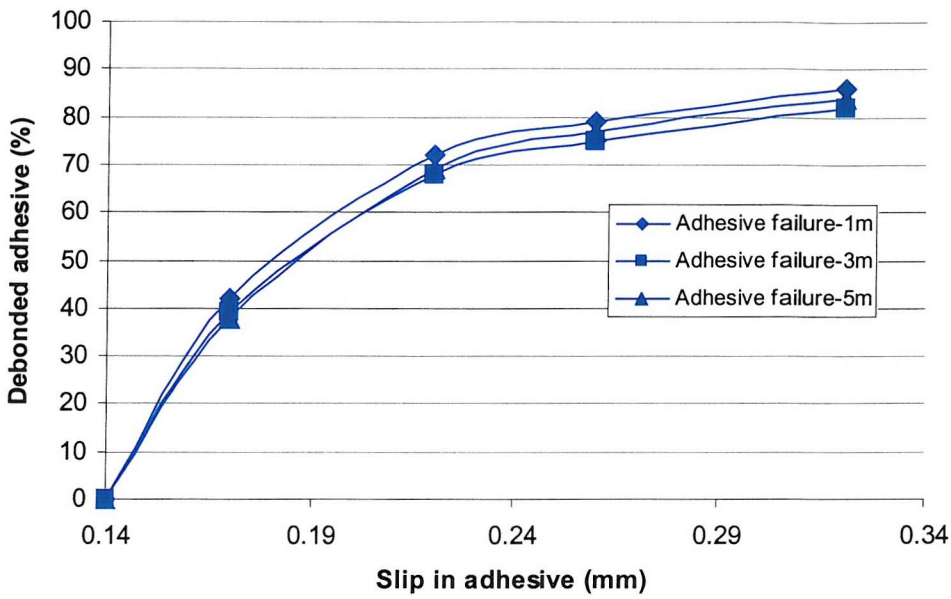

Figure 4.17 Material debonding due to slip in adhesive

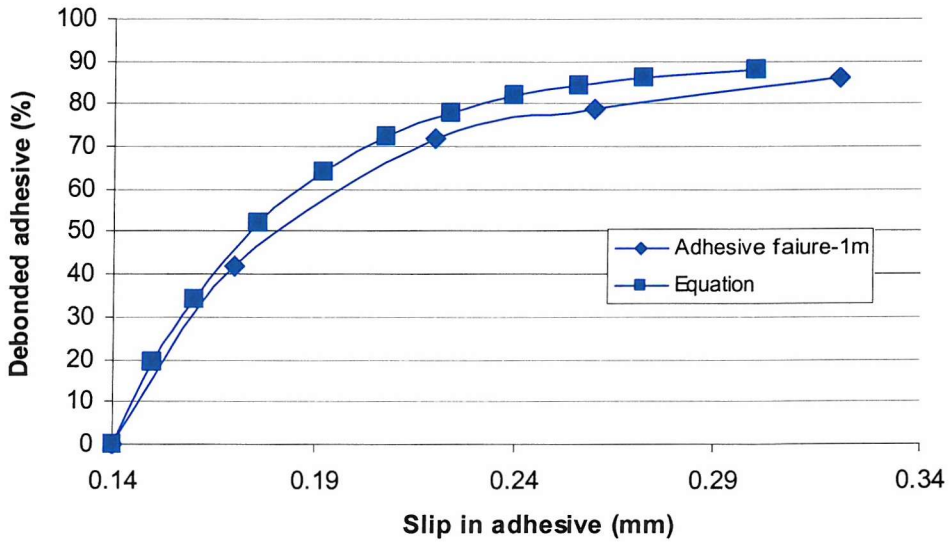

Figure 4.18 Mathematical representative of material debonding in adhesive

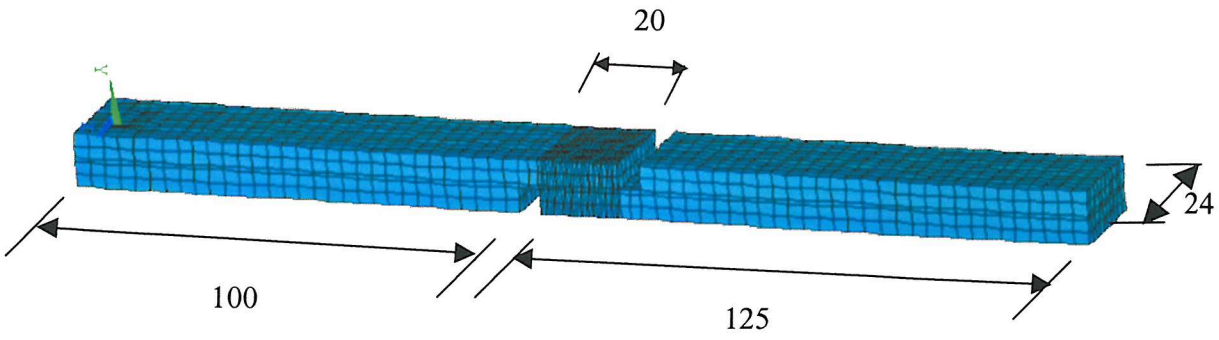

Figure 4.19 FE mesh

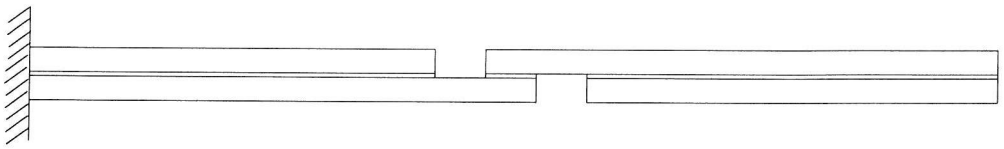

Figure 4.20 Boundary condition

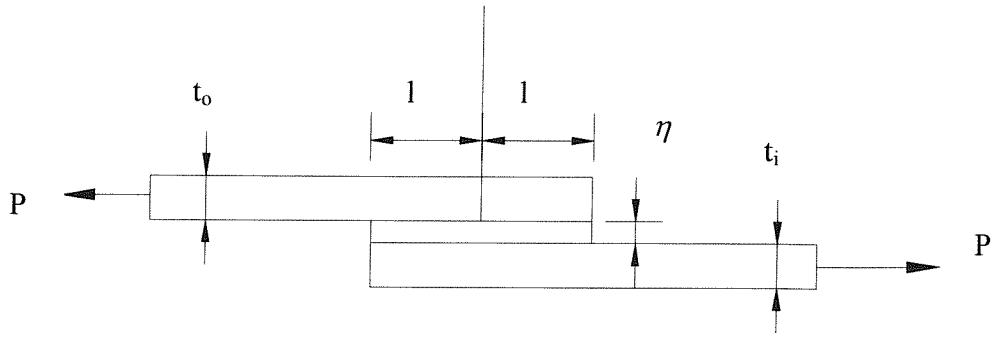

Figure 4.21 Geometric profile of a single-lap shear

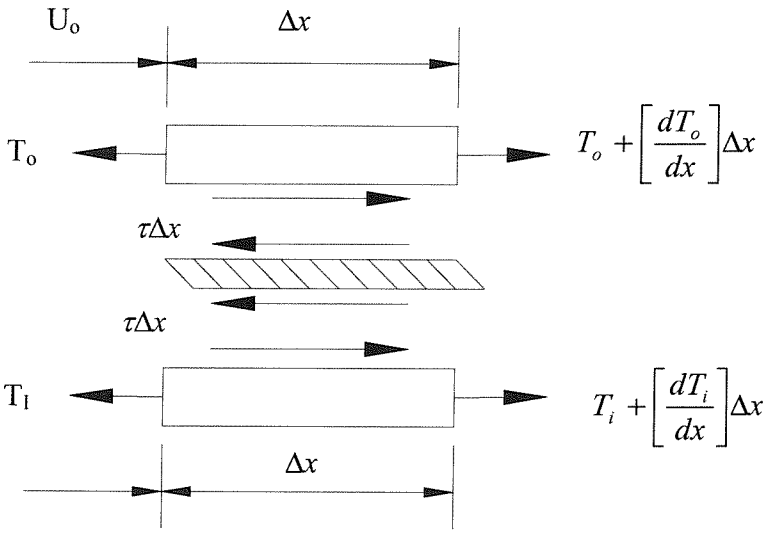

Figure 4.22 The free-body diagram of a single-lap joint- shear stress.

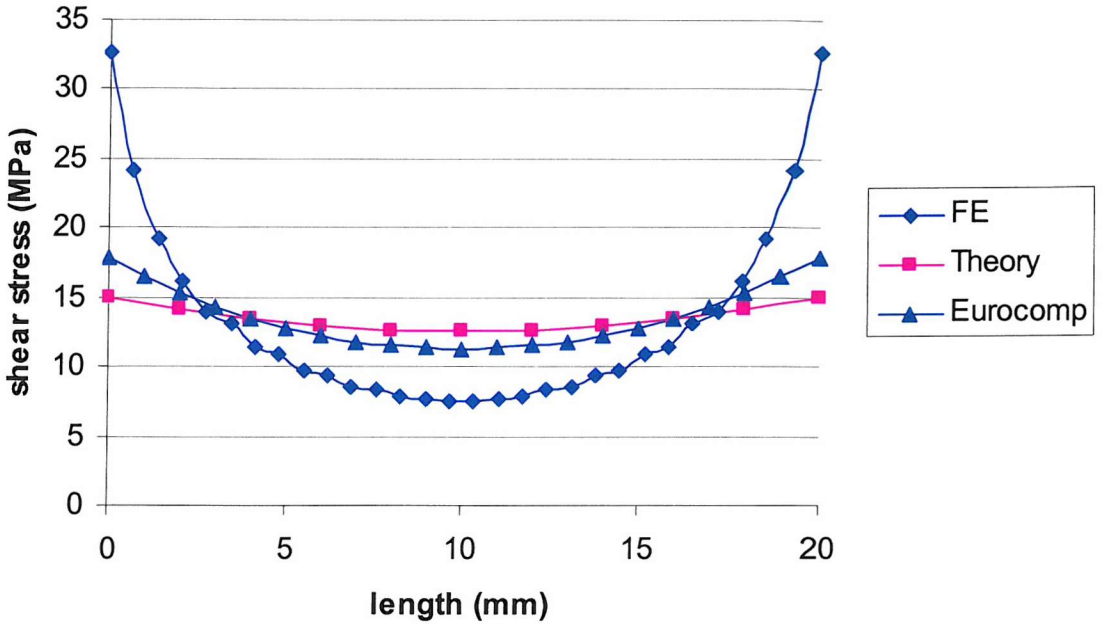

Figure 4.23 Shear distribution across the critical area for a 2 mm thick plates-steel to steel

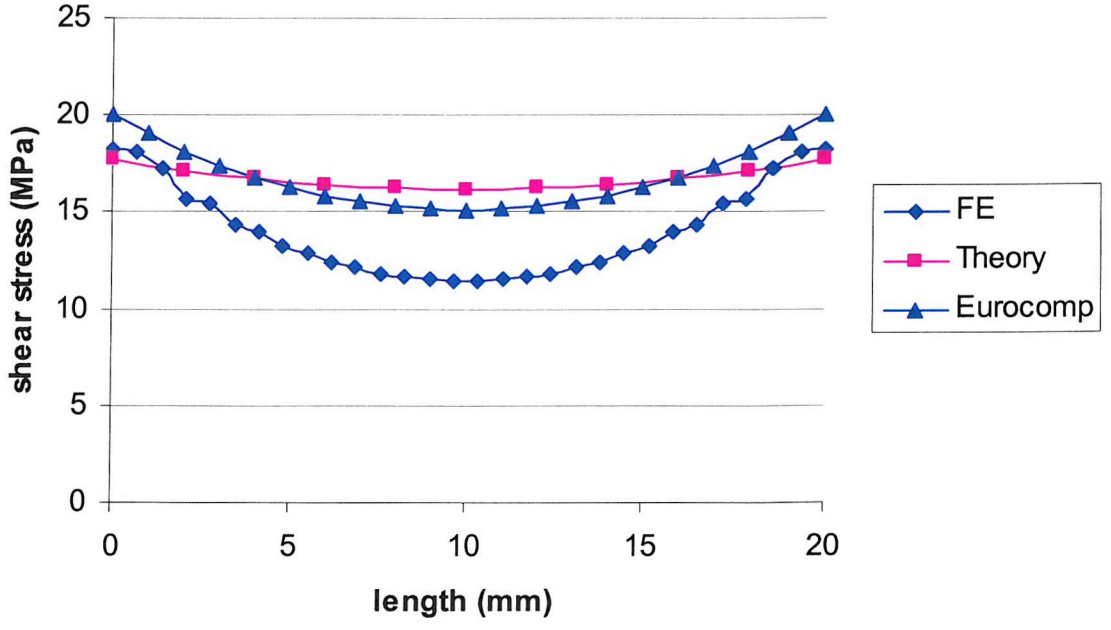

Figure 4.24 Shear distribution across the critical area for a 4 mm thick plates-steel to steel

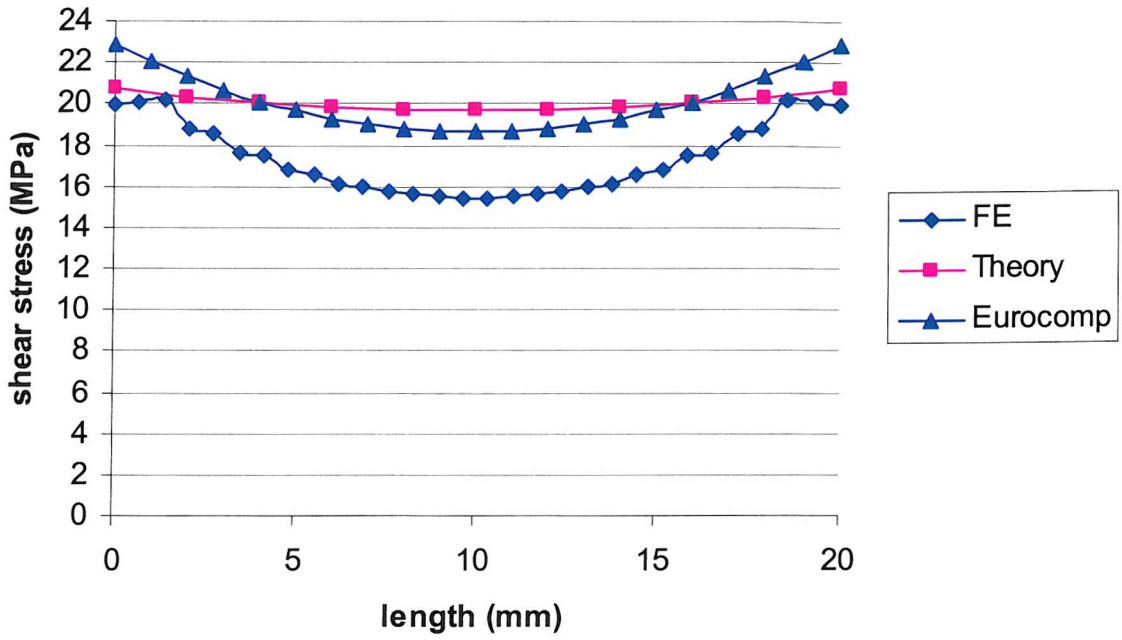

Figure 4.25 Shear distribution across the critical area for a 6 mm thick plates-steel to steel

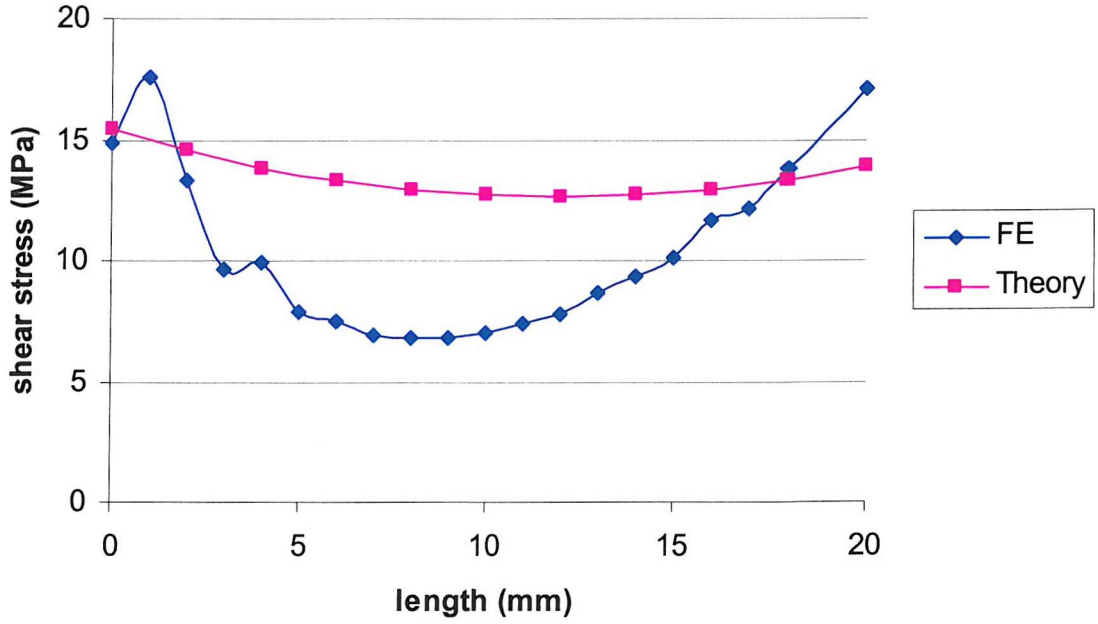

Figure 4.26 Shear distribution across the critical area for a 2 mm thick plates-steel to carbon

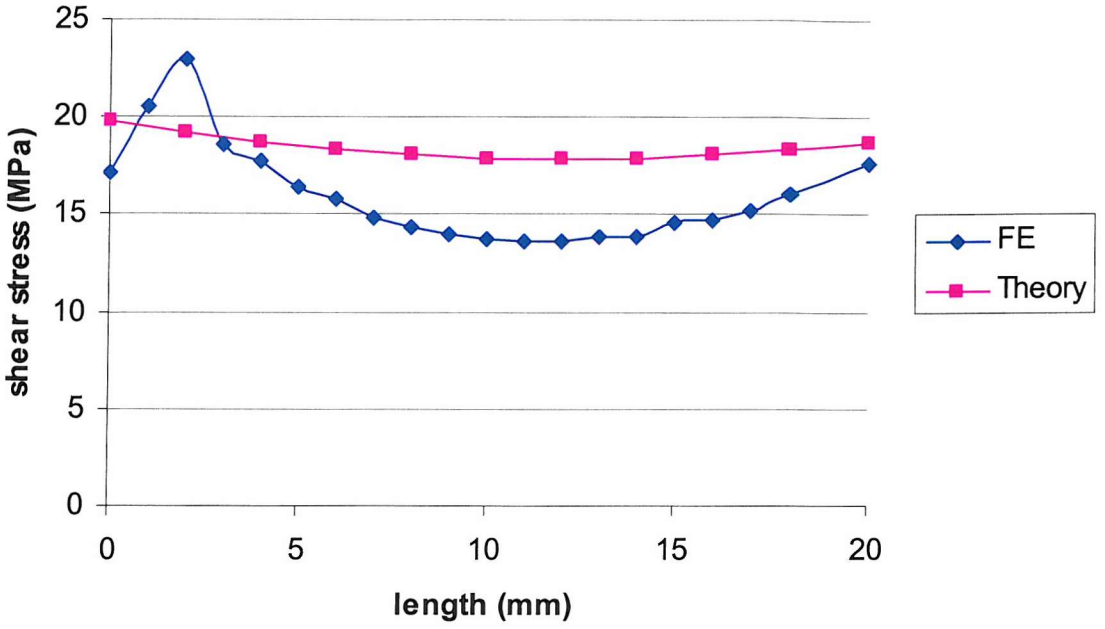

Figure 4.27 Shear distribution across the critical area for a 4 mm thick plates-steel to carbon

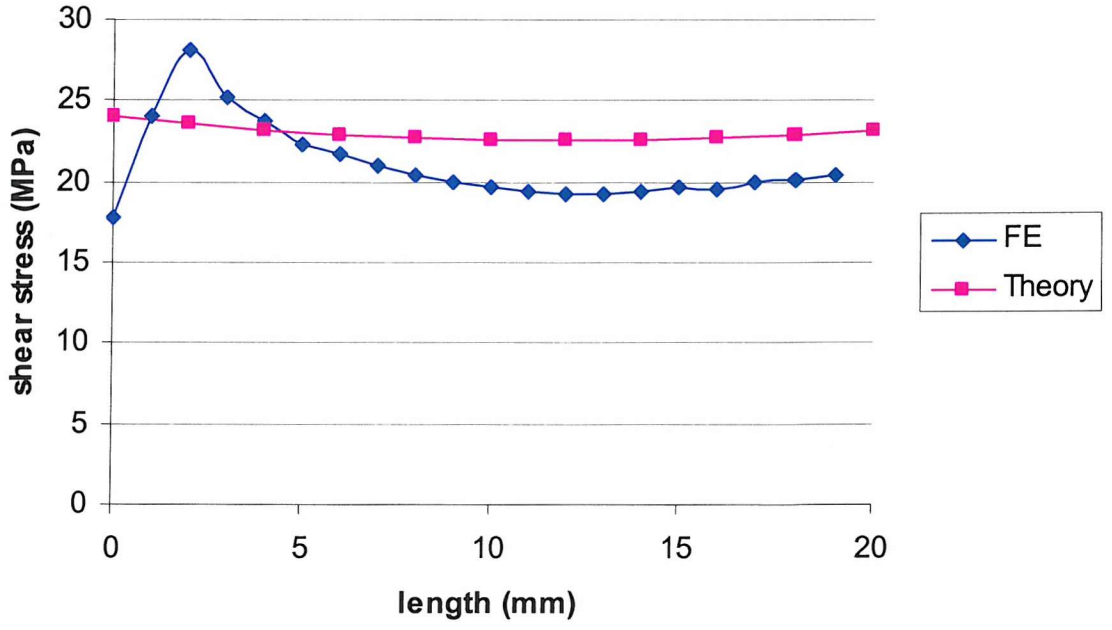

Figure 4.28 Shear distribution across the critical area for a 6 mm thick plates-steel to carbon

CHAPTER 5

AN FEA INVESTIGATION INTO CAST IRON STRUTS REINFORCED WITH CFRP

5.1 INTRODUCTION

This chapter reviews the experimental work carried out by Moy and Lillistone [1999] and details the analytical and finite element analyses of both unreinforced and reinforced cast iron struts. As previously discussed in Chapter 2 (literature review), LINK research study [Link, 2000] had focused on the usage of carbon fibre for structural rehabilitation. This project was particularly relevant to London Underground, as many of its cast iron structural holdings are over 100 years old and in need of rehabilitation.

After structural failure of one of the cast iron struts that were propping the vent shaft wall at Rotherhithe Station in London, the urgency of reinforcing the cast iron struts

for the purpose of relieving parts of the existing stresses became crucial. Three remaining struts from Rotherhithe were removed from service and tested to find their load carrying capacity, some reinforced, and some unreinforced. Each strut was 12 metres long and was cut in half as the testing machine available could only cope with specimens up to 10 meters long.

Initial testing carried out at NEL [1999] revealed local failures and cracking in the cast iron end shoes (Figure 5.1) that was believed to have been caused by premature failure. This coupled with the uncertainty of determining the amount of existing preload in the structure from the initial testing led to the commissioning of a new test regime involving fresh specimens with consistent cross sections [Moy & Lillistone, 1999]. The test procedure of the fresh specimens will be described in this Chapter.

The use of the non-linear Finite Element Method for cast iron material is well established. Studies [ABAQUS 5.8] have shown that carefully calibrated numerical models can adequately model the required behavioural characteristics of cast iron. The commonly used mesh generation and the FE analysis practices are described here with references to the ANSYS [ANSYS 6.1] and ABAQUS [ABAQUS 5.8] software used in the present study.

The FE analysis provided outputs of stresses in the adhesive and the adherends. This led to the completion of calibrated models that were used for parametric studies. The aim of this investigation was to identify the level of benefits gained with the various levels of preload prior to the reinforcement of the struts and to identify the effect of geometrical imperfection on the performance of the struts.

5.2 REVIEW OF THE EXPERIMENTAL STUDY CONDUCTED BY MOY AND LILLISTONE [1999]

With reference to the initial testing of the cast iron struts removed from the Rotherhithe station, Moy and Lillistone [1999] carried out an extensive testing regime on

six fresh cast iron struts with no existing preload, as part of the LINK project [2000]. The investigation was carried out in order to evaluate the compatibility of CFRP plates in reinforcing such structures and to monitor the benefits gained. The investigation had found that the stiffness and load carrying capacities of the struts were significantly enhanced using CFRP plates.

Details of the experiment and brief discussion have been included in this chapter as finite element models were calibrated against the experimental data obtained by Moy and Lillistone [1999]. Full data and report can be found in Moy and Lillistone [1999] report and hence only some references will be made in this section.

5.2.1 The specimens

Six struts were tested by Moy and Lillistone [1999], which included three sets of different cross-sections, identified as specimen I, II and III. The struts were tested to failure, two without reinforcement and the rest with various amounts of reinforcement. In each case the reinforcement was added while the cast iron was carrying a substantial preload.

The cross sections of the cast-iron struts were of cruciform shape. Figure 5.2 shows a typical section of specimen I, and Table 5.1 gives comparative dimensions and section properties for the sections used. The first letter represents the type of specimen, i.e., I-type 1, II-type 2, III-type3. The second letter indicates the presence of reinforcement, i.e., U-unreinforced, R-reinforced, L-lightly reinforced, H-heavily reinforced. Special castings were made to produce the specimens and these were cut square at the end to give a specimen height of 2.5m. Moy and Lillistone decided at an early stage that an eccentric load would be applied to the specimens and values for the eccentricity are also given in Table 5.1 and shown in Figure 5.3. This was done to simulate a practical environment where struts are loaded not symmetrically and hence one side of the cruciform will go in tension and the other side in compression.

Preliminary finite element analyses were conducted by MSL [1999] and they predicted the failure loads of the unreinforced cast iron struts, and the preloads applied in the tests were approximately 50% of the predicted failure loads of the unreinforced struts (Table 5.1). However, it is believed that the models used by MSL [1999] were not calibrated against any experimental data and the results were used to give an approximation of the failure load of the struts.

Before any testing an examination of each strut was carried out to measure the imperfections in each leg of the cruciform and to check the section dimensions. The maximum out of true in any leg was just over 4mm with respect to the end of the specimen. The carbon fibre composite was applied to the short arms of the cruciform as shown in Figure 5.3. The thicknesses of the composite plates used are given in Table 5.1.

5.2.2 Instrumentation

Before any loading, strain gauges were attached to both the cast iron and the carbon fibre plate at mid-height, as shown in Figure 5.3. The positions of the strain gauges have been marked by combination of numbers and letters. The prefix "C" indicates that gauge was on the carbon plate. Three lateral displacements were measured on the centreline and at the outside edge of each long leg, as shown in Figure 5.3. This checked whether the strut twisted when under load.

5.2.3 Test method

A column-testing machine was used for the experimental work. Figure 5.4 shows a schematic of the test set up. Great care was taken to ensure that the top and bottom rods lined up vertically and that the specimen was vertical in the rig ensuring the end conditions were as close as practical to pinned.

The test procedure for the unreinforced struts was straightforward. The load was increased to about 25% of the predicted failure load and then returned to zero. The load was then increased in increments until failure.

The procedure for the reinforced specimens was more complicated. Load was applied to the still unreinforced strut in increments up to the required preload. Load was then removed in increments. The load was again increased in increments and the strut was then left under the preload for at least an hour to ensure its stability. The reinforcement was then attached to the loaded strut. After curing of approximately 90 hours, the preload was removed in increments. Load was cycled in increments to the preload value and back to zero. Load was then increased until failure occurred.

5.2.4 Test results

Figures 5.5 to 5.10 show the load versus lateral deflection and load versus axial and bending strains, respectively. The axial strains were calculated as the average of the cast iron gauges 1 and 3 (see Figure 5.3) and the bending strain was calculated as half the difference between gauges 3 and 1.

Table 5.2 presents recorded failure loads for each specimen. Figures 5.11 to 5.13 present strain values across the width of the section from both specimens, reinforced and unreinforced for a quoted increment of load.

5.2.5 Discussion

5.2.5.1 Behaviour of the cast iron strut reinforced with carbon fibre plates

The experimental results showed that there was a good bond between the carbon fibre composite and the cast iron. The linear strain distribution, Figures 5.11 to 5.13, show that there was no slip between the carbon and the cast iron and that the reinforced section was behaving in a fully composite manner.

It can be seen from load versus deflection graphs (Figures 5.5 to 5.7) that the carbon reinforcement had a significant stiffening effect on the struts as the reinforced sections have steeper gradient and produce smaller strain changes for a given load increment compared to their counterparts

Table 5.2 shows the strengthening effect due to carbon reinforcement. In every reinforced strut failure was initiated in the carbon fibre on the compression arm of the cruciform cross-section. The compression failure seemed to be resulted from crushing and fibres riding past each other. Between these areas of crushing the composite appeared undamaged and was firmly bonded to the cast iron. The strain reading showed that the failed reinforcement was no longer carrying significant load.

In every case the reinforced struts carried further load after initial carbon failure. In specimens II/HR, I/R and III/R final failure was initiated in the cast iron in tension. In specimen II/LR it appeared that there was local buckling in the compression arm of the strut. As a result two pieces broke away from the compression side and the remainder of the specimen broke in half. It was reported by Moy and Lillistone [1999] that the imperfection in the cast iron could have caused the local buckling and the very thin carbon fibre plates would have had a smaller restraining effect than in any of the other specimens. Reviewing the report, the strut II/LR showed a similar imperfection pattern as the other struts and no evidence of local buckling was found in the FE analysis, which will be described later in this Chapter.

After initial failure of the carbon there was a change in position of the neutral axis (zero strain) due to the change in the effective cross section. The axis shifted toward the tension arm as the effective cross section of the compression arm reduced significantly due to carbon plate failure. There was still a linear distribution of strain across the effective part of the strut, as can be seen in Figures 5.8 to 5.10.

5.2.5.2 Preliminary FE analysis and Material properties

The initial finite element analyses carried out by MSL [1999] underestimated the failure load by between 11% and 107%. It is believed that the initial analyses did not account for the effect of non-uniform load distribution on fibre buckling strength. This has been described in details later on.

It has been possible to back calculate from the test results to obtain values for the elastic modulus of the cast iron and the carbon fibre. The method of calculation is given in Appendix E and the results are shown in Table 5.3.

Tensile and compressive tests were carried out by Moy and Lillistone [1999] on numerous cast iron coupons and rectangular specimens, respectively. The geometrical dimensions of these specimens have been illustrated in Figures 5.14 and 5.15. Specimens were taken from the cast iron cruciform and tested to failure at Southampton University [Moy, 1999]. Overall, twelve specimens were tested, seven in tension and five in compression, and the average was used for the purpose of FE analysis. Figures 5.16 show the average strain/stress curves obtained from the experiments.

There was a good agreement between the experimental elastic modulus and that obtained from the hand calculations. The method of hand calculation is given in Appendix E. The compression specimen gave an average value of 133 kN/mm^2 (Figure 5.16) and tensile specimen gave a value of 126 kN/mm^2 (Figure 5.16), which is very close to the hand calculated average value of 129 kN/mm^2.

5.2.5.3 Imperfection in the cast iron

The examination of the specimens gave an impression of the deviations of the specimens from the true line. The recorded imperfection did not exceed 4mm in all cases (for more details, please refer to Moy and Lillistone [1999]). However, from the experimental load-deflection graphs it can be seen that a typical strut will deflect (lateral

deflection) around 20 to 25mm before failure. Hence, imperfection of 4mm or more could have a significant influence on determining the overall strength of the structure.

5.3 FE MODELLING OF CAST IRON STRUT

The use of the non-linear FE method for cast iron material is well established. Study by ABAQUS 5.8 has shown that carefully calibrated numerical models can adequately model the actual mechanical behaviour of cast iron.

The FE analysis was carried out to investigate the effect of the preload levels and the imperfections on the stiffness and load bearing capacity of the struts. The FE analysis outputs in the carbon, the adhesive, and the cast iron allowed continuous monitoring of the stresses in the structure.

5.3.1 General details

The FE procedure adopted was the same as that detailed in ABAQUS 5.8. The general-purpose software package ANSYS was used for the mesh generation, and the ABAQUS package was used for the analysis and post-processing.

The dimensions of the models were the same as the experimental specimens. The cast iron, adhesive, and the carbon were modelled with 8-noded non-linear brick[1] elements, with reduced integration[2] and hourglass control[3] to prevent shear locking[4].

[1] The solid element includes isoparametric elements: quadrilateral in two dimensions and "bricks" in three dimensions. These isoparametric elements are generally preferred for most cases because they are usually the more cost-effective of the elements. They are offered with first- and second-order interpolation.

[2] Reduced integration uses a lower-order integration to form the element stiffness. The mass matrix and distributed loading use full integration. Reduced integration reduces running time, especially in three dimensions. Fully integrated elements do not hourglass but may suffer from "locking" behaviour: both shear and volumetric locking. Shear locking occurs in first-order, fully integrated elements that are subjected to bending. The numerical formulation of the elements gives rise to shear strains that do not really exist- the so-called parasitic shear. Therefore, the elements are too stiff in bending.

[3] Hourglassing [ABAQUS, 1997] can be a problem with first-order, reduced-integration elements in stress/displacement analyses. Since the elements have only one integration point, it is possible for them to

Figure 5.17 shows the finite element mesh used. Advantage was taken of any symmetry conditions in geometry to reduce computational effort. Appropriate mesh was selected where no significant benefits were gained by further refining the mesh, as explained in Chapter 4.

5.3.2 Boundary conditions

Only one quarter of the strut was considered because of symmetry. All nodes at the mid-cross section and the mid-span were restrained to produce the required symmetry, and appropriate nodes at the end of the strut were restrained to represent a pinned condition. This is illustrated in Figure 5.18.

5.3.3 Material properties

As described earlier, a series of tensile and compression test were carried out on cast iron coupons by Moy and Lillistone [1999]. The average of all collected data was considered for the FE analysis, as shown in Figure 5.16. For the carbon fibre and the adhesive, the appropriate data was collected as described in Chapter four.

5.3.4 Loading

A point load was applied to the end of the strut using the "STATIC" function, which considered the load as a static load step and selected increments using an automatic procedure as described earlier. Since ABAQUS automatically selects the increment size during the analysis, the process is usually more efficient because ABAQUS can react to nonlinear response, whereas the inexperienced user would not be

distort in such a way that the strains calculated at the integration point are all zero, which in turn, leads to uncontrolled distortion of the mesh. Second-order reduced-integration elements, with few exceptions, do not have the same difficulty.

[4] Volumetric locking [ABAQUS, 1997] occurs in fully integrated elements when the material behaviour is incompressible. Spurious pressure stresses develop at the integration points, causing an element to behave too stiffly for deformations that should cause no volume change.

able to predict this. This method is particularly valuable in cases where the response to load varies widely through the step.

5.3.5 Failure criteria

As discussed previously, failure modes of composites are strongly dependent upon geometry, loading direction, and ply orientation [Lessard and Chang, 1989]. Since the composite is loaded in-plane, only in-plane failure modes need to be considered. For CFRP plates subjected to compressive and tensile loadings, four failure modes were considered: compression, tension, buckling, and shear failure.

It is known that in-plane failure is the dominant mechanism in compression failure of fibre-dominated composites [Chang, 1986]. Compression failure can result from a combination of compressive stress σ_y and shear stress σ_{xy}. A failure index e_c^2 can be defined in terms of these stresses and the strength parameters X_c, Y_c and S_c (to be defined later). When the failure index exceeds 1.0, material failure is assumed to occur. The failure index is defined as follows:

$$e_c^2 = \left(\frac{\sigma_y}{Y_c}\right)^2 + \frac{\int_0^{\gamma_{xy}} \sigma_{xy} d\gamma_{xy}}{\int_0^{\gamma_{xy}^u} \sigma_{xy} d\gamma_{xy}} \tag{5.1}$$

where e_c^2 , σ_y and σ_{xy} are the compression failure index, compressive stress and shear stress, respectively, in each layer. In this equation, Y_c is the longitudinal compressive strength and γ_{xy}^u the ultimate shear strain. The shear stress-shear strain relationship is written as

$$\gamma_{xy} = \left(\frac{1}{G_{xy}}\right)\sigma_{xy} + \alpha\sigma_{xy}^3 \tag{5.2}$$

where G_{xy} is the (initial) ply shear modulus and α[5] a nonlinearity factor. Introducing the ply shear stress-shear strain relationship of equation (5.2) into equation (5.1) gives

[5] α is a constant that was determined experimentally by Chang. Kuo and Chang. Yen, 1986

$$e_c^2 = \left(\frac{\sigma_y}{Y_c}\right)^2 + \frac{\frac{\sigma_{xy}^2}{2G_{xy}} + \frac{3}{4}\alpha\sigma_{xy}^4}{\frac{S_c^2}{2G_{xy}} + \frac{3}{4}\alpha S_c^4} \tag{5.3}$$

where $\mathbf{S_c}$ is the in-situ ply shear strength and for laminates with linear elastic behaviour ($\alpha = 0$), Equation 5.3 can be reduced to

$$e_c^2 = \left(\frac{\sigma_y}{Y_c}\right)^2 + \left(\frac{\sigma_{xy}}{S_c}\right)^2 \tag{5.4}$$

Therefore, the compression failure criterion states that when the stresses σ_y and σ_{xy} in any one of the plies in a laminate satisfy Equation (5.3) (with $e_c^2 \geq 1$), compression failure occurs in that layer. When compression failure occurs in a layer, the longitudinal modulus E_y and Poisson's ratio ν_y of that layer are reduced to zero, i.e. the matrix can no longer carry any load in compression. However, the transverse modulus E_x, and the shear stress-strain relations remain unchanged, i.e. in the failed layer the in-plane properties are reduced as follows:

For $\sigma_y < 0$ and $e_c^2 \geq 1$

$$\begin{bmatrix} \frac{E_x}{1-\nu_x\nu_y} & \frac{E_y\nu_x}{1-\nu_x\nu_y} \\ \frac{E_x\nu_y}{1-\nu_x\nu_y} & \frac{E_y}{1-\nu_x\nu_y} \end{bmatrix} \longrightarrow \begin{bmatrix} E_x & 0 \\ 0 & 0 \end{bmatrix}$$

$$\overline{G}_{xy} = \frac{\partial f(\gamma_{xy})}{\partial \gamma_{xy}} \longrightarrow \frac{\partial f(\gamma_{xy})}{\partial \gamma_{xy}} \text{ (i.e. unchanged)}$$

Lessard and Chang [1989] had carried out an investigation into the effect of various load distributions on the critical stress values due to buckling. The study had shown that fibre composites subjected to non-uniform load distribution are typically more resistant to fibre buckling at a local level. In extreme cases, the local buckling strength can reach to almost 8 times the uniaxial compressive strength. The study has a direct relevance to this investigation and hence a brief review of their work has been included in this chapter and no further reference will be made in this section.

Fibre buckling is a very important failure mode because it frequently leads to catastrophic failure in structures subjected to compression. Therefore, it is very important that fibre-buckling failure be fully understood and predictable. All the previous analyses were developed based on the assumption that the composite was stressed uniformly due to a constant load. As a consequence, the geometry is greatly simplified to only a one-dimensional configuration with a single fibre embedded in a matrix, assuming that each fibre of a unidirectional layer shares an equal load and deforms in the same manner. The influence of one fibre on another was ignored.

However, since fibre compressive strength is directly associated with geometric stability, any disturbance in geometry and stress distribution among the fibres could significantly affect the buckling strength. Therefore, it is very important to fundamentally understand the in situ buckling strength in composites, and to determine the effect of fibre-matrix-fibre interaction on the buckling strength in composites with uniform stress distribution. Figure 5.19 shows the effect of uniform and nonuniform loading of a composite.

A variational method based on the minimum potential energy principle [Lessard and Chang, 1989] was used to develop the analysis (see Appendix F), which evaluates the critical stress as:

$$\sigma_c = \frac{E_f \pi^2}{12n^2} v_f [B_f] + \frac{G_m}{v_m}[B_\gamma] + \frac{E_m n^2 v_f^2}{v_m \pi^2}[B_e] \qquad (5.5)$$

Where

$$n = \frac{L}{t_f}$$

$$B_f = \frac{\left(\sum_{j=1}^{N} \left(k_j^i\right)^2\right)}{\left(\sum_{j=1}^{N} \alpha_j^i \left(k_j^i\right)^2\right)}$$

$$B_\gamma = \frac{1}{4}\frac{\left(\sum_{j=1}^{N-1}\left(k_j^i + k_{j+1}^i\right)^2\right)}{\left(\sum_{j=1}^{N}\alpha_j^i\left(k_j^i\right)^2\right)}$$

$$B_e = \frac{\left(\sum_{j=1}^{N-1}\left(k_j^i - k_{j+1}^i\right)^2\right)}{\left(\sum_{j=1}^{N}\alpha_j^i\left(k_j^i\right)^2\right)}$$

B_f, B_γ, and B_e are factors which affect the size of the fibre, shear, and extensional terms, respectively. These factors are influenced mainly by the way the load is distributed on the fibre system. E_m and E_f are the moduli of the matrix and fibre material, respectively. v_m and v_f are the volume fraction of the matrix and fibre respectively, and G_m is the shear modulus in the matrix, t_f and L are the width, and the length of the fibre, respectively. k_j^i are the interaction coefficients, which relate the displacement of the j^{th} fibre to the displacement of the i^{th} fibre and α_j^i is a factor that relates the load on each fibre, P_j to the load on the critical fibre, P_i.

Under a constant load distribution, without fibre imperfections, all P_j's are equal $\left(\alpha_j^i = 1\right)$. As a result, all $k_j^i \approx 1$, i.e., the displacement distribution is nearly uniform, and B_f=1, and B_γ=1, and $B_e = 1$ and the buckling expression becomes

$$\sigma_c = \frac{E_f \pi^2 v_f}{12n^2} + \frac{G_m}{\gamma_m} = \sigma_c^o \longleftrightarrow X_c^o \tag{5.6}$$

The buckling load is the well-known buckling equation for unidirectional laminates subjected to uniform loading. σ_c^o is the stress, which is assessed against X_c^o (the unidirectional ply compressive strength).

Considering the system of fibre subjected to a single concentrated load P_i on the i^{th} fibre (see Figure 5.20). Based on equation, $P_j = \alpha_j^i P_i$ (see Appendix F, Equation 19), $\alpha_j^i = 1$ and all other $\alpha_j^i = 0$. Minimising energies leads to the following "B-factors"

$$B_f = 6.72, \qquad B_\gamma = 6.65, \qquad B_e = 0.14 \tag{5.7}$$

And

$$\sigma_c = \frac{E_f \pi^2 v_f}{12n^2}(6.72) + \frac{G_m}{\gamma_m}(6.65) + \frac{E_m n^2 v_f^2}{v_m \pi^2}(0.14) \tag{5.8}$$

$$\sigma_c = 7.88\sigma_c^0 \tag{5.9}$$

The model showed that nonuniform load distributions are typically more resistance to fibre buckling at a local level. Local strengths exceed σ_c^o, therefore X_c^o is exceeded. The concentrated load shows the extreme case of putting the entire load on a single fibre, leading to a very high local buckling strength of almost 8 times the uniaxial compressive strength. The half-sinusoid loading is a "mild" stress concentration, yet the increase in local buckling strength is 35% and no increase in local buckling strength for constant loading. Thus, the effects of load distributions have a significant influence on the local fibre buckling strength.

Therefore, buckling failure occurs when the maximum compressive stress in the fibre direction exceeds the fibre buckling strength, X_c, independent of the other stress components. The failure index is defined as follows:

$$e_b^2 = \left(\frac{\sigma_y}{X_c}\right)^2 \tag{5.10}$$

Fibre buckling in a layer is a catastrophic mode of failure. Hence, after this failure index exceeds 1.0, it is assumed that the material can no longer support any loads.

$$\begin{bmatrix} \frac{E_x}{1-\nu_x\nu_y} & \frac{E_y\nu_x}{1-\nu_x\nu_y} \\ \frac{E_x\nu_y}{1-\nu_x\nu_y} & \frac{E_y}{1-\nu_x\nu_y} \end{bmatrix} \longrightarrow \begin{bmatrix} 0 & 0 \\ 0 & 0 \end{bmatrix}$$

$$\overline{G}_{xy} = \frac{\partial f(\gamma_{xy})}{\partial \gamma_{xy}} \longrightarrow 0$$

The fibre-matrix shearing and the tensile failure have been discussed in the chapter four and will not be discussed in here.

5.3.6 Model calibration

FE models are mathematical representations of the physical behaviour of structures and therefore need to be calibrated against experimental tests to demonstrate their accuracy and compatibility. The models can then be modified to predict the behaviour of the structures under different geometry and material parameters. The FE analysis procedure in this investigation consisted of static analysis. The analyses were used to investigate the overall effect and benefits of reinforcing with CFRP plates compared to the behaviour of unreinforced specimens.

The model was calibrated using the strain gauge data, obtained from the laboratory tests, carried out by Moy and Lillistone [1999], and using the average measured material properties of the cast iron, obtained from the tensile and compressive coupon tests. Figure 5.21 shows a comparison between the FE strain readings in the compression region (gauge position 3) and its experimental counterpart for specimen I. It can be seen that there is a good agreement between the two readings.

5.3.7 Preload analysis stage

Modelling the unreinforced struts was straightforward as the preload was applied in increment and returned to zero. However, the experimental procedure for the

reinforced struts required the preload to be applied to the cast iron and then removed followed by applying load increments to both cast iron and carbon fibre plate. This procedure was carried out by using a command which allows a set of elements to be activated and deactivated in the ABAQUS. Therefore, the elements which formed the adhesive and the carbon fibre plates were deactivated for the preload analysis and activated with no prior strain at completion of the preload analysis.

5.3.8 Ultimate strength analysis stage

Finite element models of the tension-compression behaviour of the struts were created which accounted for the progressive failure in the adhesive and the carbon from the tensile and compressive loading effects. This was done using a special macro, similar to that of beam model, to identify the occurrences of failure indexes in elements and reduce the mechanical properties of those elements accordingly.

A concentrated load was applied at the required eccentricity, located on the short arm, as shown in Figure 5.4 and the analyses were carried out to failure. Initial failure occurred in the carbon plate in compression where the load, on the region, was then transferred to the cast iron. This initiated the yielding in the cast iron, which progressed through out the compression arm until the strut had reached its tensile capacity in the tension arm and subsequently failed.

5.3.9 Results

The results of the FE analysis were in good agreement with the experimental results and the predicted deformation behaviour agreed with the experimentally observed behaviour. Figures 5.22 to 5.25 show the load versus lateral deflection curves predicted by the FE model and the corresponding experimental curves.

The FE models confirmed that, in all the specimens, failure initiated in the carbon fibre with the greatest compression and subsequently the load was then transferred to the

cast iron followed by final failure in the cast iron in tension. Figure 5.26 shows a typical lateral deflection of a cast iron strut under eccentric loading. Table 5.4 gives a comparison between FE and experimental bending stiffness values and shows that all FE predictions with the exception of specimen II/LR with the difference of 11% were within 5% of the experimental bending stiffness. There are several possibilities to account for the difference between the FE and the experimental predictions, which includes variation in geometric imperfections and the mechanical properties of the cast iron material. However, the differences between the FE and the experimental results are small enough to be considered acceptable.

No material failure was discovered in the adhesives, showing that the fully cured adhesive was capable of transferring the shear stress across the cast iron to the composite through the interface and was able to withstand large strains. Also no failure occurred in the tensile CFRP plate, due to the tensile strength being much greater than that of the cast iron. Hence, where the cast iron experienced tension failure, the stresses in the CFRP plate only reached a fraction of the failure stress level.

Overall, the models have shown good correlation and agreement with the experimental values. Hence, it was felt that the models did represent the physical structures and were adequate for further parametric studies.

5.4 Parametric study

The calibrated models were used in further analysis to investigate the effect of different geometric imperfections and different level of preload prior to reinforcement on the stiffness and load bearing capacity of a typical cast iron strut. Therefore, the existing models can be extrapolated to create varied environments with regard to geometric and loading conditions, respectively. Tables 5.5 and 5.6 show the range of geometric imperfections and preloads that have been computed into the FE models, respectively. The matrices are similar to those for the previous models, i.e. III/R-2mm is reinforced cast iron strut III with 2mm imperfection or III/R-30% is reinforced cast iron strut III

with 30% preload, where the maximum preload is taken from the failure load of the unreinforced cast iron that was provided by MSL [1999].

5.4.1 Imperfection study

As discussed previously the maximum out of true in any leg was just over 4mm with respect to the ends of the specimen. However, a range of geometrical imperfections was selected in such a way that the highest value in the range represented an imperfection of double the value of the recorded imperfections in the experimental procedures.

Initial stiffness and failure load of the reinforced strut 'I' under a range of geometric imperfections were analysed and results are presented in Table 5.5 and shown in Figure 5.27. The geometrical imperfection was modelled as linear from the end of the strut to mid-height of the strut.

Load versus lateral deflection curves followed the same pattern in all specimens and it can be seen from the Table 5.5 that the greatest reduction in initial stiffness due to imperfection was just below 10% and it can be seen from Figure 5.28 that the rate of stiffness change with regard to geometric imperfection is linear.

The effect of imperfection on the level of failure load has been shown in Figure 5.29. It can be seen that the failure load reduces significantly with the increase in imperfection level and adopts a polynomial pattern, which can be expressed as: $y = 200.89x^2 + 35.714x - 0.0286$, where y and x are the percentage of reduction in failure load and geometrical imperfection, respectively. Therefore, imperfection of approximately 0.3% will reduce the level of failure load by 30%.

The imperfection analysis in this investigation was selected to produce the worst case scenario and it was found that the effects on the structural stiffness are relatively small and can be neglected. The value of the initial imperfection did not affect the failure

mode of the structure but the failure load was significantly influenced with regard to the imposed geometrical imperfection.

Therefore, it is recommended that the initial imperfection should be accounted for in determining the load bearing capacity of a structure. It was also shown that the initial imperfection has a small effect on the structural stiffness. The results presented in this Chapter could be used in determining the effect of initial imperfection on the performance of similar structures.

5.4.2 Preload prior to reinforcement

The calibrated model of specimen III-R was used in further analysis to investigate the structural behaviour of cast iron strut by implementing a range of preload levels prior to reinforcement where the maximum preload was identified as the failure load of the unreinforced cast iron strut, provided by MSL [1999].

It was felt that a strut under a significant preload (50% or more of the failure load) might produce a global buckling in the structure, depending on the eccentricity of the applied load, which in turn could have an effect on the failure load and the stiffness of the structure. Therefore, it was decided that the preload should be removed prior to reinforcement, as the composite structure will be much stronger to resist buckling. Hence, in this analysis the load was applied to the unreinforced strut in increment up to the required preload. Load was then removed and the reinforcement was applied to the strut. The load was again increases in increments until failure occurred.

The question which has to be posed is "what are the benefits of carbon fibre strengthening to in-situ struts that are already under load?". This is difficult to answer and in fact prompts further question of what the level of the existing preload is. Without this information, which is almost impossible to obtain, any predictions about the amount of benefit will be rather tenuous [Moy, 1999]. Therefore, a range of preload varying from 30 to 75 percent of the failure load of the unreinforced cast iron strut was selected and

analysed. The failure load can be estimated using Dier et al. [1997] equation that was produced to estimate the failure load of a column, which will be described later in this Chapter.

Initial stiffness and failure load of the reinforced cast iron strut 'III' under a range of preload is shown in Figure 5.30 and presented in Table 5.6. The matrices are similar to those of the experimental struts, i.e. III-R30 is reinforced cast iron strut 'III' with 30 percent preload prior to reinforcement.

Load versus deflection curves followed a similar pattern in all specimens and it can be seen from the Table 5.6 that there was very little change in the initial stiffness up to the point where failure occurred in the CFRP plate in the compression zone (arm). At this stage the load that was carried by the carbon plated in the compression zone is suddenly transferred to the cast iron. As a result, the cast iron yields rapidly in the compression until the majority of the compression zone has yielded. The cast iron in the greatest tension yields, causing failure in the tension.

It can be seen from the Figure 5.30 that where carbon plate failure has occurred and the load has been shifted to the cast iron, the stiffness of the structure is affected by the level of preload prior to reinforcement. The results of the stiffness change have been tabulated and are presented on Table 5.7. It can be seen from Table 5.7 that a 45% preload prior to reinforcement will decrease the stiffness of the structure after the carbon plate failure by 27% with respect to the same specimen with no preload prior to reinforcement.

At failure of the CFRP plate in the compression zone, the load will be transferred to the cast iron. Figure 5.31 shows the effect of preload prior to reinforcement on the stiffness. The rate of change in the stiffness of the structure after the carbon plate failure can be expressed in a polynomial form of $y = 0.0123x^2 - 0.0263x + 2.008$, where x and y are the percentage level of preload prior to reinforcement and reduction in the level of stiffness after the occurrence of failure in the CFRP plate, respectively.

The effect of preload prior to reinforcement on the level of the failure load has been shown in Figure 5.32. It can be seen that the level of preload has a reduction effect on the level of failure load, and adopts a polynomial form which can be expressed as $y = 0.0024x^2 + 0.1232x + 0.2685$, where x and y are the percentage level of preload prior to reinforcement and reduction in the level of failure load, respectively.

Dier et al [1997] in the JIP1 manual considered the problem of predicting the failure load of reinforced columns in detail and produced an equation of the form [see Appendix E]

$$\frac{P_2}{P_{u2} - P_1\left(\frac{A_t}{A_g} - 1\right)} \leq 1 \qquad (5.11)$$

where P_1 is the preload, P_2 the failure load of the reinforced, preloaded strut, P_{u2} the axial load capacity of the reinforced strut, A_g the area of the transformed[6] reinforced strut and at the area of the unreinforced strut.

They also showed that, when the column is stocky[7] and does not bend significantly, this equation can be simplified to

$$\frac{P_1}{P_{u1}} + \frac{\Delta P}{P_{u2}} \leq 1 \qquad (5.12)$$

where P_{u1} and ΔP are the axial load capacity of the unreinforced column and the benefit to be obtained from strengthening the column ($\Delta P = (P_2 - P_1)$), respectively. Figure 5.33 confirms that the equation 5.12 does predict the failure load of the reinforced column with good accuracy. It can be seen from Figure 5.33 that the FE curve has approximately the same gradient as the theoretical one. However, where a column has a preload less than approximately 15%, the stresses produced in the strut are not enough to cause any

[6] Using cast iron as reference material, we can convert the carbon plate area into the cast iron using modulus ratio.

[7] For which both ratios l/h and l/b are less than 15, where l is the height, b is the width of the column and h is the depth.

plasticity and hence the structure can recover completely. Hence, at the early stages of the curve (FE) in Figure 5.33, the reduction in the level of axial capacity is zero.

5.5 CONCLUSIONS

The FE analyses have successfully simulated the behaviour of cast iron struts under eccentric loading condition and comparisons have shown that there is a good agreement between the FE analysis and experimental data.

The FE analyses have shown that the degree of geometrical imperfections causes an alteration in the magnitude of the failure load. The investigation that was carried out on strut I-R showed that 0.3% geometrical imperfection in relation to the length of the strut causes approximately 30% reduction in the strut load bearing capacity in comparison to the same strut with no imperfection.

The FE analyses also showed that different amounts of preload will cause changes in structural secondary stiffness and failure load. The investigation that was carried out on strut III-R showed that 45% preload of unreinforced failure load prior to reinforcement would cause approximately 30% reduction in the failure load.

Therefore, imperfection can significantly reduce the load bearing capacity of a strut and needs to be accounted for and identified in form of inspection. However, it is practically impossible to determine the level of the existing preload in the strut, the findings of this chapter should be used to raise awareness of the effects of preload with regard to reduction in secondary stiffness and load bearing capacity of cast iron struts.

Specimen	Dimension 'D' (mm)	Laminate position	Laminate thickness (mm)	Eccentricity (mm)	Predicted unreinforced capacity by MSL (kN)	Preload (kN)
I/U	275	Unreinforced	N/A	27.5	854	N/A
I/R	275	Short arm	3.6	27.5	854	425
II/LR	200	Short arm	1.8	20.0	415	200
II/HR	200	Short arm	3.0	20.0	415	200
III/U	150	Unreinforced	N/A	10.0	198	N/A
III/R	150	Short arm	2.4	10.0	198	100

Table 5.1 Details of section geometry and test parameters (see Figure 5.2, 5.3 and 5.4)

Specimen	Failure load (kN)	Load enhancement	Failure mode
I/U	1220	N/A	Ductile
I/R	1427	1.17	Ductile
II/LR	708	Unreinforced load unknown	Rupture
II/HR	775	1.10 ratio II/HR to II/LR	Rupture
III/U	410	N/A	Ductile
III/R	750	1.39	Rupture

Table 5.2 Details of failure loads and modes

Specimen	*Elastic modulus of cast iron (KN/mm²)*		
	Axial	Bending	Average
I/U	135	129	132
I/R	112	143	128
II/LR	128	113	120
II/HR	117	106	112
III/U	118	170	144
III/R	125	155	140
Average			129
Specimen	Elastic modulus of carbon fibre (KN/mm²)		
	Axial	Bending	Average
I/R	287	319	303
II/LR	436	168	302
II/HR	416	165	291
III/R	202	308	255
Average			288

Table 5.3 Elastic modulus values

Specimen	Bending stiffness experimental (KN)	Bending stiffness numerical (KN)	Ratio FE/Exp
I/U	101	98	0.97
I/R	170	175	1.03
II/LR	60	67	1.11
II/HR	70	74	1.05
III/U	60	58	0.96
III/R	84	87	1.03

Table 5.4 Comparison of FE and experimental values on bending stiffness.

Specimen	Initial imperfection (mm)	Ratio of initial imperfection/strut length (%)	Initial bending stiffness (KN)	Failure load (KN)	Reduction in failure load %
I-control	0	0	178.3	1541	0
I-r2	2	0.08	174.5	1490	4
I-r4	4	0.16	171.0	1370	11
I-r6	6	0.24	167.7	1240	20
I-r8	8	0.32	164.5	1040	33

Table 5.5 Details the effect of imperfection on bending stiffness and failure load of specimen I-R (I-control is specimen I with no imperfection)

Specimen	Initial preload (%)	Initial bending stiffness (KN/mm)	Failure load (KN)	Reduction in failure load %
III-control	0	89.9	628.5	0
III-R30	30	89.8	600	4.4
III-R45	45	89.8	560	10.9
III-R60	60	87.5	525	16.5
III-R75	75	87.1	490	22.1

Table 5.6 Details the effect of initial preload on bending stiffness and failure load of specimen III-R (initial preload is calculated as a percentage of the unreinforced failure load. Control specimen is defined as a specimen with no preload prior to reinforcement.)

Specimen	bending stiffness after carbon plate failure (kN/mm)	Reduction in stiffness %
III-control	13.0	0
III-R30	10.5	19
III-R45	9.5	27
III-R60	8.6	34
III-R75	3.3	75

Table 5.7 Details the effect of initial preload on stiffness of the specimen III-R after carbon plate failure (the reduction stiffness values are calculate with respect to the control specimen with has no preload prior to reinforcement).

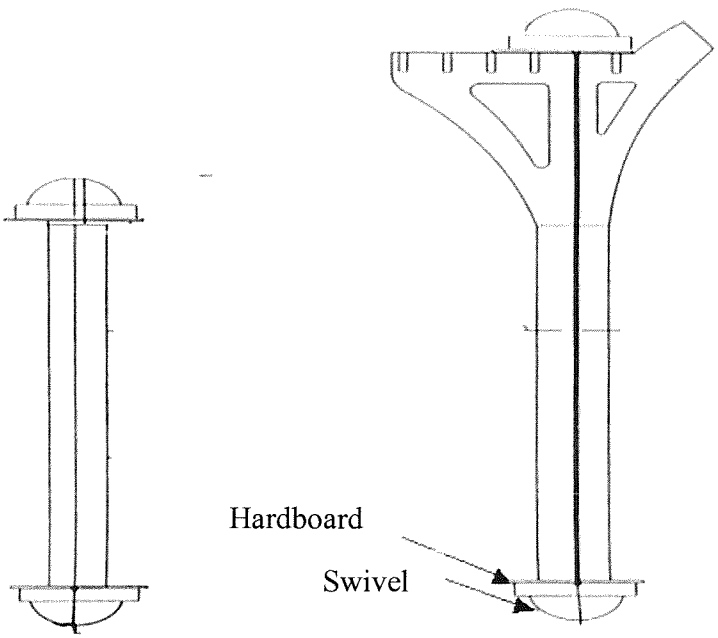

(a) Removed end shoes (b) With end shoes

Figure 5.1 Elevated view of cast iron strut

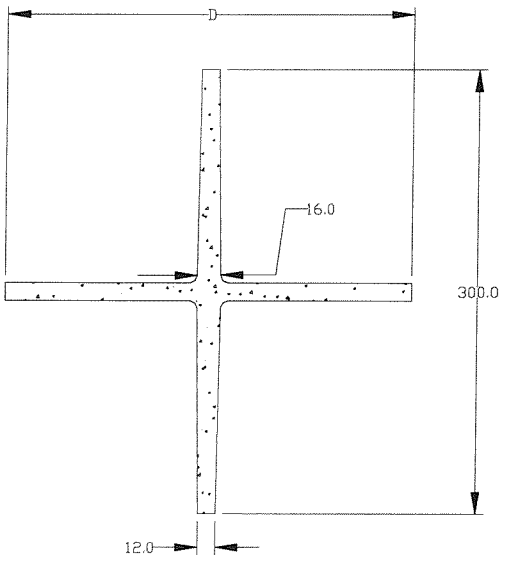

Figure 5.2 Cruciform section – specimen I

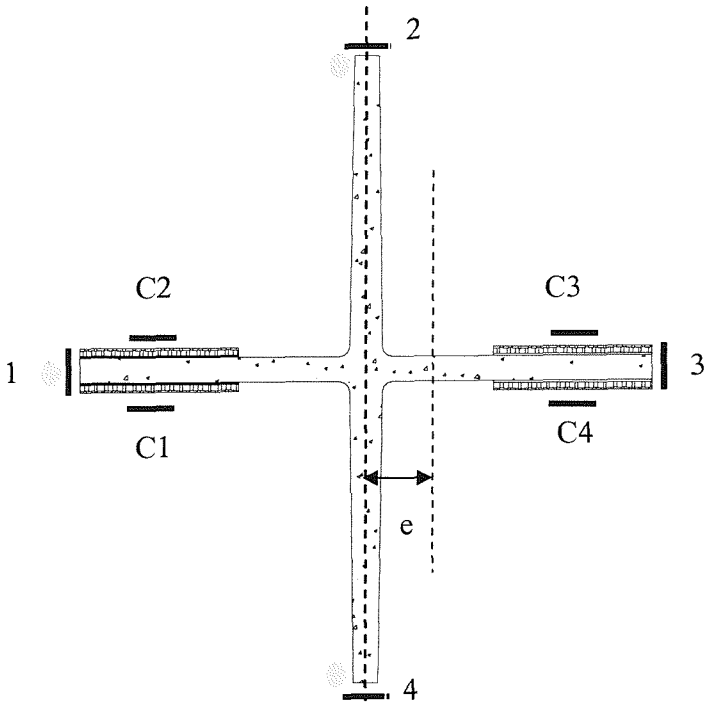

Figure 5.3 Cruciform strut section showing strain gauge positions

— Strain gauge

Displacement transducers

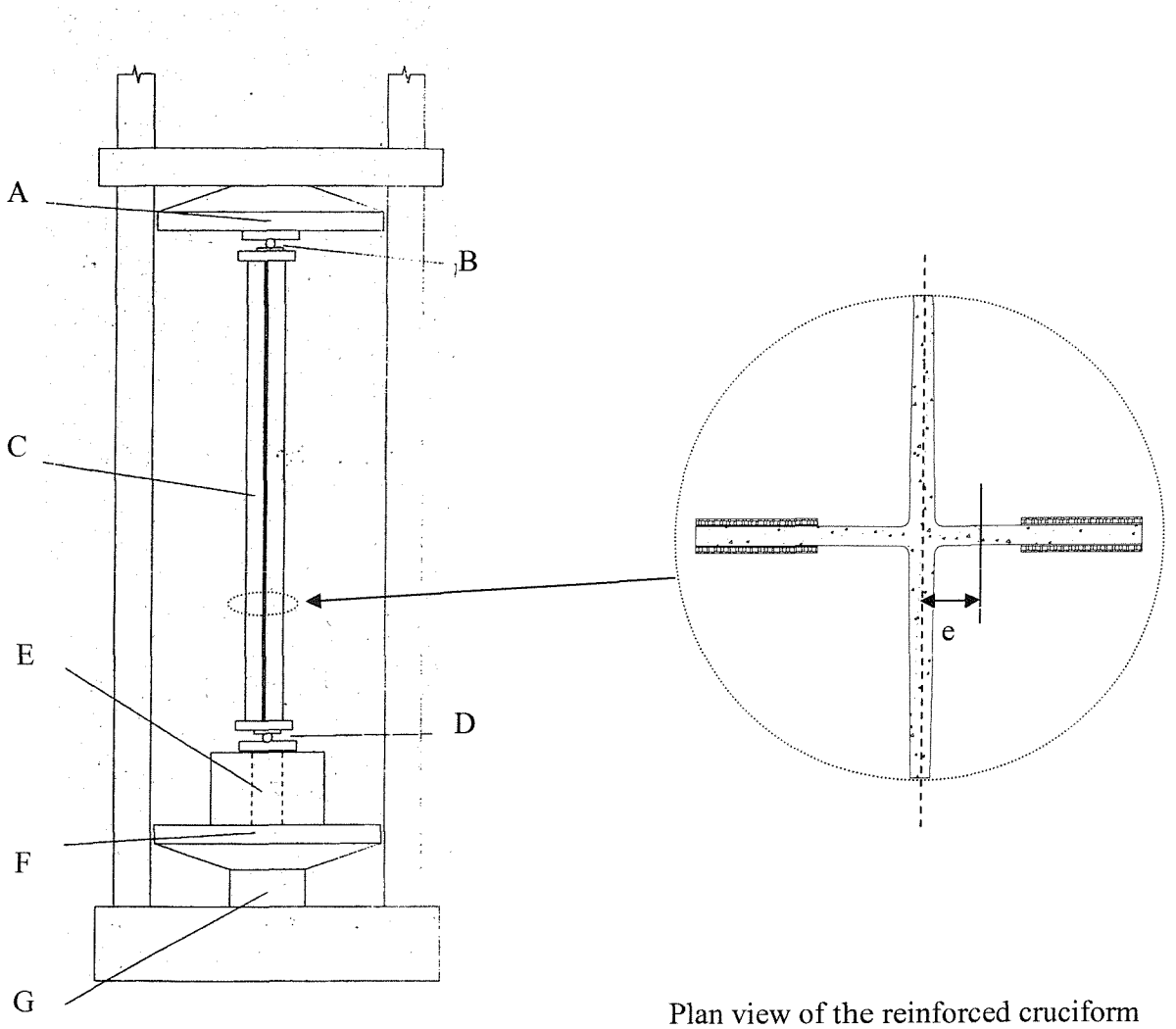

Plan view of the reinforced cruciform shaped strut

A: top platen
B, D: roller support
C: specimen
E: hydraulic jack and bracing system
F: bottom platen
G: test rig jack
e: eccentricity of the applied load

Figure 5.4 Schematic view of test set-up

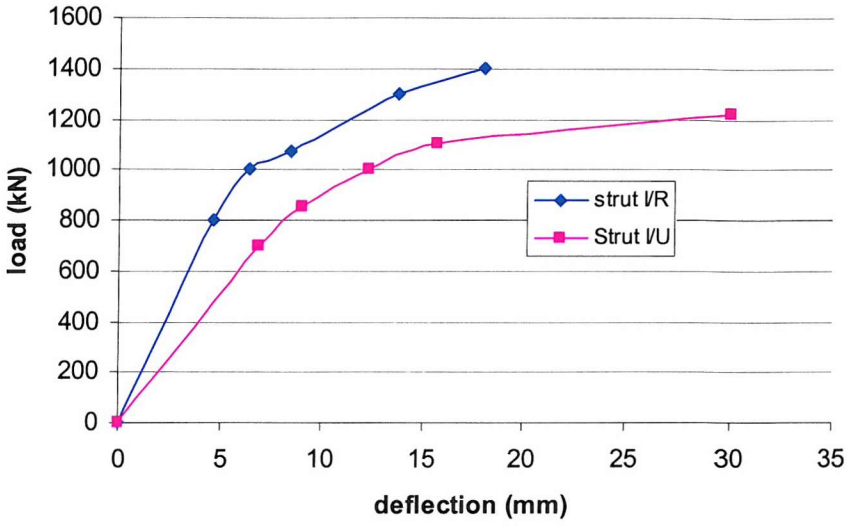

Figure 5.5 Strut I/U & I/R, comparison of load versus deflection graphs

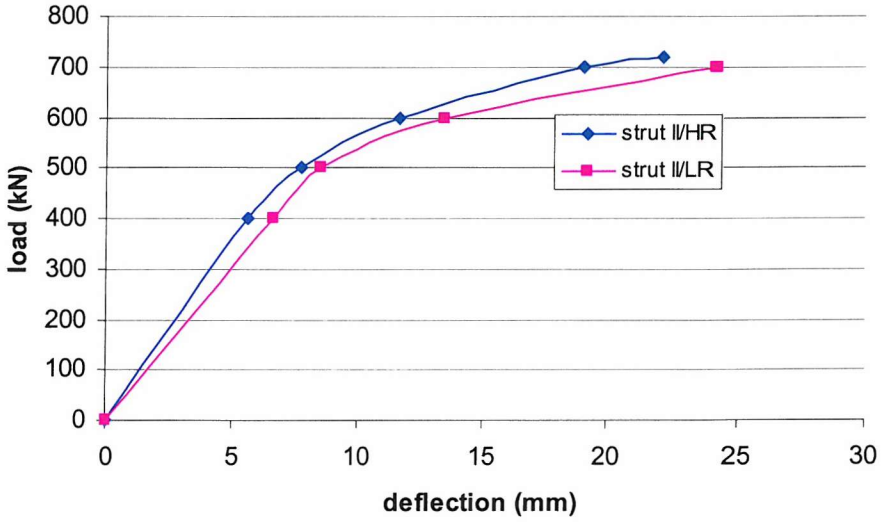

Figure 5.6 Struts II/LR & II/HR, comparison of load versus deflection graphs

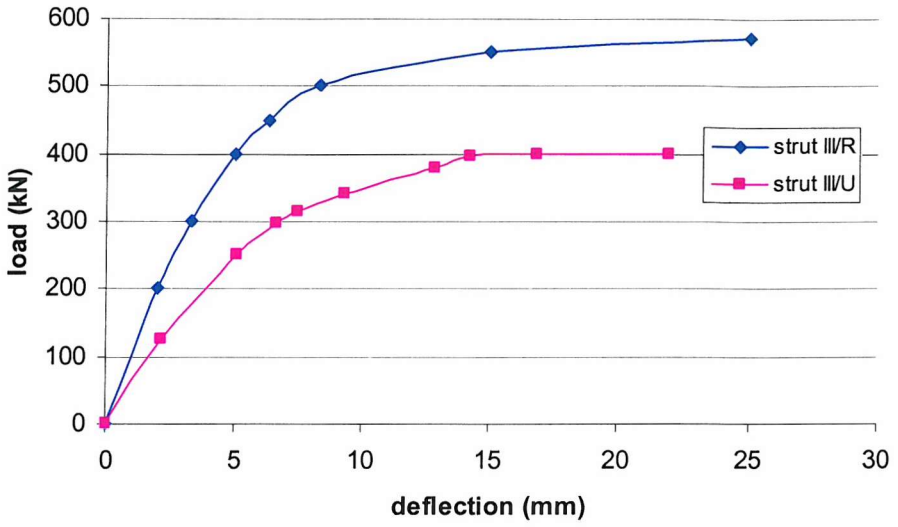

Figure 5.7 Struts III/U & III/R, comparison of load versus deflection graphs

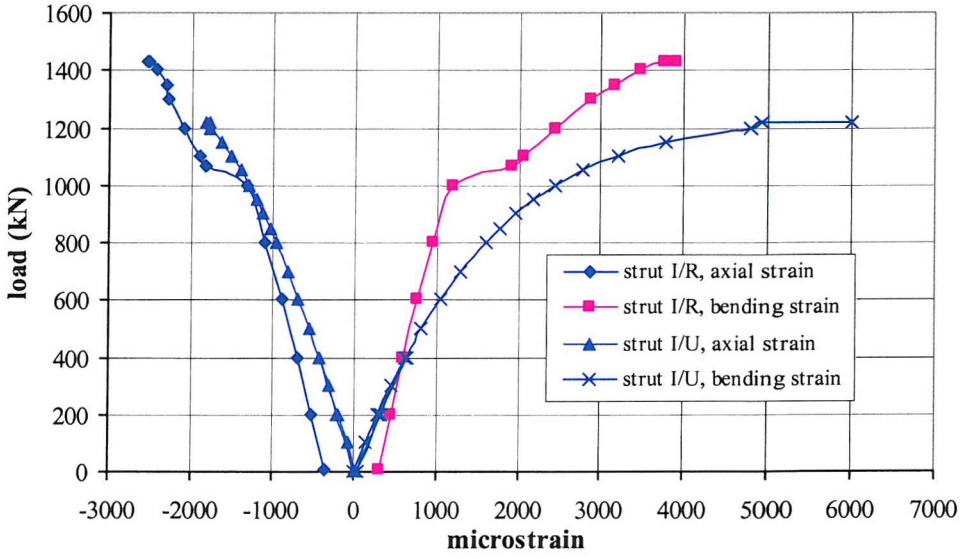

Figure 5.8 Strut I/U & I/R, comparison of load versus axial and bending strains

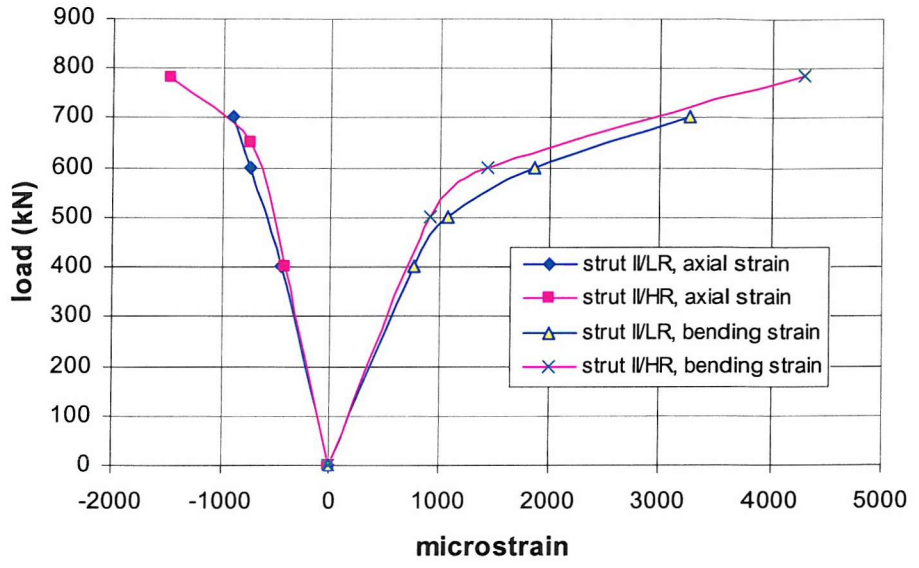

Figure 5.9 Strut II/LR & II/HR, comparison of load versus axial and bending strains

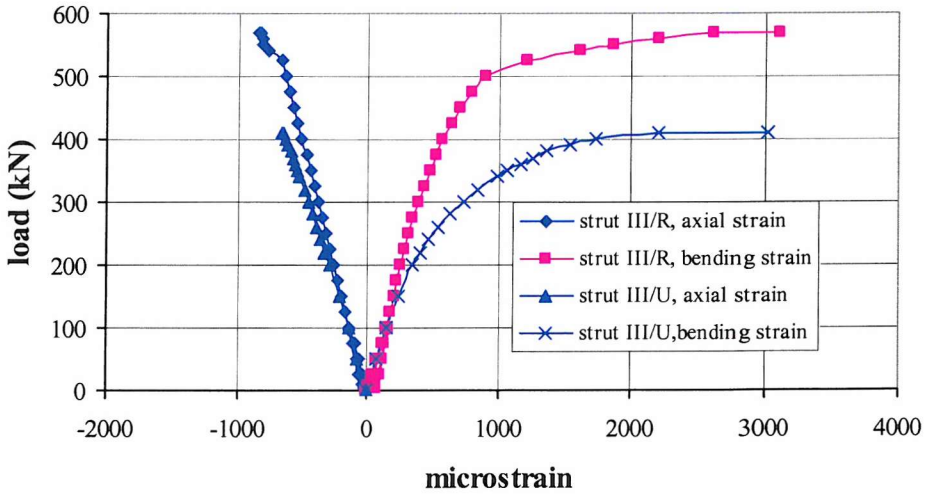

Figure 5.10 Strut III/U & III/R, comparison of load versus axial and bending strains

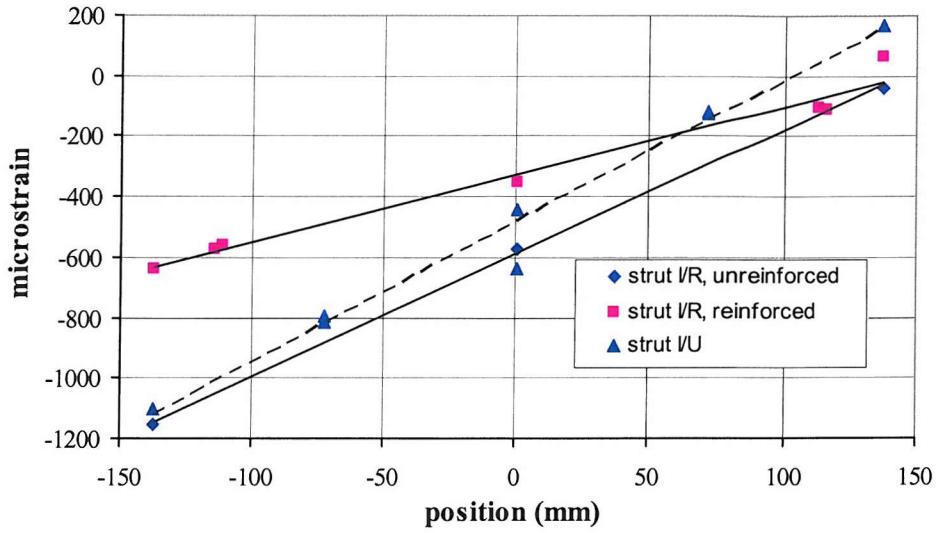

Figure 5.11 Struts I/U & I/R, comparison of strain changes in unreinforced and reinforced struts for a given load of 400kN

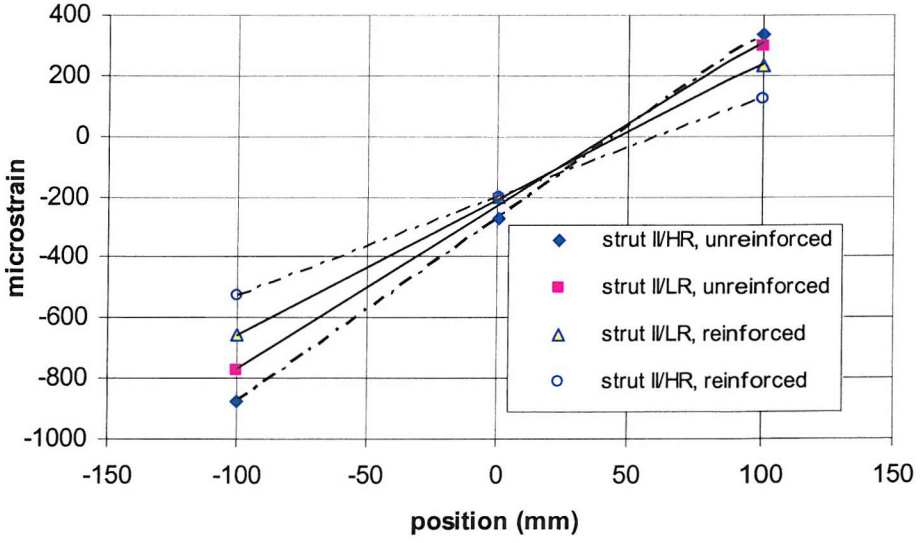

Figure 5.12 Struts II/LR & II/HR, comparison of strain changes in light reinforced and high reinforced struts for a given load of 200kN

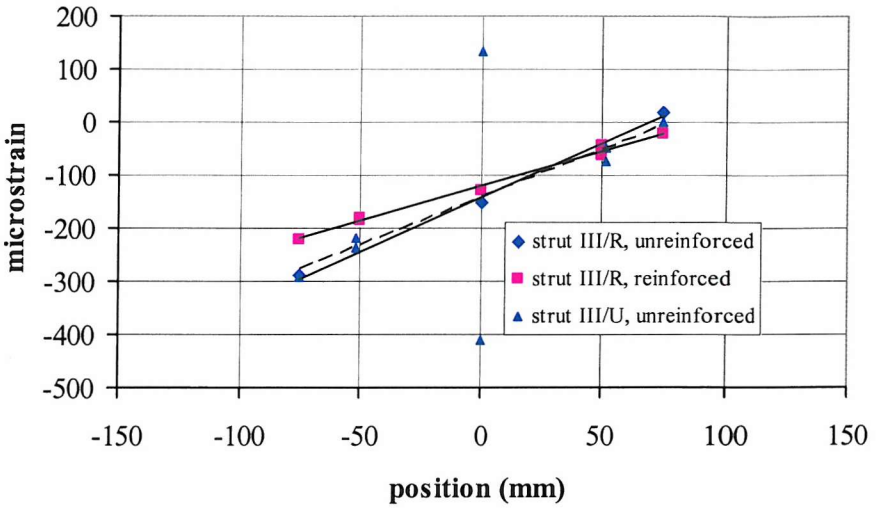

Figure 5.13 Struts III/U & III/R, comparison of strain changes in unreinforced and reinforced struts for a given load of 100kN

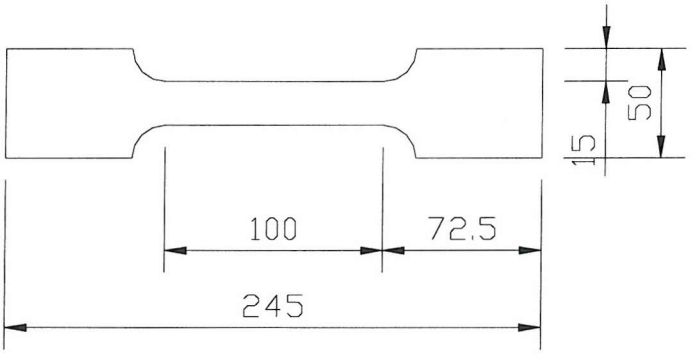

Figure 5.14 Cast iron tensile specimen (specimen is 8mm thick and all dimensions are in (mm)

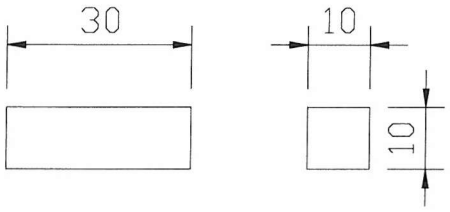

Figure 5.15 Cast iron compression specimen (all dimensions are in mm)

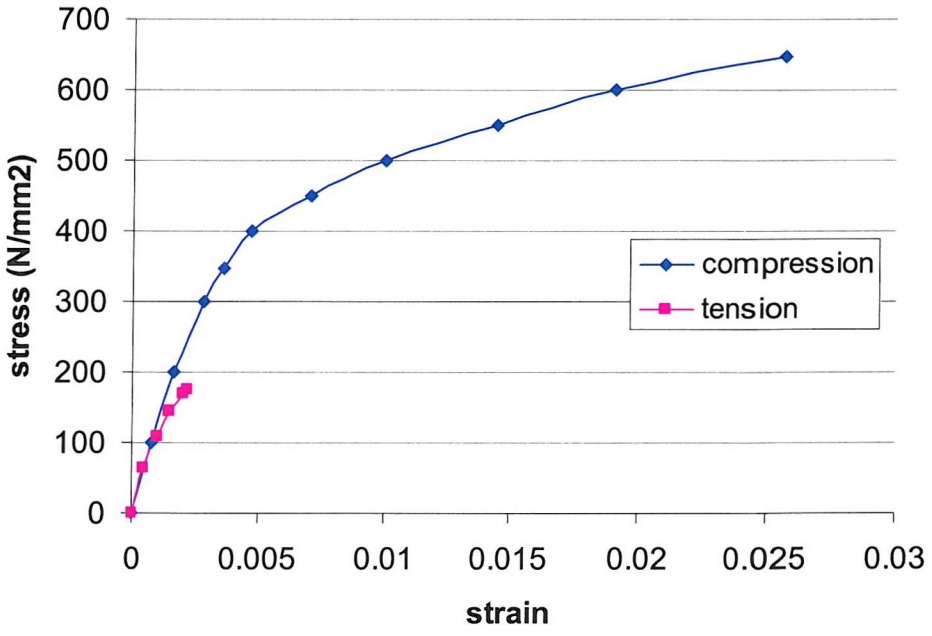

Figure 5.16 Average stress-strain curve for cast iron coupons under tensile and compression loading

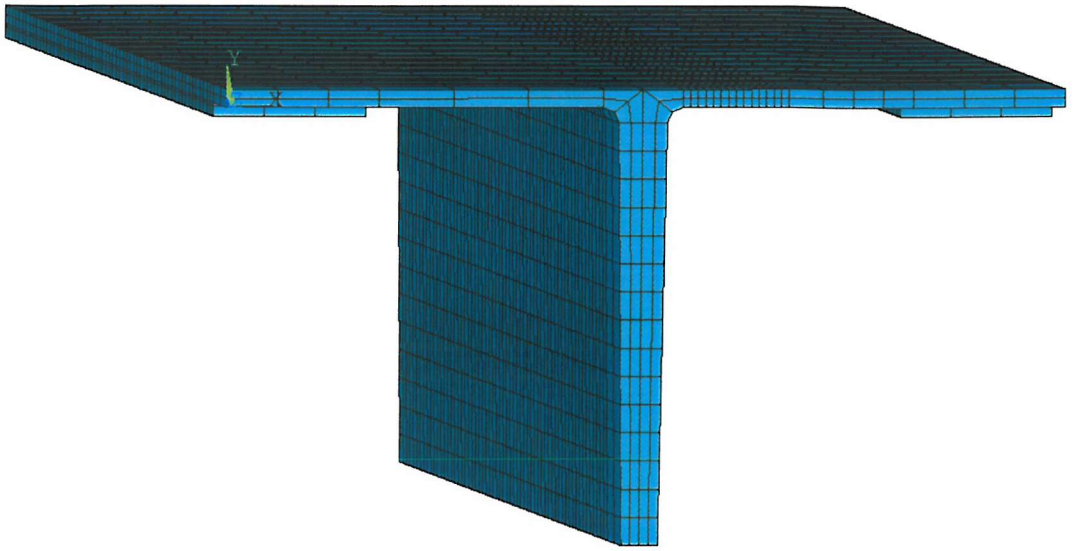

Figure 5.17 Finite element mesh for specimen I-R

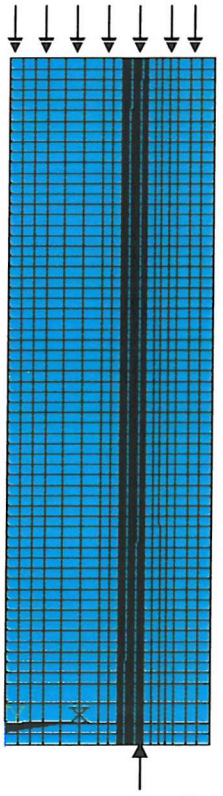

Figure 5.18 Boundary conditions to represent the symmetry

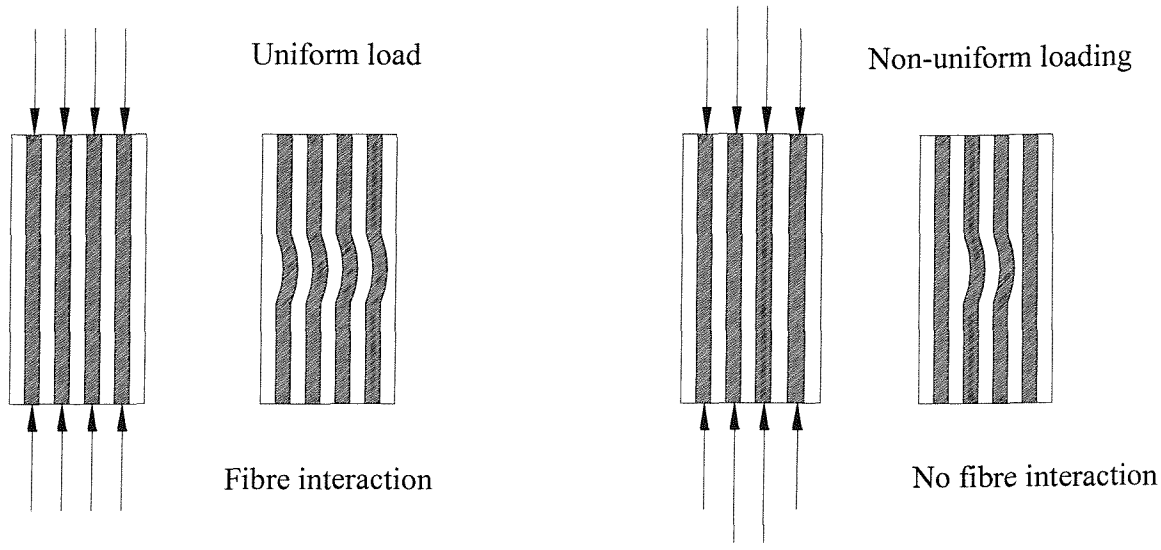

Figure 5.19 Simulation of the buckling of microfibers due to uniform and nonuniform loading conditions.

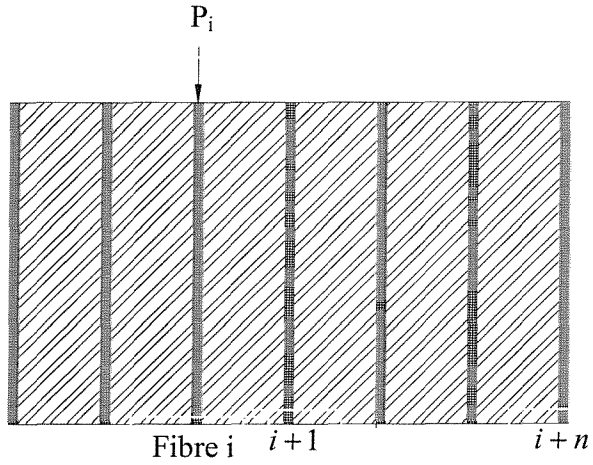

Figure 5.20 Modelling of a fiber-matrix system from a system of fibers

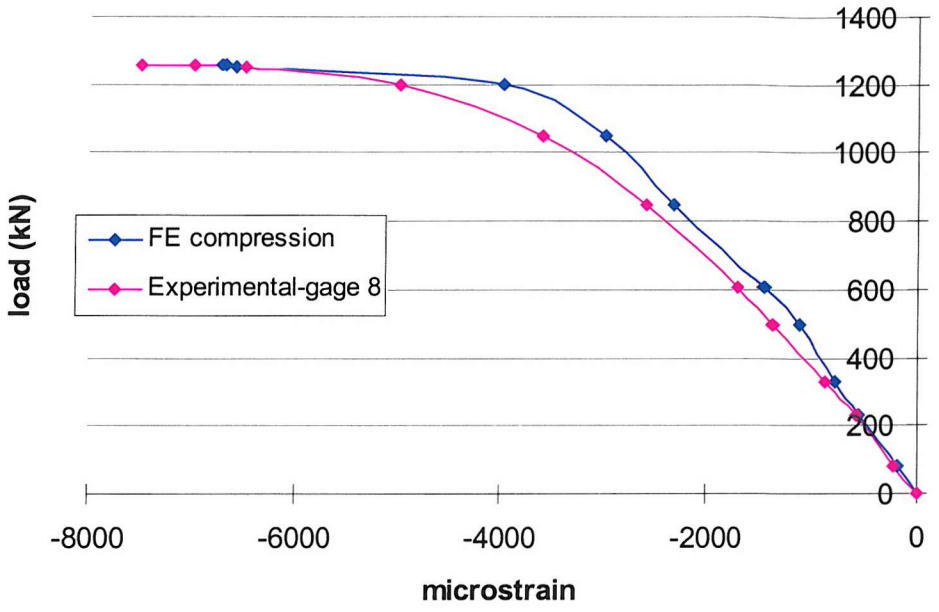

Figure 5.21 Comparison between the FE and the experimental strain reading

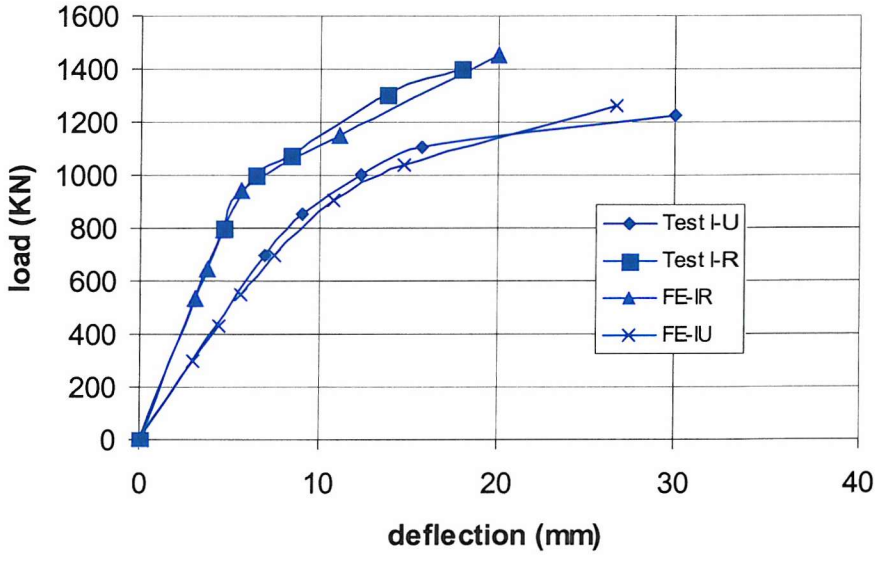

Figure 5.22 Load-deflection graph for reinforced and unreinforced specimen I

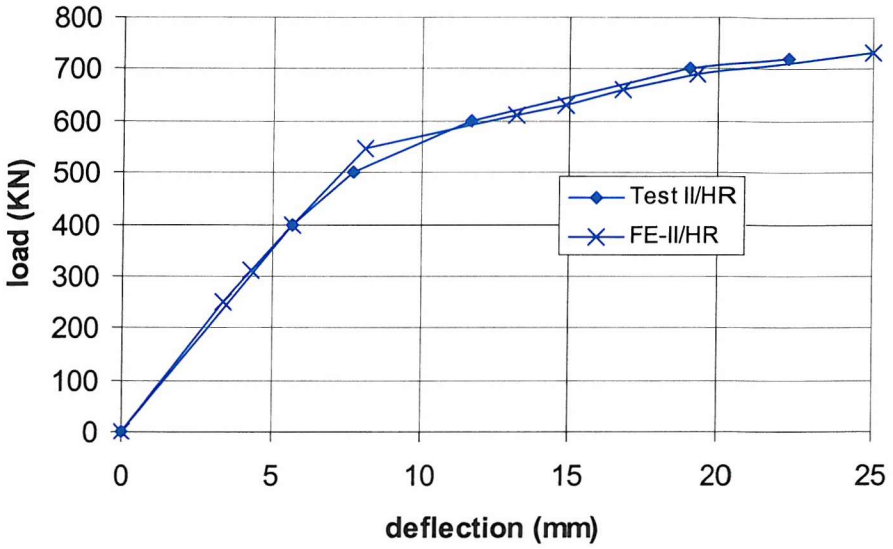

Figure 5.23 Load-deflection graph for specimen II/HR

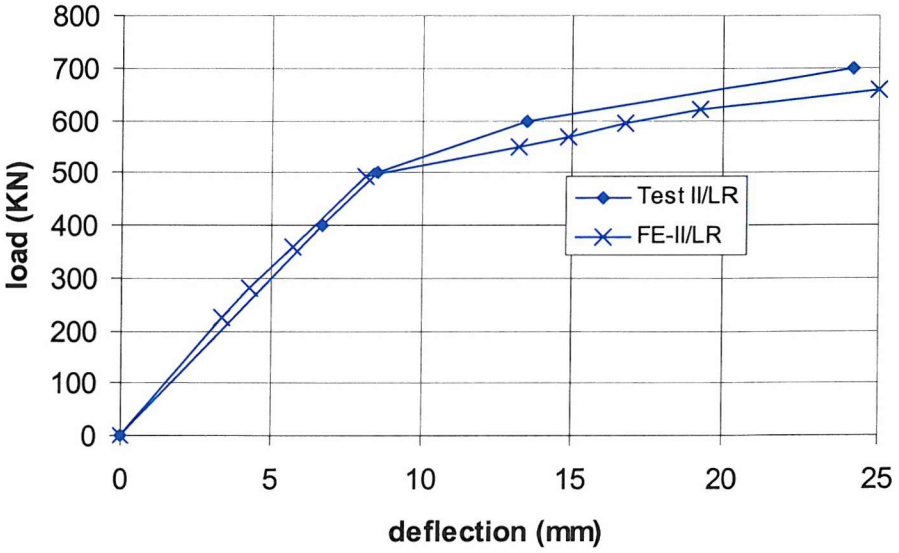

Figure 5.24 Load-deflection graph for specimen II/LR

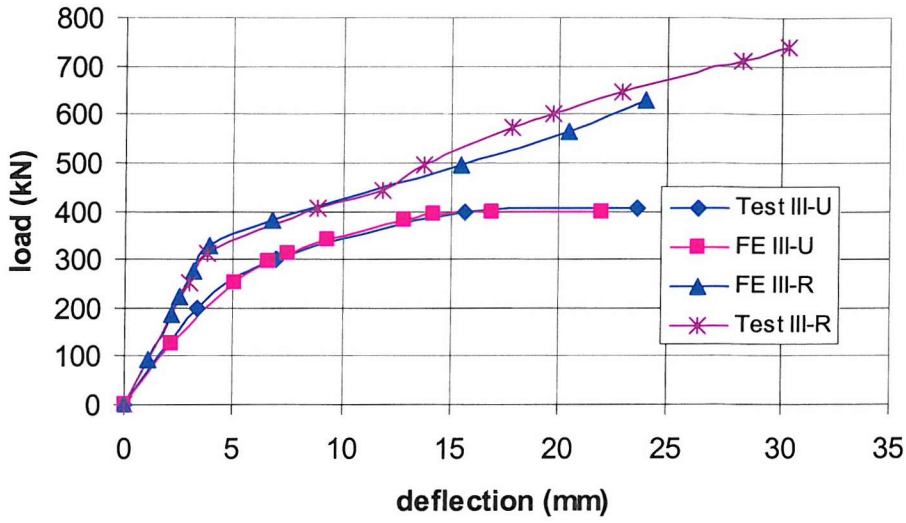

Figure 5.25 Load-deflection graph for reinforced and unreinforced specimen III

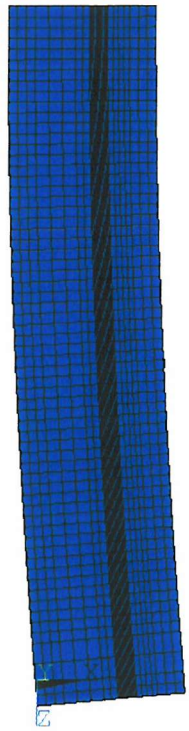

Figure 5.26 A typical cast iron strut deflection (lateral) under eccentric loading

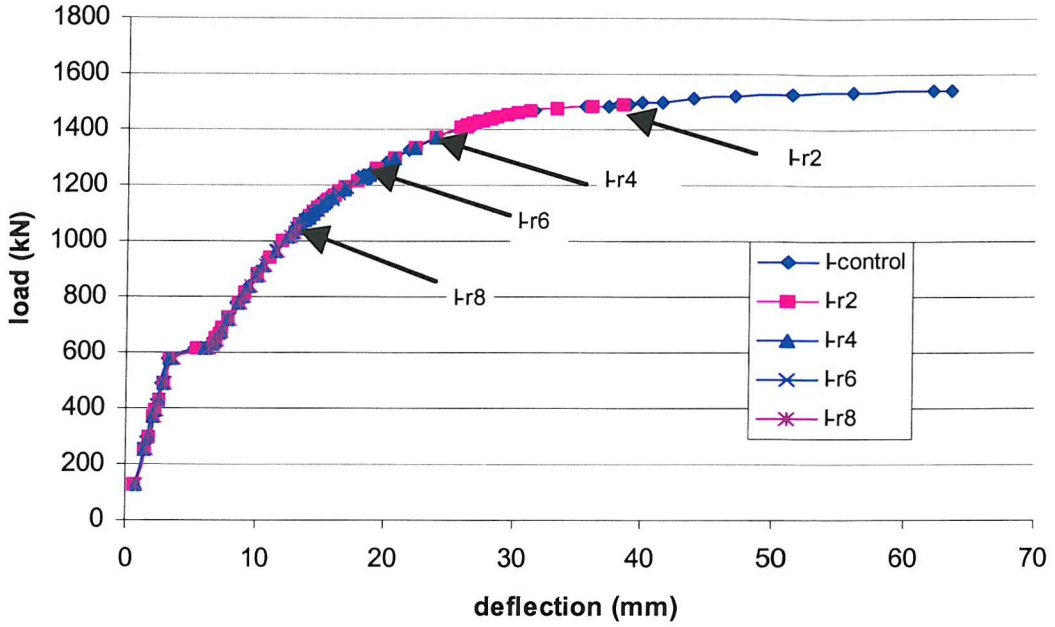

Figure 5.27 Load-deflection graph for reinforced specimen I with various level of imperfection (the arrows indicate the end of each curve)

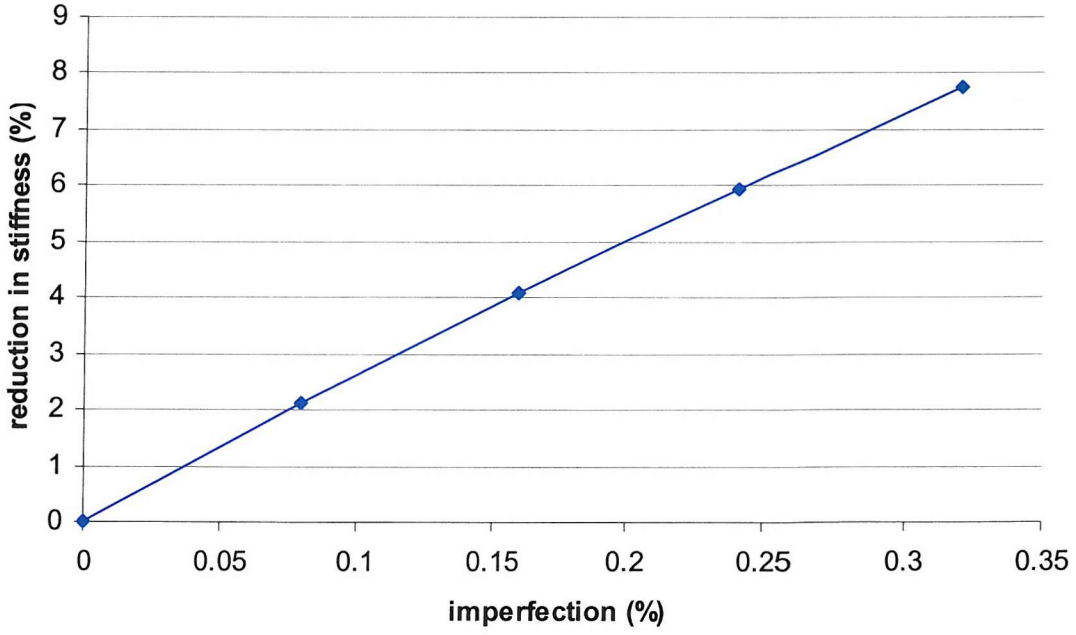

Figure 5.28 Reduction in stiffness with regard to geometrical imperfection on specimen I-R

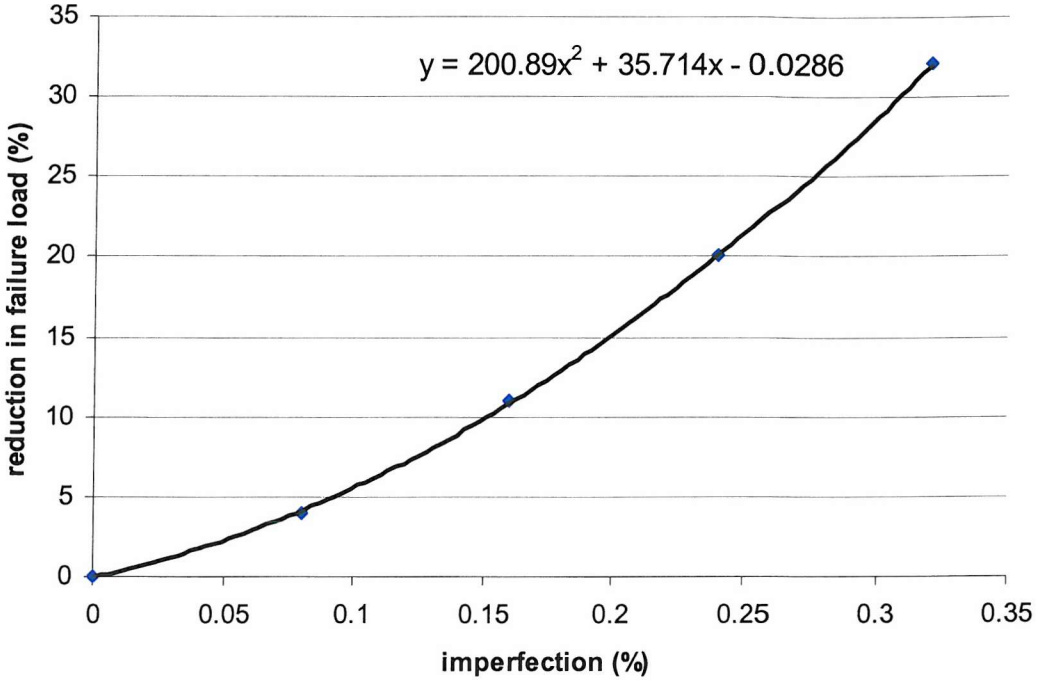

Figure 5.29 Reduction in level of failure load with regard to geometrical imperfection on specimen I-R

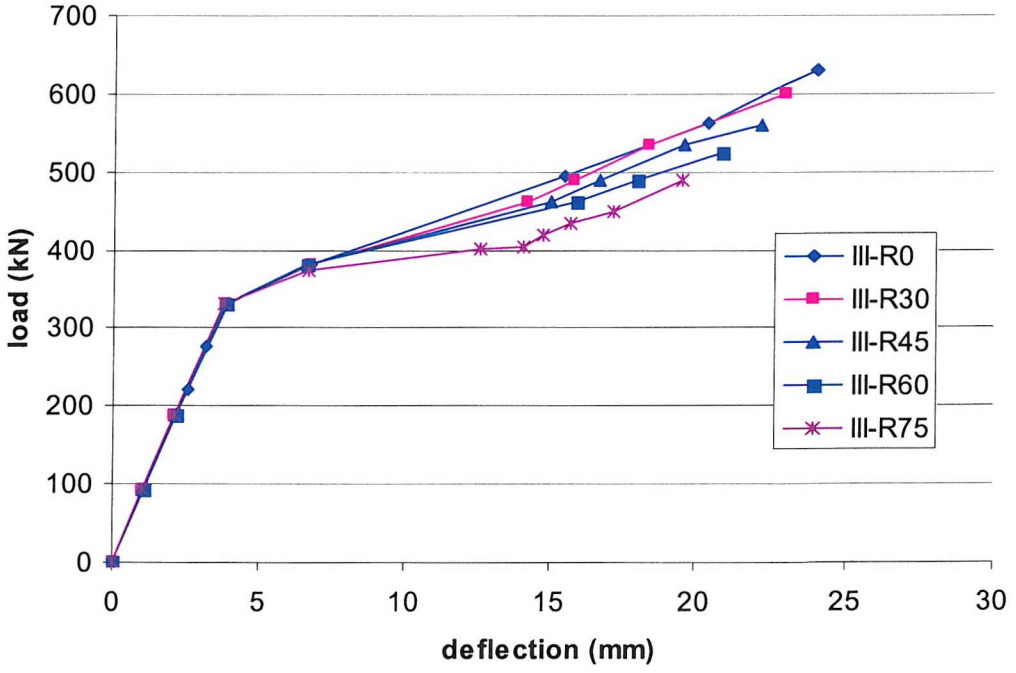

Figure 5.30 Load-deflection graph for reinforced specimen III with various level of preload

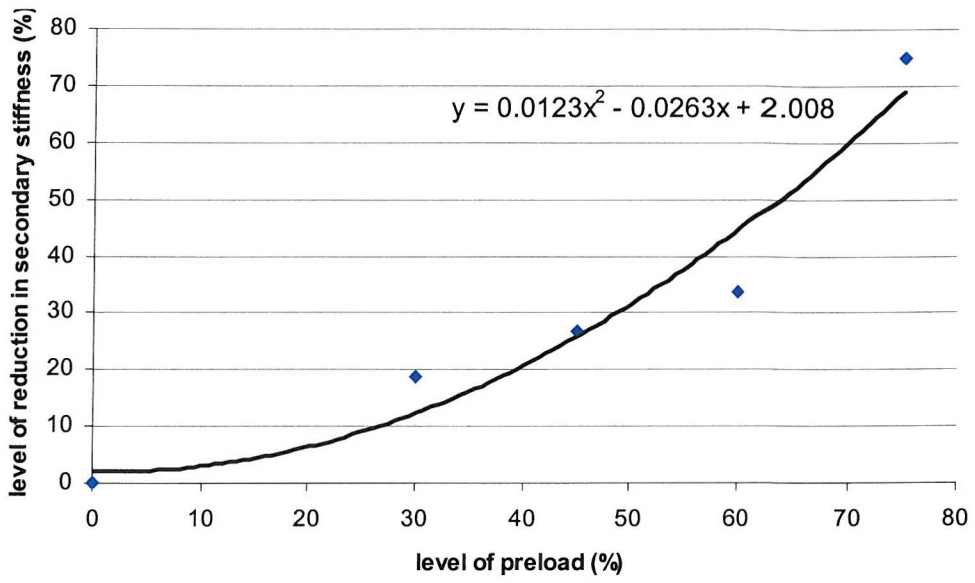

Figure 5.31 Reduction in level of stiffness after carbon fibre failure with regard to initial preload on specimen III-R

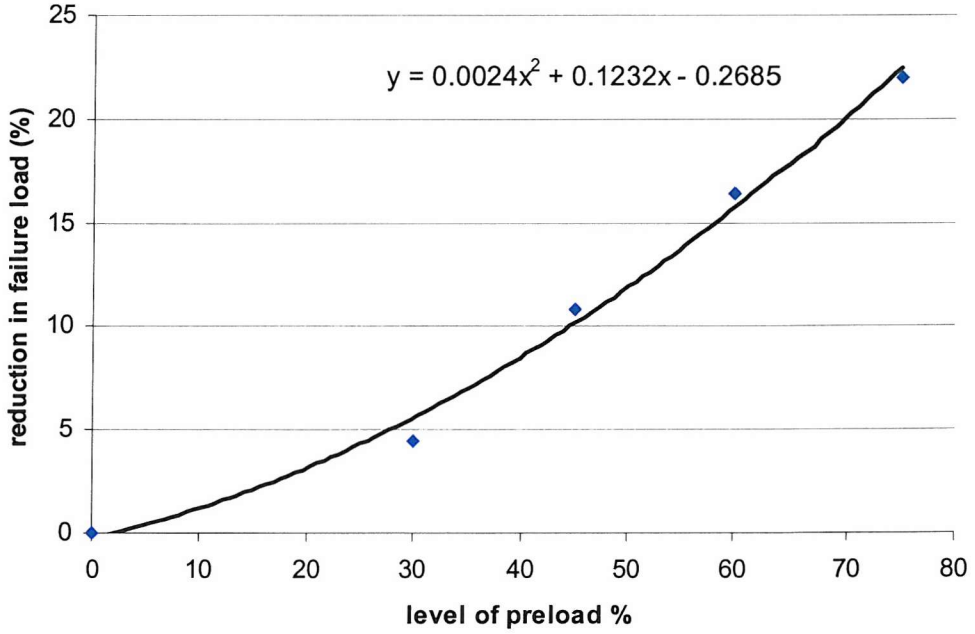

Figure 5.32 Reduction in level of failure load with regard to initial preload on specimen III-R

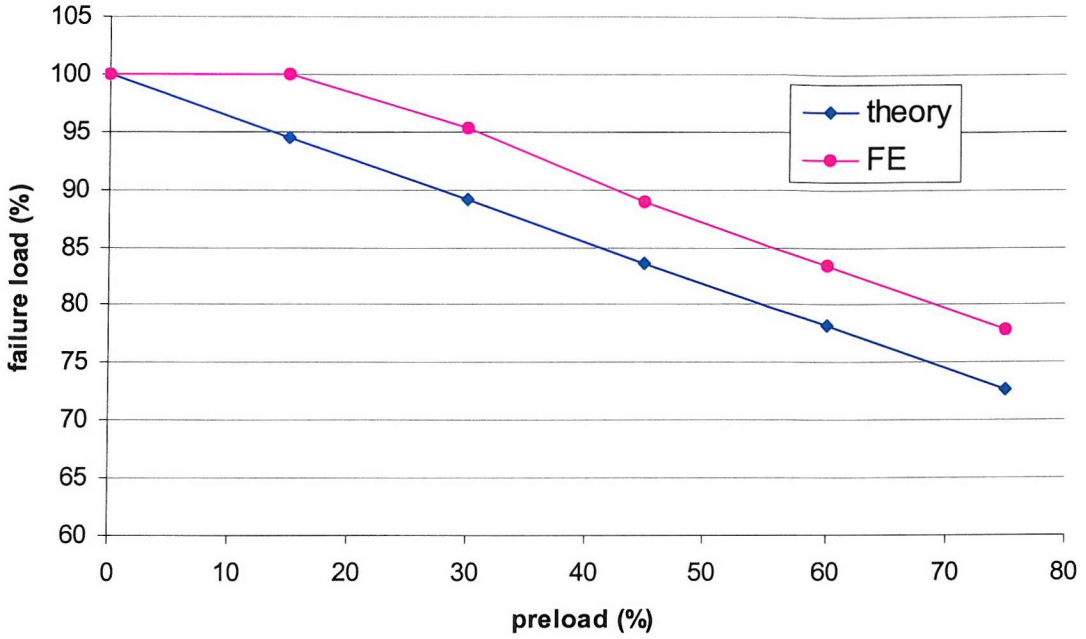

Figure 5.33 Comparison between the predicting of final failure load using FE and theoretical calculations on specimen III-R

CHAPTER 6

CONCLUSIONS AND RECOMMENDATIONS

6.1 PROJECT BRIEF

The aim of this research was to identify the benefits of strengthening metallic structures with CFRP plates while the structures are subjected to preload and imposed loading. Literature review has revealed that although a great deal of work in strengthening structures using fibre composites has been carried out, there are still major concerns regarding the performance of adhesive during the curing period. A major focus of this work was dedicated to the strengthening of railway bridges, particularly to bridges which cannot be closed during strengthening due to economic consideration. In such circumstances the adhesive that is used to bond the CFRP plates to the existing structure is subjected to cyclic loading during curing so that effectiveness of the bond between the metallic substrate and the CFRP may be affected.

The second area of the research dealt with the strengthening of cast iron struts with existing preload and geometric imperfections. Theoretical studies [Moy, 1997] have shown that the intensity of the preload affects the amount of benefit to be gained, as the tensile strength of cast iron determines when failure occurs, thus preventing the CFRP composite from developing its full structural capability. Further FE investigation was carried out into determining the benefits gained from CFRP reinforcement with respect to various levels of preload and geometrical imperfection.

In this chapter the main research findings are summarised and recommendations for further work outlined.

6.2 REINFORCED STEEL BEAMS

6.2.1 Experimental work

When strengthening structures by means of CFRP plate attached to the metallic substrate using adhesives, the adhesive will develop full strength over many hours (depending on temperature) during which the adhesive will be vulnerable to damages caused by excessive deformation which can cause debonding of the CFRP plate.

From the static tests to failure, it was found that the overall stiffness of the structure due to reinforcement using CFRP was increased by as much as 33%. However, this was greatly affected as the adhesive was subjected to cyclic loading while curing. The adhesive sustained damage in the form of debonding.

It was found that the behaviour of the reinforced beam changed from linear to nonlinear well below the failure load, which confirmed that the method of transformed sections is good enough for predicting the reinforced section behaviour. However, this was only valid where the adhesive was not subjected to any imposed loading while curing, which frequently cannot be avoided in practical situations.

The FE models developed have successfully simulated the effect of cyclic loading on the stiffness of the adhesive in the reinforced steel beams and have good agreement with the experimental data.

It has been shown that during the curing period the adhesive could only withstand a limited amount of shear deformation (slip). Beyond that limit the final shear strength of the adhesive will be reduced and eventually debonding will occur. Material failure is achieved when lateral movements in the adhesive exceed a limit. This will reduce the shear strength of the adhesive and eventually lead to debonding. Hence, it is reasonable to assume that this would be valid in all beams irrespective of their size.

The calibrated model based on 1m span beams was used in further analyses to investigate the effect of cyclic loading on the stiffness of the adhesive used in I-beams of more practical dimensions. The analysis of the 1m span beams was extended to 3m and 5m spans and it was shown that in all specimens, the debonding did follow a similar pattern as the 1m span beam.

The FE analyses have shown that excessive slip movement causes debonding of the adhesive layer and the behaviour is consistent throughout specimens, with different length and sizes. Therefore, it was concluded that, for reinforced beams, it is possible to determine the amount of material debonding in the adhesive, when it is subjected to continuous cyclic loading during adhesive curing as described in Chapter Four. It is then possible to calculate the bending stiffness of the reinforced steel beam using the area transformation method. Therefore, it is recommended that until further development in this field, whereby the extent of damage in the adhesive can be predicted with a good accuracy, finite element analysis should be conducted to determine the extent of damage due to any imposed loading.

6.2.2 Parametric study on shear stress distribution on lap-shear specimens

Debonding failure of the adhesive interface depends largely on the interfacial shear and normal stresses between the structure and the bonded plate. At the ends of the reinforcing plate there is a sudden change in the cross-section from the basic unplated member to the plate-reinforced member. Consequently, the axial force in the plate is discontinuous and leads to concentrated forces applied at the end of the plate. Hence the shear stresses at the ends of the plate can be very large. It has been shown [Ascione, L, 2000], that in circumstances the shear stress at the ends of the plate exhibited peak values much higher than those predicted by classical beam bending theory.

It was found that the lap shear behaviour with different adherends was not symmetric due to the difference in mechanical property of the adherends. Simple hand calculations are generally adequate in predicting the level of average shear stress in the adhesive layer. However, due to discontinuity at the ends, all specimens experienced significant increase in shear stress at the ends of the plates. In some cases, especially where the adherend plates are thin, the increased values were significantly higher than the predicted average values. In some cases, the shear stress exhibit peaked values of over twice the values predicted by bending theory. It is these maximum values that initiate peeling.

A pragmatic approach to this problem was adopted in order to overcome uncertainties around this issue. It is recommended that safety factors should be introduced into the beam bending theory calculations until more information is available from further research.

6.3 RINFORCED CAST IRON STRUTS

6.3.1 FE validation

The results of the FE analysis were in good agreement with published experimental results [Moy & Lillistone, 1999] and the predicted deformation behaviour of the reinforced strut agreed with the experimentally observed behaviour.

The FE models confirmed that, in all the specimens, failure initiated in the carbon fibre in greatest compression but the compression force was then transferred from the carbon fibre to the cast iron, allowing the strut to carry more load until final failure in the cast iron in tension.

No further material failure was discovered in the adhesives, as the fully cured adhesive was capable of transferring the shear stress across the cast iron/composite interface and was able to withstand large strains. Also no failure occurred in the CFRP plates in tension because the tensile strength of the CFRP was much greater than that of the cast iron. Hence, while the cast iron experienced tension yield and failure, the stresses in the CFRP plate reached only a fraction of the failure stress level.

6.3.2 Imperfection study

The calibrated models were used in further analyses to investigate the structural behaviour of cast iron strut with a range of geometric imperfections, which were implemented into the finite element model.

Load versus lateral deflection curves followed the same pattern in all specimens and the greatest reduction in initial stiffness due to imperfection was just below 8%. However, the failure load reduced significantly as the sign of the imperfection increased. The maximum imperfection of 8mm out of line of the strut caused a 30% reduction in the failure load.

The imperfections used in this investigation were selected to produce the worst possible effects and it was found that the effects on the structural stiffness were relatively small and could be neglected. However, it was found that the failure loads were significantly influenced by the geometrical imperfections.

Therefore, with regard to load carrying capacity, it is recommended that allowance should be made for the reduction in the load carrying capacity with the aid of FE analysis.

6.3.3 Preload prior to reinforcing

A range of preload varying from 30% to 75% of the FE predicted failure load of the unreinforced cast iron strut was selected and the initial stiffness and failure load of a particular reinforced cast iron strut was analysed.

The level of preload had no effect on the strut stiffness up to the point where failure occurred in the CFRP plate in the compression zone. From this point, the stiffness of the struts was found to be dependent on the level of preload existing prior to reinforcing.

It was shown that the reduction in the stiffness after CFRP plate failure was proportional to the level of preload prior to reinforcing. It was shown that with approximately 50% preload prior to reinforcing the stiffness of the structure after initial carbon plate failure was reduced by as much as 30%.

The use of FE analysis is recommended for predicting the stiffness and the failure level until further research and development in this area has resulted into series of design guidelines.

6.4 Summary

It was found that reinforcing metallic structures with CFRP plates was an effective and efficient method of reinforcement, particularly to structures that cannot be closed during strengthening. This research also outlined the need for further research and development to create better guidelines for practical use.

6.5 RECOMMENDATIONS FOR FURTHER WORK

This research has identified important issues that could improve the serviceability of metallic structures in need of strengthening and rehabilitation. The following issues need to be looked at in more detail to develop reliable design guidelines for the CFRP strengthening of metallic structures.

- There is uncertainty with regard to the shear and normal stress distributions in adhesively jointed structures. It is recommended that further research be carried out in order to develop a better understanding of the phenomena with regard to adhesively joint structures.
- Following cast-iron strut tests [Moy, 1999] pilot test programme on model steel beams with one metre span and reinforced with CFRP was carried out as part of this research. These tests appear to be the totality of testing to confirm the theoretical studies upon which the existing design guides for metallic structures have been based. Therefore, it is recommended that further testing of cast-iron beams and struts, and steel beams be carried out. The results will form a basis to confirm, or otherwise, some of the tentative recommendations given in the design guides for metallic structures. They would also form the basis for more comprehensive guidance that should encourage much wider use of polymer composites in construction.

References

ABAQUS/AQUA (1997) User's Manual Rev 5.5-5.8, Hibbit, Karlsson and Sorensen Inc., Rhode Island, USA

Adams R. D and Wake W. C (1984), structural adhesive joints in engineering, Kluwer

Albrecht G and Haensel J (1996), replacement of single cables in cable strayed and suspension bridges. Third international conference on bridge management. University of Surry, UK, 14-17 April.

Angus H T (1960), physical and engineering properties of cast iron, 2nd edition, London Boston: Butterworth.

ANSYS 6.1 (1999) User's Manuals Rev 5.5-6.1, Swanson Analysis Systems Inc., Houston, Texas, USA

Ascione L (2000), modelling of composite/concrete interface of RC beams strengthened with composite laminates, composite part B-ENG 31 (6-7):535-540

Advanced Structural SystEms for Tomorrow's infrastructure (internal report, 2002), former Mouchel Consulting Ltd, Surrey UK

Baker A. A. and Jones R. (1988) bonded repair of aircraft structures, Martinus Nijhoff Publishers

Berfsaas A and Brustad H (1993), assessment and evaluation of a railway bridge. Second international conference on bridge management, university of Surry, Guildford, UK, 18-21 April.

Bhagwan D. A (1990), Analysis and performance of fibre composites, 2nd edition, New York: Wiley

Chang fu-kuo & Lessard L B (1989) Effect of load distribution on the fibre buckling strength of unidirectional composites, Journal of Composite Material, Vol24, pp.,65-92

Chang fu-kuo (1986) A progressive damage model for laminated composites containing stress concentrations, Journal of Composite Materials, Vol 21, pp.,834-855

Chawla K K (1987), composite materials, springer-verlag, New York

Clarke J L & Spon F N (1996), EUROCOMP, structural design of polymer composites

Daniel IM and Ishao O (1994). Engineering Mechanics of Composite Materials. Oxford University Press.

Das PC (1996), safety concepts and practical implications. International symposium. ICE highways agency. London, 4-5 July.

DERA (Defence Evaluation and Research Agency, 2000), material testing – 120 years design life, part of LINK inland surface transport project IST 031 internal report

Dier et al., the JIP1 manual, chapter 8, 1997

DML (Development Royal Dockyard Ltd, 2000), Plate bonding development-final report, part of LINK inland surface transport project IST 031 internal report

Evans JE (1993), the strengthening and improvement of the structures of the Severn crossing. Second international conference on bridge management, university of Surry, Guildford, UK, 18-21 April.

Gillett. H. W (1951), The behaviour of engineering metals, 1951, **London : Published for Gillet Brothers Discount Company**

Hart-smith L. J (1973), adhesive bonded single lap joint, CR 112236, NASA Langley research centre, USA.

Hashin Z (1980) failure criteria for unidirectional fibre composites, journal of applied mechanics, Vol 47, P329-334

Hull D (1981), an introduction to composite materials, Cambridge University Press, Cambridge, U.K.

Institution of Civil Engineers (2001), design, and practice guide, FRP composites life expansion and strengthening of metallic structures, Thomas Telford UK

Karabinis. A. I and Rousakis, T. C (2002), "Concrete confined by FRP materials, a plasticity approach", ENG structures 24 (7): 923-932

Kennedy I (2001), Steel bridge strengthening: a study of assessment and strengthening experience and identification of solutions, London: Thomas Telford

Lawrence J. B (1974), Engineering applications of composites, 2nd edition, New York: Wiley

Lee W. A (1984), Adhesive in engineering design, London – design council

Lessard L B and Chang fu-kuo (1989), "Damage tolerance of laminated composites containing an open hole and subjected to compressive loading": Part I- analysis

Lessard L B and Chang fu-kuo (1989), "Damage tolerance of laminated composites containing an open hole and subjected to compressive loading": Part II- experiment

Lessells J M (1954), strength and resistance of metals, John Wiley, New York

LINK inland surface transport project IST 031 (2000), " Carbon fibre composites for structural rehabilitation and life extension, validation and design guidance, final report

Mallick P K (1988), fibre-reinforced composite, Marcel Dekker, New York.

Mays G. C (1981), Adhesively bonded joints in engineering applications, Philadelphia Pa

Metcalfe A (1974), interfaces in metal matrix composites, New York: Academic Press

Meyer R W (1985), Pultrusion technology, chapman and hall, New York.

Moy S.S.J. & Lillistone (1999) A theoretical investigation into the benefits of using carbon fibre reinforcement to increase the capacity of initially unloaded and preloaded beams and struts. Department of Civil & Environmental Engineering Research Report, University of Southampton, part of LINK inland surface transport project IST 031 internal report.

Moy S.S.J. (2000) Early age curing under cyclic loading - an investigation into stiffness development in carbon fibre reinforced steel beams. Department of Civil & Environmental Engineering Research Report, University of Southampton, part of LINK inland surface transport project IST 031 internal report

MSL (MSL engineering Ltd, 1999), Design of strengthening schemes for cast iron struts using carbon fibre reinforced plastics, part of LINK inland surface transport project IST 031 report.

Nanni A (2003), Fibre-reinforced composites for the strengthening of masonry structures, Structural Engineering International 4, P271-278

National Engineering Laboratory (1999) a report for London underground (cast iron struts in compression), part of LINK inland surface transport project IST 031 report.

Noton B (1974), engineering application of composites, New York: Academic Press

Parmley P A (1974), engineering application of composites-military aircraft, advanced composites branch, structures division, internal report

Pritchard B (1993), bridge strengthening with minimum traffic disruption. Second international conference on bridge management, university of Surry, Guildford, UK, 18-21 April.

Rabinovitch Y. F (2002), Strengthening of RC slabs with circular composite patches, composite structures, Vol 55, pp. 225-238

Richardson M. O. W (1977), Polymer engineering composites, London: Applied science publishers

Rocca R J D and Scott R J (1974), engineering application of composite-ocean engineering, Gibbs & Cox, incorporated

Roko K (1999) failure modes of sheet bonded fibre-reinforced polymer applied to brick masonry. Fourth international symposium on fibre-reinforced polymer for reinforced concrete structures, Baltimore, MID, Nov 1999, pp.305-311

Rosato D V and Grove C S (1964), filament winding, wiley, New York

Shiuh-chuan der (1999), stress analysis of adhesively-bonded lap joints, composite structure 47 (1-4): 673-678

Taljsten B (2003), Strengthening concrete beams for shear with CFRP sheets, construction and building materials, Vol 17, pp. 15-26

Bibliography

Adams R. D and Peppiatt N. A, stress analysis of adhesive bonded lap joints, J1. of strain analysis, (1974)

Admas R. D. and Peppiatt N. A, rubber model for adhesive lap joints, J1. of strain analysis. (1973)

Admas R.D. and Grant L. D. R, adhesive layer thickness as a variable in the strength of bonded joint, 16th anuual meeting of the adhesion society, Williamsburg, USA (1993)

Ahn S. H and Springer G. S, repair of composite laminates- II: models, J1 of composite materials (1998)

Ahn S. H. and Springer G. S, repair of composite laminates-I: test results, J1. of composite materials (1998)

Amijima, S. and T. Adachi. "Nonlinear Stress-Strain Response of Laminated Composites," J. of Composite Materials, 7:124-130 (1973).

Ascione, L. Feo. Modelling of composite/concrete interface of RC beams strengthened with composite laminated, J. Comp. Eng., 2000, 535-540.

Baker A. A. and Jones R. bonded repair of aircraft structures, 1988

Barnes, F. and Dier, A. F., "carbon fibre composite for the strengthening, repair and modification of offshore structures", international conference on advances in marine structures III, DERA Rosyth, U.K., May 1997.

Berndt N and Wittmoser A, grey iron as a material in shipbuilding and marine engine construction, grey iron founders' society, 1958.

Blake J. I. R, Boyd S., Nisio S. D. and Shenoi R. A. experimental determination of residual strength and stiffness of metal-composite joints under cyclic loading, 2001

Bogdanovich A. and Kizhakkethara I. Three dimensional finite element analysis of adhesively bonded plates, 1997.

Bolton J W, grey cast iron, penton, Cleveland, 1937

Bowditch M, Carbon fibre composite for strengthening and rehabilitation surface preparation development, 2000

Burns, S. W., C. T. "Failure modes for compression loaded angle-ply plates with holes". Proceeding of 4th international conference on composite structures, UK., 27-29, 1987, pp. 2.175-2.191.

Chen D, an analysis of adhesive-bonded single-lap joints. J appl mech 1983; 50:109-15.

Cheng, S., Analysis of adhesively bonded joints with non-identical adherends. J. Eng. Mech., 1991, 117, (3), 605-623.

Chow W. T. and Atluri N. composite patch repair of structures: adhesive nonlinearity, thermal cycling, and debonding, 1997.

Curtis PT (ed.). CRAG Test Methods for the Measurement of the Engineering Properties of Fibre Reinforced Plastics. Technical Report No. 88012, Royal Aerospace Establishments, 1988.

Das PC, bridge assessment and strengthening: principal and practical issues. Journal of highways. Proceeding of seminar PTRC European transport forum. University of Warwick, 12-16 September 1994.

Delale, F., Stresses in adhesively bonded joints: A closed form solution. J. Composite Mater., 1981, 15, 249-271.

Design Guidance for Strengthening of Concrete Structures using Fibre Composite Materials. The Concrete Society, Technical Note No.55. 1999 ISBN 0 9466 9184 3.
DRDL, Final report for plate bonding development trails, 2000

Drimoussis A, Cheng JJR. Shear strengthening of concrete bridge girders using carbon fibre-reinforced plastic sheets. Fourth International Bridge engineering Conference, vol. 1. San Francisco (California, USA), August 28–30, 1995:337– 47.

Flint AR and Huband MV, bridge assessment: the need for codified rules. Second international conference on bridge management, university of Surry, Guildford, UK, 18-21 April 1993.

Folks M J, short fibre reinforced thermoplastics, Wiley, Chichester, U.K., 1982.

ICE design and practice guide. FRP Composites. Life Extension and strengthening of metallic structures. Editor S.S.J. Moy. Thomas Telford Ltd, July 2001. ISBN 0 7277 3009 6.

Pahdi G.S., R.A. Shenoi, S.S.J. Moy, and G.L. Hawkins. Progressive Failure and Ultimate Collapse of Laminated Composite Plates in Bending. Composite Structures. Vol 33, No 11, 1997.

Gilletta, D. "Degradation models in finite element analysis of multilayered composite structures". Proceeding of 4th international conference on composite structures, UK, 1987, pp. 1.555-1.563.

Glover T J, BCIRA J.11, 782-793, 1963

Hahn, H. T. and S. W. Tsai. "Nonlinear Elastic Behaviour of Unidirectional Composite Laminate," J. of Composite Materials, 7:102110 (1973).

Herakovich, C. T. 1981. "on the relationship between engineering properties and delamination of composite materials". Journal of composite material, 15:336-348.

Herakovich, C. T. 1982. "Influence of layer thickness on the strength of angle-ply laminates. Journal of composite material, 16:216-227.

Hillman M H, BCIRA J.research and development, 5, 188-248, 1954

Humphreys JG., BCIRA J., 9, 609-621, 1961

Jones RM. Mechanics of Composite Materials. McGraw-Hill, 1975

Klaiber, F. W., Strengthening of single-span steel-beam bridges. Journal of the structural division, ASCE, 1982, 108(12), 2766-2780.

Klien A J, carbon/carbon: an ultrahigh-temperature composite. Adv. Compos., 38-44, March 1989.

Laszlo F and Nolle H J, J. Mechanics and physics solids, 7, no. 3, 193-208, 1959

Li G., Lee P. S. finite element and experimental studies on single-lap balanced joint in tension, 2001

Lim. C. K. Acitelli M. A. failure criteria of a typical amide cured epoxy adhesive, 1974

Menzies JB, bridge failures, hazards and social risks. International symposium. ICE highways agency. London, 4-5 July 1996.

National Engineering Laboratory, " compresiion test on cast iron struts", report for London underground ltd, 1998

Nuismer, R. J. and J. M Whitney. "Uniaxial Failure of Composite Laminates Containing Stress Concentrations," in Fracture Mechanics of Composites, ASTM STP 593, American Society of Testing and Materials, pp. 117-142 (1975).

O'Brien, T. K. 1982. "Characterization of delamination onset and growth in a composite laminate". Damage in composite materials, ASTM STP 775. K. L. Reifsnider, ed. American society for testing and material, pp. 140-167.

Pahdi, G. S, Shenoi, R. A, Moy, S. S. J, "progressive failure and ultimate collapse of laminated composite plates in bending", composite structures, Vol40, 1998, pp 227-291.

Rehder J E, Proc. Internat. Foundary Congress, Brussels, paper no 4, 313-324, 1951.

Richardson F D and Jeffes J H, J. iron steel inst, 163, 397-420, 1949

Roland, stress and strain distribution across the adhesive thickness, 1999
Rosen, B. W. "Mechanics of composite strengthening". Fibre composite materials, chapter 3, American society for metals (1965).44

Ryder GH. Strength of Materials. Cleaver-Hume Press Ltd., 1969. Rosen, B. W. "Mechanics of Composite Strengthening," Fibre Composite Materials, Chapter 3, American Society for Metals (1965).

Moy S.S.J.. Early age curing under cyclic loading - an investigation into stiffness development in carbon fibre reinforced steel beams. Department of Civil &

Environmental Engineering Research Report, University of Southampton, September 2000.

Moy S.S.J.. Lap-shear tests on specimens cut from CFRP reinforced steel beams. Department of Civil & Environmental Engineering Research Report, University of Southampton, January 2001.

Saadatmanesh H, 1994, strength and ductility of concrete columns externally reinforced with fibre composite straps, 1994.

Shiuh-Chuan Her, Stress analysis of adhesively-bonded lap-joints, composite structures, 1999, 47, 673-678

Sneddon, I. N., The distribution of stresses in adhesive joints. Chapter in adhesion, ed. Eley, D. D., Oxford University Press, 1961, pp. 207-253.

Spandenberg. L. The fatigue of metals under repeated strains, 1876.

Starnes, J. H. "Failure characteristics of Graphite-Epoxy structural component loaded in compression", in mechanics of composite materials, 1982, pp. 283-306.

Structural Materials Handbook, volume 1 – Polymer Composites. European Space Agency, ESA PSS-03-203.

Talreja, R. 1985. "Transverse cracking and stiffness reduction in composite laminates". Journal of composite materials, 19:355-375.

Tasi, S. Introduction to composite materials. Lancaster PA: Technomic publishing company (1980).

Tong. L., Effect of joint flexibility in adhesively bonded composite panel-to-flange joints. 1998, J. Comp. Eng. 287-298

Tsai, M. Y., An evaluation of analytical and numerical solutions to the single-lap joint. Int. J. Solids structures, 1994, 31, (18), 2537-2563.

Vestergren, P. and Knutsson, L., Theoretical and Experimental investigation of the buckling and post buckling characteristics of flat carbon fibre reinforced plastics panels subjected to compression or shear loads. International council of aeronautical science, paper B-101.1978, pp. 217-223.

Schelling W.. Laminated Timber Sections. Translation of paper in German communicated by J. Mallinckrodt, 1990.

Waddoups, M. E., J. R. Eisenmann amd B. E. Kaminski. "Macroscopic Fracture Mechanics of Advanced Composite Material,"J. Composite Materials, 5:446-454 (1971).

Wass, A., C. 1989. "An experimental study of the initiation and propagation of damage in compressively loaded composite laminates in the presence of a circular cutout". Proceeding of the AIAA/ASME/ASCE/AHS/ASC 30th structures, structural dynamics and materials conference, part II, mobile, AL, April 1989, pp. 1000-1011.

Whitney, J. M. and R. J. Nuismer. "Stress Fracture Criteria for Laminates Composites containing Stress Concentrations". J. Composite Materials, 8:253 – 265 (1974).

Wu, J. Z. "Stress expressions of single-lap adhesive joints of dissimilar adherends", composite structures Vol, 38, No, 1-4, 1997.

Yamada. S. E. "Analysis of laminate strength and its distribution". J. of composite materials, 12:275-284.

Yang, C. and Pang, S. S., Stress-strain analysis of single-lap composite joint under tension. J. Eng. Mater. And Tech., 1996, 118, 247-225.

Appendix A- experimental data, steel beam

- **Cyclic loading stage**
- **Bending test to failure**

Load (KN)	*Platen Deflection (mm)*	*Channel 1*		*Channel 7*	
		Ohms	*Deflection (mm)*	*Ohms*	*Deflection (mm)*
47:49 hrs					
0.91	45.36	0.00	4330.4	12.99	0.00	814.32	12.21	0.00
2.78	44.93	0.43	4339.1	13.02	-0.03	800.05	12.00	0.21
6.00	44.65	0.71	4303.1	12.91	0.08	792.34	11.89	0.33
11.84	44.32	1.04	4265.6	12.80	0.19	782.25	11.73	0.48
19.37	43.98	1.38	4199.6	12.60	0.39	755.68	11.34	0.88
30.05	43.53	1.83	4119.5	12.36	0.63	746.14	11.19	1.02
40.11	43.14	2.22	4056.5	12.17	0.82	717.01	10.76	1.46
48.81	42.82	2.54	3980.6	11.94	1.05	704.80	10.57	1.64
59.22	42.45	2.91	3930.0	11.79	1.20	686.12	10.29	1.92
62.94	42.31	3.05	3894.5	11.68	1.31	684.46	10.27	1.95
51.51	42.68	2.68	3964.2	11.89	1.10	703.26	10.55	1.67
40.12	43.06	2.30	4046.0	12.14	0.85	713.50	10.70	1.51
31.20	43.36	2.00	4106.6	12.32	0.67	729.23	10.94	1.28
21.51	43.73	1.63	4173.7	12.52	0.47	746.03	11.19	1.02
9.81	44.24	1.12	4258.1	12.77	0.22	776.26	11.64	0.57
5.44	44.46	0.90	4330.9	12.99	0.00	799.82	12.00	0.22
2.05	44.89	0.47	4338.1	13.01	-0.02	795.20	11.93	0.29
0.99	45.12	0.24	4340.0	13.02	-0.03	806.90	12.10	0.11

Table A1: Transducer readings for control beam @ 47:49

Load (KN)	*Platen Deflection (mm)*	*Channel 1*		*Channel 7*	
		Ohms	*Deflection (mm)*	*Ohms*	*Deflection (mm)*
00:25 hrs					**Cycles: 0**
0.68	19.83	0.00	4628.6	13.89	0.00	413.11	6.20	0.00
2.44	19.34	0.49	4445.7	13.34	0.55	414.80	6.22	-0.03
5.70	18.85	0.98	4345.9	13.04	0.85	415.41	6.23	-0.03
8.05	18.69	1.14	4304.0	12.91	0.97	422.06	6.33	-0.13
10.85	18.45	1.38	4277.3	12.83	1.05	402.55	6.04	0.16
12.99	18.39	1.44	4242.7	12.73	1.16	398.63	5.98	0.22
15.45	18.25	1.58	4246.8	12.74	1.15	386.77	5.80	0.40
18.07	18.13	1.70	4213.1	12.64	1.25	389.17	5.84	0.36
21.01	17.98	1.85	4189.4	12.57	1.32	378.31	5.67	0.52
23.00	17.88	1.95	4153.2	12.46	1.43	376.74	5.65	0.55
25.28	17.76	2.07	4118.9	12.36	1.53	378.06	5.67	0.53
20.14	17.98	1.85	4197.9	12.59	1.29	386.41	5.80	0.40
14.90	18.22	1.61	4263.6	12.79	1.10	395.95	5.94	0.26
10.28	18.46	1.37	4297.4	12.89	0.99	404.60	6.07	0.13
5.65	18.73	1.10	4343.5	13.03	0.86	415.70	6.24	-0.04
0.64	19.62	0.21	4561.5	13.68	0.20	406.83	6.10	0.09

Table A2: Transducer readings for SB 25 @ 00:25

Load (KN)	*Platen Deflection (mm)*	*Channel 1*		*Channel 7*	
		Ohms	*Deflection (mm)*	*Ohms*	*Deflection (mm)*
02:26 hrs					**Cycles: 2339**
Max. cyclic load: 25.04 KN					Min. cyclic load: 0.07 KN
0.36	19.61	0.00	4579.6	13.74	0.00	442.16	6.63	0.00
2.50	18.66	0.95	4466.4	13.40	0.34	416.19	6.24	0.39
4.99	18.18	1.43	4429.8	13.29	0.45	410.57	6.16	0.47
7.73	17.93	1.68	4388.7	13.17	0.57	406.19	6.09	0.54
11.04	17.69	1.92	4337.0	13.01	0.73	392.11	5.88	0.75
12.94	17.44	2.17	4321.1	12.96	0.78	390.70	5.86	0.77
16.15	17.14	2.47	4284.7	12.85	0.88	382.82	5.74	0.89
19.20	16.95	2.66	4229.8	12.69	1.05	378.37	5.68	0.96
20.61	16.65	2.96	4240.6	12.72	1.02	376.38	5.65	0.99
23.79	16.50	3.11	4238.0	12.71	1.02	371.18	5.57	1.06
25.10	16.26	3.35	4195.5	12.59	1.15	369.34	5.54	1.09
20.44	16.64	2.97	4238.0	12.71	1.02	373.18	5.60	1.03
15.13	17.09	2.52	4279.5	12.84	0.90	384.41	5.77	0.87
10.69	17.58	2.03	4345.8	13.04	0.70	393.24	5.90	0.73
5.36	18.07	1.54	4398.7	13.20	0.54	408.95	6.13	0.50
0.59	19.28	0.33	4569.3	13.71	0.03	449.12	6.74	-0.10

Table A3: Transducer readings for SB 25 @ 02:26

Load (KN)	*Platen Deflection (mm)*	*Channel 1*		*Channel 7*	
		Ohms	*Deflection (mm)*	*Ohms*	*Deflection (mm)*

06:34 hrs **Cycles: 7438**

Max. cyclic load: 25.19 KN Min. cyclic load: 0.28 KN

0.25	18.89	0.00	4550.4	13.65	0.00	435.35	6.53	0.00
2.51	18.51	0.38	4498.2	13.49	0.16	421.68	6.33	0.21
5.52	18.27	0.62	4435.1	13.31	0.35	415.21	6.23	0.30
8.23	18.13	0.76	4378.9	13.14	0.51	407.98	6.12	0.41
10.37	18.02	0.87	4374.1	13.12	0.53	404.97	6.07	0.46
12.89	17.90	0.99	4328.6	12.99	0.67	401.62	6.02	0.51
15.89	17.76	1.13	4303.7	12.91	0.74	397.77	5.97	0.56
17.75	17.67	1.22	4262.4	12.79	0.86	385.42	5.78	0.75
20.84	17.53	1.36	4275.3	12.83	0.83	378.91	5.68	0.85
22.80	17.44	1.45	4255.2	12.77	0.89	379.88	5.70	0.83
25.42	17.33	1.56	4225.3	12.68	0.98	379.90	5.70	0.83
20.55	17.02	1.87	4249.5	12.75	0.90	379.16	5.69	0.84
15.15	17.75	1.14	4304.1	12.91	0.74	387.38	5.81	0.72
10.35	17.98	0.91	4360.6	13.08	0.57	400.02	6.00	0.53
5.56	18.24	0.65	4440.1	13.32	0.33	406.42	6.10	0.43
0.36	18.96	-0.07	4537.7	13.61	0.04	433.12	6.50	0.03

Table A4: Transducer readings for SB 25 @ 06:34

Load (KN)	*Platen Deflection (mm)*	*Channel 1*		*Channel 7*	
		Ohms	*Deflection (mm)*	*Ohms*	*Deflection (mm)*

23:12 hrs **Cycles: 27278**

Max. cyclic load: 24.94 KN Min. cyclic load: 0.51 KN

0.18	18.89	0.00	4530.3	13.59	0.00	428.61	6.43	0.00
2.65	18.38	0.51	4429.9	13.29	0.30	441.90	6.63	-0.20
5.74	18.19	0.70	4380.5	13.14	0.45	437.85	6.57	-0.14
7.95	18.08	0.81	4363.3	13.09	0.50	436.83	6.55	-0.12
10.24	17.98	0.91	4316.9	12.95	0.64	426.77	6.40	0.03
12.98	17.86	1.03	4315.1	12.95	0.65	426.28	6.39	0.03
16.13	17.74	1.15	4295.5	12.89	0.70	428.91	6.43	0.00
18.19	17.66	1.23	4271.6	12.81	0.78	439.27	6.59	-0.16
20.31	17.58	1.31	4257.3	12.77	0.82	429.25	6.44	-0.01
22.51	17.50	1.39	4256.4	12.77	0.82	426.82	6.40	0.03
25.97	17.37	1.52	4221.0	12.66	0.93	426.44	6.40	0.03
20.73	17.55	1.34	4256.8	12.77	0.82	418.73	6.28	0.15
15.36	17.75	1.14	4283.6	12.85	0.74	425.03	6.38	0.05
10.83	17.94	0.95	4334.7	13.00	0.59	436.64	6.55	-0.12
5.36	18.19	0.70	4368.7	13.11	0.48	438.58	6.58	-0.15
0.16	18.90	-0.01	4525.2	13.58	0.02	465.00	6.98	-0.78

Table A5: Transducer readings for SB 25 @ 23:12

Load (KN)	*Platen Deflection (mm)*	*Channel 1*		*Channel 7*	
		Ohms	*Deflection (mm)*	*Ohms*	*Deflection (mm)*

26:02 hrs **Cycles: 31180**

Max. cyclic load: 25.08 KN Min. cyclic load: 0.59 KN

0.29	18.90	0.00	4537.0	13.61	0.00	457.35	6.86	0.00
2.71	18.39	0.51	4420.2	13.26	0.35	441.43	6.62	0.24
5.44	18.21	0.69	4395.2	13.19	0.43	441.24	6.62	0.24
8.50	18.07	0.83	4349.8	13.05	0.56	442.37	6.64	0.22
10.30	17.99	0.91	4337.8	13.01	0.60	439.94	6.60	0.26
12.77	17.88	1.02	4337.9	13.01	0.60	441.50	6.62	0.24
15.23	17.78	1.12	4304.7	12.91	0.70	433.46	6.50	0.36
20.40	17.58	1.32	4259.6	12.78	0.83	425.36	6.38	0.48
22.36	17.51	1.39	4263.8	12.79	0.82	429.43	6.44	0.42
25.63	17.39	1.51	4248.2	12.74	0.87	430.02	6.45	0.41
20.57	17.57	1.33	4260.6	12.78	0.83	425.65	6.38	0.48
15.37	17.76	1.14	4307.4	12.92	0.69	428.24	6.42	0.44
10.67	17.95	0.95	4335.9	13.01	0.60	433.15	6.50	0.36
5.27	18.20	0.70	4415.7	13.25	0.36	437.66	6.56	0.30
0.28	18.89	0.01	4525.1	13.58	0.04	458.89	6.88	-0.02

Table A6: Transducer readings for SB 25 @ 26:02

Load (KN)	*Platen Deflection (mm)*	*Channel 1*		*Channel 7*	
		Ohms	*Deflection (mm)*	*Ohms*	*Deflection (mm)*

31:14 hrs **Cycles: 37510**

Max. cyclic load: 25.04 KN Min. cyclic load: 0.53 KN

0.25	18.90	0.00	4541.6	13.62	0.00	463.76	6.96	0.00
3.02	18.35	0.55	4409.2	13.23	0.40	442.70	6.64	0.32
5.69	18.18	0.72	4390.1	13.17	0.45	449.30	6.74	0.22
7.95	18.08	0.82	4347.5	13.04	0.58	439.94	6.60	0.36
10.22	17.98	0.92	4343.2	13.03	0.60	440.70	6.61	0.35
12.77	17.87	1.03	4329.5	12.99	0.64	434.85	6.52	0.43
16.14	17.74	1.16	4304.0	12.91	0.71	434.74	6.52	0.44
18.93	17.63	1.27	4270.6	12.81	0.81	435.63	6.53	0.42
21.84	17.52	1.38	4270.8	12.81	0.81	430.34	6.46	0.50
25.45	17.39	1.51	4248.3	12.74	0.88	425.92	6.39	0.57
19.86	17.59	1.31	4291.9	12.88	0.75	438.53	6.58	0.38
14.62	17.78	1.12	4314.5	12.94	0.68	436.94	6.55	0.40
10.78	17.94	0.96	4338.4	13.02	0.61	428.86	6.43	0.52
5.42	18.18	0.72	4373.5	13.12	0.50	433.06	6.50	0.46
0.34	18.87	0.03	4510.4	13.53	0.09	460.58	6.91	0.05

Table A7: Transducer readings for SB 25 @ 31:14

Load (KN)	*Platen Deflection (mm)*	*Channel 1*		*Channel 7*	
		Ohms	*Deflection (mm)*	*Ohms*	*Deflection (mm)*
46:39 hrs					**Cycles: 56390**
Max. cyclic load: 24.97 KN					Min. cyclic load: 0.30 KN
0.20	19.17	0.00	3710.4	11.13	0.00	396.64	5.95	0.00
2.43	18.58	0.59	3598.6	10.80	0.34	386.09	5.79	0.16
5.16	18.29	0.88	3571.1	10.71	0.42	391.41	5.87	0.08
8.72	18.08	1.09	3518.7	10.56	0.58	386.45	5.80	0.15
10.98	17.99	1.18	3512.8	10.54	0.59	382.14	5.73	0.22
15.16	17.80	1.37	3469.1	10.41	0.72	376.30	5.64	0.31
18.21	17.68	1.49	3421.6	10.26	0.87	374.12	5.61	0.34
20.54	17.54	1.63	3423.0	10.27	0.86	371.72	5.58	0.37
22.29	17.48	1.69	3408.9	10.23	0.90	368.47	5.53	0.42
25.33	17.37	1.80	3383.1	10.15	0.98	354.31	5.31	0.63
19.3	17.59	1.58	3406.3	10.22	0.91	370.31	5.55	0.39
14.99	17.75	1.42	3457.3	10.37	0.76	372.88	5.59	0.36
10.4	17.95	1.22	3514.5	10.54	0.59	386.30	5.79	0.16
5.49	18.18	0.99	3562.2	10.69	0.44	394.52	5.92	0.03
0.45	18.94	0.23	3688.3	11.06	0.07	409.21	6.14	-0.19
0.17	19.03	0.14	3721.5	11.16	-0.03	409.92	6.15	-0.20

Table A8: Transducer readings for SB 25 @ 46:39

Load (KN)	*Platen Deflection (mm)*	*Channel 1*		*Channel 7*	
		Ohms	*Deflection (mm)*	*Ohms*	*Deflection (mm)*
173:43 hrs					**Cycles: 56390**
0.28	19.65	0.00	3790.6	11.37	0.00	427.00	6.41	0.00
2.81	19.02	0.63	3623.9	10.87	0.50	439.63	6.59	-0.19
5.02	18.69	0.96	3569.1	10.71	0.66	439.06	6.59	-0.18
7.51	18.53	1.12	3518.9	10.56	0.82	438.64	6.58	-0.17
10.12	18.39	1.26	3526.5	10.58	0.79	432.86	6.49	-0.09
15.18	18.16	1.49	3464.6	10.39	0.98	430.13	6.45	-0.05
20.56	17.92	1.73	3429.1	10.29	1.08	421.48	6.32	0.08
27.13	17.68	1.97	3372.6	10.12	1.25	406.35	6.10	0.31
30.02	17.57	2.08	3319.8	9.96	1.41	400.38	6.01	0.40
35.38	17.38	2.27	3318.6	9.96	1.42	390.52	5.86	0.55
41.08	17.16	2.49	3282.9	9.85	1.52	380.72	5.71	0.69
45.05	17.03	2.62	3249.5	9.75	1.62	379.59	5.69	0.71
50.04	16.85	2.80	3235.9	9.71	1.66	371.13	5.57	0.84
40.49	17.15	2.50	3266.7	9.80	1.57	373.99	5.61	0.80
30.18	17.49	2.16	3343.5	10.03	1.34	382.77	5.74	0.66
20.1	17.85	1.80	3433.7	10.30	1.07	399.20	5.99	0.42
10.18	18.27	1.38	3515.3	10.55	0.83	418.25	6.27	0.13
5.26	18.54	1.11	3572.9	10.72	0.65	421.74	6.33	0.08
0.25	19.47	0.18	3757.5	11.27	0.10	429.65	6.44	-0.04

Table A9: Transducer readings for SB 25 @ 173.43

Load (KN)	*Platen Deflection (mm)*	*Channel 1*		*Channel 7*	
		Ohms	*Deflection (mm)*	*Ohms*	*Deflection (mm)*
00:25 hrs					**Cycles: 0**
0.12	19.68	0.00	3202.4	9.61	0.00	564.66	8.47	0.00
4.08	18.94	0.74	3243.6	9.73	-0.12	538.54	8.08	0.39
8.27	18.56	1.12	3206.9	9.62	-0.01	517.73	7.77	0.70
12.90	18.29	1.39	3150.9	9.45	0.15	510.08	7.65	0.82
16.11	18.11	1.57	3129.1	9.39	0.22	496.75	7.45	1.02
20.08	17.89	1.79	3091.6	9.27	0.33	495.67	7.44	1.03
24.33	17.67	2.01	3045.9	9.14	0.47	474.07	7.11	1.36
28.59	17.46	2.22	3008.1	9.02	0.58	465.00	6.98	1.49
32.24	17.27	2.41	2956.6	8.87	0.74	474.28	7.11	1.36
35.14	17.13	2.55	2944.5	8.83	0.77	472.30	7.08	1.39
29.39	17.38	2.30	2999.0	9.00	0.61	484.13	7.26	1.21
24.26	17.62	2.06	3052.0	9.16	0.45	498.80	7.48	0.99
20.00	17.82	1.86	3098.5	9.30	0.31	506.92	7.60	0.87
15.28	18.06	1.62	3140.5	9.42	0.19	524.29	7.86	0.61
10.43	18.32	1.36	3188.0	9.56	0.04	532.77	7.99	0.48
5.29	18.68	1.00	3227.1	9.68	-0.07	551.63	8.27	0.20
0.27	19.53	0.15	3197.5	9.59	0.01	591.80	8.88	-0.41

Table A10: Transducer readings for SB 34 @ 00:25

Load (KN)	*Platen Deflection (mm)*	*Channel 1*		*Channel 7*	
		Ohms	*Deflection (mm)*	*Ohms*	*Deflection (mm)*
02:32 hrs					**Cycles: 2389**
Max. cyclic load: 33.94 KN					Min. cyclic load: 0.28 KN
0.28	19.16	0.00	3244.6	9.73	0.00	468.26	7.02	0.00
4.35	18.50	0.66	3232.5	9.70	0.04	436.86	6.55	0.47
8.40	18.15	1.01	3233.0	9.70	0.03	422.45	6.34	0.69
12.52	17.94	1.22	3186.6	9.56	0.17	414.66	6.22	0.80
17.38	17.69	1.47	3130.6	9.39	0.34	397.29	5.96	1.06
22.39	17.44	1.72	3075.5	9.23	0.51	374.17	5.61	1.41
27.15	17.20	1.96	3046.4	9.14	0.59	373.64	5.60	1.42
34.13	16.88	2.28	2970.7	8.91	0.82	357.69	5.37	1.66
30.78	17.02	2.14	3008.1	9.02	0.71	369.27	5.54	1.48
25.49	17.26	1.90	3031.0	9.09	0.64	369.50	5.54	1.48
19.76	17.52	1.64	3085.8	9.26	0.48	386.28	5.79	1.23
15.30	17.73	1.43	3131.2	9.39	0.34	400.29	6.00	1.02
10.64	17.97	1.19	3180.6	9.54	0.19	414.96	6.22	0.80
5.29	18.33	0.83	3249.0	9.75	-0.01	433.60	6.50	0.52
1.61	18.83	0.33	3240.0	9.72	0.01	453.83	6.81	0.22
0.16	19.20	-0.04	3215.9	9.65	0.09	467.35	7.01	0.01

Table A11: Transducer readings for SB 34 @ 02:32

Load (KN)	*Platen Deflection (mm)*	*Channel 1*		*Channel 7*	
		Ohms	*Deflection (mm)*	*Ohms*	*Deflection (mm)*

06:38 hrs **Cycles: 7310**

Max. cyclic load: 33.98 KN Min. cyclic load: 0.16 KN

0.52	19.38	-0.22	3193.2	9.58	0.15	484.85	7.27	-0.25
2.34	18.96	0.20	3235.6	9.71	0.03	468.61	7.03	-0.01
5.78	18.45	0.71	3245.9	9.74	0.00	448.88	6.73	0.29
8.62	18.24	0.92	3228.8	9.69	0.05	443.76	6.66	0.37
13.31	17.97	1.19	3197.9	9.59	0.14	429.68	6.45	0.58
17.05	17.77	1.39	3129.7	9.39	0.34	424.76	6.37	0.65
22.67	17.48	1.68	3066.2	9.20	0.54	411.05	6.17	0.86
26.15	17.30	1.86	3042.2	9.13	0.61	403.96	6.06	0.96
30.55	17.09	2.07	3019.0	9.06	0.68	393.04	5.90	1.13
34.60	16.90	2.26	2982.4	8.95	0.79	384.04	5.76	1.26
27.93	17.16	2.00	3055.3	9.17	0.57	392.34	5.89	1.14
22.85	17.37	1.79	3077.1	9.23	0.50	401.91	6.03	1.00
19.20	17.54	1.62	3093.4	9.28	0.45	403.75	6.06	0.97
13.50	17.82	1.34	3151.2	9.45	0.28	422.61	6.34	0.68
9.08	18.04	1.12	3198.3	9.59	0.14	432.37	6.49	0.54
4.95	18.35	0.81	3243.4	9.73	0.00	445.43	6.68	0.34
2.50	18.68	0.48	3238.7	9.72	0.02	462.89	6.94	0.08
0.57	19.17	-0.01	3197.2	9.59	0.14	482.76	7.24	-0.22

Table A12: Transducer readings for SB 34 @ 06:38

Load (KN)	*Platen Deflection (mm)*	*Channel 1*		*Channel 7*	
		Ohms	*Deflection (mm)*	*Ohms*	*Deflection (mm)*

11:47 hrs **Cycles: 13410**

Max. cyclic load: 34.27 KN Min. cyclic load: 1.9 KN

0.31	19.36	0.00	3102.2	9.31	0.00	486.25	7.29	0.00
2.52	18.84	0.52	3137.9	9.41	-0.11	475.45	7.13	0.16
5.59	18.43	0.93	3179.6	9.54	-0.23	452.09	6.78	0.51
9.32	18.14	1.22	3173.7	9.52	-0.21	443.05	6.65	0.65
14.79	17.86	1.50	3116.9	9.35	-0.04	426.63	6.40	0.89
18.74	17.68	1.68	3075.6	9.23	0.08	413.29	6.20	1.09
23.82	17.45	1.91	3057.0	9.17	0.14	413.79	6.21	1.09
28.75	17.24	2.12	3013.8	9.04	0.27	404.30	6.06	1.23
32.68	17.08	2.28	2982.3	8.95	0.36	396.78	5.95	1.34
34.21	17.02	2.34	2972.0	8.92	0.39	399.14	5.99	1.31
29.05	17.21	2.15	2976.8	8.93	0.38	399.47	5.99	1.30
24.07	17.39	1.97	3014.7	9.04	0.26	407.77	6.12	1.18
18.68	17.60	1.76	3058.8	9.18	0.13	414.18	6.21	1.08
12.56	17.86	1.50	3085.7	9.26	0.05	422.54	6.34	0.96
8.45	18.05	1.31	3135.6	9.41	-0.10	435.57	6.53	0.76
3.94	18.43	0.93	3132.7	9.40	-0.09	454.84	6.82	0.47
2.36	18.62	0.74	3131.5	9.39	-0.09	468.01	7.02	0.27
0.29	19.10	0.26	3100.4	9.30	0.01	482.56	7.24	0.06

Table A13: Transducer readings for SB 34 @ 11:47

Load (KN)	*Platen Deflection (mm)*	*Channel 1*		*Channel 7*	
		Ohms	*Deflection (mm)*	*Ohms*	*Deflection (mm)*

23:41 hrs **Cycles: 27870**

Max. cyclic load: 34.13 KN Min. cyclic load: 2.28 KN

0.28	19.14	0.00	3171.4	9.51	0.00	554.43	8.32	0.00
2.56	18.67	0.47	3185.1	9.56	-0.04	541.58	8.12	0.19
5.48	18.34	0.80	3212.3	9.64	-0.12	536.52	8.05	0.27
10.05	18.04	1.10	3182.6	9.55	-0.03	513.44	7.70	0.61
15.40	17.78	1.36	3141.6	9.42	0.09	502.18	7.53	0.78
19.93	17.58	1.56	3095.5	9.29	0.23	496.08	7.44	0.88
25.21	17.36	1.78	3053.9	9.16	0.35	489.64	7.34	0.97
30.77	17.14	2.00	3015.0	9.05	0.47	471.44	7.07	1.24
34.25	17.01	2.13	3001.6	9.00	0.51	468.79	7.03	1.28
30.06	17.15	1.99	3022.0	9.07	0.45	465.64	6.98	1.33
24.80	17.34	1.80	3054.8	9.16	0.35	473.16	7.10	1.22
19.52	17.54	1.60	3088.7	9.27	0.25	521.53	7.82	0.49
14.26	17.76	1.38	3141.0	9.42	0.09	530.66	7.96	0.36
10.36	17.93	1.21	3177.8	9.53	-0.02	538.69	8.08	0.24
4.98	18.26	0.88	3212.6	9.64	-0.12	558.87	8.38	-0.07
2.65	18.53	0.61	3192.7	9.58	-0.06	569.10	8.54	-0.22
0.27	19.00	0.14	3161.6	9.48	0.03	596.99	8.95	-0.64

Table A14: Transducer readings for SB 34 @ 23:41

Load (KN)	*Platen Deflection (mm)*	*Channel 1*		*Channel 7*	
		Ohms	*Deflection (mm)*	*Ohms*	*Deflection (mm)*

32:55 hrs **Cycles: 38980**

Max. cyclic load: 33.97 KN Min. cyclic load: 2.20 KN

0.35	18.93	0.00	3106.6	9.32	0.00	885.35	13.28	0.00
2.56	18.51	0.42	3104.0	9.31	0.01	871.95	13.08	0.20
5.21	18.25	0.68	3133.7	9.40	-0.08	873.51	13.10	0.18
10.31	17.93	1.00	3116.8	9.35	-0.03	845.24	12.68	0.60
15.26	17.71	1.22	3100.8	9.30	0.02	826.67	12.40	0.88
19.59	17.53	1.40	3082.3	9.25	0.07	826.87	12.40	0.88
24.94	17.31	1.62	3024.7	9.07	0.25	811.57	12.17	1.11
29.56	17.15	1.78	3035.5	9.11	0.21	804.25	12.06	1.22
34.28	16.97	1.96	3026.2	9.08	0.24	802.16	12.03	1.25
28.99	17.15	1.78	3015.9	9.05	0.27	801.16	12.02	1.26
24.62	17.30	1.63	3015.2	9.05	0.27	813.46	12.20	1.08
19.66	17.48	1.45	3033.1	9.10	0.22	816.19	12.24	1.04
14.57	17.68	1.25	3072.0	9.22	0.10	833.11	12.50	0.78
10.75	17.85	1.08	3106.1	9.32	0.00	842.30	12.63	0.65
5.49	18.14	0.79	3128.3	9.38	-0.07	859.91	12.90	0.38
2.72	18.44	0.49	3130.1	9.39	-0.07	866.91	13.00	0.28
0.23	18.92	0.01	3109.6	9.33	-0.01	886.56	13.30	-0.02

Table A15: Transducer readings for SB 34 @ 32:55

Load (KN)	*Platen Deflection (mm)*	*Channel 1*		*Channel 7*	
		Ohms	*Deflection (mm)*	*Ohms*	*Deflection (mm)*
47:08 hrs					**Cycles: 57620**
Max. cyclic load: 33.99 KN					Min. cyclic load: 2.12 KN
0.24	18.80	0.00	3478.3	10.43	0.00	631.99	9.48	0.00
2.41	18.32	0.48	3441.8	10.33	0.11	644.59	9.67	0.19
5.42	18.09	0.71	3432.6	10.30	0.14	639.56	9.59	0.11
10.77	17.79	1.01	3389.7	10.17	0.27	747.09	11.21	1.73
15.60	17.59	1.21	3354.6	10.06	0.37	751.14	11.27	1.79
19.97	17.43	1.37	3327.8	9.98	0.45	755.22	11.33	1.85
25.42	17.23	1.57	3288.9	9.87	0.57	745.14	11.18	1.70
29.83	17.07	1.73	3226.3	9.68	0.76	733.12	11.00	1.52
34.44	16.91	1.89	3198.6	9.60	0.84	724.36	10.87	1.39
28.26	17.12	1.68	3231.0	9.69	0.74	731.29	10.97	1.49
24.33	17.26	1.54	3278.7	9.84	0.60	743.97	11.16	1.68
20.06	17.41	1.39	3305.4	9.92	0.52	760.25	11.40	1.92
14.13	17.64	1.16	3352.3	10.06	0.38	785.27	11.78	2.30
9.32	17.85	0.95	3426.7	10.28	0.15	768.60	11.53	2.05
5.22	18.06	0.74	3432.6	10.30	0.14	769.70	11.55	2.07
2.32	18.32	0.48	3437.1	10.31	0.12	785.74	11.79	2.31
0.19	18.81	-0.01	3461.6	10.38	0.05	810.43	12.16	2.68

Table A16: Transducer readings for SB 34 @ 47:08

Load (KN)	*Platen Deflection (mm)*	*Channel 1*		*Channel 7*	
		Ohms	*Deflection (mm)*	*Ohms*	*Deflection (mm)*
00:25 hrs					**Cycles: 0**
0.03	44.29	0.00	3675.1	11.03	0.00	553.97	8.31	0.00
1.43	44.00	0.29	3617.5	10.85	0.17	553.27	8.30	0.01
4.01	43.65	0.64	3538.4	10.62	0.41	562.35	8.44	-0.13
9.64	43.23	1.06	3439.0	10.32	0.71	556.51	8.35	-0.04
14.20	42.97	1.32	3371.6	10.11	0.91	550.35	8.26	0.05
18.97	42.73	1.56	3317.1	9.95	1.07	532.24	7.98	0.33
24.19	42.46	1.83	3251.4	9.75	1.27	529.77	7.95	0.36
29.00	42.23	2.06	3198.1	9.59	1.43	516.30	7.74	0.57
34.15	41.97	2.32	3139.6	9.42	1.61	497.35	7.46	0.85
39.49	41.72	2.57	3081.4	9.24	1.78	494.31	7.41	0.89
41.90	41.60	2.69	3067.1	9.20	1.82	487.69	7.32	0.99
32.29	42.02	2.27	3160.6	9.48	1.54	501.79	7.53	0.78
22.56	42.45	1.84	3256.8	9.77	1.25	521.73	7.83	0.48
12.31	42.94	1.35	3383.1	10.15	0.88	553.42	8.30	0.01
6.32	43.29	1.00	3447.4	10.34	0.68	553.67	8.31	0.00
3.46	43.60	0.69	3548.5	10.65	0.38	551.28	8.27	0.04
0.58	44.06	0.23	3653.1	10.96	0.07	552.96	8.29	0.02

Table A17: Transducer readings for SB 42 @ 00:25

Load (KN)	*Platen Deflection (mm)*	*Channel 1*		*Channel 7*	
		Ohms	*Deflection (mm)*	*Ohms*	*Deflection (mm)*
02:06 hrs					**Cycles: 1907**
Max. cyclic load: 42.30 KN					Min. cyclic load: 4.07 KN
0.80	43.06	0.00	3479.2	10.44	0.00	761.96	11.43	0.00
3.60	42.62	0.44	3368.1	10.10	0.33	771.19	11.57	-0.14
9.17	42.29	0.77	3242.2	9.73	0.71	825.23	12.38	-0.95
14.18	42.04	1.02	3205.3	9.62	0.82	817.36	12.26	-0.83
20.10	41.76	1.30	3147.6	9.44	0.99	798.87	11.98	-0.55
23.97	41.58	1.48	3109.7	9.33	1.11	792.63	11.89	-0.46
29.23	41.35	1.71	3048.3	9.14	1.29	783.47	11.75	-0.32
35.26	41.08	1.98	2999.2	9.00	1.44	768.72	11.53	-0.10
38.76	40.93	2.13	2970.6	8.91	1.53	766.55	11.50	-0.07
41.96	40.79	2.27	2937.3	8.81	1.63	762.54	11.44	-0.01
33.82	41.13	1.93	3017.0	9.05	1.39	773.97	11.61	-0.18
24.01	41.55	1.51	3028.6	9.09	1.35	790.51	11.86	-0.43
14.12	42.01	1.05	3198.6	9.60	0.84	809.73	12.15	-0.72
4.50	42.53	0.53	3351.3	10.05	0.38	844.00	12.66	-1.23
0.80	43.06	0.00	3488.7	10.47	-0.03	858.18	12.87	-1.44

Table A18: Transducer readings for SB 42 @ 02:06

Load (KN)	*Platen Deflection (mm)*	*Channel 1*		*Channel 7*	
		Ohms	*Deflection (mm)*	*Ohms*	*Deflection (mm)*

04:13 hrs **Cycles: 4413**

Max. cyclic load: 43.10 KN Min. cyclic load: 3.92 KN

0.92	43.01	0.00	3497.3	10.49	0.00	872.39	13.09	0.00
1.58	42.89	0.12	3450.7	10.35	0.14	866.59	13.00	0.09
4.98	42.46	0.55	3338.7	10.02	0.48	840.39	12.61	0.48
9.46	42.22	0.79	3253.3	9.76	0.73	854.35	12.82	0.27
13.93	41.99	1.02	3220.8	9.66	0.83	823.26	12.35	0.74
20.59	41.67	1.34	3153.1	9.46	1.03	803.69	12.06	1.03
24.66	41.49	1.52	3101.2	9.30	1.19	800.40	12.01	1.08
30.66	41.22	1.79	3044.4	9.13	1.36	788.60	11.83	1.26
34.81	41.04	1.97	3011.5	9.03	1.46	781.70	11.73	1.36
38.83	40.87	2.14	2984.3	8.95	1.54	770.00	11.55	1.54
42.16	40.72	2.29	2932.2	8.80	1.70	767.58	11.51	1.57
34.56	41.04	1.97	3013.6	9.04	1.45	782.28	11.73	1.35
25.31	41.43	1.58	3096.3	9.29	1.20	800.20	12.00	1.08
15.00	41.91	1.10	3203.1	9.61	0.88	813.06	12.20	0.89
4.28	42.50	0.51	3347.1	10.04	0.45	894.22	13.41	-0.33
0.54	43.09	-0.08	3515.7	10.55	-0.06	879.70	13.20	-0.11

Table A19: Transducer readings for SB 42 @ 04:13

Load (KN)	*Platen Deflection (mm)*	*Channel 1*		*Channel 7*	
		Ohms	*Deflection (mm)*	*Ohms*	*Deflection (mm)*

06:34 hrs **Cycles: 7076**

Max. cyclic load: 43.18 KN Min. cyclic load: 3.02 KN

0.89	42.94	0.00	3503.8	10.51	0.00	870.11	13.05	0.00
4.05	42.49	0.45	3354.2	10.06	0.45	861.04	12.92	0.14
9.63	42.18	0.76	3265.6	9.80	0.71	889.22	13.34	-0.29
14.03	41.97	0.97	3213.7	9.64	0.87	843.60	12.65	0.40
19.18	41.70	1.24	3151.6	9.45	1.06	824.28	12.36	0.69
24.35	41.48	1.46	3107.2	9.32	1.19	817.28	12.26	0.79
29.65	41.25	1.69	3078.5	9.24	1.28	813.47	12.20	0.85
34.40	41.04	1.90	3011.2	9.03	1.48	801.68	12.03	1.03
39.40	40.84	2.10	2977.4	8.93	1.58	800.68	12.01	1.04
42.10	40.72	2.22	2988.6	8.97	1.55	798.63	11.98	1.07
34.16	41.03	1.91	3033.2	9.10	1.41	801.80	12.03	1.02
25.16	41.41	1.53	3086.7	9.26	1.25	817.50	12.26	0.79
14.90	41.88	1.06	3213.0	9.64	0.87	836.57	12.55	0.50
4.10	42.46	0.48	3329.2	9.99	0.52	879.55	13.19	-0.14
2.00	42.74	0.20	3421.6	10.26	0.25	886.63	13.30	-0.25
0.80	42.96	-0.02	3498.4	10.50	0.02	883.94	13.26	-0.21

Table A20: Transducer readings for SB 42 @ 06:34

Load (KN)	*Platen Deflection (mm)*	*Channel 1*		*Channel 7*	
		Ohms	*Deflection (mm)*	*Ohms*	*Deflection (mm)*

12:27 hrs **Cycles: 12140**

Max. cyclic load: 43.37 KN Min. cyclic load: 2.83 KN

1.07	43.78	0.00	3425.8	10.28	0.00	951.57	14.27	0.00
5.03	43.30	0.48	3310.0	9.93	0.35	955.42	14.33	-0.06
9.21	43.07	0.71	3278.2	9.83	0.44	959.08	14.39	-0.11
15.12	42.79	0.99	3210.4	9.63	0.65	970.51	14.56	-0.28
19.62	42.59	1.19	3145.2	9.44	0.84	975.74	14.64	-0.36
23.97	42.38	1.40	3097.2	9.29	0.99	941.84	14.13	0.15
28.92	42.19	1.59	3078.2	9.23	1.04	931.90	13.98	0.30
34.30	41.97	1.81	3040.8	9.12	1.16	916.83	13.75	0.52
39.91	41.74	2.04	3015.4	9.05	1.23	928.29	13.92	0.35
42.73	41.63	2.15	3003.8	9.01	1.27	920.02	13.80	0.47
35.69	41.88	1.90	3038.2	9.11	1.16	912.81	13.69	0.58
24.11	42.32	1.46	3088.1	9.26	1.01	922.59	13.84	0.43
15.84	42.66	1.12	3181.6	9.54	0.73	962.09	14.43	-0.16
4.19	43.30	0.48	3313.8	9.94	0.34	960.73	14.41	-0.14
0.97	43.72	0.06	3426.4	10.28	0.00	969.04	14.54	-0.26

Table A21: Transducer readings for SB 42 @ 12:27

Load (KN)	*Platen Deflection (mm)*	*Channel 1*		*Channel 7*	
		Ohms	*Deflection (mm)*	*Ohms*	*Deflection (mm)*

23:12 hrs **Cycles: 25260**

Max. cyclic load: 43.19 KN Min. cyclic load: 3.11 KN

0.65	43.36	0.00	3481.3	10.44	0.00	1018.46	15.28	0.00
2.00	43.13	0.23	3411.1	10.23	0.21	1027.26	15.41	-0.13
4.92	42.85	0.51	3298.0	9.89	0.55	1061.22	15.92	-0.64
9.45	42.62	0.74	3258.5	9.78	0.67	1023.19	15.35	-0.07
14.59	42.40	0.96	3231.9	9.70	0.75	1004.13	15.06	0.21
19.58	42.19	1.17	3186.9	9.56	0.88	991.68	14.88	0.40
24.16	42.00	1.36	3148.9	9.45	1.00	969.05	14.54	0.74
30.47	41.74	1.62	3111.3	9.33	1.11	987.37	14.81	0.47
34.07	41.56	1.80	3050.6	9.15	1.29	1007.41	15.11	0.17
39.58	41.36	2.00	3027.5	9.08	1.36	1026.53	15.40	-0.12
42.00	41.27	2.09	3000.7	9.00	1.44	1012.87	15.19	0.08
32.84	41.62	1.74	3076.9	9.23	1.21	1031.17	15.47	-0.19
23.99	41.96	1.40	3147.8	9.44	1.00	1046.64	15.70	-0.42
13.12	42.42	0.94	3217.1	9.65	0.79	1055.86	15.84	-0.56
4.86	42.82	0.54	3306.0	9.92	0.53	1063.64	15.95	-0.68
2.26	43.07	0.29	3389.6	10.17	0.28	1067.67	16.02	-0.74
0.94	43.29	0.07	3470.6	10.41	0.03	1081.70	16.23	-0.95

Table A22: Transducer readings for SB 42 @ 23:12

Load (KN)	*Platen Deflection (mm)*	*Channel 1*		*Channel 7*	
		Ohms	*Deflection (mm)*	*Ohms*	*Deflection (mm)*

26:08 hrs **Cycles: 28770**

Max. cyclic load: 43.10 KN Min. cyclic load: 3.50 KN

0.75	43.18	0.00	3477.7	10.43	0.00	640.63	9.61	0.00
2.62	42.88	0.30	3405.9	10.22	0.22	636.01	9.54	-0.07
5.23	42.66	0.52	3298.9	9.90	0.54	638.79	9.58	-0.03
9.52	42.45	0.73	3279.6	9.84	0.59	643.28	9.65	0.04
14.54	42.23	0.95	3221.1	9.66	0.77	628.18	9.42	-0.19
19.57	42.02	1.16	3171.2	9.51	0.92	625.95	9.39	-0.22
24.27	41.80	1.38	3126.5	9.38	1.05	769.60	11.54	1.93
29.04	41.62	1.56	3089.9	9.27	1.16	757.77	11.37	1.76
34.27	41.42	1.76	3047.0	9.14	1.29	780.04	11.70	2.09
38.91	41.25	1.93	3038.8	9.12	1.32	751.83	11.28	1.67
42.57	41.12	2.06	3011.0	9.03	1.40	752.21	11.28	1.67
34.15	41.43	1.75	3043.7	9.13	1.30	748.16	11.22	1.61
24.97	41.77	1.41	3117.1	9.35	1.08	751.78	11.28	1.67
14.29	42.21	0.97	3221.3	9.66	0.77	772.96	11.59	1.98
4.74	42.67	0.51	3229.2	9.69	0.75	791.60	11.87	2.26
2.73	42.85	0.33	3370.7	10.11	0.32	801.05	12.02	2.41
0.78	43.17	0.01	3479.1	10.44	0.00	809.70	12.15	2.54

Table A23: Transducer readings for SB 42 @ 26:08

Load (KN)	*Platen Deflection (mm)*	*Channel 1*		*Channel 7*	
		Ohms	*Deflection (mm)*	*Ohms*	*Deflection (mm)*

95:26 hrs **Cycles: 33680**

0.77	44.39	0.00	3427.4	10.28	0.00	569.64	8.54	0.00
2.43	44.19	0.20	3384.6	10.15	0.13	574.63	8.62	-0.07
4.11	43.99	0.40	3372.0	10.12	0.17	569.16	8.54	0.01
9.63	43.63	0.76	3281.5	9.84	0.44	576.45	8.65	-0.10
14.06	43.39	1.00	3202.7	9.61	0.67	563.19	8.45	0.10
19.22	43.17	1.22	3207.4	9.62	0.66	561.35	8.42	0.12
24.72	42.93	1.46	3129.4	9.39	0.89	544.04	8.16	0.38
29.03	42.74	1.65	3108.0	9.32	0.96	531.45	7.97	0.57
34.88	42.50	1.89	3124.0	9.37	0.91	529.04	7.94	0.61
39.28	42.31	2.08	3029.9	9.09	1.19	516.48	7.75	0.80
44.35	42.11	2.28	3033.5	9.10	1.18	505.71	7.59	0.96
49.54	41.91	2.48	2986.3	8.96	1.32	503.18	7.55	1.00
38.64	42.3	2.09	3025.6	9.08	1.21	514.53	7.72	0.83
29.36	42.66	1.73	3084.5	9.25	1.03	556.64	8.35	0.20
19.38	43.06	1.33	3166.2	9.50	0.78	574.25	8.61	-0.07
9.1	43.52	0.87	3269.6	9.81	0.47	591.00	8.87	-0.32
4.61	43.78	0.61	3309.1	9.93	0.35	601.73	9.03	-0.48
2.41	44.05	0.34	3383.0	10.15	0.13	589.48	8.84	-0.30
0.72	44.29	0.10	3431.8	10.30	-0.01	588.01	8.82	-0.28

Table A24: Transducer readings for SB 42 @ 95:26

Load (KN)	*Platen Deflection (mm)*	*Channel 1*		*Channel 7*	
		Ohms	*Deflection (mm)*	*Ohms*	*Deflection (mm)*
00:25 hrs					**Cycles: 0**
0.69	19.48	0.00	5723.6	17.17	0.00	844.94	12.67	0.00
5.66	18.32	1.16	5583.4	16.75	0.42	815.67	12.24	0.44
11.25	18.02	1.46	5480.5	16.44	0.73	803.79	12.06	0.62
14.68	17.85	1.63	5455.2	16.37	0.81	794.45	11.92	0.76
22.58	17.47	2.01	5400.7	16.20	0.97	779.05	11.69	0.99
25.58	17.34	2.14	5342.4	16.03	1.14	773.34	11.60	1.07
29.90	17.14	2.34	5317.4	15.95	1.22	757.67	11.37	1.31
36.11	16.86	2.62	5241.7	15.73	1.45	747.34	11.21	1.46
40.27	16.68	2.80	5205.2	15.62	1.56	741.29	11.12	1.55
45.08	16.47	3.01	5194.0	15.58	1.59	728.66	10.93	1.74
49.95	16.27	3.21	5123.2	15.37	1.80	718.52	10.78	1.90
39.82	16.68	2.80	5212.1	15.64	1.53	737.75	11.07	1.61
30.38	17.08	2.40	5277.7	15.83	1.34	751.23	11.27	1.41
19.24	17.58	1.90	5413.1	16.24	0.93	774.95	11.62	1.05
10.26	18.04	1.44	5481.7	16.45	0.73	795.12	11.93	0.75
0.72	19.03	0.45	5720.3	17.16	0.01	843.31	12.65	0.02

Table A25: Transducer readings for SB 50 @ 00:25

Load (KN)	*Platen Deflection (mm)*	*Channel 1*		*Channel 7*	
		Ohms	*Deflection (mm)*	*Ohms*	*Deflection (mm)*
05:17 hrs					**Cycles: 7448**
Max. cyclic load: 49.53 KN					Min. cyclic load: 0.75 KN
0.60	19.61	0.00	5517.9	16.55	0.00	837.17	12.56	0.00
5.02	18.66	0.95	5627.6	16.88	-0.33	798.76	11.98	0.58
10.51	18.18	1.43	5541.5	16.62	-0.07	813.52	12.20	0.35
15.44	17.93	1.68	5496.2	16.49	0.07	802.64	12.04	0.52
20.15	17.69	1.92	5428.7	16.29	0.27	794.14	11.91	0.65
25.04	17.44	2.17	5403.8	16.21	0.34	781.44	11.72	0.84
31.44	17.14	2.47	5337.3	16.01	0.54	768.58	11.53	1.03
35.41	16.95	2.66	5283.2	15.85	0.70	761.14	11.42	1.14
41.72	16.65	2.96	5204.6	15.61	0.94	749.10	11.24	1.32
45.01	16.50	3.11	5151.3	15.45	1.10	743.16	11.15	1.41
50.40	16.26	3.35	5127.8	15.38	1.17	746.38	11.20	1.36
40.95	16.64	2.97	5221.3	15.66	0.89	752.13	11.28	1.28
30.77	17.09	2.52	5366.5	16.10	0.45	751.13	11.27	1.29
20.20	17.58	2.03	5432.6	16.30	0.26	787.40	11.81	0.75
10.31	18.07	1.54	5545.6	16.64	-0.08	803.29	12.05	0.51
0.72	19.28	0.33	5513.0	16.54	0.01	858.60	12.88	-0.32

Table A26: Transducer readings for SB 50 @ 05:17

Load (KN)	*Platen Deflection (mm)*	*Channel 1*		*Channel 7*	
		Ohms	*Deflection (mm)*	*Ohms*	*Deflection (mm)*

15:54 hrs **Cycles: 20340**

Max. cyclic load: 49.49 KN Min. cyclic load: 0.77 KN

0.66	18.96	0.00	8236.4	24.71	0.00	841.14	12.62	0.00
4.91	18.31	0.65	8211.2	24.63	0.08	828.99	12.43	0.18
11.43	17.91	1.05	8106.5	24.32	0.39	818.04	12.27	0.35
15.21	17.72	1.24	8064.5	24.19	0.52	813.51	12.20	0.41
20.73	17.44	1.52	8009.3	24.03	0.68	800.08	12.00	0.62
25.02	17.24	1.72	7937.6	23.81	0.90	795.77	11.94	0.68
30.02	17.00	1.96	7902.3	23.71	1.00	789.76	11.85	0.77
35.35	16.74	2.22	7805.9	23.42	1.29	782.56	11.74	0.88
39.94	16.53	2.43	7780.0	23.34	1.37	781.80	11.73	0.89
44.91	16.29	2.67	7700.4	23.10	1.61	755.40	11.33	1.29
49.85	16.10	2.86	7679.1	23.04	1.67	744.23	11.16	1.45
39.50	16.54	2.42	7750.8	23.25	1.46	755.48	11.33	1.28
30.93	16.93	2.03	7847.8	23.54	1.17	770.34	11.56	1.06
20.30	17.43	1.53	7985.4	23.96	0.75	793.24	11.90	0.72
9.52	18.00	0.96	8117.6	24.35	0.36	832.25	12.48	0.13
0.30	19.07	-0.11	8503.4	25.51	-0.80	1084.27	16.26	-3.65

Table A27: Transducer readings for SB 50 @ 15:54

Load (KN)	*Platen Deflection (mm)*	*Channel 1*		*Channel 7*	
		Ohms	*Deflection (mm)*	*Ohms*	*Deflection (mm)*

20:05 hrs **Cycles: 25290**

Max. cyclic load: 49.66 KN Min. cyclic load: 0.55 KN

0.76	19.55	0.00	5721.1	17.16	0.00	881.07	13.22	0.00
5.19	18.61	0.94	5767.5	17.30	-0.14	838.17	12.57	0.64
10.19	18.17	1.38	5761.5	17.28	-0.12	812.02	12.18	1.04
15.43	17.87	1.68	5715.6	17.15	0.02	800.09	12.00	1.21
21.76	17.54	2.01	5654.3	16.96	0.20	782.83	11.74	1.47
25.88	17.33	2.22	5595.7	16.79	0.38	780.05	11.70	1.52
31.33	17.06	2.49	5554.2	16.66	0.50	767.78	11.52	1.70
35.99	16.84	2.71	5495.3	16.49	0.68	756.71	11.35	1.87
40.21	16.64	2.91	5452.6	16.36	0.81	753.45	11.30	1.91
45.44	16.39	3.16	5383.7	16.15	1.01	756.97	11.35	1.86
49.99	16.19	3.36	5392.2	16.18	0.99	737.50	11.06	2.15
40.65	16.57	2.98	5467.3	16.40	0.76	720.59	10.81	2.41
29.84	17.06	2.49	5587.1	16.76	0.40	779.27	11.69	1.53
19.87	17.54	2.01	5658.1	16.97	0.19	815.20	12.23	0.99
10.54	18.01	1.54	5779.3	17.34	-0.17	829.31	12.44	0.78
0.61	19.40	0.15	5720.2	17.16	0.00	891.06	13.37	-0.15

Table A28: Transducer readings for SB 50 @ 20:05

Load (KN)	*Platen Deflection (mm)*	*Channel 1*		*Channel 7*	
		Ohms	*Deflection (mm)*	*Ohms*	*Deflection (mm)*

23:20 hrs **Cycles: 29150**

Max. cyclic load: 49.69 KN Min. cyclic load: 0.55 KN

0.62	19.49	0.00	5745.0	17.24	0.00	892.45	13.39	0.00
5.12	18.51	0.98	5781.4	17.34	-0.11	849.86	12.75	0.64
10.16	18.07	1.42	5744.2	17.23	0.00	838.87	12.58	0.80
15.21	17.80	1.69	5703.7	17.11	0.12	816.89	12.25	1.13
21.40	17.49	2.00	5630.8	16.89	0.34	804.74	12.07	1.32
25.48	17.27	2.22	5591.6	16.77	0.46	796.75	11.95	1.44
29.86	17.06	2.43	5545.2	16.64	0.60	780.93	11.71	1.67
35.23	16.80	2.69	5477.1	16.43	0.80	774.33	11.61	1.77
40.31	16.55	2.94	5425.5	16.28	0.96	761.66	11.42	1.96
45.35	16.32	3.17	5392.4	16.18	1.06	750.82	11.26	2.12
50.40	16.10	3.39	5344.8	16.03	1.20	746.88	11.20	2.18
38.11	16.62	2.87	5427.7	16.28	0.95	759.47	11.39	1.99
29.82	16.99	2.50	5508.6	16.53	0.71	783.48	11.75	1.63
19.37	17.50	1.99	5631.2	16.89	0.34	810.95	12.16	1.22
10.37	17.96	1.53	5739.2	17.22	0.02	833.48	12.50	0.88
0.65	19.31	0.18	5748.3	17.24	-0.01	900.78	13.51	-0.12

Table A29: Transducer readings for SB 50 @ 23:20

Load (KN)	*Platen Deflection (mm)*	*Channel 1*		*Channel 7*	
		Ohms	*Deflection (mm)*	*Ohms*	*Deflection (mm)*

40:07 hrs **Cycles: 49630**

Max. cyclic load: 49.52 KN Min. cyclic load: 0.21 KN

0.62	19.61	0.00	4616.3	13.85	0.00	1002.78	15.04	0.00
5.16	18.65	0.96	4676.0	14.03	-0.18	983.86	14.76	0.28
10.82	18.15	1.46	4685.0	14.06	-0.21	977.83	14.67	0.37
15.81	17.82	1.79	4627.6	13.88	-0.03	958.99	14.38	0.66
19.81	17.62	1.99	4564.1	13.69	0.16	948.50	14.23	0.81
25.21	17.33	2.28	4505.3	13.52	0.33	925.90	13.89	1.15
30.33	17.09	2.52	4461.1	13.38	0.47	914.03	13.71	1.33
35.85	16.82	2.79	4384.1	13.15	0.70	918.23	13.77	1.27
40.58	16.60	3.01	4313.7	12.94	0.91	910.69	13.66	1.38
45.44	16.36	3.25	4228.0	12.68	1.16	892.45	13.39	1.65
50.18	16.15	3.46	4170.2	12.51	1.34	899.85	13.50	1.54
39.74	16.59	3.02	4322.6	12.97	0.88	914.45	13.72	1.32
30.51	17.00	2.61	4449.0	13.35	0.50	919.29	13.79	1.25
19.65	17.51	2.10	4570.0	13.71	0.14	951.26	14.27	0.77
10.43	17.99	1.62	4661.3	13.98	-0.14	974.12	14.61	0.43
0.56	18.94	0.68	4609.7	13.83	0.02	1083.58	16.25	-1.21

Table A30: Transducer readings for SB 50 @ 40:07

Load (KN)	*Platen Deflection (mm)*	*Channel 1*		*Channel 7*			
		Ohms	*Deflection (mm)*	*Ohms*	*Deflection (mm)*		
00:25 hrs							**Cycles: 0**
0.43	45.17	0.00	4408.8	13.23	0.00	761.33	11.42	0.00
0.88	44.96	0.21	4406.7	13.22	0.01	766.78	11.50	-0.08
5.28	44.33	0.84	4312.3	12.94	0.29	743.83	11.16	0.26
11.85	43.92	1.25	4216.1	12.65	0.58	712.38	10.69	0.73
17.71	43.60	1.57	4201.0	12.60	0.62	706.71	10.60	0.82
25.74	43.18	1.99	4114.4	12.34	0.88	685.34	10.28	1.14
31.78	42.88	2.29	4066.4	12.20	1.03	674.75	10.12	1.30
37.33	42.62	2.55	4019.2	12.06	1.17	667.18	10.01	1.41
46.53	42.18	2.99	3937.5	11.81	1.41	640.51	9.61	1.81
52.41	41.19	3.98	3871.0	11.61	1.61	631.39	9.47	1.95
58.84	41.60	3.57	3807.9	11.42	1.80	614.72	9.22	2.20
62.70	41.42	3.75	3776.6	11.33	1.90	606.58	9.10	2.32
53.56	41.81	3.36	3823.9	11.47	1.75	630.09	9.45	1.97
40.90	42.35	2.82	3954.4	11.86	1.36	650.57	9.76	1.66
30.71	42.80	2.37	4015.5	12.05	1.18	681.44	10.22	1.20
20.53	43.29	1.88	4090.0	12.27	0.96	700.46	10.51	0.91
10.54	43.80	1.37	4186.9	12.56	0.67	713.82	10.71	0.71
5.52	44.08	1.09	4229.2	12.69	0.54	739.43	11.09	0.33
1.19	44.67	0.50	4389.4	13.17	0.06	769.70	11.55	-0.13

Table A31: Transducer readings for SB 62 @ 00:25

Load (KN)	*Platen Deflection (mm)*	*Channel 1*		*Channel 7*			
		Ohms	*Deflection (mm)*	*Ohms*	*Deflection (mm)*		
03:13 hrs							**Cycles: 3275**
Max. cyclic load: 62.00 KN							Min. cyclic load: 8.75 KN
0.58	43.92	0.00	4418.5	13.26	0.00	782.13	11.73	0.00
5.30	43.22	0.70	4249.8	12.75	0.51	783.77	11.76	-0.02
10.16	42.95	0.97	4204.7	12.61	0.64	741.40	11.12	0.61
15.28	42.70	1.22	4150.2	12.45	0.80	723.92	10.86	0.87
21.63	42.39	1.53	4102.1	12.31	0.95	710.80	10.66	1.07
26.90	42.15	1.77	4034.9	12.10	1.15	688.40	10.33	1.41
36.13	41.74	2.18	3993.8	11.98	1.27	679.19	10.19	1.54
46.18	41.30	2.62	3896.9	11.69	1.56	654.88	9.82	1.91
56.10	40.87	3.05	3812.1	11.44	1.82	640.02	9.60	2.13
62.03	40.16	3.76	3783.1	11.35	1.91	630.59	9.46	2.27
53.01	40.98	2.94	3838.9	11.52	1.74	638.24	9.57	2.16
41.45	41.47	2.45	3945.5	11.84	1.42	657.76	9.87	1.87
30.23	41.96	1.96	4009.4	12.03	1.23	689.05	10.34	1.40
19.74	42.43	1.49	4089.1	12.27	0.99	718.63	10.78	0.95
9.82	42.93	0.99	4202.3	12.61	0.65	732.73	10.99	0.74
5.08	43.21	0.71	4242.9	12.73	0.53	758.89	11.38	0.35
0.57	43.90	0.02	4427.6	13.28	-0.03	781.69	11.73	0.01

Table A32: Transducer readings for SB 62 @ 03:13

Load (KN)	*Platen Deflection (mm)*	*Channel 1*		*Channel 7*	
		Ohms	*Deflection (mm)*	*Ohms*	*Deflection (mm)*

06:33 hrs **Cycles: 7278**

Max. cyclic load: 62.12 KN Min. cyclic load: 3.77 KN

0.60	45.10	0.00	4360.8	13.08	0.00	806.17	12.09	0.00
5.06	44.18	0.92	4237.1	12.71	0.37	785.00	11.78	0.32
10.43	43.81	1.29	4191.6	12.57	0.51	739.96	11.10	0.99
16.13	43.53	1.57	4152.1	12.46	0.63	734.82	11.02	1.07
23.75	43.19	1.91	4091.0	12.27	0.81	706.36	10.60	1.50
29.97	42.89	2.21	4030.5	12.09	0.99	694.80	10.42	1.67
37.42	42.54	2.56	3988.4	11.97	1.12	679.61	10.19	1.90
47.00	42.10	3.00	3917.8	11.75	1.33	669.44	10.04	2.05
54.65	41.74	3.36	3858.8	11.58	1.51	650.33	9.75	2.34
61.83	41.31	3.79	3837.2	11.51	1.57	636.13	9.54	2.55
48.74	41.83	3.27	3928.2	11.78	1.30	653.16	9.80	2.30
42.33	42.21	2.89	3946.0	11.84	1.24	655.85	9.84	2.25
32.27	42.73	2.37	4034.3	12.10	0.98	687.19	10.31	1.78
20.68	43.30	1.80	4125.0	12.38	0.71	713.51	10.70	1.39

Table A33: Transducer readings for SB 62 @ 06:33

Load (KN)	*Platen Deflection (mm)*	*Channel 1*		*Channel 7*	
		Ohms	*Deflection (mm)*	*Ohms*	*Deflection (mm)*

06:45 hrs **Cycles: 7278**

Max. cyclic load: 62.12 KN Min. cyclic load: 3.77 KN

0.70	44.78	0.00	4400.9	13.20	0.00	849.29	12.74	0.00
8.12	43.88	0.90	4187.5	12.56	0.64	800.44	12.01	0.73
19.81	43.29	1.49	4100.2	12.30	0.90	777.20	11.66	1.08
30.35	42.78	2.00	4008.7	12.03	1.18	760.56	11.41	1.33
40.43	42.31	2.47	3919.1	11.76	1.45	743.19	11.15	1.59
49.73	41.89	2.89	3800.6	11.40	1.80	727.69	10.92	1.82
61.78	41.42	3.36	3701.2	11.10	2.10	721.68	10.83	1.91
49.88	41.91	2.87	3789.4	11.37	1.83	723.84	10.86	1.88
40.49	42.25	2.53	3879.0	11.64	1.57	735.60	11.03	1.71
31.43	42.72	2.06	4009.8	12.03	1.17	778.34	11.68	1.06
20.39	43.20	1.58	4065.4	12.20	1.01	778.37	11.68	1.06
10.23	43.72	1.06	4157.3	12.47	0.73	799.61	11.99	0.75
0.53	44.79	-0.01	4417.9	13.25	-0.05	887.79	13.32	-0.58

Table A34: Transducer readings for SB 62 @ 06:45

Load (KN)	*Platen Deflection (mm)*	*Channel 1*		*Channel 7*	
		Ohms	*Deflection (mm)*	*Ohms*	*Deflection (mm)*
24:46 hrs					**Cycles: 7880**
0.57	45.57	0.00	4342.6	13.03	0.00	855.24	12.83	0.00
4.76	44.68	0.89	4331.6	12.99	0.03	804.56	12.07	0.76
9.57	44.26	1.31	4294.7	12.88	0.14	784.21	11.76	1.07
20.03	43.69	1.88	4228.4	12.69	0.34	768.30	11.52	1.30
29.69	43.18	2.39	4146.3	12.44	0.59	738.09	11.07	1.76
40.79	42.69	2.88	4044.9	12.13	0.89	726.54	10.90	1.93
50.26	42.27	3.30	3971.7	11.92	1.11	727.62	10.91	1.91
59.48	41.86	3.71	3897.3	11.69	1.34	686.32	10.29	2.53
63.08	41.72	3.85	3867.3	11.60	1.43	679.62	10.19	2.63
49.81	42.44	3.13	3971.7	11.92	1.11	698.62	10.48	2.35
41.65	42.82	2.75	4064.6	12.19	0.83	722.65	10.84	1.99
29.41	43.28	2.29	4130.8	12.39	0.64	738.93	11.08	1.74
20.35	43.60	1.97	4199.3	12.60	0.43	769.75	11.55	1.28
9.97	44.12	1.45	4284.6	12.85	0.17	785.48	11.78	1.05
4.97	44.52	1.05	4342.4	13.03	0.00	800.69	12.01	0.82
0.57	45.45	0.12	4359.1	13.08	-0.05	868.98	13.03	-0.21

Table A35: Transducer readings for SB 62 @ 24:46

Load (KN)	*Platen Deflection (mm)*	*Channel 1*		*Channel 7*	
		Ohms	*Deflection (mm)*	*Ohms*	*Deflection (mm)*
47:41 hrs					**Cycles: 7880**
Max. cyclic load: 25.04 KN					Min. cyclic load: 0.53 KN
0.90	45.67	0.00	4334.0	13.00	0.00	882.05	13.23	0.00
6.10	44.64	1.03	4318.6	12.96	0.05	798.50	11.98	1.25
11.50	44.20	1.47	4277.0	12.83	0.17	782.90	11.74	1.49
18.78	43.82	1.85	4228.8	12.69	0.32	775.45	11.63	1.60
26.70	43.42	2.25	4163.8	12.49	0.51	749.26	11.24	1.99
35.78	42.98	2.69	4096.6	12.29	0.71	734.14	11.01	2.22
47.90	42.40	3.27	4012.3	12.04	0.97	705.53	10.58	2.65
55.87	42.06	3.61	3941.4	11.82	1.18	693.81	10.41	2.82
62.22	41.80	3.87	3897.6	11.69	1.31	690.19	10.35	2.88
49.38	42.33	3.34	3981.3	11.94	1.06	702.71	10.54	2.69
36.70	42.88	2.79	4093.6	12.28	0.72	735.25	11.03	2.20
26.45	43.34	2.33	4164.0	12.49	0.51	746.13	11.19	2.04
18.75	43.70	1.97	4221.1	12.66	0.34	782.95	11.74	1.49
9.72	44.17	1.50	4301.6	12.90	0.10	796.29	11.94	1.29
5.56	44.59	1.08	4319.6	12.96	0.04	795.64	11.93	1.30
0.95	45.56	0.11	4336.2	13.01	-0.01	981.95	14.73	-1.50

Table A36: Transducer readings for SB 62 @ 47:41

--------load-------			--------Deflection-------						Average	
			gage47	zero		gage45	zero			
Psi	N		ohm	ohm	mm	ohm	ohm	mm	mm	shifted
Bed in										
0	0		381.64	0	0	271.09	0	0	0	
400	19620		420.94	39.30	0.55	316.07	44.98	0.67	0.61	
800	39240		441.97	60.33	0.84	322.36	51.27	0.76	0.80	
Loading										
200	9.81		421.41	39.77	0.56	305.00	33.91	0.51	0.53	0.23
400	19.62		437.29	55.65	0.78	323.53	52.44	0.78	0.78	0.48
800	39.24		469.05	87.41	1.22	359.35	88.26	1.32	1.27	0.97
1200	58.86		503.77	122.13	1.71	393.82	122.73	1.83	1.77	1.47
1400	68.67		522.94	141.30	1.98	416.36	145.27	2.16	2.07	1.77
1600	78.48		541.64	160.00	2.24	430.81	159.72	2.38	2.31	2.01
1800	88.29		566.76	185.12	2.59	453.89	182.80	2.72	2.66	2.36
2000	98.10		595.20	213.56	2.99	478.90	207.81	3.10	3.04	2.74
2200	107.91		622.72	241.08	3.38	504.76	233.67	3.48	3.43	3.13
2400	117.72		656.63	274.99	3.85	537.36	266.27	3.97	3.91	3.61
2600	127.53		704.11	322.47	4.51	575.75	304.66	4.54	4.53	4.23
2800	137.34		754.49	372.85	5.22	624.16	353.07	5.26	5.24	4.94
3000	147.15		890.00	508.36	7.12	780.00	508.91	7.58	7.35	7.05
3300	161.87		1712.70	1331.06	18.63	1002.52	731.43	10.90	14.77	14.47

Table A37: Transducer readings for the bending test-control beam

--------load-------			--------Deflection-------			--------Deflection-------			Average	
			gage3	zero		gage5	zero	gage 5		
Psi	N		ohm		mm	ohm		mm	mm	shifted
Bed in										
0	0		243.25	0.00	0.00	207.01	0.00	0.00	0.00	
400	19.62		284.19	40.94	0.57	253.71	46.70	0.70	0.63	
600	29.43		302.95	59.70	0.84	287.15	80.14	1.19	1.01	
800	39.24		323.00	79.75	1.12	299.23	92.22	1.37	1.25	
Loading										
	0.00									0.00
200	9.81		272.90	29.65	0.42	240.87	33.86	0.50	0.46	0.26
600	29.43		305.84	62.59	0.88	283.51	76.50	1.14	1.01	0.81
800	39.24		322.89	79.64	1.11	303.78	96.77	1.44	1.28	1.08
1000	49.05		350.17	106.92	1.50	323.52	116.51	1.74	1.62	1.42
1200	58.86		370.00	126.75	1.77	338.00	130.99	1.95	1.86	1.66
1400	68.67		390.76	147.51	2.07	364.97	157.96	2.35	2.21	2.01
1600	78.48		409.66	166.41	2.33	385.41	178.40	2.66	2.49	2.29
1800	88.29		435.38	192.13	2.69	409.82	202.81	3.02	2.86	2.66
2000	98.10		461.49	218.24	3.06	442.84	235.83	3.51	3.28	3.08
2200	107.91		493.17	249.92	3.50	483.30	276.29	4.12	3.81	3.61
2400	117.72		529.68	286.43	4.01	504.61	297.60	4.43	4.22	4.02
2600	127.53		576.83	333.58	4.67	557.09	350.08	5.22	4.94	4.74
2800	137.34		653.55	410.30	5.74	640.88	433.87	6.46	6.10	5.90
3000	147.15		774.11	530.86	7.43	762.29	555.28	8.27	7.85	7.65
3200	156.96		955.70	712.45	9.97	977.86	770.85	11.49	10.73	10.53
3300	161.87		1107.02	863.77	12.09	1104.40	897.39	13.37	12.73	12.53

Table A38: Transducer readings for the bending test-SB34

--------load--------			---------Deflection-------						Average	
			gage47	zero		gage45	zero			
Psi	N		ohm	ohm	mm	ohm	ohm	mm	mm	shifted
Bed in										
0	0		227.83	0.00	0.00	4.80	0.00	0.00	0.00	
400	19.62		300.71	72.88	1.02	83.07	78.27	1.17	1.09	
800	39.24		353.10	125.27	1.75	123.82	119.02	1.77	1.76	
Loading										
	0.00									0.00
200	9.81		276.62	48.79	0.68	97.70	48.91	0.73	0.71	0.31
800	39.24		353.06	125.23	1.75	148.83	100.04	1.49	1.62	1.22
1200	58.86		401.88	174.05	2.44	180.37	131.58	1.96	2.20	1.80
1400	68.67		423.04	195.21	2.73	199.37	150.58	2.24	2.49	2.09
1600	78.48		447.16	219.33	3.07	217.05	168.26	2.51	2.79	2.39
1800	88.29		476.75	248.92	3.48	234.49	185.70	2.77	3.13	2.73
2000	98.10		523.18	295.35	4.13	265.79	217.00	3.23	3.68	3.28
2200	107.91		583.55	355.72	4.98	307.75	258.96	3.86	4.42	4.02
2500	122.63		766.12	538.29	7.54	403.16	354.37	5.28	6.41	6.01
2600	127.53		877.13	649.30	9.09	481.01	432.22	6.44	7.77	7.37

Table A39: Transducer readings for the bending test-SB42

--------load--------			---------Deflection-------						Average	
			gage47	zero		gage45	zero			
Psi	N		ohm	ohm	mm	ohm	ohm	mm	mm	shifted
Bed in										
0	0		398.11	0.00	5.57	181.74	0.00	2.71	4.14	
800	39.24		518.73	120.62	7.26	271.79	90.05	4.05	5.66	
Loading										
	0.00									0.00
150	7.36		439.64	41.53	6.15	228.65	46.91	3.41	4.78	0.18
800	39.24		515.82	117.71	7.22	302.49	120.75	4.51	5.86	1.26
1200	58.86		570.59	172.48	7.99	343.95	162.21	5.12	6.56	1.96
1400	68.67		603.17	205.06	8.44	368.69	186.95	5.49	6.97	2.37
1600	78.48		626.65	228.54	8.77	394.24	212.50	5.87	7.32	2.72
1800	88.29		663.66	265.55	9.29	423.23	241.49	6.31	7.80	3.20
2100	103.01		694.05	295.94	9.72	456.08	274.34	6.80	8.26	3.66
2300	112.82		744.81	346.70	10.43	499.64	317.90	7.44	8.94	4.34
2500	122.63		834.10	435.99	11.68	584.71	402.97	8.71	10.19	5.59
2600	127.53		954.12	556.01	13.36	684.41	502.67	10.20	11.78	7.18

Table A40: Transducer readings for the bending test-SB50

--------load-------			--------Deflection-------			
Psi	N		gage47 ohm	zero ohm	mm	shifted
Bed in						
0	0		453.23	0.00	6.35	
800	39.24		550.97	97.74	7.71	
Loading						
100	4.91		453.23	0.00	6.35	0.00
400	19.62		510.60	57.37	7.15	0.65
800	39.24		554.33	101.10	7.76	1.26
1200	58.86		599.90	146.67	8.40	1.90
1600	78.48		661.09	207.86	9.26	2.76
2000	98.10		726.64	273.41	10.17	3.67
2200	107.91		774.13	320.90	10.84	4.34
2400	117.72		872.12	418.89	12.21	5.71
2500	122.63		1005.68	552.45	14.08	7.58

Table A41: Transducer readings for the bending test-SB62

Appendix B

- **Strain measurements**

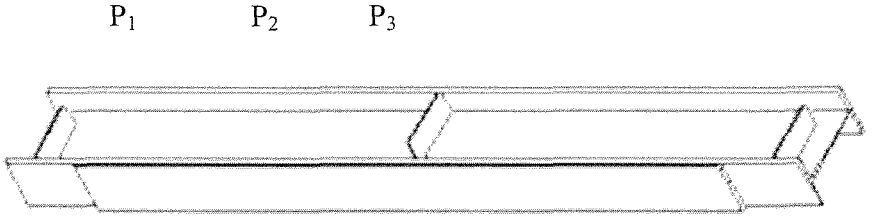

Figure B1: positioning of strain gauges along the beam

P: Position
Tflange: Top flange
Bflange: Bottom flange
Axia1: longitudinal axis
Axis2: transverse axis

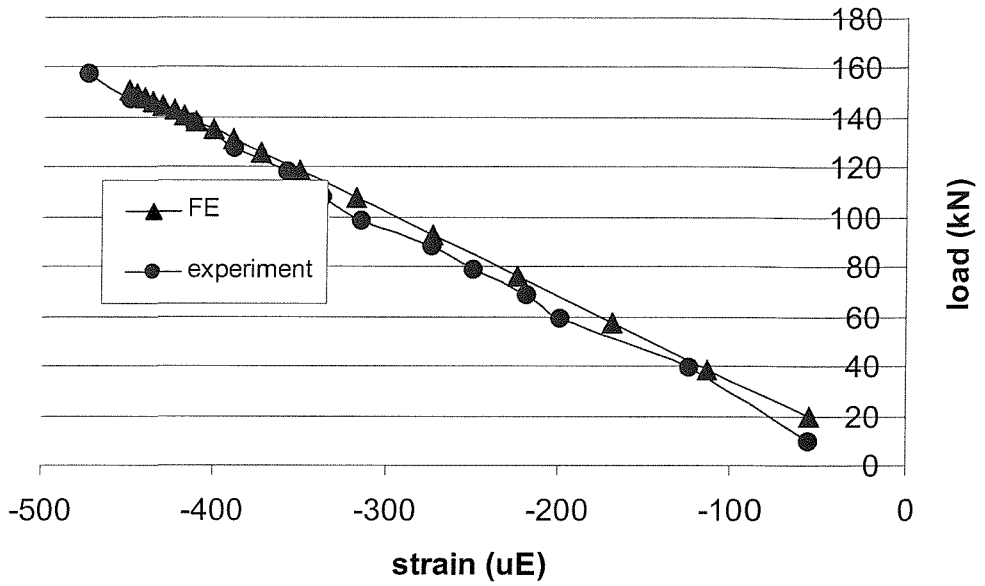

Figure B2 Load-strain curve for control specimen-top flange, position 1

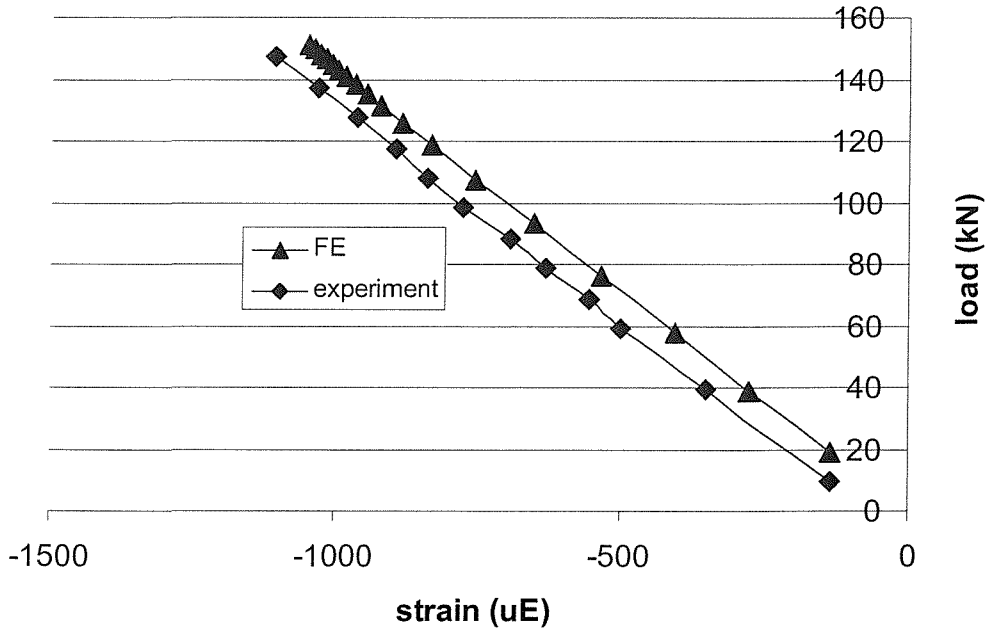

Figure B3 Load-strain curve for control specimen-top flange, position 2

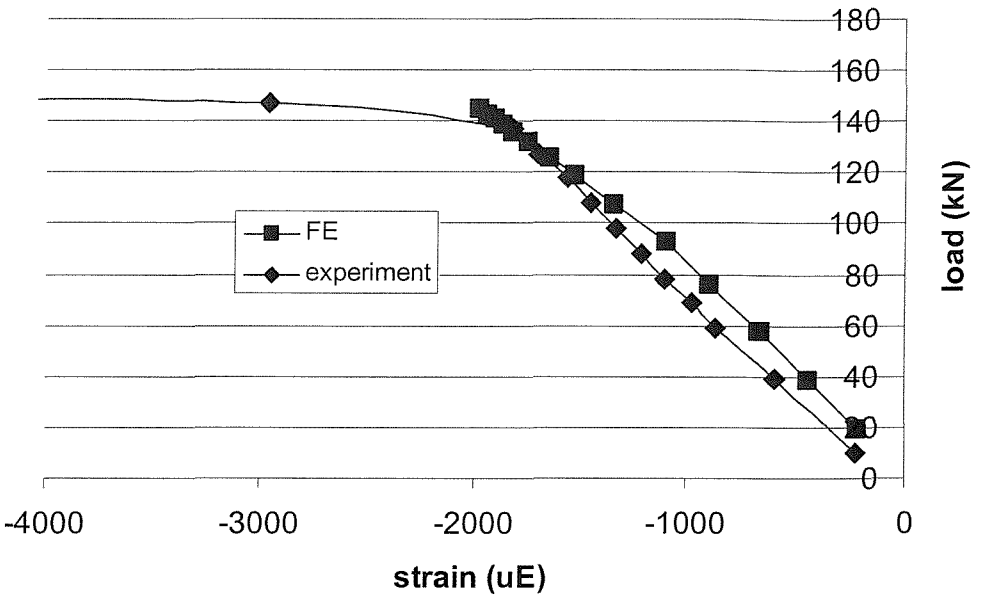

Figure B4 Load-strain curve for control specimen-top flange, position 3

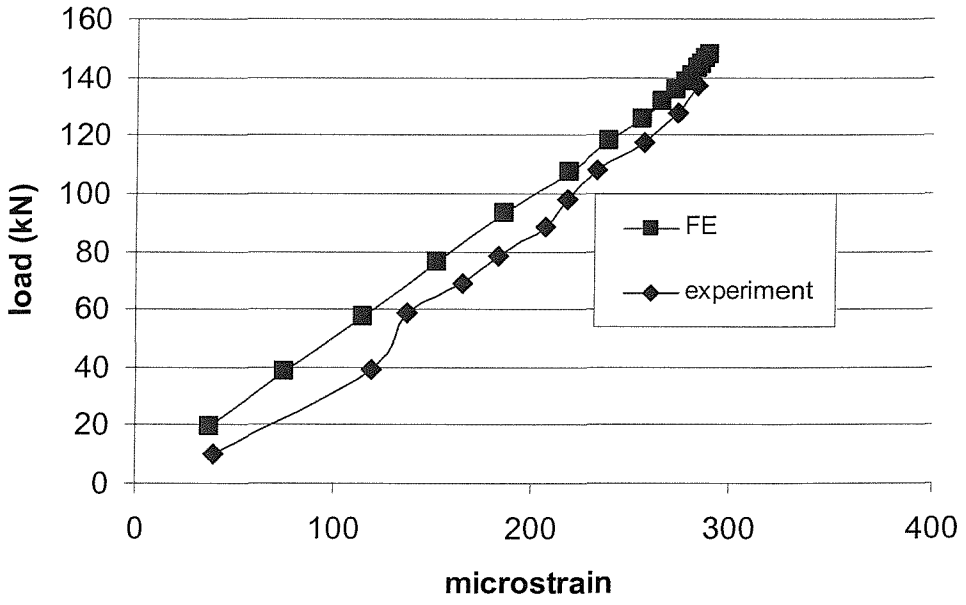

Figure B5 Load-strain curve for control specimen-bottom flange, position 1

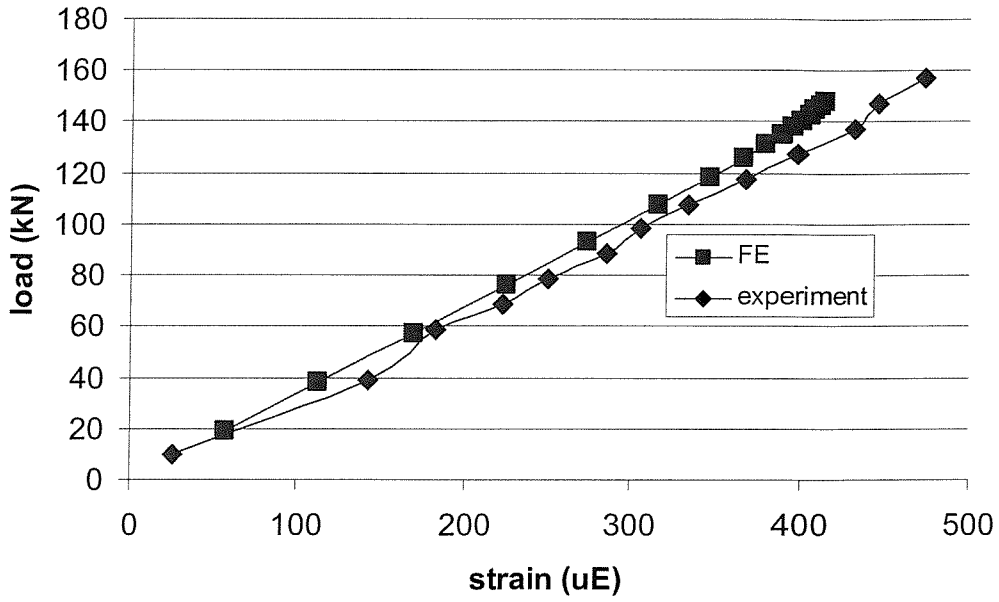

Figure B6 Load-strain curve for control specimen-bottom flange, position 2

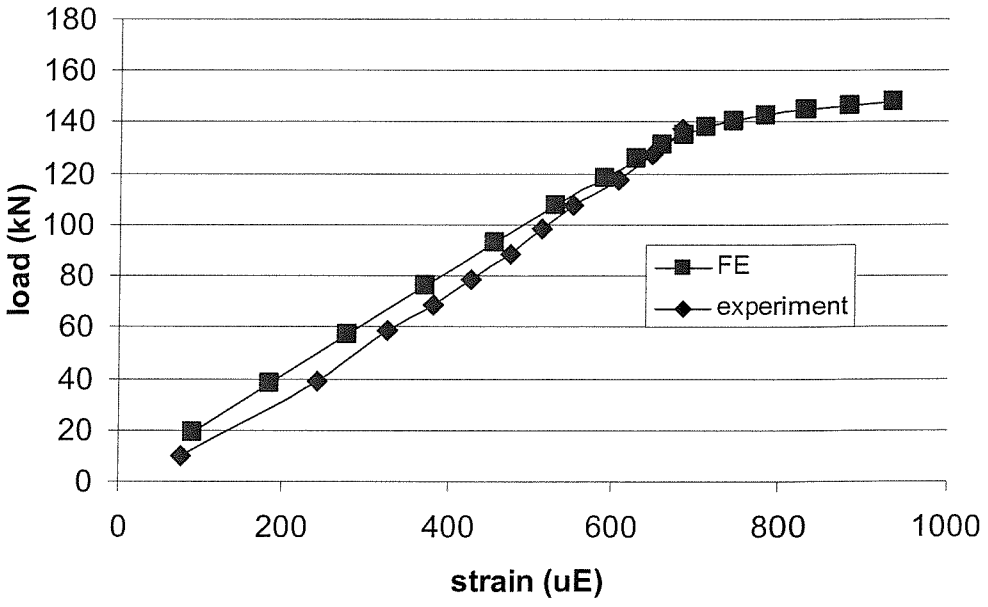

Figure B7 Load-strain curve for control specimen-bottom flange, position 3

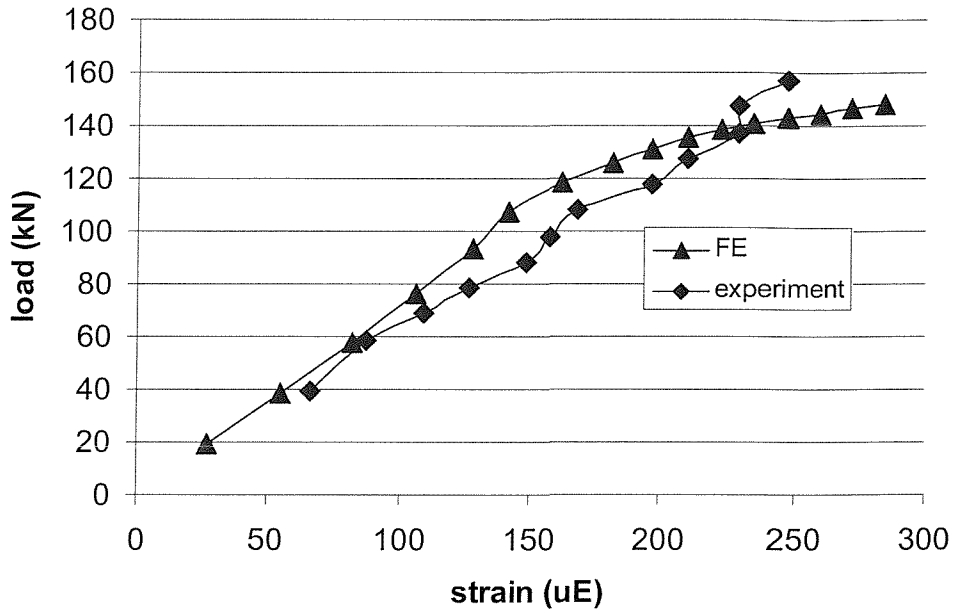

Figure B8 Load-strain curve for control specimen-carbon, position 1

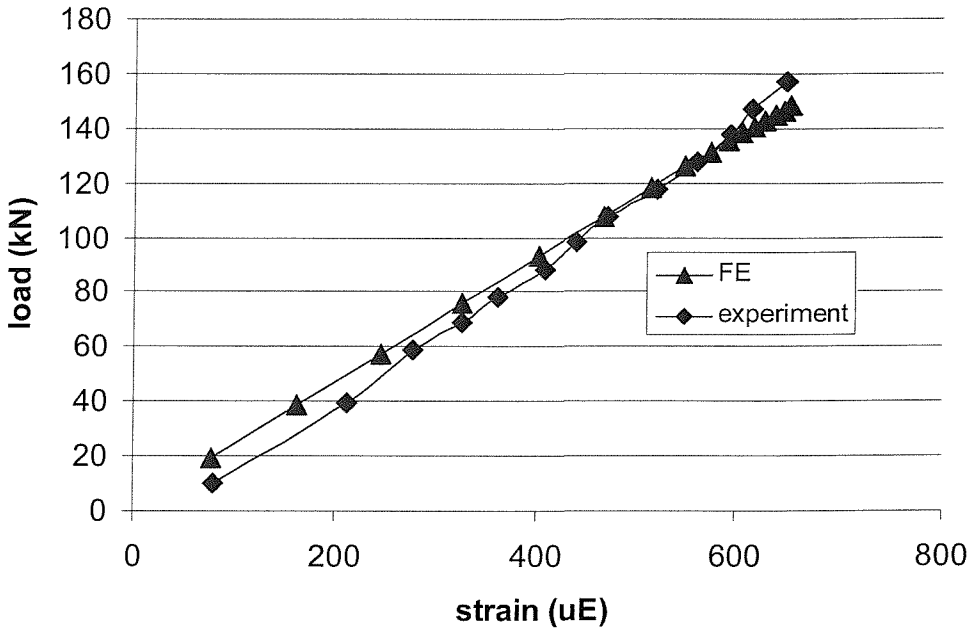

Figure B9 Load-strain curve for control specimen-carbon, position 2

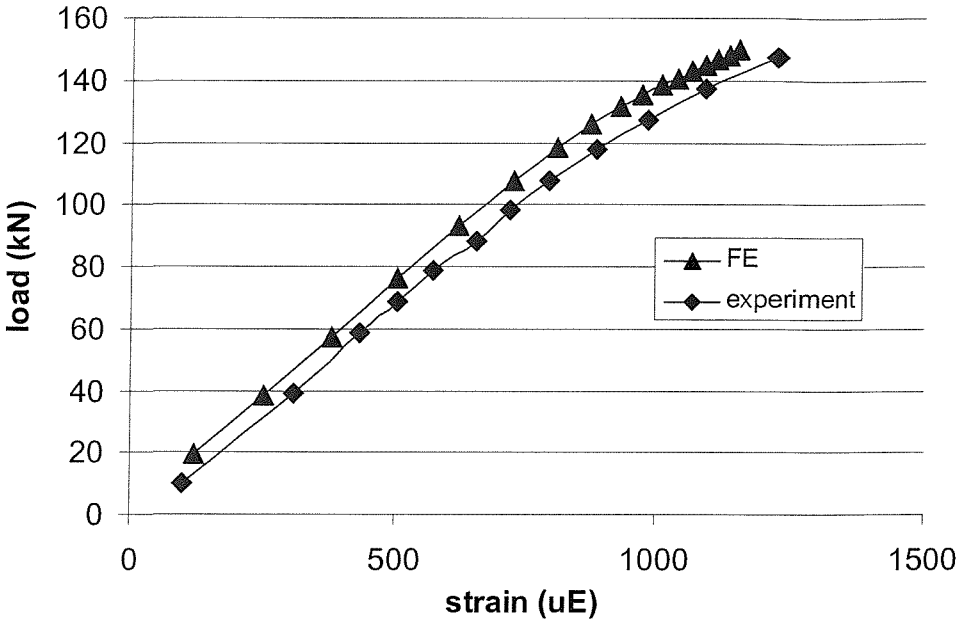

Figure B10 Load-strain curve for control specimen-carbon, position 3

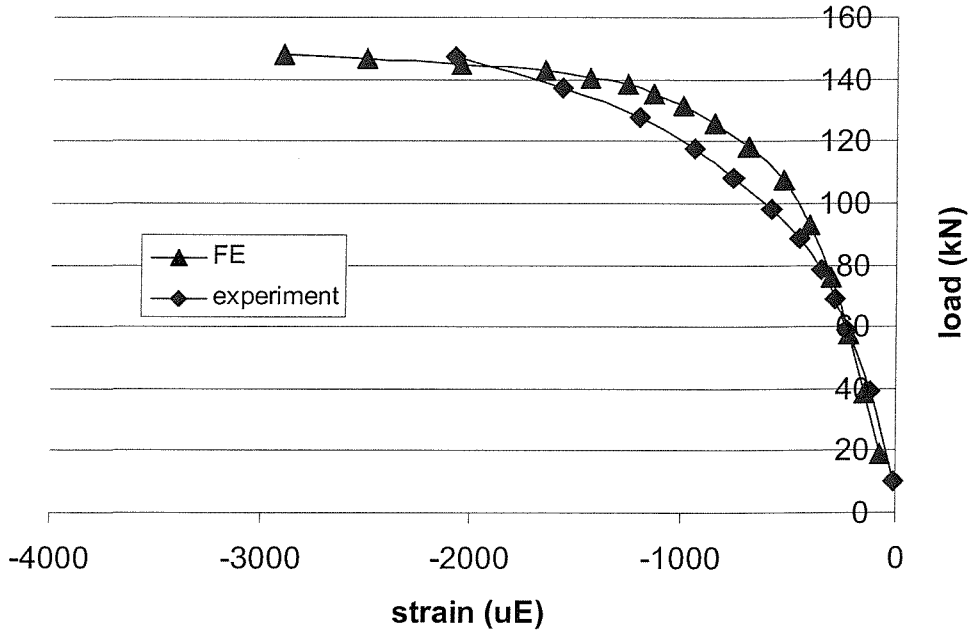

Figure B11 Load-strain curve for control specimen-web, position 3

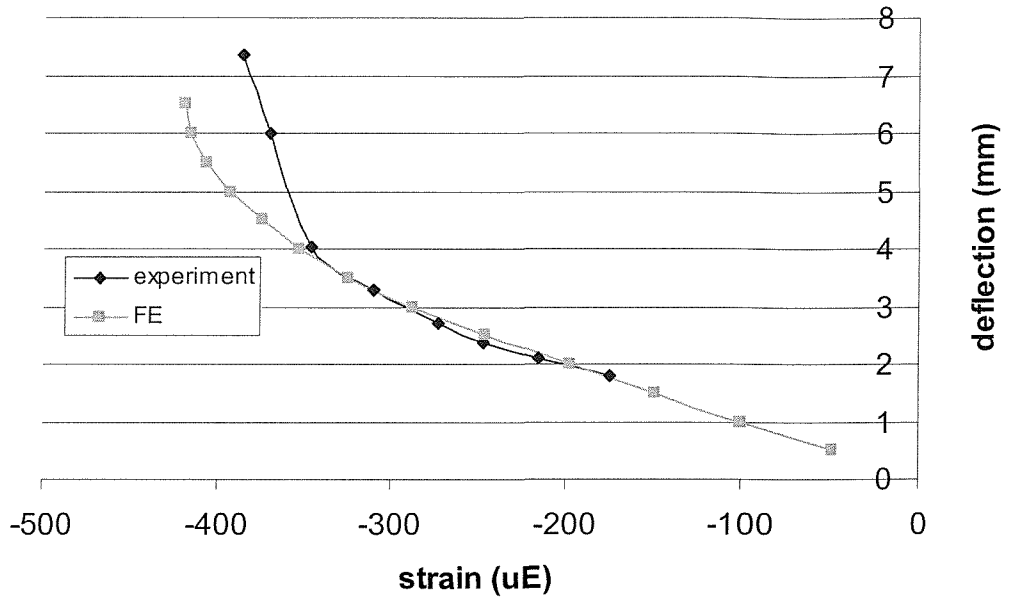

Figure B12 Load-strain curve SB42-top flange, position 1

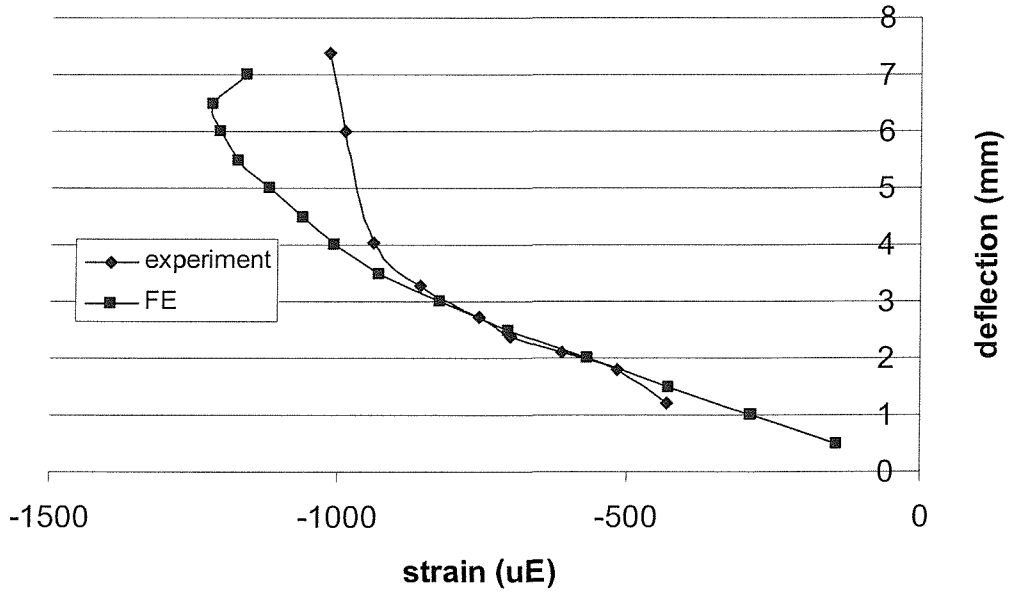

Figure B13 Load-strain curve for SB42-top flange, position 2

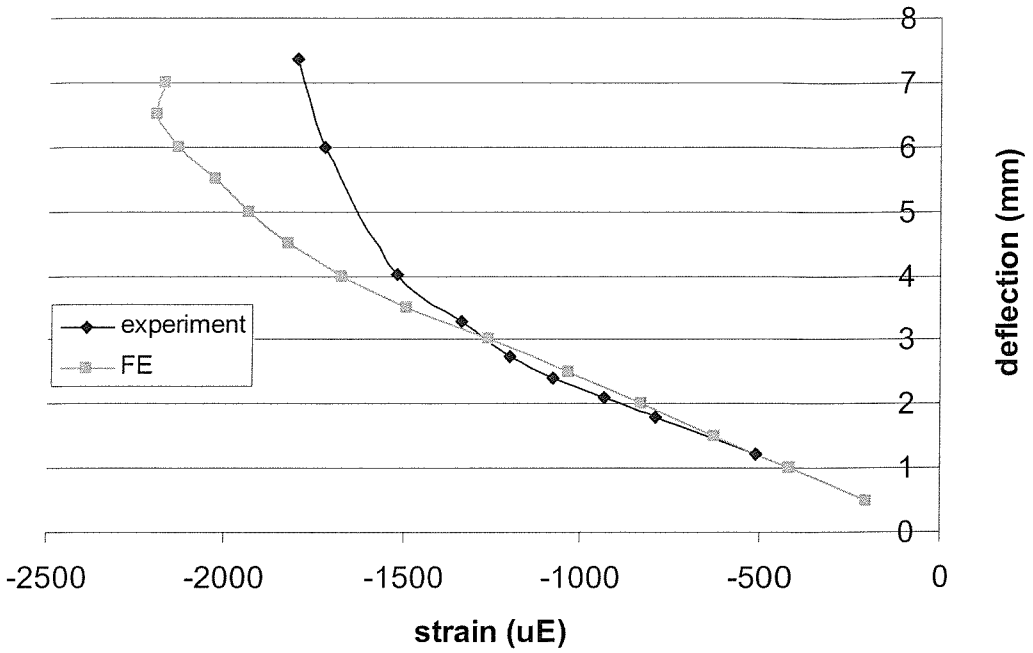

Figure B14 Load-strain curve for SB42-top flange, position 3

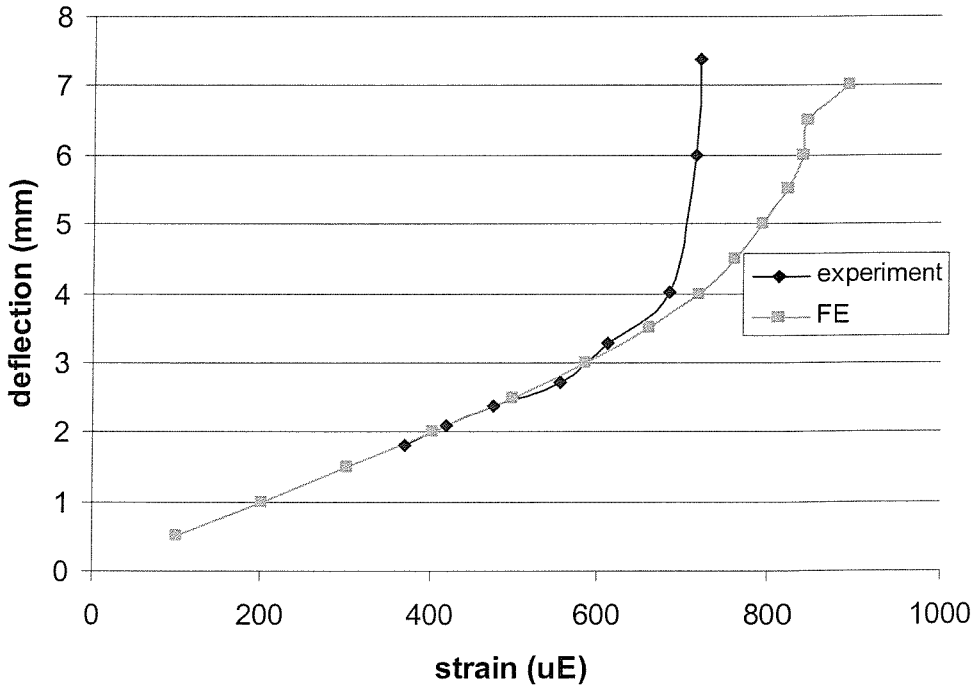

Figure B15 Load-strain curve for SB42-bottom flange, position 2

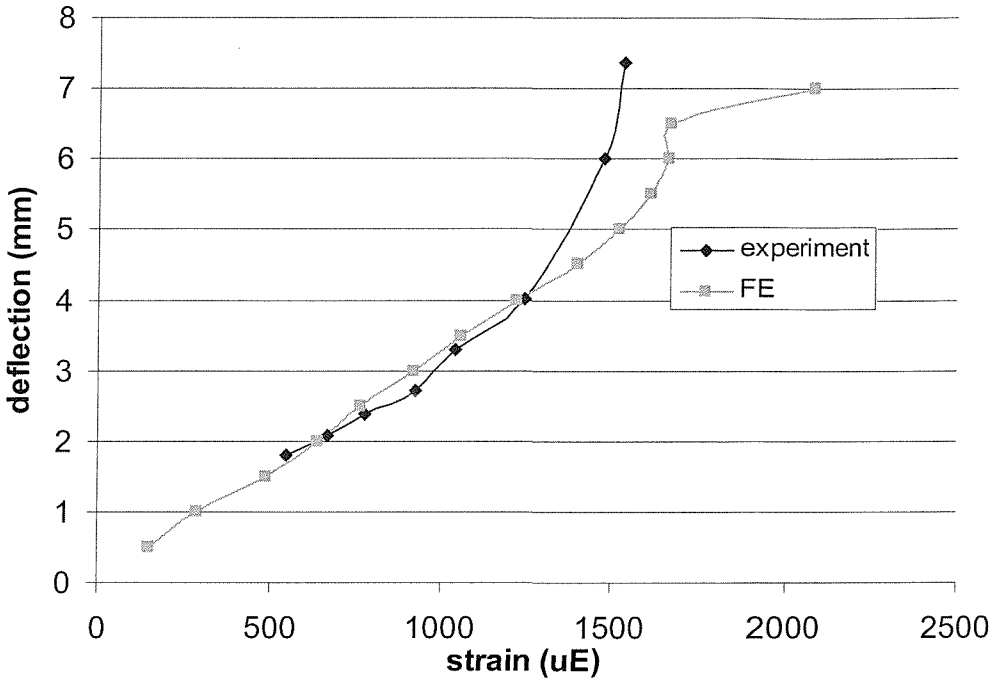

Figure B16 Load-strain curve for SB42-bottom flange, position 3

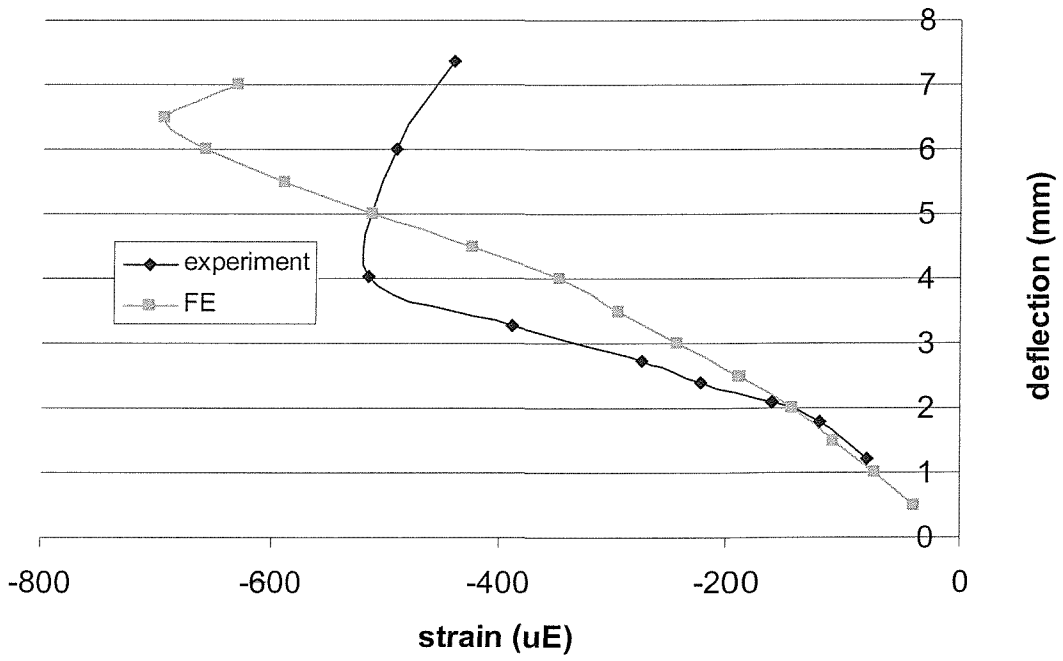

Figure B17 Load-strain curve for SB42-web

Appendix C

- **Bending stiffness**
- **Slip**
- **Shear stress**

Behavioural prediction of the test specimens

Transforming the CFRP to equivalent reference material

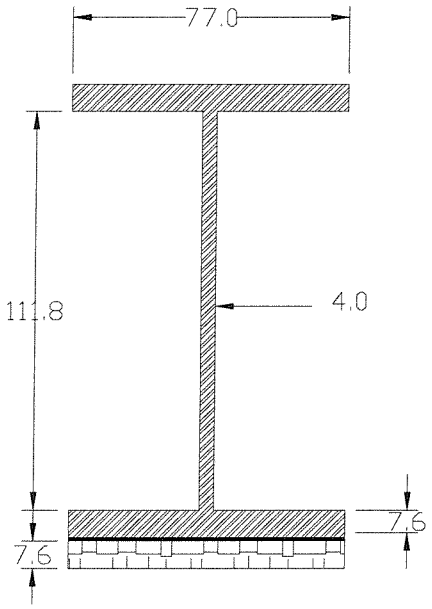

Figure C.1 Cross-sectional dimension

$$\text{The effective width} = \frac{E_c}{E_s} * \text{width}$$

$$= \frac{310}{194} * 76$$

$$= 121 \text{ mm}$$

Where, E_c is the Young's modulus of carbon, and E_s the Young's modulus of steel.

Calculating the neutral axis

Sections	Area A (mm^2)	Centre H (mm)	A*H (mm^3)	$Bd^3/12$ (mm^4)	D^2 (mm^2)	Ixx (mm^4)
1	577.6	3.8	2194.88	2780.18	7098.06	4,102,619.64
2	447.2	63.5	28397.2	465805.01	602.7	735,332.45
3	577.6	123.2	71160.32	2780.18	1235.5	716,404.98
4	920	130.8	120336	4426.34	1827.56	1,685,781.54
Total	2522.4		222088.4			7,240,138.61

Table C.1 Calculating the second moment of area

Centroid = AH/A

$$= \frac{222088.4}{2522.4} = 88.05 \text{ mm (from the top)}$$

Second moment of area = $bd^3/12 + AH^2$

For a single point load at mid-span

$$\delta = \frac{pL^3}{48EI}$$

δ = Vertical deflection

P = point load

L = span

$$\therefore \text{Bending stiffness } \left(\frac{p}{\delta}\right) = \frac{48EI}{L^3}$$

For the beams tested, L=1.15 m

$$\therefore \text{Bending stiffness } = \frac{48x194xI}{1150^3}$$

$$= 6.1 \times 10^{-6} \text{ I}$$

For the bare steel beam

Bending stiffness = $6.1 \times 10^{-6} \times 467.7 \times 10^4$

= 29.08 kN/mm

For the reinforced beam

Bending stiffness = $6.1 \times 10^{-6} \times 724 \times 10^4$

= 44.65 kN/mm

Shear stresses

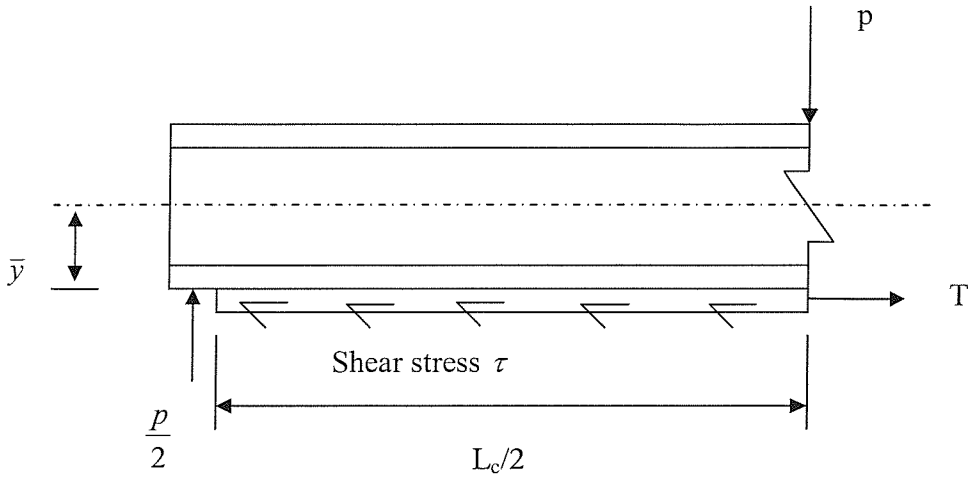

Figure C.2 forces across the reinforced beam

The shear force is constant over each half span and is equal to p/2. Hence shear stress τ is also constant. Say shear force = Q

For horizontal equilibrium

$$T = \frac{BL_c}{2}.\tau$$

B = width of carbon plate

Also

T = Bt. Average direct stress in carbon

t = thickness of carbon plate

Using engineering bending theory

$$T = Bt.\ \frac{M}{I}\left(\frac{\bar{y}+[\bar{y}-t]}{2}\right)$$

$$= Bt.\ \frac{M}{I}\left(\bar{y}-\frac{t}{2}\right)$$

$$= Bt.\ \frac{pL}{4I}\left(\bar{y}-\frac{t}{2}\right)$$

L = span of beam

$$\therefore \quad \frac{BL_c}{2}.\tau = Bt.\frac{pL}{4I}\left(\bar{y} - \frac{t}{2}\right)$$

$$\therefore \quad \tau = \frac{Q}{I}\frac{L}{L_c}\left(\bar{y} - \frac{t}{2}\right)t$$

For the test beams

L = 1.16 m

L_c = 0.98 m

. t = 7.6 mm

I = 724.0 cm

$\bar{y}$ = 46.55 mm

$$\tau = \frac{Q}{724.0x10^4}\frac{1.16}{0.98}\left(46.55 - \frac{7.6}{2}\right)7.6$$

$\therefore$ = 0.0000532 Q N/mm^2

P (KN)	Q (N)	τ (N/mm^2)
25	12500	0.67
34	17000	0.856
42	21000	1.0
50	25000	1.259
62	31000	1.6

Table C.2 Calculating the shear stress in adhesive at various load level

Steel-carbon slip before cure

When the steel beam is loaded, the tension (bottom) flange will increase in length. Although the carbon plate is in contact, no shear will be transferred across the adhesive. Consequently there will be relative slip between the steel and the carbon.

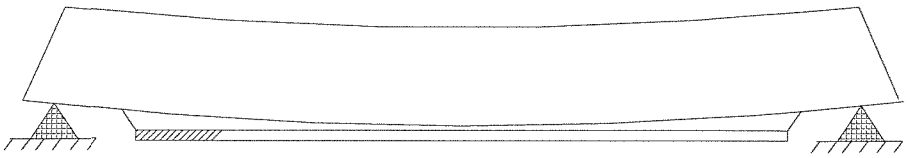

Figure C.3 Beam under point load

Using Engineering bending formula

$$\frac{M}{I} = \frac{\vartheta}{h}$$

$$\therefore \quad \varepsilon = \frac{Mh}{EI}$$

$\therefore$ Total extension over half of the length of the carbon plate is

$$\int_{L_1}^{L/2} \varepsilon . dx = \int_{L_1}^{L/2} \frac{Mh}{EI} . dx$$

$$= \int_{L_1}^{L/2} \frac{Pxh}{2EI}.dx = \frac{Ph}{4EI}\left[x^2\right]_{L_1}^{\frac{L}{2}}$$

$$= \frac{Ph}{4EI}\left[\frac{L^2}{4} - L_1^2\right]$$

h (before curing occurs) $= \frac{127}{2} = 63.5$ mm

$$L_1 = \frac{1100 - 980}{2} = 60 \text{ mm}$$

The slip is equal to the difference in extension of the steel beam and carbon.

$$\therefore \quad \text{Slip} = \frac{P * 63.5}{4 * 194{,}000 * 473 * 10^4}\left[\frac{1100^2}{4} - 60^2\right]$$

$= 5.171 \text{ x } 10^{-6} \text{ P mm}$ (P in N)

P (KN)	Slip (mm)
25	0.129
34	0.176
42	0.217
50	0.258
62	0.32

Table C.3 Slip at each end of the carbon with different loading

Theoretical prediction about the behaviour of the test specimens

Transforming the CFRP to equivalent reference material

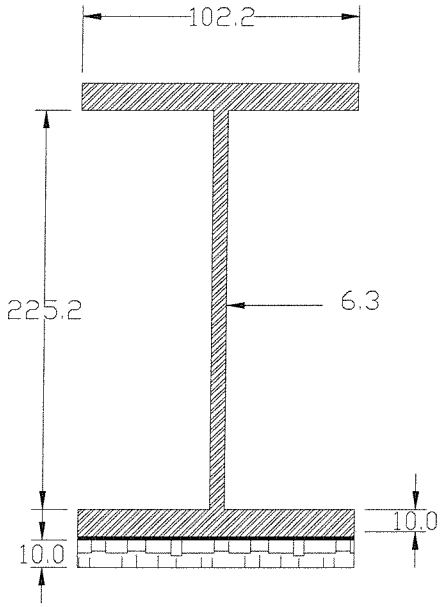

Figure C.4 Cross-sectional dimension

$$\text{The effective width} = \frac{E_c}{E_s} * \text{width}$$

$$= \frac{310}{194} * 102.2$$

$$= 163 \text{ mm}$$

Where, E_c is the Young's modulus of carbon, and E_s the Young's modulus of steel.

Calculating the neutral axis

Sections	Area A (mm^2)	Centre H (mm)	A*H (mm^3)	$Bd^3/12$ (mm^4)	D^2 (mm^2)	Ixx (mm^4)
1	1022	5	5110	8516.6	25090.5	25,651,007
2	1418.7	122.6	173932.6	5996039	1664.6	8,357,607
3	1022	240.2	245484.4	8516.6	5898.24	6,036,518
4	1630	250.2	407826	13583.3	7586.41	12,379,415
Total	5092.7		832353			52,424,547

Table C.4 Calculating the second moment of area

Centroid = AH/A

$$= \frac{832353}{5092.7} = 163.4 \text{ mm (from the top)}$$

Second moment of area = $bd^3/12 + AH^2$

For a single point load at mid-span

$$\delta = \frac{pL^3}{48EI}$$

δ = Vertical deflection

P = point load

L = span

$$\therefore \text{Bending stiffness } \left(\frac{p}{\delta}\right) = \frac{48EI}{L^3}$$

For the beams tested, L=3.0 m

$$\therefore \text{Bending stiffness } = \frac{48x194xI}{3000^3}$$

$$= 3.448\text{x } 10^{-7}$$

For the unreinforced steel beam

Bending stiffness = $3.448\text{x } 10^{-7}$ x 3508 x 10^4

= 12.09 KN/mm

For the reinforced beam

Bending stiffness = $3.448\text{x } 10^{-7}$ x 5242 x 10^4

= 18.07 KN/mm

Shear stresses

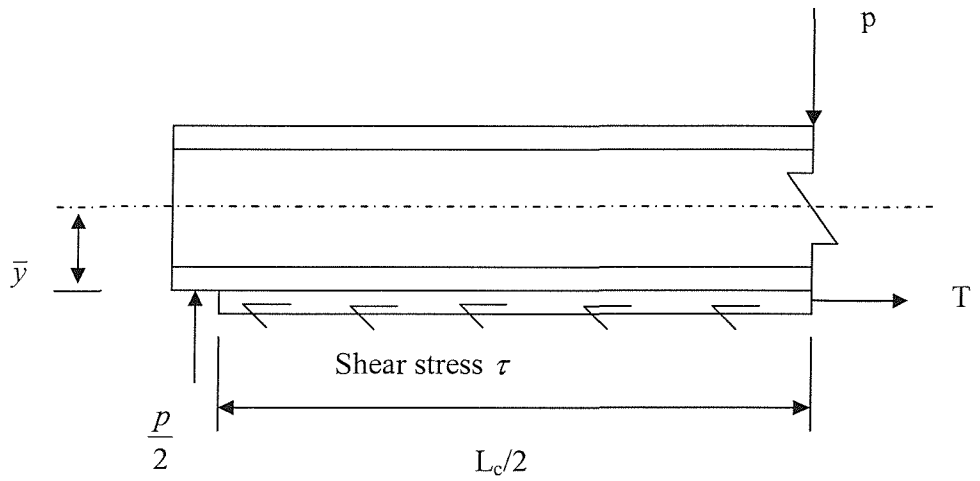

Figure C.5 forces across the reinforced beam

The shear force is constant over each half span and is equal to p/2. Hence shear stress τ is also constant. Say shear force = Q

For horizontal equilibrium

$$T = \frac{BL_c}{2}.\tau$$

B = width of carbon plate

Also

T = Bt. Average direct stress in carbon

t = thickness of carbon plate

Using engineering bending theory

$$T = Bt.\ \frac{M}{I}\left(\frac{\bar{y}+[\bar{y}-t]}{2}\right)$$

$$= Bt.\ \frac{M}{I}\left(\bar{y}-\frac{t}{2}\right)$$

$$= \text{Bt.}\ \frac{pL}{4I}\left(\bar{y} - \frac{t}{2}\right)$$

L = span of beam

$$\therefore \quad \frac{BL_c}{2}.\tau = Bt.\frac{pL}{4I}\left(\bar{y} - \frac{t}{2}\right)$$

$$\therefore \quad \tau = \frac{Q}{I}\frac{L}{L_c}\left(\bar{y} - \frac{t}{2}\right)t$$

For the test beams

L = 3.0 m

L_c = 2.98 m

t = 10.0 mm

I = 5242.0 cm^4

$\bar{y}$ = 91.8 mm

$$\tau = \frac{Q}{5242x10^4}\frac{3.0}{2.98}\left(91.8 - \frac{10.0}{2}\right)10.0$$

$\therefore$ = 0.0000166 Q N/mm^2

P (kN)	Q (N)	τ (N/mm^2)
17	8500	0.141
21	10500	0.174
25	12500	0.207
31	15500	0.257

Table C.5 Calculating the shear stress in adhesive at various load level

Steel-carbon slip before cure

When the steel beam is loaded, the tension (bottom) flange will increase in length. Although the carbon plate is in contact, no shear will be transferred across the adhesive. Consequently there will be relative slip between the steel and the carbon.

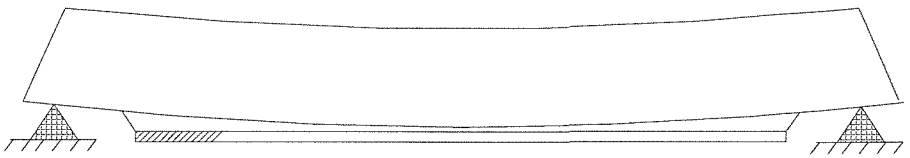

Figure C.6 Beam under point load

Using Engineering bending formula

$$\frac{M}{I} = \frac{\vartheta}{h}$$

$$\therefore \quad \varepsilon = \frac{Mh}{EI}$$

$\therefore$ Total extension over half of the length of the carbon plate is

$$\int_{L_1}^{L/2} \varepsilon.dx = \int_{L_1}^{L/2} \frac{Mh}{EI}.dx$$

$$= \int_{L_1}^{L/2} \frac{Pxh}{2EI}.dx = \frac{Ph}{4EI}\left[x^2\right]_{L_1}^{\frac{L}{2}}$$

$$= \frac{Ph}{4EI}\left[\frac{L^2}{4} - L_1^2\right]$$

h (before curing occurs) $= \frac{260.4}{2} = 130.2$ mm

$$L_1 = \frac{3000 - 2880}{2} = 60 \text{ mm}$$

The slip is equal to the extension of the steel beam, since the change in length of the carbon plate will be negligible.

$$\therefore \quad \text{Slip} = \frac{P*130}{4*194{,}000*4005*10^4}\left[\frac{3000^2}{4} - 60^2\right]$$

$= 9.39 \text{ x } 10^{-6} \text{ P mm}$ (P in N)

P (KN)	Slip (mm)
17	0.159
21	0.197
25	0.234
31	0.291

Table C.6 Slip at each end of the carbon with different loading

Theoretical prediction about the behaviour of the test specimens

Transforming the CFRP to equivalent reference material

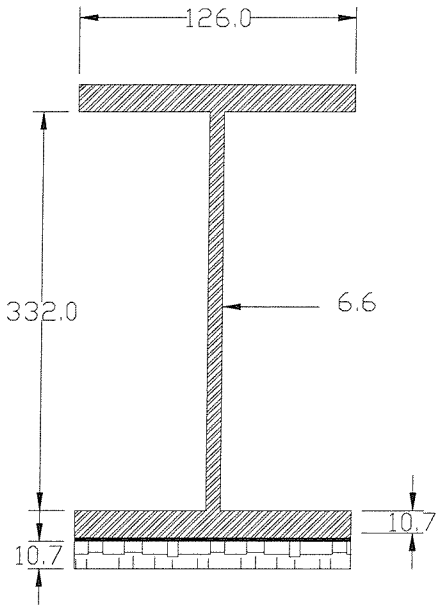

Figure C.7 Cross-sectional dimension

$$\text{The effective width} = \frac{E_c}{E_s} * \text{width}$$

$$= \frac{310}{194} * 126$$

$$= 201.3 \text{ mm}$$

Where, E_c is the Young's modulus of carbon, and E_s the Young's modulus of steel.

Calculating the neutral axis

Sections	Area A (mm^2)	Centre H (mm)	A*H (mm^3)	$Bd^3/12$ (mm^4)	D^2 (mm^2)	Ixx (mm^4)
1	1348.2	5.35	7212.87	12863	51551	69,513,921
2	2191.2	176.7	387185	20126902	3102	26,921,004
3	1348.2	348.05	469241	12863	13375	18,045,038
4	2153.91	358.75	772715	246601	15964	34,631,620
Total	7041.51		1636353			149,111,583

Table C.7 Calculating the second moment of area

Centroid = AH/A

$$= \frac{1636353}{7041.51} = 232.4 \text{ mm (from the top)}$$

Second moment of area = $bd^3/12 + AH^2$

For a single point load at mid-span

$$\delta = \frac{pL^3}{48EI}$$

δ = Vertical deflection

P = point load

L = span

$$\therefore \text{Bending stiffness } \left(\frac{p}{\delta}\right) = \frac{48EI}{L^3}$$

For the beams tested, L=5.0 m

$$\therefore \text{Bending stiffness } = \frac{48x194xI}{5000^3}$$

$$= 7.45 \times 10^{-8}$$

For the bare steel beam

Bending stiffness = $7.45 \times 10^{-8} \times 10129 \times 10^4$

= 7.55 KN/mm

For the reinforced beam

Bending stiffness = $7.45 \times 10^{-8} \times 14911 \times 10^4$

= 11.1 KN/mm

Shear stresses

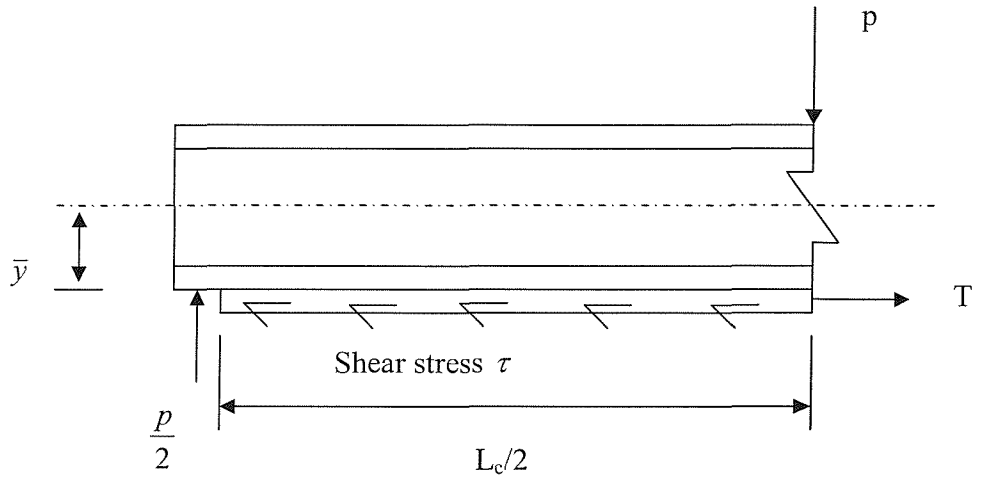

Figure C.8 forces across the reinforced beam

The shear force is constant over each half span and is equal to p/2. Hence shear stress τ is also constant. Say shear force = Q

For horizontal equilibrium

$$T = \frac{BL_c}{2}.\tau$$

B = width of carbon plate

Also

T = Bt. Average direct stress in carbon

t = thickness of carbon plate

Using engineering bending theory

$$T = Bt.\ \frac{M}{I}\left(\frac{\bar{y}+[\bar{y}-t]}{2}\right)$$

$$= Bt.\ \frac{M}{I}\left(\bar{y}-\frac{t}{2}\right)$$

$$= Bt.\ \frac{pL}{4I}\left(\bar{y}-\frac{t}{2}\right)$$

L = span of beam

$$\therefore \quad \frac{BL_c}{2}.\tau = Bt.\frac{pL}{4I}\left(\bar{y} - \frac{t}{2}\right)$$

$$\therefore \quad \tau = \frac{Q}{I}\frac{L}{L_c}\left(\bar{y} - \frac{t}{2}\right)t$$

For the test beams

L = 5.0 m

L_c = 4.89 m

. t = 10.7 mm

I = 14911.0 cm^4

$\bar{y}$ = 131.7 mm

$$\tau = \frac{Q}{14911x10^4}\frac{5.0}{4.89}\left(131.7 - \frac{10.7}{2}\right)10.7$$

$\therefore$ = 0.00000927 Q N/mm^2

P (kN)	Q (N)	τ (N/mm^2)
13	6500	0.060
16	8000	0.074
19	9500	0.088
23	11500	0.106

Table C.8 Calculating the shear stress in adhesive at various load level

Steel-carbon slip before cure

When the steel beam is loaded, the tension (bottom) flange will increase in length. Although the carbon plate is in contact, no shear will be transferred across the adhesive. Consequently there will be relative slip between the steel and the carbon.

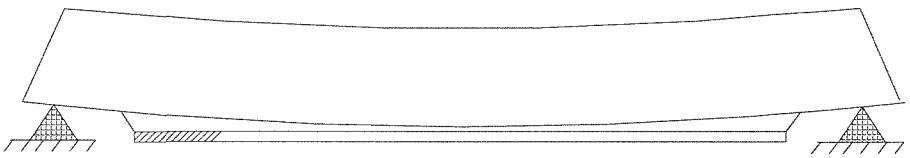

Figure C.9 Beam under point load

Using Engineering bending formula

$$\frac{M}{I} = \frac{\vartheta}{h}$$

$$\therefore \quad \varepsilon = \frac{Mh}{EI}$$

$\therefore$ Total extension over half of the length of the carbon plate is

$$\int_{L_1}^{L/2} \varepsilon.dx = \int_{L_1}^{L/2} \frac{Mh}{EI}.dx$$

$$= \int_{L_1}^{L/2} \frac{Pxh}{2EI}.dx = \frac{Ph}{4EI}\left[x^2\right]_{L_1}^{\frac{L}{2}}$$

$$= \frac{Ph}{4EI}\left[\frac{L^2}{4} - L_1^2\right]$$

h (before curing occurs) $= \frac{312}{2} = 156$ mm

$$L_1 = \frac{5000 - 4880}{2} = 60 \text{ mm}$$

The slip is equal to the extension of the steel beam, since the change in length of the carbon plate will be negligible.

$$\therefore \quad \text{Slip} = \frac{P*156}{4*194{,}000*10170*10^4}\left[\frac{5000^2}{4} - 60^2\right]$$

$= 1.23 \times 10^{-5}$ P mm (P in N)

P (KN)	Slip (mm)
13	0.159
16	0.196
19	0.233
23	0.283

Table C.9 Slip at each end of the carbon with different loading

Appendix D

- **Single lap-shear theory**

Single-lap joint theory, Shiyh-Chuan (1999)

The geometric profile of a single-lap joint is shown in Figure1. The free-body-diagram of an infinitesimal element is the overlap region is shown in Figure A. The force equilibrium of upper and lower adherend in Figure B yields to the following differential:

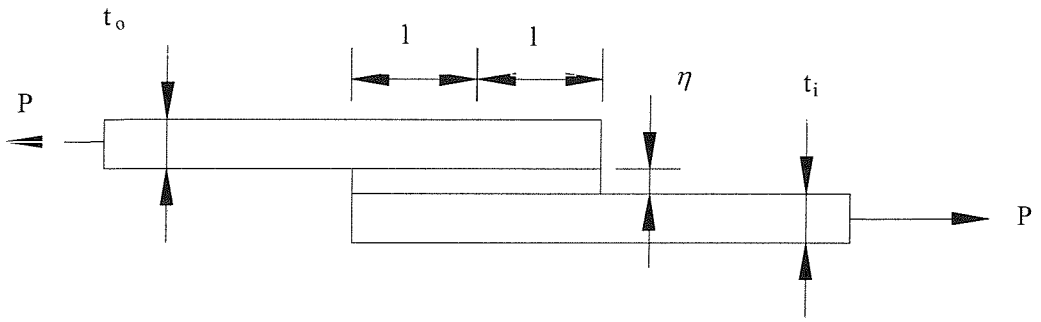

Figure D1 Geometric profile of a single-lap shear

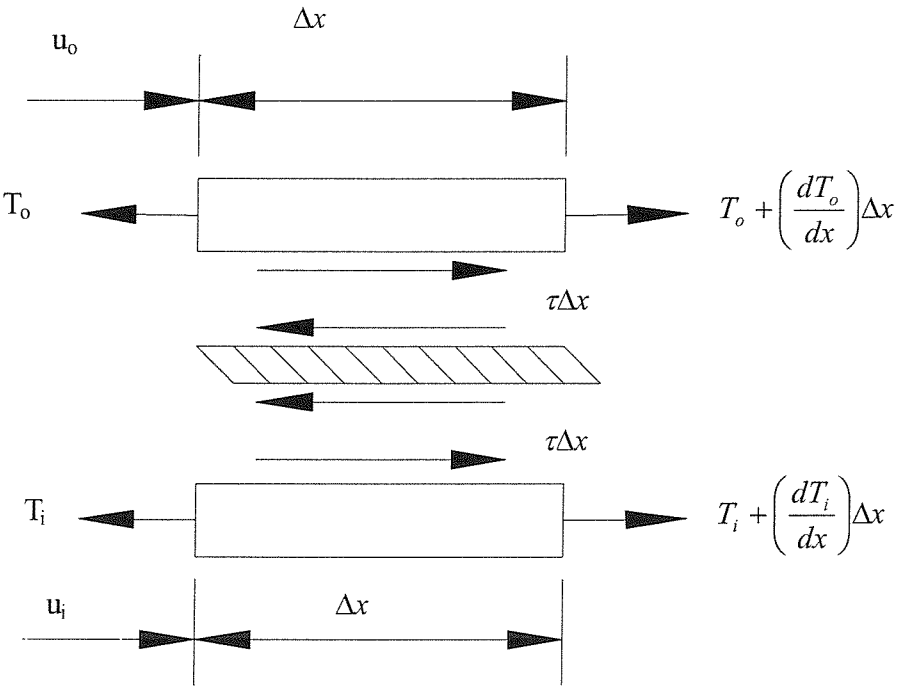

Figure D2 The free-body diagram of a single-lap joint.

$$\frac{dT_0}{dx} + \tau = 0, \tag{1}$$

$$\frac{dT_i}{dx} - \tau = 0 \tag{2}$$

where T_0, T_i in equations (1) and (2) represents longitudinal tension per unit width in the upper and lower adherend, respectively, τ is the shear stress in the adhesive layer. The longitudinal displacement-strain relationships of adherends are:

$$\frac{du_0}{dx} = \varepsilon_0 = \frac{\sigma}{E} = \frac{T_0}{E_0 t_0} \tag{3}$$

$$\frac{du_i}{dx} = \varepsilon_i = \frac{\sigma}{E} = \frac{T_i}{E_i t_i} \tag{4}$$

where u_o, ε_o, E_o and t_o are the longitudinal displacement, strain, Young's modulus, and thickness of the upper adherend, respectively. u_i, ε_i, E_i and t_i are the respective components relative to the lower adherend.

The differential equations (1) and (2) can be combined together through the shear deformation in the adhesive layer as follows:

$$\tau = G_a \gamma = \frac{G_a}{\eta}(u_i - u_0) \tag{5}$$

where G_a is the shear modulus of adhesive, γ and η are the shear strain and thickness of the adhesive layer, respectively.

Taking the derivative with respect to x of equation (5) and (1), yields:

$$\frac{d\tau}{dx} = \frac{G_a}{\eta}\left(\frac{du_i}{dx} - \frac{du_0}{dx}\right), \tag{6}$$

$$\frac{d^2 T_0}{dx^2} = -\frac{d\tau}{dx} \tag{7}$$

Substituting equation (6) and (3), (4) into equation (7) yields:

$$\frac{d^2 T_0}{dx^2} = -\frac{G_a}{\eta}\left(\frac{du_i}{dx} - \frac{du_0}{dx}\right) = -\frac{G_a}{\eta}\left(\frac{T_i}{E_i t_i} - \frac{T_0}{E_0 t_0}\right). \tag{8}$$

The force balance in Figure 3 requires that the sum of the longitudinal forces in upper and lower adherend equals to the applied force P, i.e.

$$P = T_i + T_0 \quad \text{or} \quad T_i = P - T_0. \tag{9}$$

Substituting equation (9) into (8), one can obtain a second-order differential equation of T_0 with respect to x as follows:

$$\frac{d^2T_0}{dx^2} = -\frac{G_a}{\eta}\left(\frac{P-T_0}{E_i t_i} - \frac{T_0}{E_0 t_0}\right)$$

$$\frac{d^2T_0}{dx^2} = \frac{G_a}{\eta}\left(\frac{-P}{E_i t_i}\right) + \frac{G_a}{\eta}\left(\frac{1}{E_i t_i} + \frac{1}{E_0 t_0}\right)T_0$$

$$\frac{d^2T_0}{dx^2} - \frac{G_a}{\eta}\left(\frac{1}{E_i t_i} + \frac{1}{E_0 t_0}\right)T_o = -\frac{G_a P}{E_i t_i \eta}$$

$$\frac{d^2T_0}{dx^2} - \lambda^2 T_o = -\frac{G_a P}{E_i t_i \eta} \tag{10}$$

where

$$\lambda^2 = \frac{G_a}{\eta}\left(\frac{1}{E_i t_i} + \frac{1}{E_0 t_0}\right)$$

The associated boundary conditions are

$$\begin{aligned} T_o &= 0, \qquad x = l \\ T_o &= P, \qquad x = -l \end{aligned} \tag{11}$$

Where l is the half length of the bonded region.

The solution of differential equation (10) can be written as

$$T_0 = A\sinh(\lambda x) + B\cosh(\lambda x) + \frac{PE_o t_o}{\left(E_o t_o + E_i t\right)}. \tag{12}$$

The integration constants A and B can be solved by applying the boundary conditions in equation (11). As a result, the longitudinal tension, T_o and T_i, in upper and lower adherend and the shear stress τ in the adhesive layer can be expressed as the following form:

$$T_o = P\left[-\frac{1}{2}\frac{\sinh(\lambda x)}{\sinh(\lambda l)} + \frac{E_i t_i - E_o t_o}{2(E_i t_i + E_o t_o)}\frac{\cosh(\lambda x)}{\cosh(\lambda l)} + \frac{E_o t_o}{(E_i t_i + E_o t_o)}\right] \tag{13}$$

$$T_i = P\left[1 + \frac{1}{2}\frac{\sinh(\lambda x)}{\sinh(\lambda l)} - \frac{E_i t_i - E_o t_o}{2(E_i t_i + E_o t_o)}\frac{\cosh(\lambda x)}{\cosh(\lambda l)} - \frac{E_o t_o}{(E_i t_i + E_o t_o)}\right] \tag{14}$$

$$\tau = \frac{P\lambda}{2}\left[\frac{\cosh(\lambda x)}{\sinh(\lambda l)} - \frac{E_i t_i - E_o t_o}{(E_i t_i + E_o t_o)}\frac{\sinh(\lambda x)}{\cosh(\lambda l)}\right] \tag{15}$$

Appendix E- cast iron strut

- **Derivation of interaction equation for preloaded columns**
- **Prediction of material properties from test results**

Derivation of interaction equation for preloaded columns

For preloaded columns, the effect of the induced stresses (due to the existing load (P_1) at the time of strengthening) on the response of the reinforced composite column needs to be taken into account. The capacity criterion to be satisfied is derived as follows:

$$P_1 = A_g \sigma_{a1} \tag{1}$$

where

σ_{a1} is the average failure stress of the unreinforced column due to the existing load (P_1)

$$P_{u1} = A_g \sigma_{f1} \tag{2}$$

where

σ_{f1} is the average failure stress of the unreinforced column,

P_{u1} is the axial load capacity of the unreinforced column.

The flexure buckling load that the reinforced column can withstand is:

$$P_2 = A_g \sigma_{a1} + A_t (\sigma_{a2} - \sigma_{a1}) \tag{3}$$

The axial load capacity of the reinforced column is:

$$P_{u2} = A_t \sigma_{f2} \tag{4}$$

where

A_t is the area of the transformed section,

σ_{f2} is the average stress in the reinforced column at failure.

Conservatively, the reinforced column fails when:

$$\sigma_{a2} = \sigma_{f2}$$

i.e. when

$$P_2 = A_g \sigma_{a1} + A_t (\sigma_{f2} - \sigma_{a1}) \tag{5}$$

Substituting ($P_{u2} = A_t \sigma_{f2}$) in equation (3) gives:

$$P_2 = P_1 + P_{u2} - A_t \sigma_{a1} \frac{A_g}{A_g} \tag{6}$$

Substituting ($P_1 = A_g \sigma_{a1}$) in equation (6) and rearranging, we get:

$$P_2 = P_{u2} - P_1\left(\frac{A_t}{A_g} - 1\right) \tag{7}$$

This gives the required interaction equation:

$$\frac{P_2}{P_{u2} - P_1\left(\frac{A_t}{A_g} - 1\right)} \leq 1.0$$

Prediction of material properties from test results

Unreinforced

The following equations can be derived from the stress-strain relationship and the engineers bending formula:

$$F = E_c A_c \varepsilon_{ca}$$

and

$$F(\delta + e) = \frac{E_c I_c \varepsilon_{cb}}{y_{max}}$$

where

F = applied force

δ = transverse deflection

e = eccentricity of applied force

E_c = elastic modulus of cast iron

A_c = area of strut section

ε_a = axial strain in the cast iron

I_c = second moment of area of strut section

y_{max} = maximum distance from section centroid to edge of section

Values for the various quantities can be calculated from the section dimensions or found from the test results. Two values for E_c can be calculated from the axial and bending behaviour of the strut.

Reinforced

A similar approach for the reinforced section gives

$$F = E_c(A_c + mA_r)\varepsilon_a$$

and

$$F(\delta + e) = E_c \frac{(I_c + mI_r)}{y_{max}} \varepsilon_b$$

where

A_r =area of carbon fibre reinforcement

I_r = second moment of area of carbon fibre reinforcement

Appendix F

- **Buckling failure theory**

Buckling failure – review

A review of Change and Lessard (1989) investigation into fibre buckling failure of fibre reinforced composites was carried out to investigate the level of fibre interaction due to uniform and non-uniform loading. The investigation was especially focused on understanding the effect of fiber-matrix interaction due to nonuniform loading on fiber buckling strength of unidirectional composites. An analytical model based on the energy principle was developed for predicting the fiber buckling strength of unidirectional composites. Numerical solutions were generated from the model to study the effect of fiber-matrix interaction on the fiber buckling strength of composites subjected to different types of loadings.

Fiber buckling is a very important failure mode because it frequently leads to catastrophic failure in structures subjected to compression. Therefore, it is very important that fiber-buckling failure be fully understood and predictable. All the previous analyses were developed based on the assumption that the composite was stressed uniformly due to a constant load. As a consequence, the geometry is greatly simplified to only a one-dimensional configuration with a single fiber embedded in a matrix, assuming that each fiber of a unidirectional layer shared an equal load and deformed in the same manner. The influence of one fiber on another was ignored.

However, since fiber compressive strength is directly associated with geometric stability, any disturbance in geometry and stress distribution among the fibers could significantly effect the buckling strength. Therefore, it is very important to fundamentally understand the in situ buckling strength in composites, and to determine the effect of fiber-matrix-fiber interaction on the buckling strength in composites with uniform stress distribution. Figure F1, shows the effect of uniform and nonuniform loading of composite. A variational method based on the minimum potential energy principle is used to develop the analysis. Consider that a unidirectional composite consist of N identical continuous fiber embedded uniformly in a matrix, as shown in Figure F2. It is assumed that each

fiber can deform in an individual manner and that the i^{th} fiber has its lateral displacement denoted as $w_i(x)$.

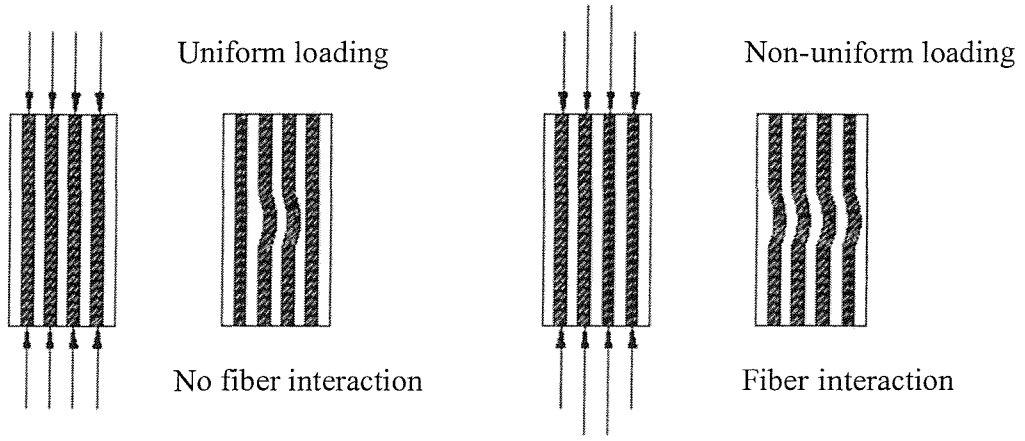

Figure F1: Simulation of the buckling of microfibers due to uniform and nonuniform loading conditions.

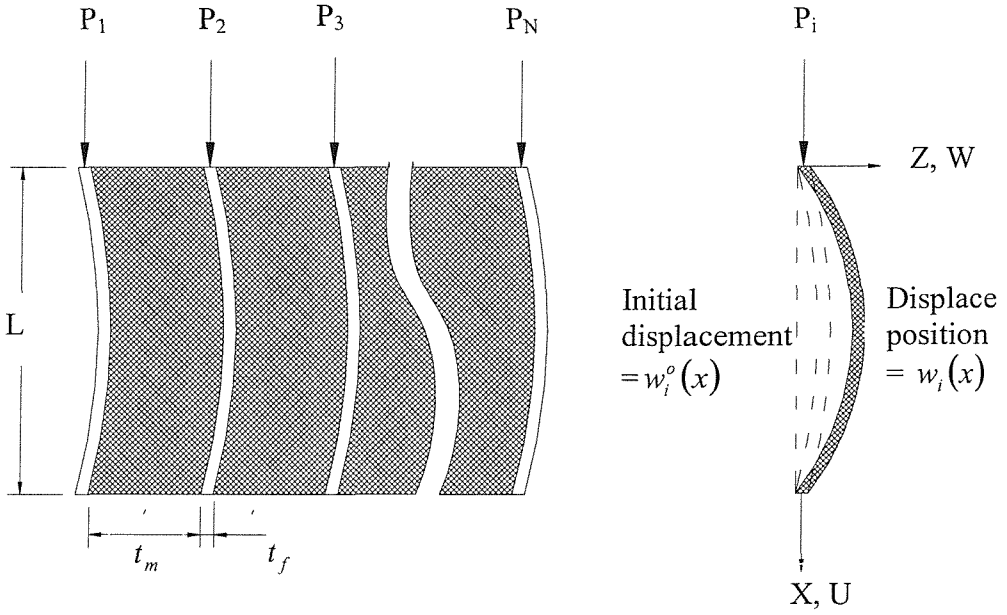

Figure F2: The modelling of a fiber-matrix system using N loaded fibers. Each fiber has initial imperfection $w_i^o(x)$ and displaced $w_i(x)$.

It is further assumed that (1) the matrix supports non of the compressive loads, (2) the fiber has an initial imperfection, described by specifying an initial lateral displacement $w_i^0(x)$ along the length of the fiber, and (3) the material has linear stress-strain relationships. Based on these assumptions, the compressive load is distributed over the fibers. The load carried on the i^{th} fiber is denoted as P_i. The lateral displacement of the i^{th} fiber relative to imperfection id denoted by:

$$\overline{w}_i(x) = w_i(x) - w_i^o(x) \tag{1}$$

The total potential energy of the system can be broken down into four terms:

1. Strain energy due to fiber bending
2. Strain energy due to matrix extension
3. Strain energy due to matrix shearing
4. Work done by the applied load

Each term can be calculated separately and will be elaborated upon below. The summation of each term forms the total potential energy of the system.

The strain energy due to bending of the i^{th} fiber, can be expressed as

$$\prod_i^f = \frac{1}{2}\int_0^l E_f I_f \left(\frac{\partial^2 \overline{w}_i(x)}{\partial x^2}\right)^2 dx \tag{2}$$

This is the strain energy in the matrix due to extensional strain, resulting from the relative lateral displacements of adjacent fibers, i.e.,

$$\prod_{i,i+1}^e = \frac{E_m b t_m}{2}\int_o^l (\varepsilon_{i,i+1})^2 dx \tag{3}$$

Where E_m is the extensional modulus of the matrix ε is the extensional strain, and the subscripts "$i, i+1$" denote that the matrix under consideration is between the i^{th} and i^{th+1} fibers.

The strain energy of the matrix due to shearing can be approximately expressed as:

$$\prod_{i,i+1}^{\gamma} = \frac{G_m b t_m}{2} \int_o^l (\gamma_{i,i+1})^2 dx \tag{4}$$

Where G_m is the shear modulus, and the shear strain γ is the average strain in the matrix between the i^{th} and the i^{th+1} fibers.

The work done by the load P_i to the I^{th} fiber can be expressed as:

$$\prod_i^p = -\frac{P_i}{2} \int_0^l \left[\left(\frac{\partial w_i(x)}{\partial x} \right)^2 - \left(\frac{\partial x_i^o(x)}{\partial x} \right)^2 \right] dx \tag{5}$$

Expressions for $\varepsilon_{i,i+1}$ and $\gamma_{i,i+1}$ can be found from kinematic deformations in terms of the displacements of the i^{th} and the i^{th+1} fibers. Under a compressive load, the fibers bend, causing two points on adjacent fibers to move away from or toward each other (horizontally) and to move parallel to each other (vertically). Horizontal motion causes extensional deformation in the matrix while vertical motion results in shear deformation, as shown in Figure F3.

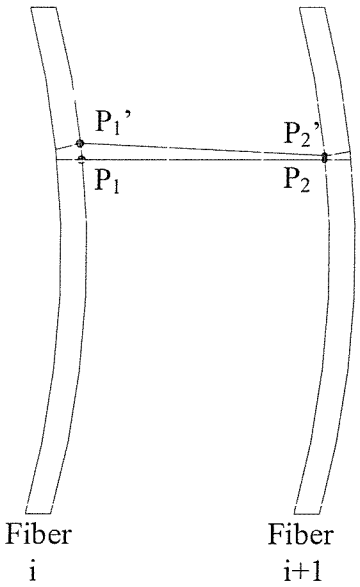

Figure F3: Kinematics of fiber deformation. Showing two fibers i and $i+1$, and two points initially deformed at p_1 and p_2 respectively, and finally displaced to p_1' and p_2' respectively.

It has been shown [Hyer, 1986], two corresponding points on adjacent fibers i and $i+1$ are labelled p_1 and p_2. Initially, the two points are parallel, vertically, a certain lateral distance apart. The deformation state is represented by p'_1 and p'_2. The points are moved with respect to each other, both horizontally and vertically, causing extensional and shear deformations, respectively. By definition, the strain-displacement relationships under small deflection for matrix extension and shearing are defined as:

$$\varepsilon = \frac{\partial w}{\partial z} \tag{6}$$

$$\gamma = \frac{\partial w}{\partial x} + \frac{\partial u}{\partial z} \tag{7}$$

In term of actual displacements, the average extensional strain, $\varepsilon_{i,i+1}$, in a matrix, due to the relative movement, can be approximated as:

$$\varepsilon_{i,i+1} = \frac{\left[\overline{w}_{i+1}(x) - \overline{w}_i(x)\right]}{t_m} \tag{8}$$

Considering equation (17), the first term of the shear deformation can be approximated as:

$$\frac{\partial w}{\partial x} = \frac{1}{2}\left(\frac{\partial \overline{w}_i(x)}{\partial x} + \frac{\partial \overline{w}_{i+1}(x)}{\partial x}\right) \tag{9}$$

The second term is related to the change of slope of the line joining point p_1 and p_2 resulting in the following approximation:

$$\frac{\partial u}{\partial z} = \frac{\frac{t_f}{2}\left(\frac{d\overline{w}_i(x)}{dx} + \frac{d\overline{w}_{i+1}(x)}{dx}\right)}{t_m}, \tag{10}$$

thus, the shear strain, $\gamma_{i,i+1}$, in a matrix is

$$\gamma_{i,i+1} = \frac{1}{2}\left(1 + \frac{t_f}{t_m}\right)\left(\frac{\partial \overline{w}_i(x)}{\partial x} + \frac{\partial \overline{w}_{i+1}(x)}{\partial x}\right) \tag{11}$$

Combining equation (13), (14), (18), and (21) leads to the following expressions for extensional strain energy and shearing strain energy for the matrix between the i^{th} and i^{th+1} fibers.

$$\prod_{i,i+1}^{e} = \frac{E_m t_m b}{2} \int_0^l \left(\frac{\overline{w}_i(x) - \overline{w}_{i+1}(x)}{t_m} \right)^2 dx \tag{12}$$

$$\prod_{i,i+1}^{\lambda} = \frac{G_m t_m b}{8} \left(1 + \frac{t_f}{t_m} \right)^2 \int_0^l \left(\frac{\partial \overline{w}_i(x)}{\partial x} + \frac{\partial \overline{w}_{i+1}(x)}{\partial x} \right)^2 dx \tag{13}$$

Summing equation (14), (15), (22) and (23) the total potential energy of a fiber-matrix composite containing N fibers can be expressed as

$$\prod = \sum_{i=1}^{N} \prod_i^f + \sum_{i=1}^{N} \prod_i^p + \sum_{i=1}^{N-1} \prod_{i,i+1}^e + \sum_{i=1}^{N-1} \prod_{i,i+1}^{\gamma} \tag{14}$$

Accordingly, equation (24) is the total potential energy for the system containing multiple variables, w_j (x) (where $j=1 \rightarrow N$). Taking the variation of the total potential energy will lead to equilibrium equations for the system, from which a critical load can be determined. For uniform loading, all the $w_j(x)$ terms can be considered equal, and equation (14) will be reduced to a simple one-nonuniform loading, the displacement of each fiber may not be the same and they will consequently influence each other. In order to determine the critical load of the system, the influence of one fiber deformation on the others has to be determined. Here, a decay distance is introduced to evaluate the degree of interaction among fibers.

Consider that the system of fibers given in Figure F2 can be modelled as a series of parallel fibers on elastic foundations with a spring constant k_s and k_f, as shown in Figure F4. The spring constant $k's$ can be determined from an energy balance. Spring constant for matrix:

$$K_s = bE_m \frac{L}{t_f} \frac{v_f}{v_m},$$

Spring constant for a fiber:

$$K_f = \frac{32}{5} b E_f \left(\frac{t_f}{L}\right)^3 \quad (15)$$

Where E_m and E_f are the moduli of the matrix and fiber material, respectively. v_m and v_f are the volume fraction of the matrix and fiber respectively, and b, and t_f and L are the depth, width, and length of the fiber, respectively. If there is a lateral force introduced to produce a lateral displacement at the i^{th} fiber, owing to fiber-spring interaction, such a displacement will disturb the displacement field of the surrounding fibers. These displacements can be related to the displacement of the i^{th} fiber by solving a set of simultaneous equation or using recursion relationships

$$W_f(x) = k_j^i w_i(x) \quad (16)$$

Where k_j^i are the interaction coefficients, which relate the displacement of the j^{th} fiber to the displacement of the i^{th} fiber

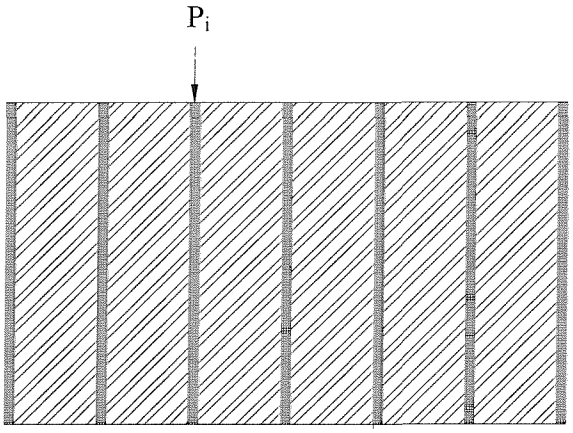

(a) Step1: aligned fibers in an elastic matrix

Fiber i $i+1$ $i+n$

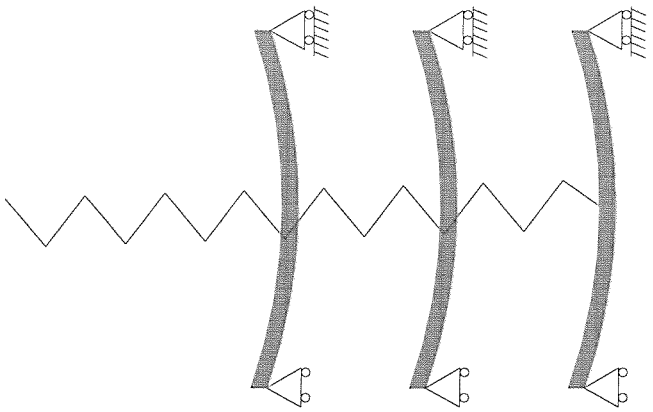

(b) Step 2: matrix modelled as springs, fibers modelled as beams

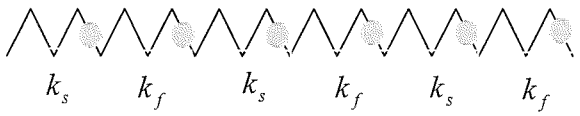

(c) Step 3: matrix spring constant calculated as k_s, fiber constant calculated as k_f

Figure F4: Modelling of a fiber-matrix system from a system of fibers and matrix to a system of spring.

Now, considering a system of N fibers subjected to a nonuniform loading, the magnitude of the displacement of each fiber, sharing different portions of the load, will not be the same. As a consequence, the fibers interact with each other and result in nonzero extensional strain energy. It is useful to examine the energy terms using the equation for sinusoidal waveforms and ignoring initial imperfections,

$$w_j(x) = A_j \sin\left(\frac{\pi x}{L}\right)$$

$$w_j^o(x) = 0 \qquad (17)$$

For a system of fibers in which only the i^{th} fiber is loaded (see Figure F4(a)), the displacements of other surrounding fibers can be related to A_i through the decay distance assumption, i.e.,

$$A_j = k_j^i A_i \tag{18}$$

Note that because of the decay distance assumption, the problem with a single loaded fiber can be related to each other and can be written in terms of a single load parameter. For this problem, the displacement of fibers can also be formulated by the decay distance assumption, with the aid of the superposition method. The displacement of each fiber is the sum of the displacements caused by the load acting on the fiber and the displacements due to the nonuniform load distribution. The magnitudes of the displacements for the loaded fiber due to each individual load are related to each other proportionately to the magnitude of the loads on fibers. Thus, the fiber with the largest displacement can be easily determined. This fiber is most likely to buckle and is called the "critical fiber" (call it fiber "j").

Thus, each load P_j (where $j = 1 \rightarrow N$) on the jth fiber can be related to the load on the critical fiber, P_i, by a factor α_j^i, i.e.,

$$P_j = \alpha_j^i P_i \tag{19}$$

All the displacement amplitudes A_j can be related to the displacement on the critical fiber, A_i, by a factor k_j^i, i.e., $A_j = k_j^i A_i$. The sum of the total energies for this system of fibers can thus be expressed as:

$$\begin{aligned}\Pi &= \sum_{i=1}^{N}\Pi_i^f + \sum_{i=1}^{N}\Pi_i^p + \sum_{i=1}^{N-1}\Pi_{i,i+1}^e + \sum_{i=1}^{N-1}\Pi_{i,i+1}^\gamma \\ &= \frac{1}{2}E_f I_f\left(\frac{\pi}{L}\right)^4\left(\frac{L}{2}\right)\left(\sum_{j=1}^{N}(A_j)^2\right) - \frac{1}{2}\left(\frac{\pi}{L}\right)^2\left(\frac{L}{2}\right)\left(\sum_{j=1}^{N}P_j A_j^2\right) \\ &+ \frac{E_m b}{2t_m}\left(\frac{L}{2}\right)\left(\sum_{j=1}^{N-1}(A_j - A_{j+1})^2\right) \\ &+ \frac{G_m t_m b}{8}\left(1+\frac{t_f}{t_m}\right)^2\left(\frac{\pi}{L}\right)^2\left(\frac{L}{2}\right)\left(\sum_{j=1}^{N-1}(A_j + A_{j+1})^2\right)\end{aligned} \tag{20}$$

Substituting the known relationships between forces, and the known relationships between displacements yields.

$$\prod = \frac{1}{2}E_f I_f\left(\frac{\pi}{L}\right)^4\left(\frac{L}{2}\right)A_i^2\left(\sum_{j=1}^{N}\left(K_j^i\right)^2\right) - \frac{1}{2}\left(\frac{\pi}{L}\right)^2\left(\frac{L}{2}\right)P_i A_i^2\left(\sum_{j=1}^{N}\alpha_j^i\left(k_j^i\right)^2\right)$$
$$+ \frac{E_m b}{2t_m}\left(\frac{L}{2}\right)A_i^2\left(\sum_{j=1}^{N-1}\left(k_j^i - k_{j+1}^i\right)^2\right)$$
$$+ \frac{G_m t_m b}{8}\left(1+\frac{t_f}{t_m}\right)^2\left(\frac{\pi}{L}\right)^2\left(\frac{L}{2}\right)A_i^2\left(\sum_{j=1}^{N-1}\left(k_j^i + k_{j+1}^i\right)^2\right) \qquad (21)$$

The summation of total energy in equation (31) is in term of only one variable, A_i. Minimizing the potential energy of the system with respect to this variable,

$$\frac{\partial\prod}{\partial A_i} = 0 \qquad (22)$$

Now, solving for P_i, the critical load,

$$P_i = E_f I_f\left(\frac{\pi}{L}\right)^2\left[\frac{\sum_{j=1}^{N}\left(k_j^i\right)^2}{\sum_{j=1}^{N}\alpha_j^i\left(k_j^i\right)^2}\right] + \frac{E_m b}{t_m}\left(\frac{L}{\pi}\right)^2\left[\frac{\sum_{j=1}^{N-1}\left(k_j^i - k_{j+1}^i\right)^2}{\sum_{j=1}^{N}\alpha_j^i\left(k_j^i\right)^2}\right]$$
$$+ \quad G_m t_m b\left(1+\frac{t_f}{t_m}\right)^2\left[\left(\frac{1}{4}\right)\frac{\sum_{j=1}^{N-1}\left(k_j^i + k_{j+1}^i\right)^2}{\sum_{j=1}^{N}\alpha_j^i\left(k_j^i\right)^2}\right] \qquad (23)$$

P_i is the critical load on the i^{th} fiber, but it is more useful to think about a critical stress in this region of the composite.

$$\sigma_c = \frac{P_i v_f}{b t_f}, \qquad I_f = \frac{1}{12}b t_f^3 \qquad (24)$$

Furthermore, by introducing the following parameters and simplifying variables,

$$n = \frac{L}{t_f},\ v_f = \frac{t_f}{t_f + t_m},\ v_m = \frac{t_m}{t_f + t_m},\ t_m = t_f\frac{v_m}{v_f} \qquad (25)$$

Equation (23) yields

$$\sigma_c = \frac{E_f \pi^2}{12n^2} v_f [B_f] + \frac{G_m}{v_m}[B_\gamma] + \frac{E_m n^2 v_f^2}{v_m \pi^2}[B_e] \tag{26}$$

Where

$$B_f = \frac{\left(\sum_{j=1}^{N} (k_j^i)^2\right)}{\left(\sum_{j=1}^{N} \alpha_j^i (k_j^i)^2\right)}$$

$$B_\gamma = \frac{1}{4} \frac{\left(\sum_{j=1}^{N-1} (k_j^i + k_{j+1}^i)^2\right)}{\left(\sum_{j=1}^{N} \alpha_j^i (k_j^i)^2\right)}$$

$$B_e = \frac{\left(\sum_{j=1}^{N-1} (k_j^i - k_{j+1}^i)^2\right)}{\left(\sum_{j=1}^{N} \alpha_j^i (k_j^i)^2\right)}$$

B_f, B_γ, and B_e are factors which effect the size of the fiber, shear, and extensional terms, respectively. These factors are influenced mainly by the way the load is distributed on the fiber system. The fiber-buckling model can be used to generate useful results. The following numerical studies were performed to illustrate the kind of results obtained from the fiber-buckling model.

1. Constant applied load: used to simulate the uniaxial compressive strength
2. Single concentrated load: used to observe maximum support of unloaded fibers

Under a constant load distribution, without fiber imperfections, all P_j's are equal $(\alpha_j^i = 1)$. As a result, all $k_j^i \approx 1$, i.e., the displacement distribution is nearly uniform, and B_f=1, and B_γ=1, and $B_e = 1$ and the buckling expression becomes

$$\sigma_c = \frac{E_f \pi^2 v_f}{12n^2} + \frac{G_m}{\gamma_m} = \sigma_c^o \longleftrightarrow X_c^o \tag{27}$$

The buckling load is the well-known buckling equation for unidirectional laminates subjected to uniform loading. σ_c^o is the stress, which can be best, be compared to X_c^o (the unidirectional ply compressive strength).

Consider the system of fiber subjected to a single concentrated load P_i on the i^{th} fiber (see Figure F5). Based on equation (29), $\alpha_j^i = 1$ and all other $\alpha_j^i = 0$. Minimising energies leads to the following "B-factors"

$$B_f = 6.72, \qquad B_\gamma = 6.65, \qquad B_e = 0.14 \tag{28}$$

And

$$\sigma_c = \frac{E_f \pi^2 v_f}{12n^2}(6.72) + \frac{G_m}{\gamma_m}(6.65) + \frac{E_m n^2 v_f^2}{v_m \pi^2}(0.14) \tag{29}$$

$$\sigma_c = 7.88\sigma_c^0 \tag{30}$$

The result, equation (41), means that for a "point " load, the stress concentration can be almost 8 times the uniaxial compressive strength before local buckling occurs.

This model shows why it is not sufficient to consider only the unidirectional compressive strength parameter X_c^o. The boundary may be able to withstand a stress up to 8 times X_c^o. The model shows that nonuniform load distributions are typically more resistant to fiber buckling at a local level. Local strength exceed σ_c^o, therefore X_c^o is exceeded. The case of the single concentrated load shows the extreme case of putting the entire load on a single fiber, leading to a very high local buckling strength of almost 8 times the uniaxial compressive strength.

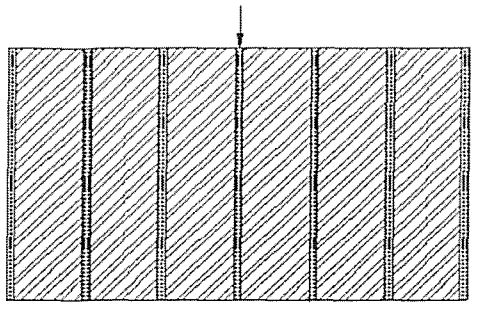

(a) Concentrated load

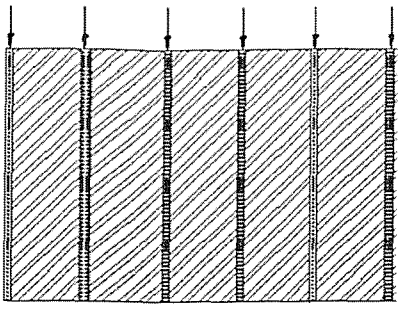

(b) Uniform load

Figure F5: Two examples of loaded fiber-matrix systems used to demonstrate the fiber-buckling model.